

A Combinatorial Approach to Study Structure- Activity Relationships of Myosins and Dynamins Using Small Molecule Modulators

Von der Naturwissenschaftlichen Fakultät
der Gottfried Wilhelm Leibniz Universität Hannover
zur Erlangung des Grades

Doktor der Naturwissenschaften
Dr. rer. nat.

genehmigte Dissertation
von

M. Sc. Jayashankar Selvadurai
geboren am 14.09.1982 in Thiruvavarur (India)

2012

Referent: Prof. Dr. Dietmar Manstein

Korreferent: Prof. Dr. Markus Kalesse

Tag der Promotion: 24.05.2012

Erklärung

Hiermit erkläre ich, Jayashankar Selvadurai, dass ich meine Dissertation selbständig verfasst und die benutzten Hilfsmittel und Quellen sowie gegebenenfalls die zu Hilfeleistungen herangezogenen Institutionen vollständig angegeben habe.

Contents

Acknowledgements	VI
Abbreviations	VIII
Summary	X
Zusammenfassung	XII
CHAPTER 1	1
Introduction	1
1. Introduction	2
1.1 GTP-Binding Proteins	3
1.1.1 General Overview	3
1.1.2 Dynamin and Dynamin Related Proteins	5
1.1.2.1 Large GTPases: The Dynamin Superfamily	6
1.1.2.2 Classical Dynamins	9
1.1.2.3 Dynamin Like Proteins (DLPs) and Dynamin Related Proteins (DRPs).....	12
1.1.2.4 Vps1p	14
1.1.2.5 Mgm1p/OPA1	14
1.1.2.6 Plant Dynamins	15
1.1.2.7 Mx Proteins	16
1.1.2.8 Guanylate-Binding Proteins (GBPs)/Atlastins.....	16
1.1.2.9 Bacterial Dynamin-Like Proteins	16
1.1.3 GTPase Activity of Dynamins	17
1.1.4 Dynamin: a Molecular Motor or a Regulatory Protein	18
1.1.5 Dynamins and Their Interacting Partners.....	20
1.1.5.1 Drp1- Cdks	20
1.1.5.2 Dynamin1 and Amphiphysin1-SH3 Domain	22
1.2 ATP Binding Proteins: Myosin	23
1.2.1 Molecular Properties of Myosins	26
1.2.2 Architecture and Structure Details of Myosins	26
1.2.3 The Myosin II Motor Domain of <i>D. discoideum</i>	29
1.2.4 The Cross Bridge Cycle	31
1.3 Diseases Related to Myosin and Dynamin Dysfunction	33
1.3.1 Small Molecule Effectors of Myosins and Dynamins	34
CHAPTER 2.....	36
Materials and Methods	36
2.1 Buffer Recipes.....	37
2.2 Competent Cells	38
2.3 Transformation of Plasmid DNA into Competent Cells	38

2.4 Plasmid DNA Isolation	39
2.5 <i>D. discoideum</i> Growth on Plates and in Shaking Culture	39
2.6 <i>D. discoideum</i> Electroporation	40
2.7 Preparation and Cryo-Conservation of <i>D. discoideum</i> Spores.....	41
2.8 Polymerase Chain Reaction (PCR)	41
2.9 Restriction Enzyme Mediated Digestion of DNA.....	42
2.10 Separation of DNA-Fragments on Agarose Gels	42
2.11 Purification of DNA from PCR Reactions and Agarose Gels	43
2.12 Ligation of DNA Fragments	43
2.13 SDS Polyacrylamide Gel Electrophoresis (SDS-PAGE).....	43
2.14 Western Blotting	44
2.15 Analytical Protein Preparations.....	45
2.16 Purification of DynaminA.....	46
2.17 Purification of DynaminA Domains Fused to Myosin II Motor Domain of <i>D. discoideum</i>	47
2.18 GST-Amphiphysin1-SH3 Domain Purification	48
2.19 Purification of Dynamin1	49
2.20 Purification of Dynamin Related Protein1	51
2.21 Purification of Minimal Construct GG1 (dynamin1) and GGA (dynaminA).....	52
2.22 Steady-State Kinetics	54
2.23 Stopped Flow Kinetics	56
2.24 <i>In-vitro</i> Motility Assay	57
2.24.1 Buffers.....	57
2.24.2 Actin Labelling.....	57
2.24.3 Flow Cell Construction	58
2.24.4 Assay Procedure	58
2.24.5 Hardware and Software	59
2.25 Microscale Thermophoresis	59
2.26 Live Cell Total Internal Reflection Fluorescence (TIRF) Microscopy	60
2.27 Mass Spectrometry	60
2.28 Crystallization of Proteins and Crystal Handling.....	61
2.28.1 X-Ray Diffraction	61
2.28.2 Hanging and Sitting Drop Vapor Diffusion	63
2.28.3 Cryo-Protection of Crystals.....	64
2.28.4 Crystal Mounting for Data Collection.....	64
2.28.5 Data Collection and Processing.....	65
2.28.6 Structure Solution, Refinement and Model Building.....	65
2.28.7 Simulated Annealing	66

2.28.8 Model Building, Structure Interpretation and Figure Preparations.....	66
2.28.9 Data Processing Software and Modules.....	67
CHAPTER 3.....	68
Results.....	68
3.1 Functional Characterization of Dynamin Related Protein1 (Drp1)	69
3.1.1 Ionic Strength Dependence and Cooperativity of Drp1 GTPase Activity	69
3.1.2 Transient Kinetic Characterization of Drp1 Interactions with Nucleotides	70
3.1.2.1 GTP Binding to Drp1	71
3.1.2.2 GDP Binding to Drp1.....	73
3.1.2.3 Nucleotide Dissociation Kinetics of Drp1	74
3.1.2.4 Summary of Nucleotide Binding and Nucleotide Dissociation Kinetics.....	77
3.2 Mdivi-1 and Sertraline Binding Properties to Drp1	78
3.3 Assembly Properties of Drp1 Studied by Dynamic Light Scattering	79
3.3.1 Salt Dependence of Drp1 Self-Assembly.....	80
3.3.2 Influence of Sertraline and Mdivi-1 on Drp1 Self-Assembly	81
3.3.3 Effect of Sertraline on GTP- γ -S Induced Drp1 Self-Assembly	82
3.4 Assembly Properties of Drp1 Studied by Analytical Ultra-Centrifugation (AUC)	84
3.4.1 Concentration Dependence of Oligomer Formation	84
3.4.2 Influence of GTP- γ -S on Drp1 Oligomerization.....	85
3.4.3 Influence of GDP on Drp1 Self-Assembly	85
3.4.4 Influence of GTP- γ -S and GDP on Drp1 Self-assembly.....	86
3.5 Drp1 Acts as Substrate of the Cdk2/CyclinA Complex.....	87
3.5.1 Mass Spectrometry Analysis of Drp1 Phosphorylation	89
3.5.2 FRET-Based Displacement Experiments of the CyclinA/p27 Complex by Drp1 and Dynamin1	90
3.6 Binding Affinity of Drp1 for Cardiolipin and the Influence of Nucleotides on Drp1- Cardiolipin Interaction	92
3.7 Homology Modeling and Structural Analysis of the Drp1 GTPase Domain in Complex with Nucleotides and Cardiolipin.....	95
3.8 Crystallization Experiments of Drp1.....	99
3.9 Use of Psychotropic Drugs as Potential Dynamin and Drp1 Modulators.....	100
3.9.1 Fluvoxamine and Sertraline are Potent Inhibitors of Drp1 and Dynamin1 GTPase Activity.....	102
3.9.2 Engineering, Production, and Crystallization of Genetically Modified Dynamin1 Constructs for High Resolution Structure Determination	105
3.9.2.1 Engineering of Various Full-Length and Truncated Dynamin1 Constructs	105
3.9.2.2 GTPase Activity Test of Various Dynamin1 Constructs	110
3.9.2.3 SH3-Domain Mediated Binding of Amphiphysin1 to Dynamin1	111
4. Small Molecule Effectors of Myosin Motor Activity	112
4.1 Structure-Based Identification of Myosin VI Specific Inhibitors	112

4.1.1 Functional Characterization of Myosin VI Specific Inhibitors.....	116
4.1.2 Inhibition of Myosin VI ATPase Activity by PBPh and TIP.....	117
4.1.3 Inhibition of Myosin VI Cellular Function by Halogenated Phenols	118
4.2 Carbazoles as Modulators of Myosin Motor Activity.....	121
4.2.1 Free Energy Calculations of Carbazoles Binding to Myosins Using a Molecular Mechanics Approach.....	124
4.2.2 Inhibiting Potency of Pre-Selected Carbazoles on Myosin ATPase Activity.....	130
4.3 Crystal Structure of the Myosin II Motor Domain in Complex with 2,3,4,6,8- pentachlorododecahydro-1 <i>H</i> -carbazol-1-ol (KIN86).....	134
4.3.1 Structural Characterization of the KIN86 Binding Site	134
4.3.2 B-Factor Analysis of the X-ray Structures of the Myosin II Motor Domain in Complex with Different Inhibitors.....	139
Discussion	142
5.1 The Combinatorial Approach.....	143
5.1.1 Psychotropic Drugs as Potent Effectors of Dynamin1 and Drp1	143
5.1.1.1 Characterization of Sertraline as a New Allosteric Inhibitor of Drp1 Self-Assembly.....	145
5.1.1.1.1 Drp1 Acts as a Substrate of Cdk2/CyclinA.....	146
5.1.1.1.2 ATP Increases Drp1 Binding Affinity to Mitochondrial Lipids	147
5.1.1.2 Molecular Engineering of Optimized Dynamin Constructs for Structure Determination and Functional Studies	148
5.1.2 Small Molecule Effectors of Myosin	148
5.1.2.1 Mechanism and Specificity of Myosin Inhibition by Halogenated Carbazoles and Phenols	149
5.2 Outlook.....	153
References	154
Curriculum Vitae	181
Conference and Workshops	182

Acknowledgements

I am grateful to Prof. Dr. Dietmar J. Manstein for giving me the opportunity and a wonderful laboratory atmosphere to pursue my doctoral thesis. I am deeply indebted to him for providing me with a fascinating and challenging project and for giving me great scientific freedom combined with guidance.

I thank Dr. Roman Fedorov, for his valuable inputs in the area of statistical crystallography and also for taking me to the synchrotron facilities within Germany. I take this opportunity to thank Prof. Dr. Georgios Tsiavaliaris for teaching me stopped flow techniques and for his valuable discussion on various scientific topics like mechano-transductions and chemical biology of myosin IXb. I would also like to thank PD Dr. Ute Curth for her advice and for her help in performing analytical ultracentrifuge experiments. I thank Dr. Andreas Pich for his advice and support in performing mass spectrometry experiments. I thank Dr. Igor Chizhov for his interesting discussion on chemical kinetics and his philosophical inputs about science in general. I would like to thank Dr. Thomas Reubold for his discussion on dynamin projects and his guidance for preparing interesting chemical biology project on various dynamins. His advice and constant discussions has evoked severe interest in me to learn more on biology of apoptosis.

I take this opportunity to thank Dr. Vasantha pattabhi and Dr. D. Velumurugan, University of Madras, India, for their encouragement, confidence in my abilities and for providing great moral support. I am especially indebted to Dr. Amit Sharma, International Centre for Genetic Engineering and Biotechnology (ICGEB), for providing me an opportunity to learn the protein purification techniques and cell culture handlings and for his moral support to pursue my doctorate in the field of structural biology.

I want to thank the staff at the synchrotrons DESY in Hamburg, ESRF in Grenoble for their help during data collection and providing knowledge in synchrotron physics.

I am grateful to Dr. Joachim Greipel and Andreas Blakowitz from the Institute for Biophysical Chemistry, Hannover Medical School for their excellent support in all aspects of the computational facilities. In particular I would like to thank Lina Sell and Jennifer

Colshorn for helping me in contract arrangements and official work related to the administrative departments of Hannover Medical School and Leibniz University Hannover.

I thank Dr. Amrita Rai and Dr. Manuel Taft for their endurance in listening and answering my questions related to various experimental results. I want to thank Petra Baruch, Christian Wassman, Claudia Thiel and all the people from the Institute for Biophysical Chemistry and Structural Analysis for providing me with a great and lively ambience.

I am grateful to Dr. Folma Buss and the members of her group at the Department of Clinical Biochemistry, Cambridge Institute for Medical Research, for teaching me TIRF microscopy and allowing me to perform cell biological experiments related to myosin VI and myosin Ib.

Special thanks to my friends Rajesh Kolli, Gunnar Weninger, Krishna Chinthalapudi, Sarah Heissler, Anne Hennig, Mattias Preller, and Jonathan Rodatus Petrowitz for their support in the laboratory, their willingness to share knowledge, and for their friendship beyond the realms of bench work.

I am very grateful to my grandmother, parents and teachers who supported and encouraged me in all aspects of life and for the values what they have taught me.

Abbreviations

<i>A. thaliana</i>	<i>Arabidopsis thaliana</i>
AAA ⁺	ATPases associated with cellular activities
ADL	Arabidopsis dynamin-like
ADP	Adenosine-5'-diphosphate
ARF	ADP Ribosylation Factors
Arf	ADP-Ribosylation factor
ATP	Adenosine-5'-triphosphate
BDLP	Bacterial dynamin like protein
bp	Base pair
<i>C. elegans</i>	<i>Caenorhabditis elegans</i>
CCP4	Collaborative Computational Project No. 4
cDNA	Complementary DNA
CNS	Crystallography & NMR system
COOT	Crystallographic Object-Oriented Toolkit
CV	Column volume
<i>D. discoideum</i>	<i>Dictyostelium discoideum</i>
<i>D. melanogaster</i>	<i>Drosophila melanogaster</i>
Da	Dalton
DEAE	Diethylaminoethyl
Dlp	Dynamin like protein
DMSO	Dimethyl sulfoxide
DNA	Deoxy-ribo nucleic acid
dNTP	2'-deoxy-ribo 5'-triphosphate nucleotide
DRP	Dynamin related protein
DTT	Dithiothreitol
<i>E. coli</i>	<i>Escherichia coli</i>
EDTA	Ethylene diamine-tetra-acetic acid
EF-G	Elongation factor G
EF-Tu	Elongation factor thermo unstable
EM	Electron microscopy
ER	Endoplasmic reticulum
EYFP	Enhanced yellow fluorescent protein
FtsZ	Filamentous temperature sensitive Z
g	Gram
<i>g</i>	Gravitational force
GAP	GTPase activating protein
GDI	Guanine nucleotide-dissociation inhibitor
GDP	Guanosine 5'-diphosphate
GED	GTPase effector domain
GEF	Guanine nucleotide exchange factor
GMP	Guanosine 5'-monophosphate
GOLD	Genetic Optimisation for Ligand Docking
G-protein	GTP-binding protein
GST	Glutathione S transferase
GTP	Guanosine 5'-triphosphate
GTPase	Guanosine 5'-triphosphate phosphatase
GTP- γ S	Guanosine 5'-O-(3-thiotriphosphate)
hGBP1	Human guanylate binding protein1
hr	Hour

HSP	Heat shock protein
IPTG	Isopropyl β -D-1-thiogalactopyranoside
kb	Kilo base (pairs)
M	Molar
MES	2-[N-Morpholino]ethanesulfonic acid
MGL	Molecular Graphics Laboratory
Mgm1	Mitochondrial genome maintenance 1
min	Minute
ml	Milli litre
mM	Milli molar
MR	Molecular replacement
M-Ras	Membrane-anchored RAS
Mx	Myxovirus resistance
NF- κ B	Nuclear factor kappa-light-chain-enhancer of activated B cells
ng	Nano gram
Ni-NTA	Ni ²⁺ -nitrilotriacetate;
Nm	Nano meter
NTS	N-terminal sequence
OD	Optical density
OPA1	Optic atrophy 1
PBS	Phosphate buffered saline
PCR	Polymerase chain reaction
PEG	Polyethylene glycol
PH	Pleckstrin homology
PMSF	Phenylmethylsulfonyl fluoride
PRD	Proline rich domain
QNS	Glutamine asparagine serine-rich domain
Ran	Ras related nuclear protein
Rap	Ras related protein
RAS	Rat sarcoma
Rheb	Ras homolog enriched in brain
Rho	Ras homology
Rpm	Rotation per minute
<i>S. cerevisiae</i>	<i>Saccharomyces cerevisiae</i> (baker's yeast)
<i>S. pombe</i>	<i>Schizosaccharomyces pombe</i> (fission yeast)
SDS	Sodium lauryl sulfate
SDS-PAGE	SDS-polyacrylamide gel electrophoresis
TBS	Tris buffered silane
TBST	TBS with tween
TGN	Trans Golgi network
TIRF	Total internal reflection fluorescence
Tris	Tris [hydroxymethyl] aminomethane
Vps1	Vacuolar protein sorting 1
w/v	Weight per volume
ZPCK	N-Carbobenzyloxy-L-phenylalanyl chloromethyl ketone

Summary

Dynamin1, dynamin related protein1 (Drp1) and a selection of myosins are the proteins used in this work to investigate how small molecules can modulate their enzymatic activity. Myosins use ATP to generate mechanical force; whereas dynamins use GTP binding and hydrolysis to generate force in the nucleotide induced self-assembled structure. Nucleotide-dependent conformational changes of myosins and dynamins are involved in specified cellular functions with the force generated. Membrane remodeling, squeezing of invaginated vesicles, mitochondrial fissioning are a few to mention for dynamins. Muscle contraction, cargo transport, maintenance of stereociliary bundles in the inner ear, are some of the force mediated functions associated with myosins. Malfunction of the myosins and dynamins are implicated in cancer, cardiomyopathies, blindness, epilepsy and neurodegenerative diseases. Combination of mutagenesis, genetic manipulation, siRNA knock down, and biophysical techniques like X-ray diffraction have been used during the course of this work to characterize the proteins function *in vivo* and *in vitro*. The chemical biological studies on these proteins in combination with other tools assisted in understanding how small molecules can modulate their enzymatic properties like hydrolysis activities, sliding of myosins on actin and self-assembly properties of Drp1 to mention a few.

In the first part of this work, protein engineering of dynamin1 was used in generating stable, oligomerization incompetent mutant forms. A minimal functional fusion dynamin1, containing the N-terminal GTPase domain and C-terminal GED domain was produced to address how small molecules influence on the bundle signaling element (BSE) formed by these two domains. The non-classical dynamin Drp1 specific modulator, sertraline which is a psychotropic drug was identified after systematic studies on Drp1's assembly property in an ionic dependent manner. Computational analysis using comparative structure method with *D. discoideum* dynaminA GTPase domain identified R247 in Drp1 GTPase domain as a key interacting residue for cardiolipin binding to Drp1 which is equivalent residue to R239 in dynaminA. This Drp1-cardiolipin interaction is nucleotide dependent and affinity of cardiolipin is 50 fold higher to Drp1 in the presence of ATP. Similar computational method was used in producing stable monomeric forms of dynamin2 and dynamin3 and was used in crystallization experiments. Protein-small molecule affinity in this work was studied by using the state of the art biophysical technique, microscale thermophoresis (MST).

In the second part of the thesis, we screened a series of halogenated 1-OH-carbazoles for their potency to activate or inhibit the enzymatic activity of myosin motors from different classes.

Myosin activity was measured following ATP turnover in the presence of 30 mM F-actin and using an *invitro* motility assay. Additionally, we determined the binding mode for this class of effector molecules by co-crystallizing selected 1-OH-carbazoles with the *Dictyostelium* myosin-II motor domain. The identification of the allosteric binding site on myosin-II provided the basis for the identification of compounds that show greater potency towards other myosin isoforms with the help of molecular docking studies. 3,4,6-tribromododecahydro-1*H*-carbazol-1-ol was identified as a myosin-Ib specific inhibitor with an IC₅₀ value of 4.2 ± 2.1 μM. 2,4,6-triiodophenol and pentabromophenol specifically inhibited myosin-VI ATPase activity with IC₅₀ values of 7.9 ± 1.9 μM and 13.7 ± 2.9 μM, respectively. X-ray crystallography was used to determine structural details of small molecule effector-myosin II motor domain complex. The crystal structure of the myosin II motor domain of *D. discoideum* complexed with pentachlorocarbazole was solved at 2.7 Å resolutions. Our results demonstrate the potential of combining biochemical, X-ray crystallographic and modeling approaches in the search for potent allosteric effectors of enzyme function. Homology modeling of myosin IXb and docking studies with various halogen-substituted carbazoles assisted in identifying compounds that have modulating effect on myosin IXb *in-vitro*. The calculated free energy of binding of the small molecules to the myosins from the docking studies was used as one of the criterion to select the compounds to test them in *in-vitro* assay. 3,4-dibromo,6-methyl-1*H*-carbazol-1-ol, specifically inhibited the actin-activated ATPase rate of myosin IXb in *invitro* assay, was one of the compound selected from the molecular docking analysis.

Thus, my work in chemical biology of dynamin, dynamin related protein1 and myosin is valuable tool for ligand based drug discovery. The knowledge of the structure and binding mode of the compounds facilitates to identify class- and isoform-specific inhibitors through the analysis of the pharmacophore of the binding sites. Small molecule modulators can be used as cell biological tools, like sertraline which was identified, inhibited the mitochondrial fissioning (preliminary data), which in turn is a proof for its modulating effect on Drp1. Thus, structural and functional characterization of dynmain, dynamin related protein1 and myosin by small molecules in a chemical biological perspective provides interesting and illuminating scientific principles for drug like molecule's discovery. The impact of this work will be on the development of human health, which is a major factor for any growing society.

Keywords:

Small molecules, myosin VI, phenols

Zusammenfassung

Dynamine, Dynamin verwandte Proteine¹ (Drp1) und Myosine zählen alle zu den Motorproteinen. Sie werden durch die Hydrolyse von GTP- oder ATP-Nukleotiden angetrieben. Sie üben alle ihre Motoraktivität aus, um spezifische zelluläre Funktionen durchzuführen mit der generierten Kraft. Das Abschnüren von invaginerten Vesikeln, die Teilung von Mitochondrien, Ladungstransport, Aufrechterhaltung von Stereozilienbündeln im inneren Ohr und Muskelkontraktion sind einige der Funktionen, die zu nennen sind. Fehlfunktion der Motorproteine steht im Zusammenhang mit der Ausbildung von Krebs, Blindheit, Kardiomyopathie, Epilepsie und neurodegenerativen Erkrankungen. Ortsspezifische Mutagenese, genetische Manipulation, siRNA knock down, Microarray-Technologie, biophysikalische Techniken, wie NMR und Röntgenbeugung haben unser Verständnis von Motorproteinen verbessert. Die Grundlage der vorliegenden Arbeit wird durch die Untersuchungen verschiedener Klassen kleiner Moleküle, die die Motoraktivität verändern, Proteinengineering und Röntgenkristallographie gebildet. Halogenierte Carbazole, Phenole und psychotrope Wirkstoffe wurden auf ihre biologischen Aktivitäten getestet. Myosine verschiedenster Klassen und Isoformen der gleichen Klasse wurden rekombinant hergestellt und für die Untersuchung der Verbindungen auf ihre Spezifität und Affinität verwendet. Der Myosin Ib-spezifische Inhibitor 3,4,6-Tribromdodecahydro-1*H*-carbazol-1-ol mit einem IC₅₀ von 4,2 ± 2,1 µM, die Myosin VI-spezifischen Inhibitoren 2,4,6-Triiodphenol und Pentabromphenol mit IC₅₀ von 7,9 ± 1,9 µM bzw. 13,7 ± 2,9 µM und der Dynamin-verwandte Protein 1-spezifische Modulator Sertralin, der zu den psychotropen Wirkstoffen zählt, wurden identifiziert. Die Kristallstruktur von Myosin II im Komplex mit Pentachlorcarbazol wurde bis zu einer Auflösung von 2,7 Å gelöst. Diese Struktur zeigte den Bindungsmodus des Carbazols, mit dem es möglich erscheint, die Unterschiede in der biologischen Aktivität verschiedenster halogener Carbazole auf die Motorfunktion von Myosinen zu erklären. Homologiemodellierung von Myosin IXb und Dockingstudien mit unterschiedlichen Halogen-substituierten Carbazolen unterstützten die Identifizierung von Substanzen mit höheren theoretischen Affinitätswerten. 3,4-Dibrom-6-methyl-1*H*-carbazol-1-ol inhibierte spezifisch die Aktin-aktivierte ATPase-Rate von Myosin IXb. Im Fall der Dynamine, zeigten vergleichende, strukturunterstützte Mutagenesestudien die Bedeutung von R247 für die Drp1-Funktion. Mutation von R247 spielt eine Rolle in der Ausbildung länglichgeformten Mitochondrien. Der gleiche Ansatz diente auch der Darstellung der monomeren Formen von Dynaminen und Dynamin-verwandten Proteinen mit den entsprechenden Mutationen. Protein-Liganden-Wechselwirkungen wurden durch neue

Techniken, wie Microscale Thermophorese, untersucht. Chemisch-biologische Studien dieser Motorproteine sind für die ligandenbasierte Wirkstoffentwicklung von Bedeutung. Das Verständnis der Struktur und des Bindungsmodus der Substanzen ermöglicht die Identifizierung Klassen- und Isoformspezifischer Inhibitoren durch die Analyse des Pharmakophors der Bindungsstelle. Kleine molekulare Modulatoren können als zellbiologische Werkzeuge verwendet werden, Sertralin, das durch unsere Screens identifiziert wurde, inhibiert die Mitochondrienspaltung, was einen Nachweis für seinen modulierenden Effekt auf Drp1 darstellt. Zelluläre Prozesse, wie Apoptose können durch die Verwendung solcher Substanzen untersucht werden, da Mitochondrienspaltung und Apoptose miteinander in Beziehung stehen.

Aus diesem Grund liefern strukturelle und funktionale Charakterisierungen von Motorproteinen aus chemisch-biologischer Betrachtungsweise interessante und erleuchtende wissenschaftliche Grundlagen für die Entwicklung Wirkstoff-ähnlicher Moleküle. Die Bedeutung dieser Arbeit wird die Entwicklung menschlicher Gesundheit betreffen, die einen wesentlichen Faktor für jede wachsende Gesellschaft darstellt.

Schlüsselwörter:

Niedermolekulare Wirkstoffe, Myosine VI, Phenole

CHAPTER 1

Introduction

1. Introduction

“Movement is life, Stagnation is death” (law of Dharma). All types of cells have a common feature, which give them the shape and rigidity to maintain their static and dynamic properties. This common feature is attributed to well controlled spatiotemporal interactions of molecular motors with cytoskeletal proteins. The cytoskeletal proteins are broadly classified into microfilaments, intermediate filaments and microtubules. Cytoskeleton remodeling coordinated with the motor proteins is crucial for maintenance of cell physiological functions, cell development, survival and proliferation. Nanoscopic to macroscopic movements in living systems are driven by biological molecular motors that are designed to convert chemical energy into mechanical motion (Oster, 2000 ; Oster, 2000 ; Oster, 1999 ; Wang, 1998 ; Elston, 1998) where conformational changes in the motor domains are amplified and transmitted to their lever arms, which lead to large intramolecular conformational changes (Spudich, 2001 ; Vale, 2000). Starting with flagella rotary motion in bacteria, polymerase migration on nucleic acid templates, cargo disposal to destined targets within cells, spindle pole separation and opposed chromatin movement during cell division, movement of entire cells by retraction are all carried out by motor proteins (Berg, 2003; Endow, 1991; McMacken et al., 1977). The central feature of molecular motors is the generation of force as a consequence of nucleotide induced conformational changes. Amongst the best known molecular motors are myosins that use the actin filament for transport functions and generation of contractile forces, while kinesins and dyneins are microtubule-based motors. Like the classical motor proteins myosin, kinesin and dyneins, dynamin owe the ability to generate force through a mechanism that involves nucleotide-dependent conformational changes and self assembly in the course of executing their cellular functions (Kull, 1998 ; Marx, 1998; Gulick, 1998 ; Sack, 1997). Thus, the family of dynamin proteins can be regarded in the broadest sense as GTP-dependent molecular motors. Dynamin are regarded as molecule possessing both motor-like mechanochemical properties and GTPase-like regulatory functions.

The focus of this thesis is to find specific small molecule probes to modulate the enzymatic properties of myosins and dynamins. Identifying specific small molecule probes provides a powerful tool to study the motor functions and to probe the complex biological processes of myosin and dynamin.

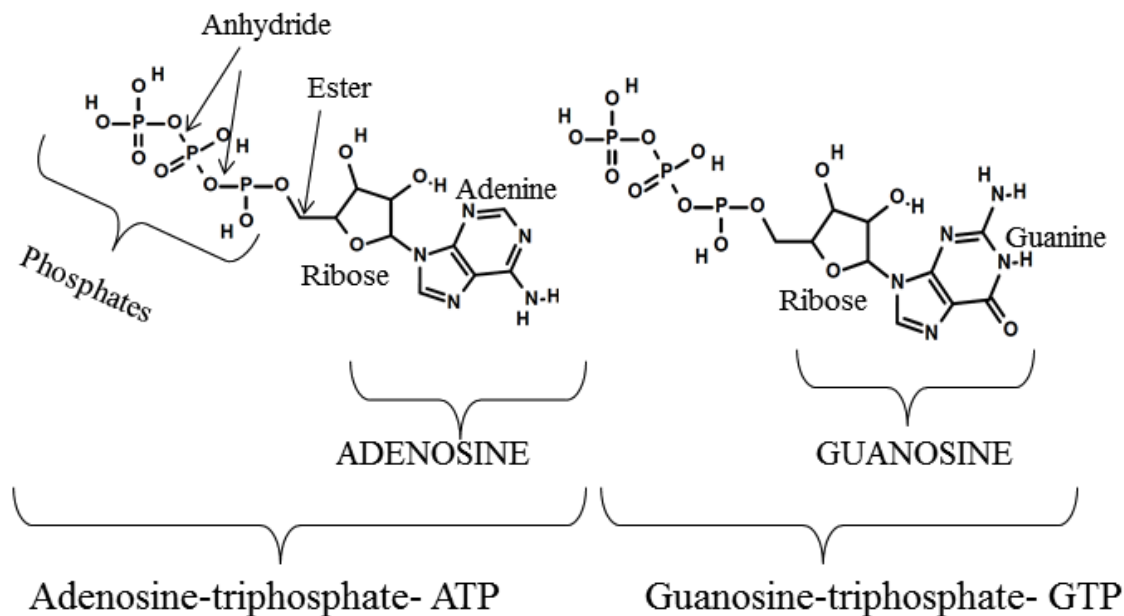


Figure 1: Chemical structure of adenosine triphosphate (ATP) and guanosine triphosphate (GTP).

1.1 GTP-Binding Proteins

1.1.1 General Overview

GTP binding proteins regulate a wide range of important cellular functions such as cell proliferation, regulation of senescence, cell survival, induction of tumor cell invasion, metastasis, cell movement, phagocytosis, growth cone guidance, and cytokinesis nuclear transport, angiogenesis, exocytic and endocytic pathways, vesicle budding, movement along cytoskeletal elements, vesicle targeting, translocation of newly made polypeptides across membranes and so on (Bos, 1992; Bourne and Stryer, 1992; Campuzano and Modolell, 1980; Chrzanowska-Wodnicka and Burrige, 1992; David-Pfeuty et al., 1979; Ellis and Mellor, 2000; Lad et al., 1980; Ridley, 2001; Rosenblatt et al., 1980; Slebos and Rodenhuis, 1992). The characteristic G-domain is conserved in all GTPases. Based on sequence similarity and cellular function, GTPases can be classified into many different subfamilies. Well known members are:

- 1: The Ras family members (Ras, Rap, Ral, M-Ras, Rab, Rin, Rho, Rac, Ran and ARF).
- 2: The α -subunit of hetero-trimeric G proteins.
- 3: The translation factors of protein biosynthesis (IF, EF and RF).
- 4: The signal recognition particles (SRP54, Ffh) and their receptors (SR α / β , FtsY).
- 5: Large GTPase of the dynamin and dynamin-like protein families, (Dynamin1, Vsp1p, hGBP1).

GTPases function by either responding to or controlling the activity of a range of upstream and accessory proteins like guanine nucleotide dissociation inhibitors (GDIs), guanine nucleotide exchange factors (GEFs), and GTPase-activating proteins (GAPs), with the strength of the specific interaction critically depending on the nucleotide state of the G-proteins (**Fig. 2**). Binding and hydrolysis of GTP induces transitions between at least four different conformational states,

- 1: GDP-bound form,
- 2: The nucleotide-free form,
- 3: The GTP-bound form,
- 4: The transition state during hydrolysis.

The effector molecules are only bound in the GTP-bound state, which is also referred to as the “on” state. The GDP-bound state is referred to as the “off” state, because no interactions with effector molecules and thus no signal transduction events can take place while the protein is in this state. GDP dissociation and GTP hydrolysis are mediated by guanine nucleotide exchange factor (GEFs), guanine nucleotide-dissociation inhibitor (GDI), and the GTPases-activating proteins (GAPs). The GTPase cycle, is activated by GEFs, which promote the release of GDP and allow its replacement by GTP. This reaction is negatively regulated by GDIs. Active GTP-bound GTPases can then promote the activation of different effectors until they return to their GDP-bound inactive state upon hydrolysis of the GTP into GDP, which is catalyzed by GAPs. Thus the GTPase activity is controlled and regulated by GAPs, GDIs and GEFs.

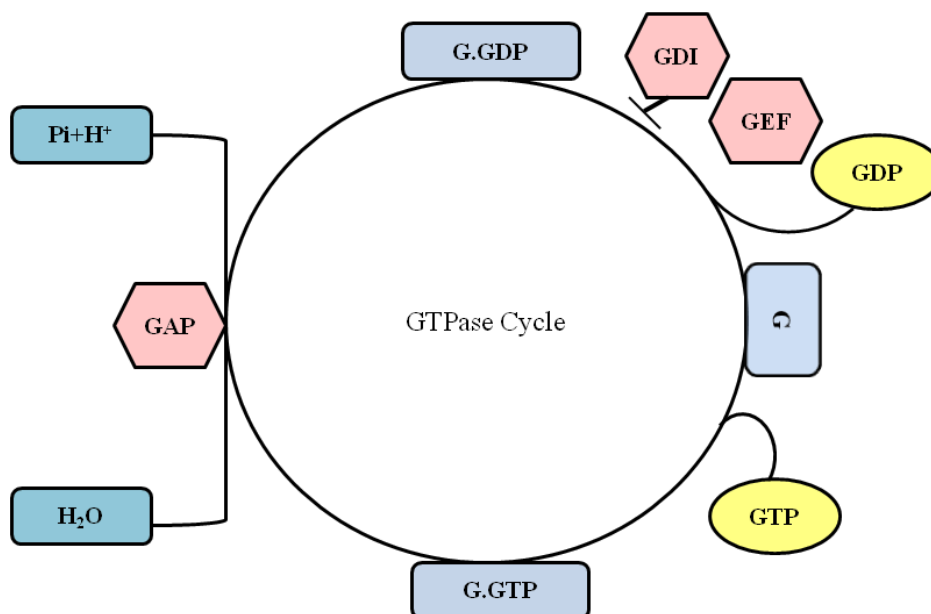


Figure 2: The GTPase cycle, inactive GDP-bound GTPases are activated by guanine nucleotide exchange factors (GEF), which promote the release of GDP and allow its replacement by GTP. This reaction is negatively regulated by guanine nucleotide dissociation inhibitors (GDI). Active GTP-bound small GTPases can then promote the activation of different effectors until they return to their GDP-bound inactive state upon hydrolysis of the GTP into GDP, which is catalyzed by GTPase activating proteins (GAP).

1.1.2 Dynamin and Dynamin Related Proteins

Dynamins are generally classified as ‘large GTPases’. In addition to having a larger GTPase domain, dynamin and dynamin related proteins are distinguished from other GTPases by their low GTP affinities and GTP-dependent oligomerization. In addition, members of the dynamin family were shown to interact with lipid membranes and this interaction increases their GTPase activity. The following table summarizes the functions of some of the dynamin superfamily members.

Table 1: Summary of the dynamin superfamily and their cellular functions.

Protein	Localization	Functions
Dynamin	Plasma membrane, Golgi, endosomes	Vesicle formation , fission
Vps1	Golgi	Vesicle formation, transport
Dnm1/Drp1	Mitochondrial outer membrane	Mitochondrial fission, Morphology
Mgm1/Msp1/OPA1	Mitochondrial inner or outer membrane, or matrix	Mitochondrial morphology
Pragmoplastin	Cell wall	Membrane morphology
ADL	Cell wall, chloroplast	Membrane bio-genesis
hGBP1	Cytoplasm	Antiviral activity
Mx	Cytoplasm, Nucleus	Antiviral activity

1.1.2.1 Large GTPases: The Dynamin Superfamily

Dynamin is a high molecular weight, cytoplasmic guanosine triphosphatase; the dynamin family has been investigated for the involvement in endocytosis, even though dynamin was primarily investigated for a novel microtubule-based motors. In particular, dynamins capacity for rapid recycling of clathrin-coated vesicles at the *D. melanogaster* synapse first became apparent from independent studies carried out by Koenig and Ikeda, 1989; Koenig et al., 1989; Poodry and Edgar, 1979; Ramaswami et al., 1994. Various studies have also confirmed the role of dynamins in membrane fission events, anti-viral activity, plant cell plate formation and chloroplast biogenesis.

Dynamin family members share common structural features but the overall degree of sequence similarity and homology varies among the different family members, in agreement with their diverse functions. The structural similarity is mostly attributed to the conserved core of the GTPase domain which comprises approximately 160 amino acid residues, and consists of a mixed six-stranded β -sheet that is surrounded by five α -helices, whereas the Ras protein has 184 amino-acid residues that is considered to be the minimal GTP binding protein. The minimal distinguishing architectural features that are common to all the dynamins are the GTPase domain (~300 amino acids) containing the tripartite GTP-binding motifs (G1, G2, G3

and G4) (**Fig. 4**), which are required for the guanine–nucleotide binding and hydrolysis. The G1 motif, which is also known as P-loop, coordinates the phosphates of the GTP nucleotide. The P-loop is also known as Walker A motif, is a GTP or ATP binding motif found in most of the nucleotide binding proteins and found in most cellular organisms and is contained in 10 to 18% of all gene products (Ramakrishnana et al., 2001). This motif has the pattern of *GXXXXGK (T/S)* where *X* is any amino acid and *G, K, T* and *S* are glycine, lysine, threonine, and serine respectively. Whereas the reported consensus sequence of the Walker B motif is *(R/K) XXXXGXXXXLhhhhD*, where *R, K, G, L* and *D* denote arginine, lysine, glycine, leucine, and aspartic acid residues respectively. *X* represents any of the 20 standard amino acids and *h* denotes a hydrophobic amino acid. Structurally, P-loop NTPases are α/β proteins that contain regularly recurring α - β units with the β -strands forming a central, (mostly) parallel β -sheet surrounded on both sides by α -helices. During nucleotide hydrolysis the P-loop does not significantly change its conformation, but stays bound to the remaining phosphate groups. P-Loop binding has been shown to cause structural changes in the bound nucleotide (**Fig. 3**), and in the distant Walker B motif which consists of a conserved aspartate (or, less commonly, glutamate) residue. The aspartate residue coordinates magnesium ions and the glutamate is essential for the nucleotide hydrolysis. G2-motif which has a conserved threonine amino acid residue is involved in catalysis and is also referred to as switch1. The G3 motif, which is also known as switch2, containing the amino acid sequence *DXXG* is responsible for interaction with the γ -phosphate of the nucleotide. The fourth motif, interacting with base and ribose of GTP is the G4 motif.

Dynamins have a larger GTPase domain than the classical small GTPases like Ras. Moreover dynamins and dynamin-related proteins have the distinguished property of oligomerization-dependent GTPase activation. The minimal functional and structural domains necessary to belong to the dynamin superfamily are the GTPase, Middle and GED domains. Additional domains are present in most non-classical members and allow specific targeting to sites of action. Domain organization of dynamins consists of five distinct domains. They are as follows:

- 1: Large amino-terminal **GTPase domain**, containing three GTP-binding motifs.
- 2: A self-assembly region, **Middle domain** with potential self-assembly properties.
- 3: A **Pleckstrin homology domain (PH)**, involved in membrane binding.
- 4: A coiled-coil domain also called **GTPase effector domain** that stimulates the GTPase activity and participates in self-assembly.
- 5: And a **Proline/Arginine-rich domain (PRD)** that was found to increase dynamin–dynamin interactions and contains several SH3-binding sites for binding dynamin to its interacting partners.

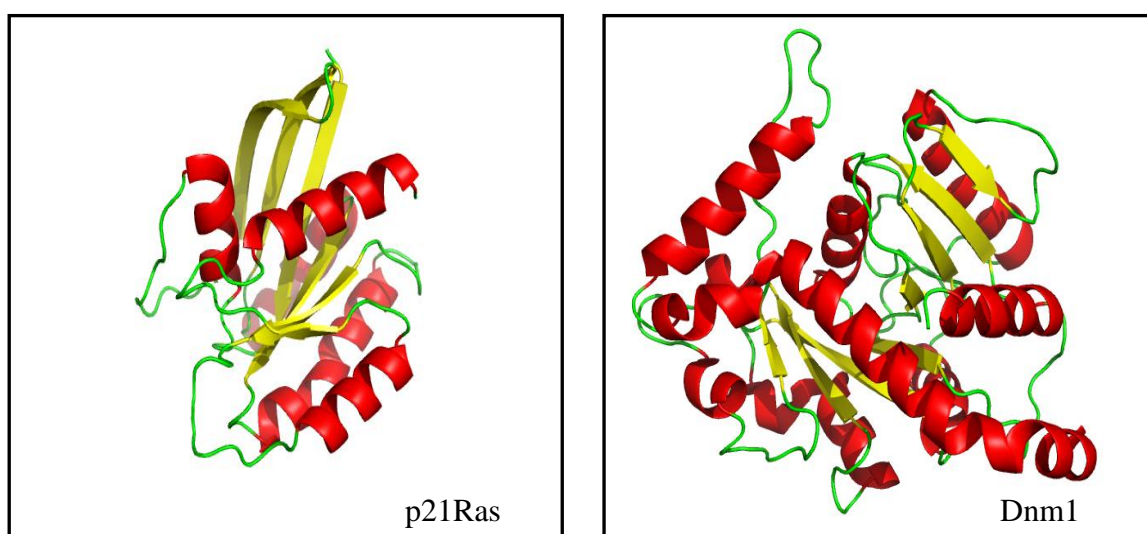


Figure 3: Cartoon representation of the small GTPase p21Ras GTPase domain and the large GTPase Dnm1 GTPase domain. Pdb id: 1ctq (p21Ras) and 2aka (Dnm1). The common central core has β - sheets surrounded by helices.

Dyn3	GGQSAGKS	IVTR	DLPGIT	TKLD
Dyn1	GGQSAGKS	IVTR	DLPGMT	TKLD
Dyn2	GGQSAGKS	IVTR	DLPGIT	TKLD
DymA	GSQSSGKS	IVTR	DLPGIT	TKLD
Drp1	GTQSSGKS	IVTR	DLPGMT	TKLD
Ras	GAGGVGKS	DPTI	DTAGQE	NKCD
	G1- P-loop	G2 – switch1	G3 - switch2	G4

Figure 4: Comparison of G-domain motifs, G1-G4 of dynamins, dynamin related proteins (Drp) and a small GTPase (pRas).

1.1.2.2 Classical Dynamins

Classical dynamins have five identifiable domains, a GTPase domain, a middle domain, a PH domain, a GED, and a PRD. The middle domain of classical dynamins lacks sequence similarity to other known structural motif. The middle domain has been implicated in dynamin self assembly. The PH and PRD domains are responsible for protein-protein interactions and protein targeting. The PH domain can additionally interact with lipid membranes, while the PRD domain binds to the Src-Homology-3 (SH3) domain of interacting proteins (Praefcke and McMahon, 2004).

While *D. melanogaster* and *C. elegans* have only one gene for dynamin (Chen et al., 1991; Clark et al., 1997; van der Blik and Meyerowitz, 1991) mammals have three dynamin genes with distinct tissue distributions. Dynamin1 is restricted to neurons with 5 splice variants, dynamin2 is ubiquitously expressed and has 4 splice variants, and dynamin3 is expressed predominantly in testis but also found in lung and brain (Urrutia et al., 1997). Alternative splicing creates at least 27 variants showing differential expression in mammalian tissue (Cao et al., 1998; McNiven et al., 2000a). Domain organization of classical dynamins to non-classical dynamins is shown in the **Fig. 5**.

Dynamin1 was first purified from calf brain as a microtubule-binding protein (Obar et al., 1990). Cloning of the dynamin cDNA revealed a GTP binding site, which was found to show homology to anti-viral MX proteins and the yeast vacuolar sorting protein Vps1p (Obar et al., 1990). Purified dynamin1 was found to have a specific GTPase activity, which is stimulated to high levels by microtubules (Obar et al., 1990). The *D. melanogaster* dynamin homolog is the product of the *shibire* gene, a locus previously implicated in endocytosis (Chen et al., 1991; van der Blik and Meyerowitz, 1991). Flies carrying a temperature sensitive mutation in their *shibire* gene have a pleiotropic phenotype. Around the endocytic cups or necks long spirals were observed. Further, increase in temperature resulted in rapid reversible paralysis, which was considered as most striking phenotype (Chen *et al.*, 1991). The paralysis is due to a defect at the presynaptic membrane (**Fig. 6**) (Kosaka and Ikeda, 1983a, b). EM analysis showed an accumulation of endocytic pits whose necks are encircled by single or double electron dense bands (Koenig and Ikeda, 1999, 2007). Over expression of dynamin with mutations K44E and S45N in the GTP binding domain in cultured cells have a dominant negative effect on receptor-mediated endocytosis. Coated pits failed to become constricted and coated vesicles failed to bud, while coated pit assembly, invagination, and the

recruitment of receptors into coated pits were unaffected (Damke et al., 1994). In GTP γ S treated nerve terminals, tubular invaginations of the plasmalemma were found. The walls of these invaginations were decorated by transverse electron-dense rings showing positive immuno reactivity for dynamin (Takei et al., 1995). Dynamin was shown to be identical to dephosphin, a substrate of protein kinase C that undergoes stimulus-dependent dephosphorylation at the nerve termini, suggesting a role in rapid synaptic vesicle recycling (Robinson et al., 1993).

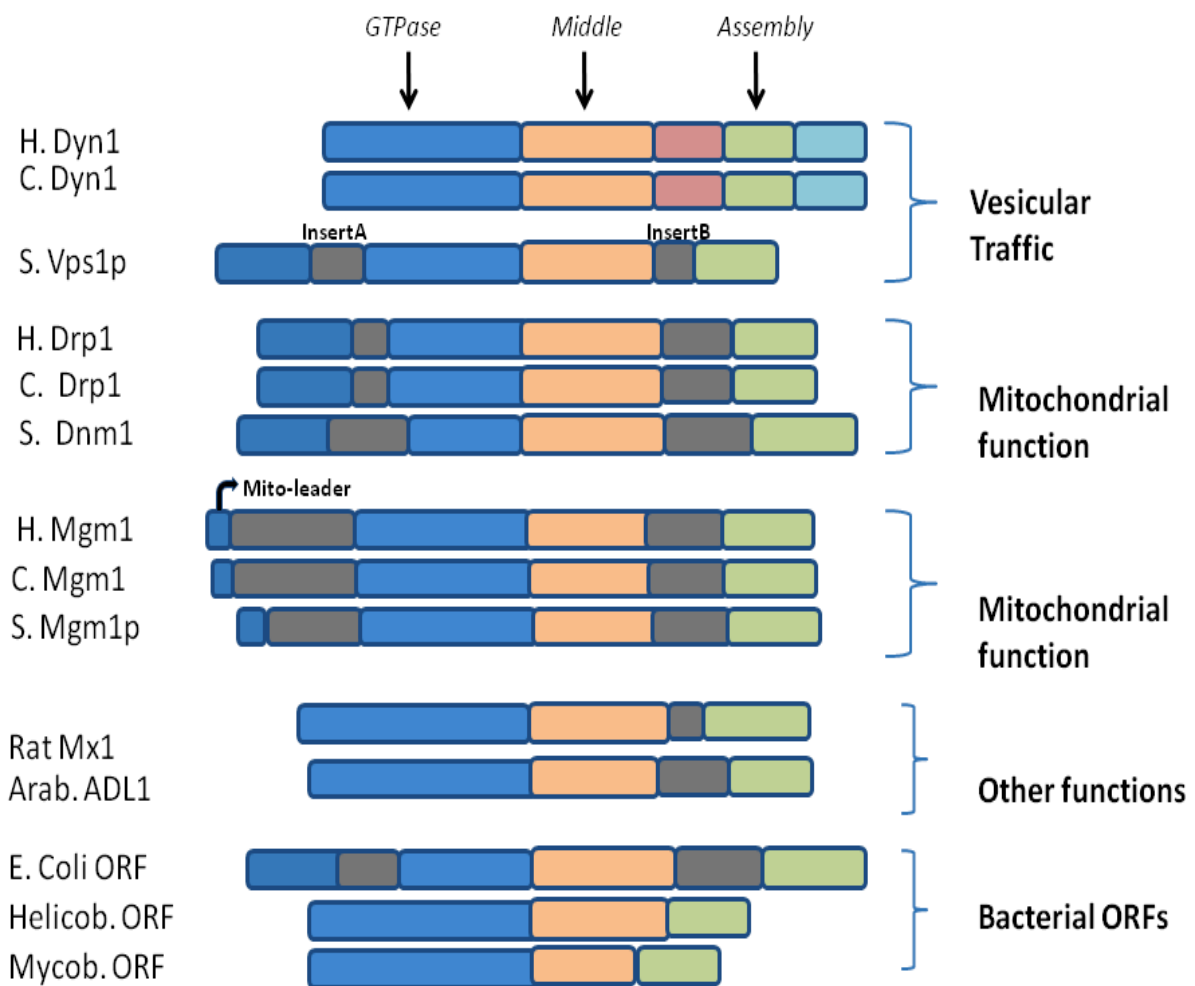


Figure 5: Domain organization of various dynamins, dynamin like and dynamin related proteins. PH domains (red), PRD domain (light blue) are also shown. The corresponding identifiers for the ORFs for *E. coli* GenBank J05620, *H. pylori* GenBank AE000605 and *M. tuberculosis* GenBank Z95324. Modified and color coded cartoon representation of various dynamins. Inspired by Alexander M. Van der Blik (van der Blik, 1999).

All of these data point towards an important role of dynamin in the release of vesicles from the plasma membrane. Structural analysis of dynamin1 shows that it exists as a tetramer (Muhlberg et al., 1997) that can assemble into rings and spirals (Hinshaw and Schmid, 1995) and forms helical tubes on a lipid bilayer (Sweitzer and Hinshaw, 1998; Takei et al., 1995). These structures are similar to collared structures seen at the base of coated pits of *Shibire* flies. The structure of mammalian dynamin1 GTPase domain in the nucleotide-free state was solved by using X-ray crystallography (Reubold et al., 2005).

Another mammalian dynamin, dynamin2, has been proposed to play a role in endocytosis (Altschuler et al., 1998; Henley et al., 1998; Kasai et al., 1999; Volchuk et al., 1998), at the trans Golgi network (Jones et al., 1998; Yang et al., 2001), as a signal transduction molecule regulating transcription (Fish et al., 2000), or as a link to the actin cytoskeleton (McNiven et al., 2000a; McNiven et al., 2000b; Slepnev et al., 2000). Dynamin 2 interacts with cortactin and regulates actin assembly. A dynamin2 mutant with decreased affinity for GTP was found to have decreased actin dynamics within the cortical actin network.

Mutants of cortactin that show less binding to the Arp2/3 complex or dynamin2 have decreased actin dynamics. Dynamin2 promotes the association of actin filaments nucleated by Arp2/3 complex and cortactin with phosphatidylinositol 4, 5-bisphosphate (PIP₂)-containing lipid vesicles (Schafer, 2002, 2004). It is also important in mediating focal adhesion and stress-fiber formation (Yoo et al., 2005). Dynamin2 mutation induces prominent decoration of microtubules. Further, it has been reported that dynamin2 is required for proper dynamic instability of microtubule, hence is essential for organelle motility (Otsuka et al., 2009; Tanabe and Takei, 2009). Mutations in the dynamin2 protein were found in patients with Charcot-Marie-Tooth (CMT) disease, which is an inherited peripheral neuropathy.

Along with dynamin2, dynamin3 is also highly expressed in the testis. Dynamin3 does not colocalize with clathrin, suggesting that these two dynamins have distinct functions in sertoli cells. Mice lacking the *klotho* gene, which functions as an aging-suppressor, show deficiencies in spermatogenesis alongside drastically reduced expression levels of dynamin2 and dynamin3 in the testis, indicating a possible association of these proteins with spermatogenesis (Kamitani et al., 2002). Over expression of a specific dynamin3 splice variant in mature neurons caused a marked remodeling of dendritic spines. This suggests that

dynamin3 is a postsynaptic dynamin that interacts with Homer. This interaction plays a significant role in dendritic spine morphogenesis and remodeling (Gray et al., 2003). A specific dynamin3 splice variant interacts with cortactin and modulates actin-membrane dynamics in developing neurons (Gray et al., 2005). Recently, it has been shown that dynamin3 is additionally involved in the growth and development of mega karyocytes (Reems et al., 2008).

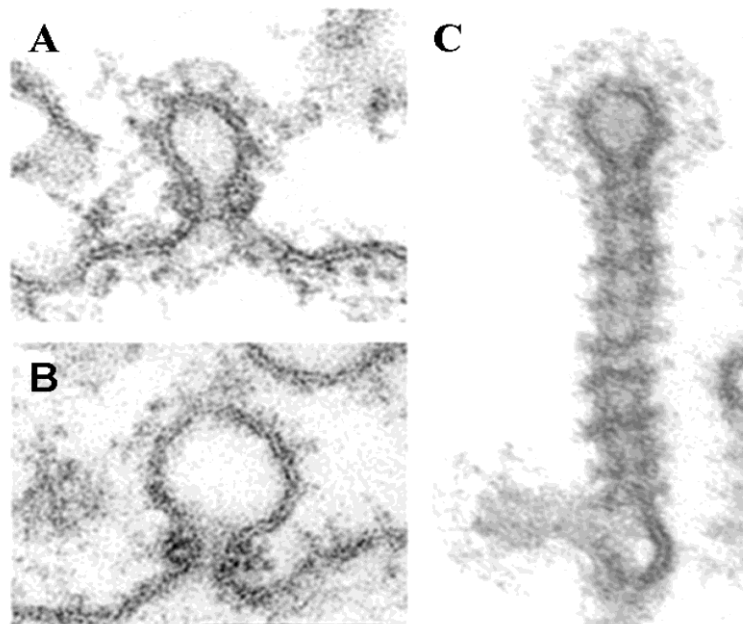


Figure 6: (A-B) Electron micrograph of clathrin-coated pit from *D. melanogaster* shibire nerve termini with a dense collar material seen at neck. (C) Invaginating tubule decorated with a striation pattern and a terminal clathrin-coated pit are observed in synaptosomes treated with GTP γ S (Kosaka and Ikeda, 1983a; Takei et al., 1996).

1.1.2.3 Dynamin Like Proteins (DLPs) and Dynamin Related Proteins (DRPs)

Compared to the five-domain structure of classical dynamins, DLPs lack the PH and PRD domains **Fig. 7**. From yeast to humans, there is at least one DLP homologue per organism involved in mitochondrial division. Like classical dynamins, DLP oligomerize into

multimers and form rings. Recently it has been reported that the mutation A395D in the middle domain of human Dlp1 is lethal, as a consequence of defects in mitochondrial and peroxisomal fission (Waterham et al., 2007). Sequence homology does not allow distinguishing the regions between the middle domain and PH domain in dynamin-like proteins. However, some Dlps such as *A. thaliana* ADL2 contain a region that binds specifically to phosphatidylinositol-4-phosphate (PtdIns4P) and may have a similar function as the PH domain (Kim et al., 2001). This domain is also responsible for the recruitment of proteins at the constriction site in mitochondria, which acts as pseudo-PRD domain.

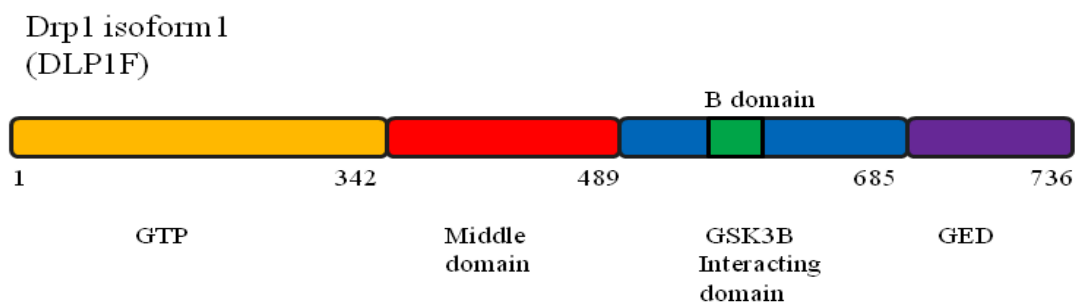


Figure 7: Domain organization of Drp1 Isoform1. Drp1 contains several domains characteristic of dynamin family such as GTPase domain, a middle domain, a GTPase effector domain (GED). Drp1 has also a glycogen synthase kinase 3 beta (GSK3 β) interacting domain and uncharacterized B domain.

The levels of Drp1 mRNA are high in brain, moderate in skeletal and heart muscle and low in other tissues (Smirnova et al., 1998). Drp1 was thought initially to play a role in vesicular transport similar to that of dynamin (Imoto et al., 1998). However, dominant-negative mutations in human Drp1 have no effect on the secretory or on the endocytic pathway (Smirnova et al., 1999), but have a dramatic effect on mitochondrial distribution. The yeast homolog of Drp1, Dnm1p is one of three dynamin related proteins in yeast (Gammie et al., 1995). Dnm1p has been found to be localized to sites of mitochondrial division. Cryo-EM studies have proven the role of Dnm1p's mechano-chemical role which is important during mitochondrial division (Mears et al., 2010). The mitochondria in Dnm1p mutant yeast cells collapse into a clump near the nucleus, which normally have peripheral distribution (Smirnova et al., 2001). Initially these proteins were implicated in vesicle trafficking (Gammie et al., 1995). Both Dnm1p and Drp1 have later been localized to the outer membrane of mitochondria at constriction or fission sites. Cells transfected with mutants of

these proteins show a defect in mitochondria fragmentation (Bleazard et al., 1999; Labrousse et al., 1998; Labrousse et al., 1999; Otsuga et al., 1998; Sesaki and Jensen, 1999; Smirnova et al., 2001; Smirnova et al., 1998). DynaminA from *D. discoideum* is most closely related to the Dnm1p subfamily (Wienke et al., 1999).

Inhibition of Drp1 by overexpression of a dominant-negative mutant leads the loss of the mitochondrial membrane potential and the release of cytochrome C which causes a reproducible swelling to the organelle. Inhibition of Drp1 blocks cell death, implicating mitochondrial fission as an important step in apoptosis (Frank et al., 2001; Phillips et al., 2001). Ishihara and Mihara have shown that Drp1 is essential for embryonic development and required for synapse formation in mice (Ishihara et al., 2009; Masaike et al., 2007; Taguchi et al., 2007). Transfection of Drp1 and their K38A mutant leads to constriction of ER membrane with periodic Drp striation, providing an insight into the close associations of mitochondria and the endoplasmic reticulum (Pitts et al., 1999; Yoon et al., 2000; Yoon et al., 1998; Yoon et al., 2001).

1.1.2.4 Vps1p

The absence of the PRD and the PH domain makes Vps1p non-classical dynamin in the yeast *S. cerevisiae*. Vps1p is involved in vesicle trafficking from the Golgi (Rothman et al., 1990; Wilsbach and Payne, 1993). Vps1p seems to function in vesicle trafficking at the Golgi rather than at the plasma membrane, (Nothwehr et al., 1995; Wilsbach and Payne, 1993) and is probably involved in the formation of clathrin coated vesicles at the Trans Golgi network (TGN) (Bensen et al., 2000). Vps1p also controls the number of peroxisomes in *S. cerevisiae*, since in a Vps1p mutant only one or two giant peroxisomes remain. Analogous to the function of other dynamin-related proteins, Vps1p is also involved in a membrane fission event that is required for the regulation of peroxisome abundance (Hoepfner et al., 2001; Vizeacoumar et al., 2006).

1.1.2.5 Mgm1p/OPA1

The domain architecture of this family of proteins is similar to that of DLPs, except for the additional mito-leader sequence at their amino terminal. Mgm1p and Msp1p both have a large N-terminal extension that contains a mitochondrial targeting sequence (Jones and Fangman, 1992; Pelloquin et al., 1999a; Pelloquin et al., 1999b). Mgm1p is the third dynamin

family member in *S. cerevisiae* that defines its own subfamily (Jones and Fangman, 1992). Mgm1 homologues are *S. pombe* Msp1p (Pelloquin et al., 1998), human OPA1 (Alexander et al., 2000; Delettre et al., 2000) and a homolog in *C. elegans*. Mgm1p was found to be necessary for mitochondrial genome maintenance. Mgm1p is localized to mitochondria, but it is controversial whether it associates with the outer membrane or localizes to the intermembrane space (Shepard and Yaffe, 1999; Wong et al., 2000). *S. pombe* Msp1p was localized to the matrix side of the inner mitochondrial membrane and its overproduction leads to an alteration of mitochondrial structure and function.

Optic atrophy1 (OPA1) is the only known human dynamin with a mitochondrial targeting sequence and is thought to function similar to that of Mgm1p. Mutations in human OPA1 give rise to dominant optic atrophy, a glaucoma that is caused by atrophy of retinal ganglion cells and the optic nerve, resulting in blindness (Delettre et al., 2001). RNAi knockdown of OPA1 expression in cultured cells results in mitochondrial fragmentation, disruption of cristae structure and a loss of the mitochondrial membrane potential. This leads to apoptosis (Olichon et al., 2003). OPA1 mutation R445H associated with dominant optic atrophy impairs oxidative phosphorylation and mitochondria fusion (Zanna et al., 2008).

1.1.2.6 Plant Dynamins

Mostly plant dynamins are involved in chloroplast division (Gao et al., 2003; Miyagishima et al., 2003). They all lack the PRD and the PH domain, except for ADL3. Phragmoplastin and ADLs (*Arabidopsis* dynamin-like) are higher plant members of the dynamin family. Phragmoplastin from soybean localizes to the cell plate in dividing cells (Gu and Verma, 1996). ADL1 (Park et al., 1997) was localized to the thylakoid membranes of chloroplasts and might be involved in the biogenesis of thylakoids (Park et al., 1998). ADL2 is localized to chloroplasts by its N-terminal amino acids and is most closely related to Dnm1p (Kang et al., 1998). ADL2b was observed to localize at the tips and at the constriction sites of mitochondria and is involved in *Arabidopsis* mitochondrial division. The *Arabidopsis* dynamin-related proteins DRP3A and DRP3B play key roles in both mitochondrial and peroxisomal fission (Fujimoto et al., 2009).

1.1.2.7 Mx Proteins

Mx proteins are interferon induced anti-viral proteins of 70 to 80 kDa found in all vertebrates. They are capable of inhibiting the multiplication of negative stranded RNA viruses like influenza virus by abolishing virus polymerase function (Pavlovic et al., 1993; Pitossi et al., 1993). Mx proteins are not associated with membranes but localize to the cytoplasm (e.g. mouse Mx2) or the nucleus (e.g. mouse Mx1) (Zurcher et al., 1992a, b, c). Mx family proteins contain an N-terminal GTPase domain and variable C-terminal domains, depending on their function and location. Mx proteins exert their antiviral function by various mechanisms, e.g. by binding to the nucleocapsid and blocking nuclear import (Kochs and Haller, 1999a, b) or by inhibiting viral transcription (Praefcke et al., 1999). Mx proteins have been shown to assemble into homo oligomers (Melen et al., 1992). Similar to the GED of classical dynamin, human MxA contains a C-terminal domain that is involved in activating GTPase activity and promotes oligomerization (Haller et al., 1998). It has been shown that a functional GTP-binding motif is necessary for virus inhibition.

1.1.2.8 Guanylate-Binding Proteins (GBPs)/Atlastins

These proteins are arguably the least conserved members of the dynamin family. hGBP1 is a type-II interferon inducible large GTPase of 67 kDa with intracellular anti-pathogenic activity and their antiviral activity is lower compared to that of Mx proteins (Anderson et al., 1999). Like dynamin, hGBP1 displays low nucleotide affinity, is stable in the absence of nucleotide, and undergoes nucleotide dependent oligomerization (Praefcke et al., 1999; Prakash et al., 2000a; Prakash et al., 2000b). The crystal structure of hGBP1 shows differences in the connectivity of secondary structure elements compared to dynamin1 but the intramolecular interactions are thought to be similar to those that have been predicted for dynamins for their GTP and GED domains. GBPs are not found in *D. melanogaster* or *C. elegans*, but there is a weak homologue in *A. thaliana*. Unlike dynamin, GBPs can hydrolyse GTP not only to GDP, but also to GMP (Prakash et al., 2000a).

1.1.2.9 Bacterial Dynamin-Like Proteins

Many eubacteria have dynamin-like proteins that consist of GTPase domain, middle domain and GED. *yjda* is an *E. coli* ORF with a predicted GTPase domain sequence that is characteristic of dynamin family members (GenBank J05620). The predicted protein has C-

terminal domains and putative coiled-coils as in other dynamin family members. This suggests that the Yjda protein forms a multimeric assembly with mechano-chemical properties similar to those of dynamin. Other bacteria such as *H. pylori* and *M. tuberculosis* have similar ORFs with unknown functions (van der Blik, 1999). The structure of the bacterial dynamin like protein (BDLP) from *N. punctiforme* has been solved by X-ray crystallography in presence and absence of GDP. Similar to dynamins, BDLP also undergoes helical self-assembly and tubulates lipid bilayer (Low and Lowe, 2006).

1.1.3 GTPase Activity of Dynamins

Purified dynamin exists in tetramer/monomer equilibrium under high salt condition, higher than 300 mM NaCl (Binns et al., 1999) and forms ring and spiral structures under low salt conditions, lower than 50 mM NaCl (Hinshaw and Schmid, 1995). Assembly into rings or spirals is a common feature of dynamins (van der Blik, 1999). Classical dynamin (Hinshaw and Schmid, 1995; Takei et al., 1995), Dlp1 (Smirnova et al., 2001; Yoon et al., 2001), phragmoplastin (Zhang et al., 2000), ADL2 (Kim et al., 2001), dynaminA (Klockow et al., 2002) and Mx proteins (Kasai et al., 1999) have been shown to form rings or spirals. The GED is important for self-assembly (Okamoto et al., 1999; Smirnova et al., 1999) and an interaction of the GED with the GTPase domain and with the middle domain was shown biochemically and by yeast two-hybrid analysis (Muhlberg et al., 1997; Smirnova et al., 1999). Interactions between the GED and the GTPase and middle domain were found in Mx proteins as well (Praefcke et al., 1999; Schumacher and Staeheli, 1998). GED interaction with the GTPase domain stimulates GTPase activity (Muhlberg et al., 1997). The mechanisms of dynamin's basal and assembly-stimulated hydrolysis are unknown. The issue whether it acts by accelerating GDP release or rather like a classical GAP via an arginine finger is not settled yet (Marks et al., 2001; Sever et al., 1999). The recent crystal structure of human dynamin1-derived minimal GTPase-GED fusion protein, which is a dimeric in the presence of the transition state mimic $\text{GDP}\cdot\text{AlF}_4^-$, gave insights on how assembly stimulated GTP hydrolysis might be achieved.

Dynamins display low nucleotide affinity compared to small GTPases (μM range) and have a high basal turnover rate with reported values ranging from $8\text{-}30 \times 10^{-3} \text{ sec}^{-1}$ (Marks et al., 2001; Sever et al., 2000a, b). The GTPase activity shows co-operativity to its oligomerization induced GTPase rate and reaches a value of $1\text{-}5 \text{ sec}^{-1}$ at a dynamin concentration of $1 \mu\text{M}$ (Stowell et al., 1999; Tuma and Collins, 1994). Assembly on suitable

templates leads to an increase in GTPase activity, e.g. a 16-fold increase upon assembly on microtubules (Obar et al., 1990). The highest activation found so far has been observed after assembly on lipid nano tubes that led to a 1000-fold increase in GTPase activity (Marks et al., 2001; Sever et al., 2000a, b). Point mutations in the human dynamin1 GTPase domain, mainly in their G1, G2, G3 and G4, the GTP binding motifs, dramatically lowered both the rate of assembly stimulated GTP hydrolysis activity and the affinity for GTP (Damke et al., 2001a; Damke et al., 2001b; Song et al., 2004a; Song et al., 2004b).

1.1.4 Dynamin: a Molecular Motor or a Regulatory Protein

There is a long running debate whether dynamin is a motor protein or works as a regulatory GTPase. Dynamin self-assembles into rings or spirals in low salt conditions or in the presence of lipid nanotubes (Sweitzer and Hinshaw, 1998). This stimulates GTPase activity over 100-fold. Dynamin rings accumulate at the neck of the endocytic cup. GTP hydrolysis by dynamin induces a conformational change, which in turn is responsible for force generation and leads to membrane fission. These observations led to the first model for the function of dynamins **Fig. 8**. The model suggests that dynamins assemble in the GTP-bound form and form collar-like structures at the deep invaginated coated pits. GTP hydrolysis causes one of two conformational changes, either constriction of assembled structure or helical expansion, which leads to the pinching-off of coated vesicles. According to Stowell *et al.*, this model of molecular spring is called as ‘Pinchase’.

On the other hand, some data support a model where dynamin functions as a classical signaling GTPase. An Arg to Ala point mutation in the GED was reported to have a reduced assembly stimulated GTPase activity, while the basal turn-over rate is normal. Cells transfected with this R725A mutant showed increased endocytosis in contrast to the expected reduction (Sever et al., 1999), suggesting that dynamin functions like other GTPase superfamily members, as a regulatory enzyme. GTP-bound dynamin recruits downstream effectors to the coated pit; the effectors in turn mediate coated vesicle formation. As the neck narrows and vesicle formation is about to complete, dynamin self-assembly triggers GTP hydrolysis, which terminates interactions with downstream effectors (**Fig. 8**, arrow3). Impairment of self-assembly in the GED mutants will prolong the GTP-bound state and hence, accelerate vesicle formation.

Dynamin is an important component of the endocytic machinery, to understand its role as a mechano-chemical enzyme or as a regulatory protein, it is important to understand dynamin's oligomerization-stimulated GTPase activity. Whether it generates force or it inhibits the signal between the adapter proteins in the downstream by its assembly-stimulated hydrolysis rate. This is possible once structures of dynamin in different nucleotide states have been solved. But still there is no evident which nucleotide states are functionally important.

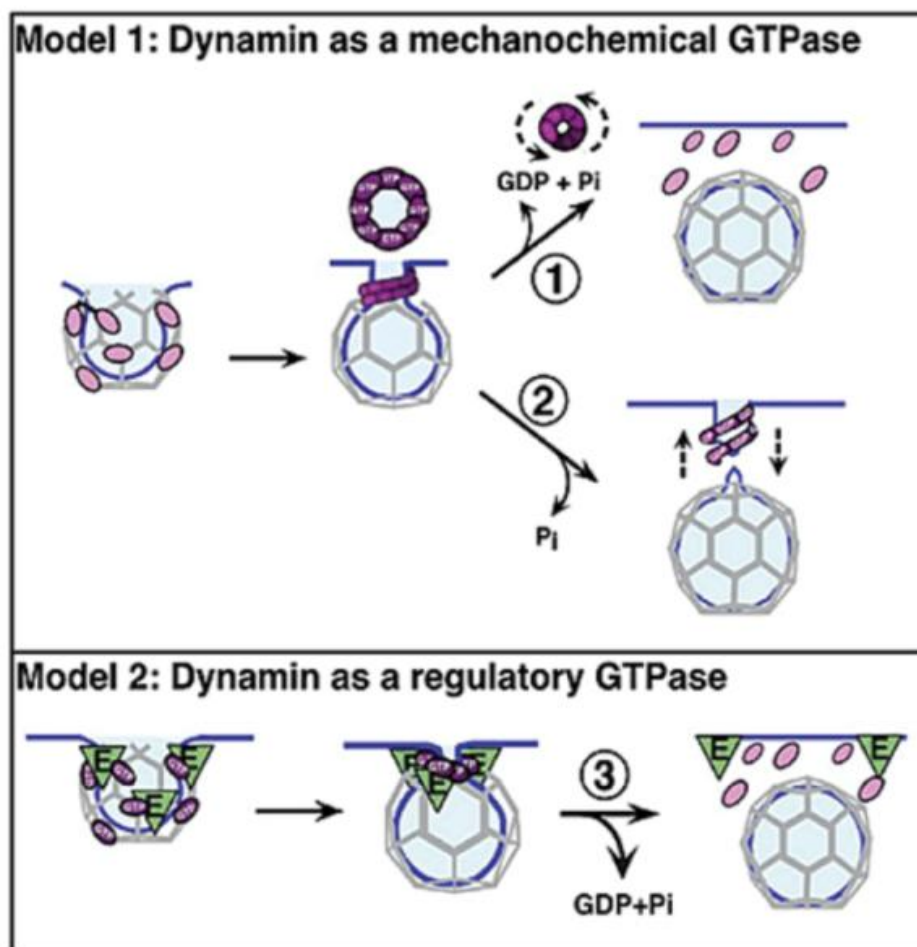


Figure 8: Two models of dynamin function. **Model 1:** As a mechanochemical enzyme, dynamin uses chemical energy released from GTP hydrolysis for fission of the neck of a coated pit, either by constricting dynamin collars (arrow 1) or by expanding (arrow 2) the helical pitch of dynamin rings. **Model 2:** As a regulatory enzyme, the dynaminGTP complex, which is localized to coated pits, recruits and/or activates effector molecules that are required for vesicle formation. GTP hydrolysis triggered by assembly of dynamin at the neck (arrow 3) serves to terminate interactions with downstream effectors (Song and Schmid, 2003).

1.1.5 Dynamins and Their Interacting Partners

1.1.5.1 Drp1- Cdks

Cyclin dependent kinases (Cdks) belong to the family of threonine/serine kinase (ST – kinases), and require cyclins, to functionally construct and activate their active site. Cdk2 is formed by two lobes (**Fig. 9**). The N-terminal lobe contains a G-loop in which phosphorylation of the residue T14 and Y15, renders the Cdk/cyclin complex inactive. The bigger C-terminal lobe contains the T-loop also called activation loop, in which phosphorylation of T160 is crucial for the Cyclin/Cdk complex activation. Cdks are regulatory components during proliferation, differentiation, and apoptosis in neuron and other cells. Cdks are present throughout the mammalian cell cycle. Their cyclin partners undergo a periodic synthesis and destruction cycle, which means the concentration of cyclin, varies from G1 to M phase in cell cycle **Fig. 10**. In vertebrates, the earliest cell divisions are very different from normal adult cell divisions. At very early stage cell divisions are rapid and synchronous, but there are long gaps from the thirteenth cell division just after midblastula transition. Cyclins A, B, E and Cdk-1 and 2 are controlling elements during embryonic cell division, whereas Cyclin D-1, 2, 3 and Cdk-4, 6 are very important during normal adult cell division. Regulation of mitochondrial dynamics during mitosis is important to assure that daughter cells inherit them. Improper mitochondrial numbers have been implicated in a number of diseases. Previous studies from two-hybrid screen have shown that *Xenopus* protein XDrp1 interacts with both embryonic and somatic forms of cyclinA, but not with B type cyclins (Funakoshi et al. 1999).

In addition Cdk5/p35 is known to phosphorylate dynamin1 and amphiphysin1 (Nguyen and Bibb, 2003; Tomizawa et al., 2003). In contrast to other Cdks, Cdk5 does not depend on cyclins to get activated nor for its substrates to get phosphorylated (Tomizawa et al., 2002). But, Cdk2 in neurons initiates death by suppressing E2F-1/Rb- dependent transcription at neuronal G1/S check point (Nguyen et al., 2002). Thus, it became apparent to study on dynamin1 and Drp1-Cdk2/cyclinA interactions individually. An assay system was developed to check for the dynamin1 and Drp1's phosphorylation status by the cyclin dependent kinase2/cyclinA complex. This led to discover the novel phosphorylation site in Drp1.

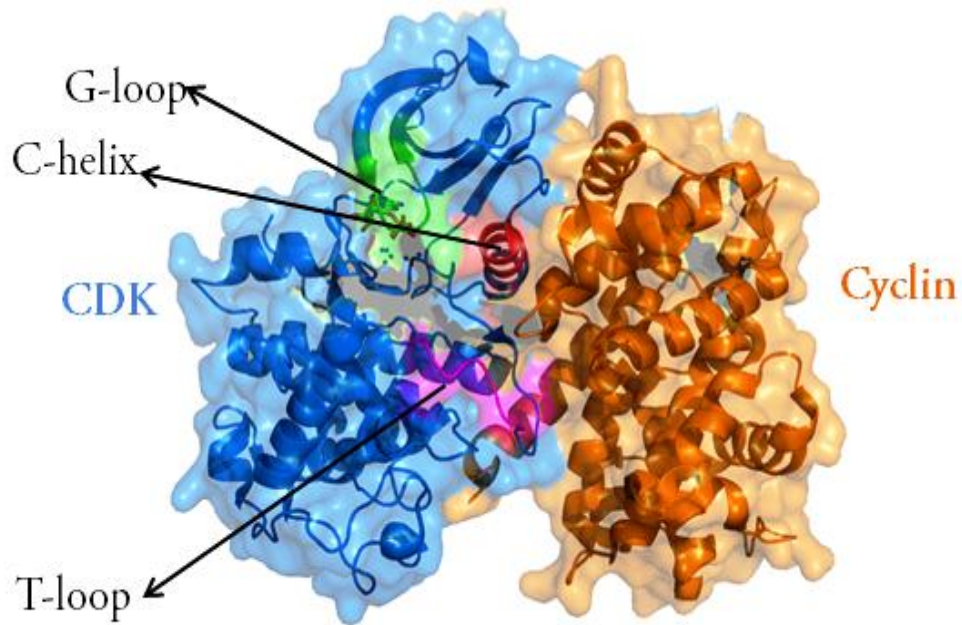


Figure 9: Cartoon representation of Cdk/Cyclin complex of the PDB id: 3qhw. The blue surface and blue cartoon represents the Cdk and the orange surface and the cartoon represents the cyclin. The T-loop is shown in pink surface, C-helix in red surface and G-loop in green surface.

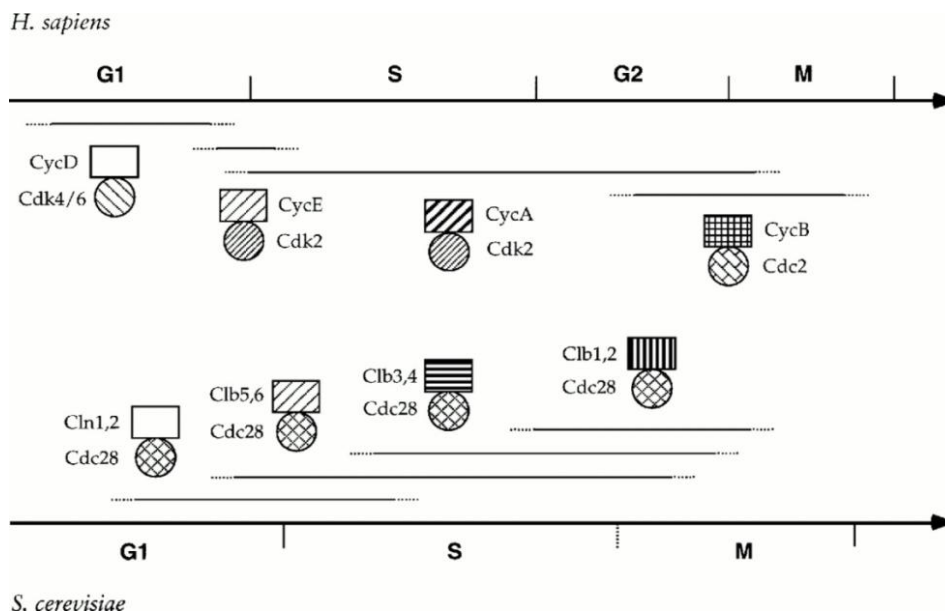


Figure 10: Sketch of the regulatory proteins cyclins and cdks at various cell-cycle phases (Morgan, 1997).

1.1.5.2 Dynamin1 and Amphiphysin1-SH3 Domain

Amphiphysin proteins are highly conserved from yeast to human. Their domain organization starts with an amino-terminal BAR (Bin1-Amphiphysin-Rvs) domain, a central variable domain and a carboxyl-terminal Src homology 3 domain (SH3) **Fig. 11** and **Fig. 12**. BAR domains initiate membrane bending by mediating interactions with acidic phospholipids and homo/heterodimerization (Farsad et al., 2001; Slepnev et al., 1998; Takei et al., 1999). SH3 domain mediates protein-protein interactions and in amphiphysins, this domain interacts with dynamin1 and synaptojanin1 (David et al., 1996; McPherson et al., 1996).

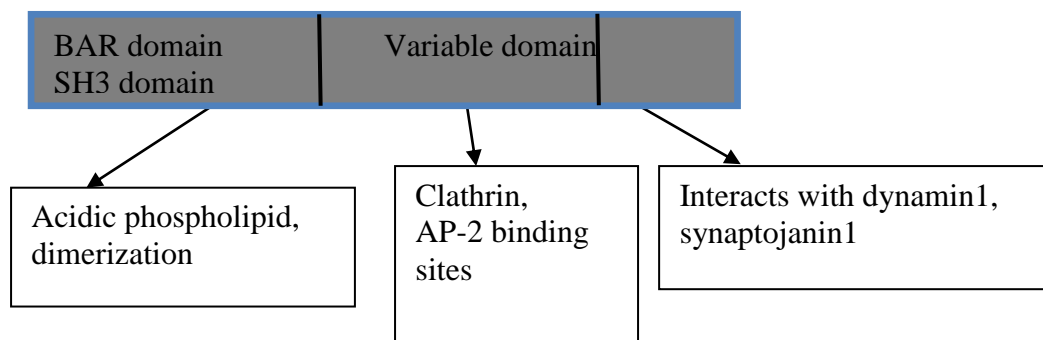


Figure 11: Domain organization and sequence annotation of amphiphysin.

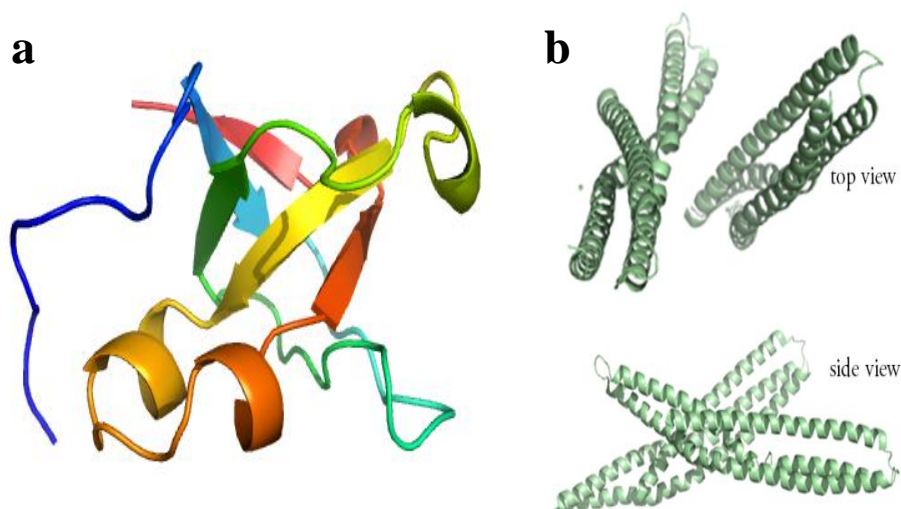


Figure 12: (a) Cartoon representation of SH3 domain (pdb id: 1bb9) and (b) BAR domain (pdb id: 2fic).

There are two isoforms of amphiphysin in mammals, amphiphysin1 which expresses in brain, and amphiphysin2 expresses as splice variant in brain at high levels as well as in striated muscle. Muscle amphiphysins do not have clathrin and AP-2 binding sites (Antoine et al., 1999; Di Paolo et al., 2002; Farsad et al., 2001), and are independent of clathrin coats or in other words clathrin independent functions (Antoine et al., 1999; Leprince et al., 2003; Leprince et al., 1997; Saiz et al., 1999; Wechsler-Reya et al., 1997a; Wechsler-Reya et al., 1997b; Wechsler-Reya and Barres, 1997). Amphiphysin2 forms heterodimers with amphiphysin1 and are localized with presynaptic cytomatrix (Bauerfeind et al., 1998). They are enriched at coated endocytic intermediates. The role of amphiphysin in presynaptic vesicle endocytosis is important and dynamin1, synaptojanin1 are their endocytic intermediate interaction partners (Shupliakov et al., 1997), Mutations in Rvs, the amphiphysin homolog in *S.cerevisiae* causes defects in endocytosis (Lombardi and Riezman, 2001). Amphiphysin plays vital role in actin dynamics during synaptic vesicle recycling in neurons (Sivadon et al., 1995). Disrupting the interactions of amphiphysin2 with dynamin1 by proline-arginine rich domain peptide (PRDp) stalls fissioning in reticulospinal presynaptic axon.

1.2 ATP Binding Proteins: Myosin

Myosins are members of hydrolase enzyme family, capable of converting chemical energy of ATP hydrolysis directly into mechanical energy to generate force and directed movement. Myosins are involved in a wide spectrum of biochemical and biophysical events in the eukaryotic cells. These include movement of cells, load-dependent anchoring, cytokinesis, vesicle transport, golgi organization, sensory signal transduction, cortical tension maintenance and neurite outgrowth (Brown and Bridgman, 2003a; Brown and Bridgman, 2003b; Sellers, 1999; Wylie et al., 1998; Yumura and Uyeda, 2003).

The interplay between myosins and actin filaments are not only necessary for cellular events, but in some cases they are also needed to maintain or to form organized structures like stereo-cilia of inner hair cells. The interaction between myosins and actin is an example for cytoskeletal remodeling owing to the concept of cellular dynamics. Class 2 muscle myosins were studied extensively and became the founding member of myosin superfamily, for this reason it has been called as conventional myosin, whereas other myosins are called

Table 2: Different classes of myosin and their functional motifs.

Myosin Class	Motifs	Function
MI	Polybasic domain	Anionic phospholipid binding
MII	Coiled-coil	Cytokinesis, muscle contractility
MIII	Protein kinase domain	Signaling in photo transduction
MVI	Reverse gear	Transport, reverse movement, hearing
MXVI	Ankyrin repeats	Protein-protein interaction
MXVIII	PDZ	Protein-protein interaction
MXV	Extended	Stereocilia formation, actin bundling, hearing
MX	PH domain	Phospholipid binding
MVII,MX,MXII,MXV	FERM	Binding to membrane associated proteins
MIX	Rho-GAP	Regulation of actin
MI,MIV	SH3	Protein-protein interaction
MV,MX	PEST	Calpain recognition vesicle transport, smooth ER, centrosomes
MIV,MVII,MX,MXII,MXV	MyTH4	Microtubule binding

1.2.1 Molecular Properties of Myosins

Though myosin motor domains are highly conserved, the kinetics varies between different classes and isoforms. The fraction of time spent by myosin on actin filament during the acto-myosin ATPase cycle is called duty ratio. The duty ratio may be low or high depending on the class of myosins, myosin II have low duty ratio. Other relevant properties are the processivity and directionality, which are crucial factors for any given myosins. Motors that have to carry or transport cargo usually have high duty ratio, thus walk several steps along the actin filament without detachment. But those myosins which detach after a short or single step, i.e. motors with low duty ratio are not functionally suited to carry out cargo transport within the cells. Such motors with low duty ratio combine together or form molecular assemblies to perform their functions, whereas class 2 and class 18 myosins being the exceptions, one best example is the conventional myosins during muscle contraction (Geeves and Holmes, 1999) which works as molecular assemblies. In regard to directionality, the plus end of the actin points towards the cell periphery. So, in which case the myosins that walk towards the cell periphery are plus end directed myosins such as myosin I, myosin V. Whereas myosin VI (Wells et al., 1999) move towards the minus end of the filament. There are some indications that myosin IX also move towards the minus end of the filament, i. e. from the plasma membrane to the interior of the cell. Hence, the duty ratio, processivity and directionality parameterize any given myosins.

1.2.2 Architecture and Structure Details of Myosins

The main architectural elements of the myosin structure are the myosin head, the neck region/ lever arm and the tail domain (**Fig. 14**). The myosin head can further be subdivided into motor domain where ATP hydrolysis and actin binding takes place. The lever arm contains variable number of (0 to 7) binding sites for calmodulin-like light chains. The lever-arm produces the force upon the conformational change during strong actin binding and product release after ATP hydrolysis, and the magnitude of this force depends on the length of the neck. The lever arm is the regulatory part of the myosin motor head which homes essential and regulatory light chains at least in the case of myosin II. Several studies on the motor domain have led to a model for force transduction that supposes, the N-terminal SH3-like- β -barrel subdomain (absent in class-I myosin) and the upper and lower 50 kDa domains (primary topological elements in motor domain) remain relatively unchanged due to conformational restriction with respect to actin in the acto-myosin complex. And the force is

produced mostly from a rigid body movement of the neck along with the converter domain, which is a subdomain of the myosin motor domain that connects the neck **Fig. 15**. They are triggered by the conformational changes in the motor domain (mainly in the U50 kDa). The outcome of the movement of the lever arm is called “power stroke”. The involvement of switch I and switch II in the complex communication pathways between the nucleotide binding pocket and actin binding region have improved our understanding (Reubold et al., 2003) about the affinity of myosin motor to actin, nucleotide and products (like ADP, P_i) and the generated force. Loop 1, near the nucleotide binding pocket which is about 25 kDa from the amino-terminus and Loop 2 near the actin binding interface, which is about 75 kDa from the amino-terminus, were considered to be highly dynamic part of the motor domain.

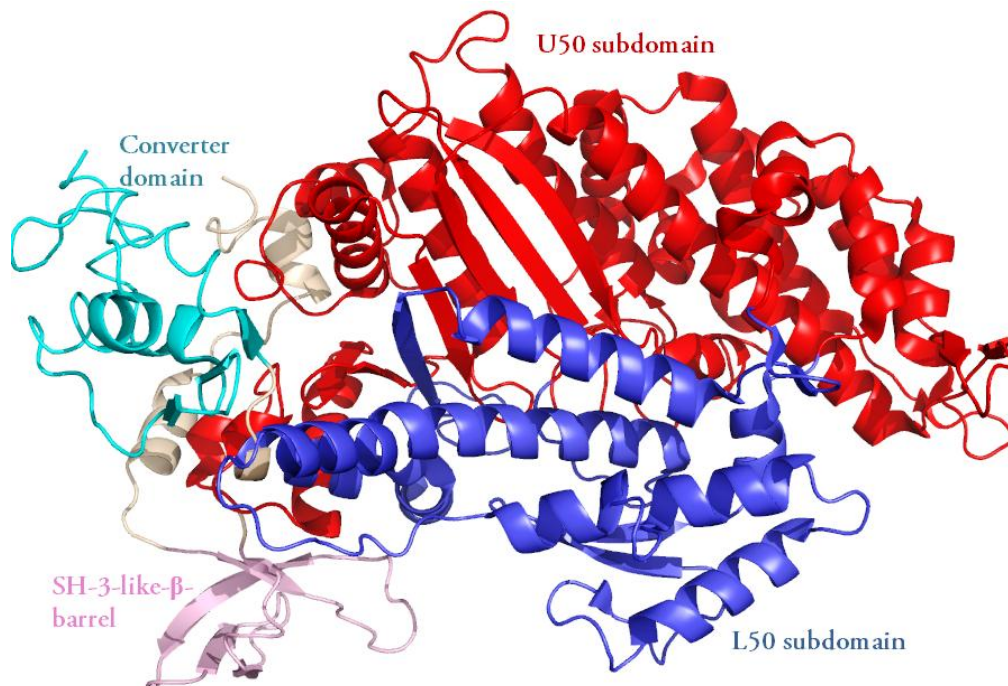


Figure 14: The cartoon representation of the myosin motor domains includes SH-3-like- β -barrel in pink, Lower 50 kDa in blue, Upper 50 kDa in red domain and converter domain in cyan.

Myosin as a protein family shares a high structural similarity between their motor domains. Among the myosins, myosin VI has a unique insert of about 50 amino acids at the converter region. The varying length and spacer between IQ motifs could affect the stiffness of the neck, the relative disposition of the heads and possibly the regulation of unconventional

myosin (Sellers, 2000). Important parameters of myosin motors, like step size and sliding velocity are characterized by the amount of converter rotation and the length of the neck region .

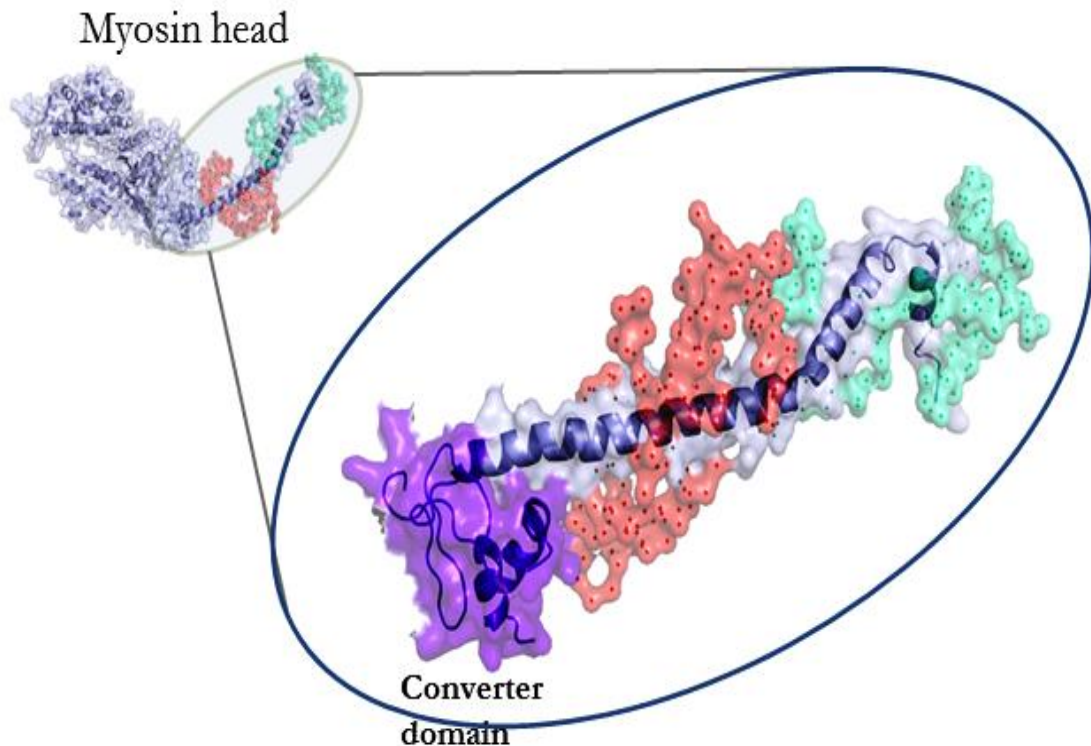


Figure 15: C-terminal converter domain (purple) connecting the motor domain and the neck region. Surface representation of essential light chain (red) and regulatory light chain (cyan) are also shown.

The soluble fragment obtained upon limited proteolysis of myosin, is called subfragment1 or S1 **Fig. 16**. The S1 or myosin head contains as said above, the motor domain and neck region. The motor domain comprises the ATP binding pocket and the actin binding site. Thus, understanding the conformational changes taking place within this fragment can be translated into the understanding of the mechanics of the myosin motor and its implication in contractility, rigidity and movement in the cellular context. The complete picture of the coupling between the acto-myosin reaction cycle and the generated force may be evident from understanding myosins with different nucleotide bound state or crystal structures in different conformation of the lever arm or intelligent protein engineering or high resolution electron microscopic acto-myosin complex structures. This might change the paradigm of muscle

biology. The attempt to perturb the intrinsic mechanical properties by small molecule effectors is an interesting approach in the myosin field, and in further chapters of my thesis I have addressed and added some more value in the direction of myosin's chemical biology.

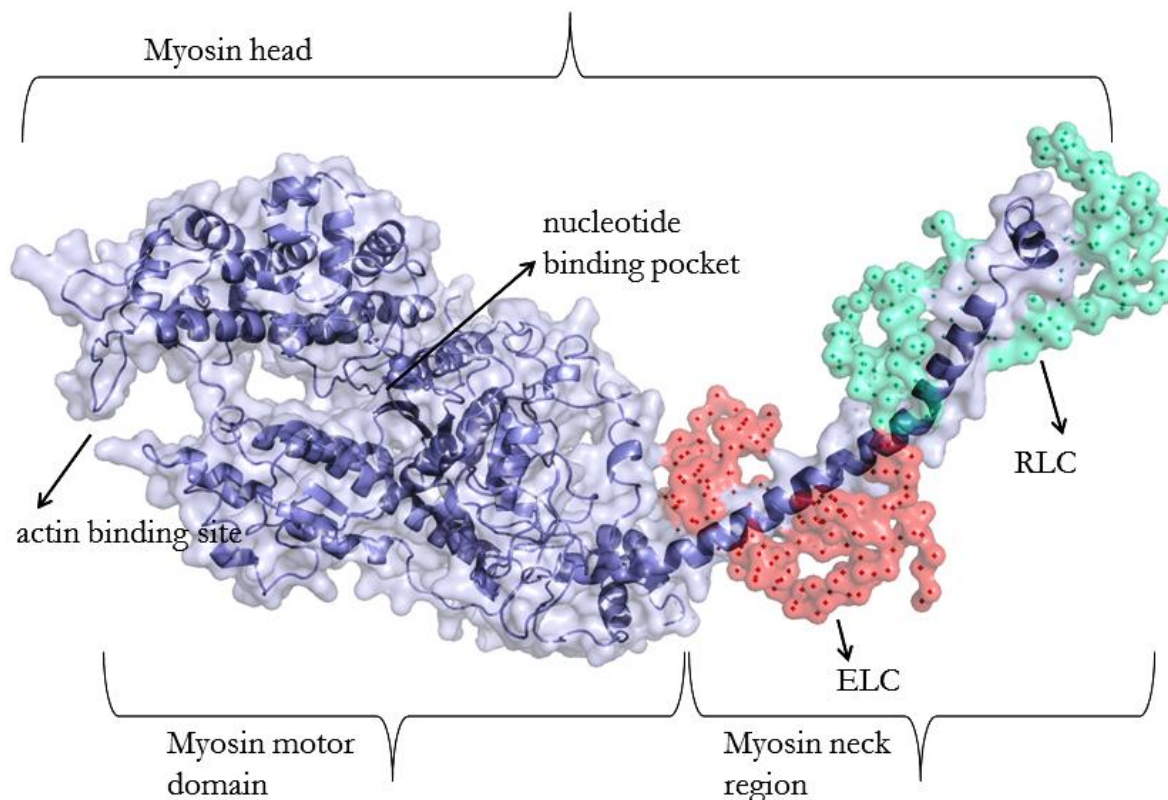


Figure 16: Cartoon and surface representation of proteolytic fragment of myosin from *G. gallus* generated by papain digestion. Motor domain and myosin neck region are in cartoon and surface representation (blue surface). The essential light chain is shown in red and regulatory light chain is shown in cyan. The coordinates of the myosin structure is obtained from the pdb id 2mys (Rayment et al., 1993).

1.2.3 The Myosin II Motor Domain of *D. discoideum*

D. discoideum conventional myosin II is an abundant protein that has been shown to be involved in cytokinesis, cell protrusion and development (Bosgraaf, 2006; Hostetter, 2004). This conventional motor has been used in our studies not only to modulate their kinetic properties by small molecule modulators, but to obtain the structural details of the motor domain in complex with nucleotide transition analogs and small molecule modulators.

Part of the myosin-actin interface, the so-called cardiomyopathy loop (CM-loop), the mutation of R403Q in human cardiac myosin at this interaction site causes familial hypertrophic cardiomyopathy (Sasaki et al., 2002, 2003). Loop 2 is another interacting motif for actin through ionic interactions. The strut-loop is a four amino acid loop – ⁵⁹⁰DPLE⁵⁹³ which has an extended conformation, they keeps the upper and lower 50 kDa domains apart thus acting as a mechanical strut. Variations in the length of strut-loop have been implicated in weak actin association to myosin. Amino acid residues ⁴⁵⁷DISGFE⁴⁶² form the switch II; the switch II keeps hold the water that attacks ATP **Fig. 17 and Fig. 18**. This loop acts as the door and opens up during the phosphate release but this model is still under debate. The long helix from 466 to 497 (the sequence numbers are according to the myosin II structure of *D. discoideum*), which connects the central core and the actin binding helix-loop-helix motif has a kink at residue 485 and this kink is stabilized by F506, L508 and I687. This relay helix transduces and amplifies local rearrangements due to conformational changes during ATP hydrolysis to the converter and the lever arm regions. Mutation of key residues like F506G, F487A in the relay helix has been shown to perturb the communication between the catalytic pocket and the acting binding regions (Tsiavaliaris et al., 2002).

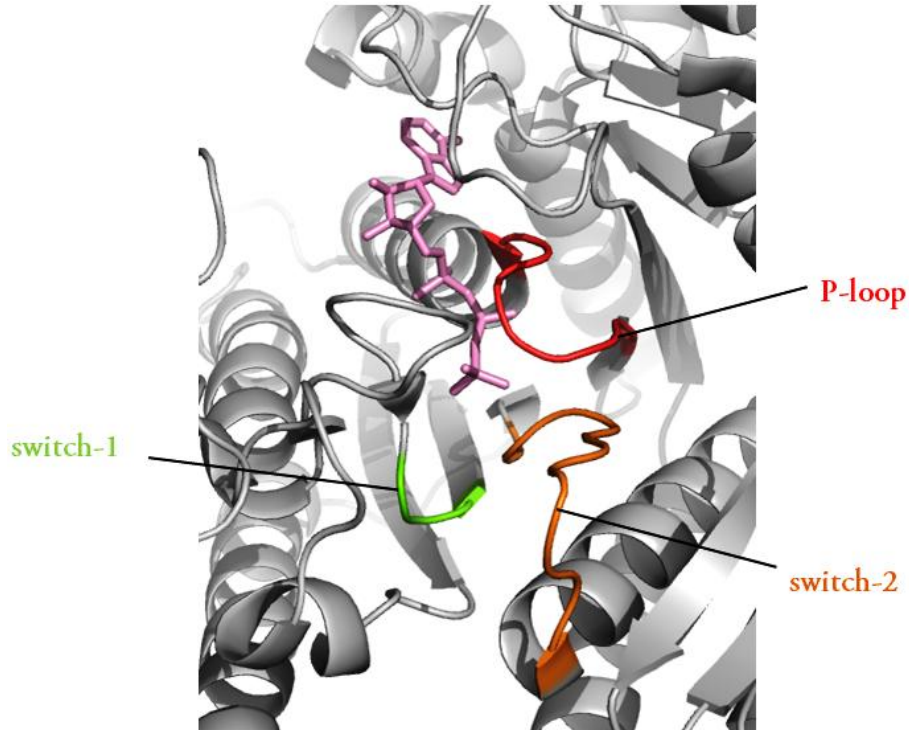


Figure 17: The ATP binding loops switch 1 (green), switch 2 (orange) and the P-loop (red) forms the active site. The nucleotide is shown in stick representation (pink).

Motor domains with artificial lever arm of myosin II from *D. discoideum* can be purified in sufficient quantity for kinetic and structural studies. Translation of the mechanism obtained from this model myosin can be used to understand the basics of the molecular mechanisms of other higher eukaryotic and mammalian myosins.

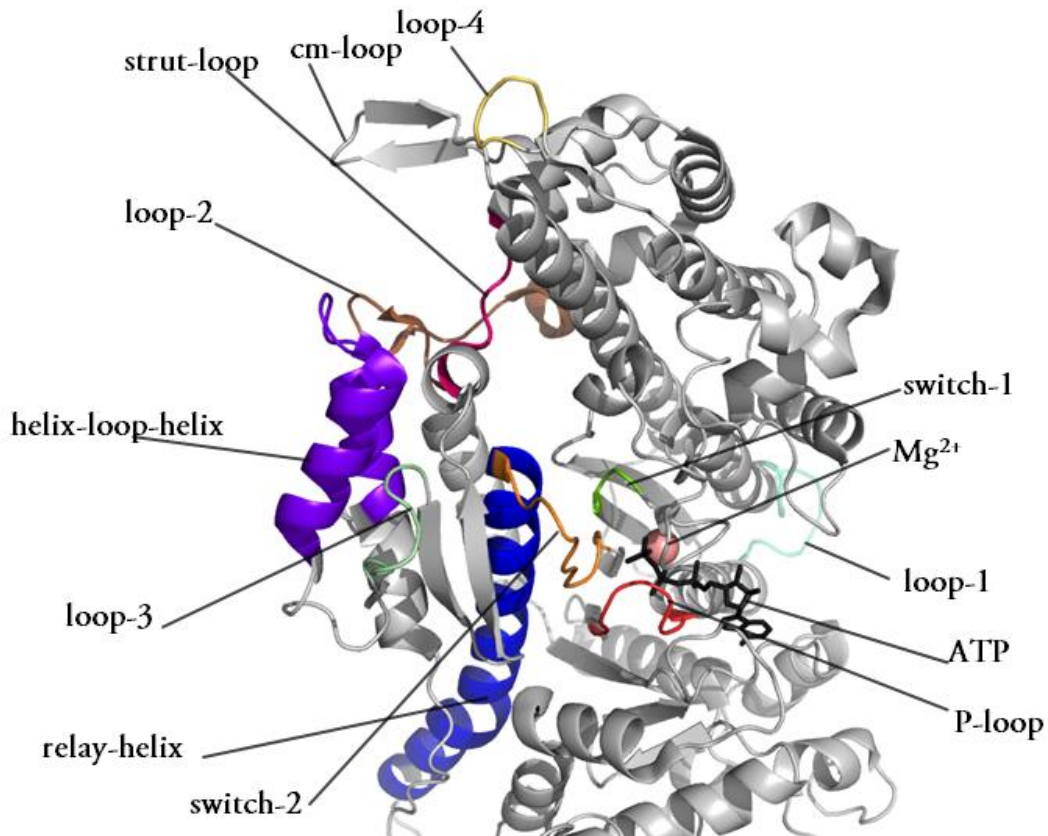


Figure 18: Structural and functional elements of myosin motor domain.

1.2.4 The Cross Bridge Cycle

The cross bridge cycle can be explained with the reaction scheme shown in **Fig. 19** with six states from *a* to *f*, for simplification. Nucleotide-free myosin strongly binds to actin in the so called rigor complex (state *a*). The affinity of myosin to actin is strong in this state. ATP binds to the rigor complex to form *A.M.T*. ATP binding to the acto-myosin complex causes dissociation of actin to form *M.T* (state *b*). ATP is hydrolyzed by myosin resulting in *M.D.P_i*, which is a state where myosin has weak affinity for actin (state *c*). At state *e*, P₁ release leads to the force generating power stroke, followed by ADP release from *A.M.D*, culminating in a

rigor cross bridge state $A \cdot M$ to bring about the next cycle (Cooke, 1995; Geeves et al., 2005; Geeves and Holmes, 2005).

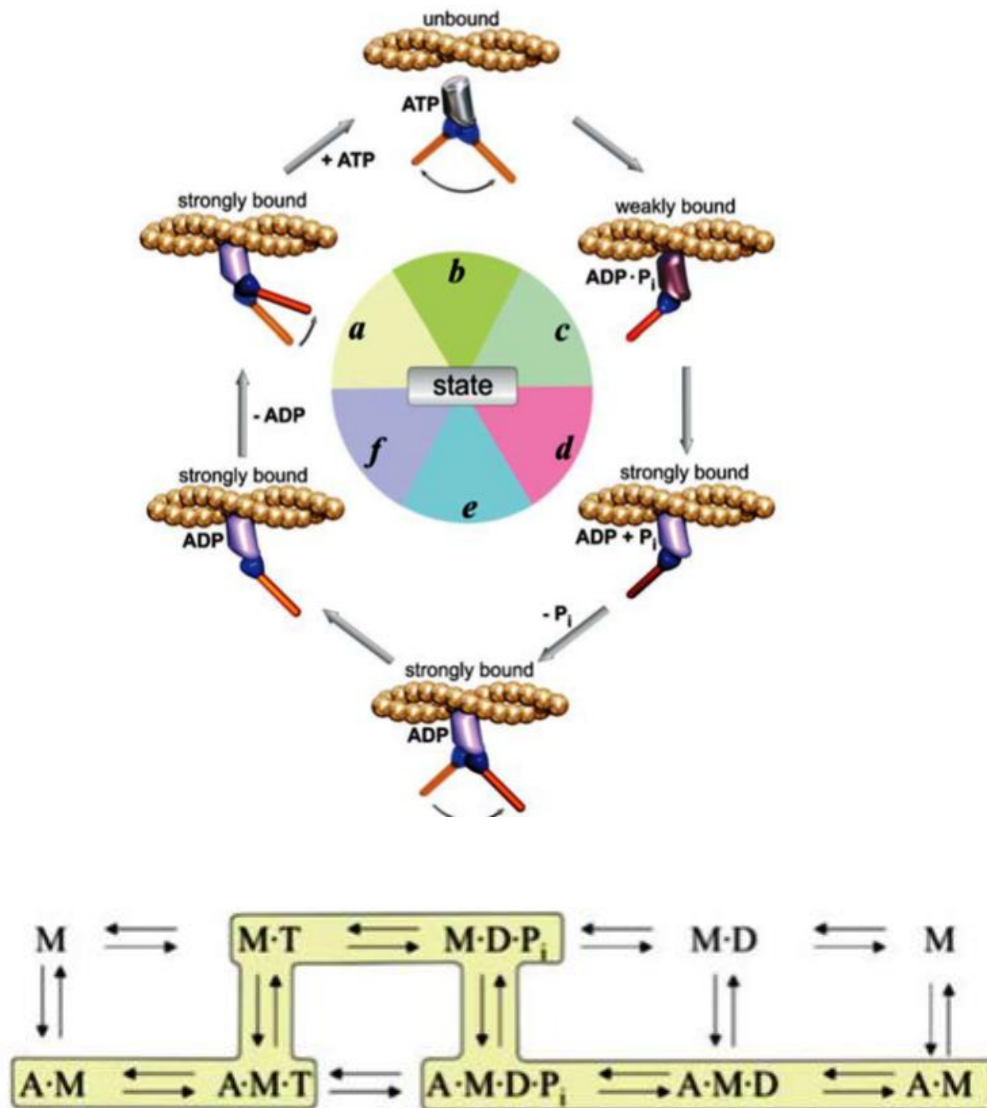


Figure 19: (a) Scheme showing the acto-myosin energy conversion cross bridge cycle (adopted from (Geeves et al., 2005)). Myosin is strongly bound to actin in the rigor complex in the state a. The equilibrium is shifted upon nucleotide binding during which myosin is released from actin. Upon hydrolysis of the bound nucleotide, myosin has weak affinity for actin like shown in the state c. Upon P_i release myosin produces pre-powerstroke. Later ADP release causes myosin to enter into the next cycle during which the lever arm produces the powerstroke. (b) The pathway of the cross bridge cycle and the model adopted to explain the chemical kinetics reactions, where, A -Actin; M -Myosin; T -ATP; D -ADP; P_i -Inorganic Phosphate are the corresponding acronyms.

1.3 Diseases Related to Myosin and Dynamin Dysfunction

Laing early onset distal myopathy, myosin storage myopathy, Familial Hypertrophic Cardiomyopathy (FHC), Fukuyama-type congenital muscular dystrophy, amyotrophic lateral sclerosis are some of the diseases caused by myosins (Banks and Fisher, 2008; Hirokawa et al., 2010; Lopez et al., 2008; Walsh et al., 2010a; Walsh et al., 2010b). The summary of the diseases and related myosins causing them are shown in **Table 3**. According to a keyword search for myosins performed at the Drug Bank database (<http://www.drugbank.ca>), a bioinformatics and cheminformatics resource that combines detailed drug (i.e. chemical, pharmacological and pharmaceutical) and drug target (i.e. sequence, structure, and pathway) information, 17 approved small molecule drugs are targeting myosin related diseases .

Table 3: Various classes of myosins and related diseases caused by them.

Myosin	Diseases
β -cardiac myosin II	Familial hypertrophic cardiomyopathy(FHC)
Myosin III	Distal arthrogyryposis (congenital contractures of limbs)
Myosin V	Griscelli disease (Hypo-pigmentation)
Myosin VI	Hearing loss
Myosin VIIA	Usher syndrome (Deafness and vision loss)
Myosin IX	May-Hegglin anomaly (Thrombocytopenia)
Myosin XV	Deafness, loss in balance

1.3.1 Small Molecule Effectors of Myosins and Dynamins

Small molecules act as an agonists or antagonists. When such molecules bind to their target proteins they can lead to changes in local ionic concentration, permeability, diffusion rate, and conformational changes. These small molecules can be characterized as activators, inhibitors or modulators of the target proteins according to the specific activity brought about by the small molecules.

Myosin displays a potential therapeutic target, because they are involved in diversified functions like transport of cargos inside the cells, muscle contractions and sensory signal processes. The interaction of myosin signifies its role in fundamental cellular processes. They can bind to membrane associated proteins, phospholipids, and to microtubules. They are also involved in signaling process; they communicate between proteins and propagate the processed communications, thereby actively involving in signaling within cellular milieu. Since myosin is involved in various cellular functions, they are prone to be lethal to the cells when they are unable to be functional. Characterizing such motors is the first thing in understanding the diseases caused by their malfunctions (Savoia, 2010 ; Savoia, 2010 ; Veugelers et al., 2004). In cases like *Toxoplasma gondii* parasites, myosinA is involved in the host cell invasion and parasite's locomotion (Dobrowolski et al., 1997; (Heaslip, 2010 ; Heaslip, 2010). Small molecule inhibitors or activators that are class specific and isoform specific for myosin could be used to modulate the enzymatic activity. 2,3-butanedione-2-monoxime; 4-Methyl-N-(phenylmethyl)benzenesulfonamide,(±)-1,2,3,3a-Tetrahydro-3a-hydroxy-6-methyl-1-phenyl-4H-pyrrolo[2,3-b]quinolin-4-one;2,4-dichloro-6-(3,4,5-tribromo-1H-pyrrole-2-yl)phenol or tribromodichloropseudilin; pentachloropseudilin; pentabromopseudilin (PBP) and resveratrol are reported to act as myosin small molecule effectors (Chinthalapudi et al., 2011; Higuchi and Takemori, 1989; Kagawa et al., 2006; Preller et al., ; Ramamurthy et al., 2004; Watanabe et al., 2010).

In case of dynamin related protein1 or dynamin1, small molecules that inhibits mitochondrial division, endocytosis have been shown to play vital roles as therapeutic targets. Inhibiting Drp1 activity reduces the mitochondrial morphological phenotype that is exclusive for some disease conditions like Parkinson's, Alzheimer's and Huntington's diseases. Ischemia, which is characterized by shortage of blood supply to a particular tissue results in low levels of oxygen or glucose in the tissue. In such case, reperfusion takes place in ischemic

tissues, which causes oxidative stress and lead to local inflammation. During reperfusion, programmed cell death (PCD) is activated. Drp1 initiates mitochondrial fragmentation in the reperfusion injury area to release cytochrome c, ultimately leading to the caspase activation and apoptosis. It has been shown that in cardio-myocytes conditioning, inhibition or over-expression of dominant negative Drp1 mutant K38A saves cells from stimulated ischemic/reperfusion injury (SIRI). But, on the other hand, dysfunction of fusion proteins leads to lowered mitochondrial respiration, alteration in mtDNA, which leads to neurological disorders like Dominant Optic Atrophy (DOA) and Charcot-Marie-Tooth type 2A diseases (CMT2A). Inhibition of Drp1 in such cells can reduce the severity of the disease conditions by reducing the fusion process. On the other hand, classical dynamin1 inhibitors have been shown to be effective in the treatment for epilepsy. Dynasore, tyrphostins, iminodyn are some of the known inhibitors that are reported so far for dynamins and dynamin related proteins (Hill et al., 2001; Hill et al., 2005; Hill et al., 2009; Hill et al., 2004; Odell et al., 2010; Tanaka and Youle, 2008).

CHAPTER 2

Materials and Methods

2.1 Buffer Recipes

Buffer A

RbCl 12 g/l
MnCl₂·4H₂O 50 mM
Potassium acetate, pH 7.5, 30 ml of 1 M stock solution
CaCl₂·2H₂O 1.5 g/l
Glycerol 150 g/l
Adjust the pH to 5.8 with 0.2 M acetic acid

Buffer B (per liter)

MOPS, pH 6.8, 20 ml of a 0.5 M stock solution
RbCl 1.2 g
CaCl₂·2H₂O 11.0 g
Glycerol 150 g

Buffer P1

Tris.Cl, pH 8.0, 50 mM
EDTA 10 mM
RnaseA 100 µg/ml

Buffer P2

NaOH 200 mM
SDS (w/v) 1%

Buffer P3

Potassium acetate, pH 5.5, 3.0 M

Buffer QBT (equilibration buffer)

NaCl 750 mM
MOPS, pH 7.0, 50 mM
Isopropanol (V/V) 15%
Triton X-100 (V/V) 0.15%

Buffer QC (Wash buffer)

NaCl 1.0 M
MOPS, pH 7.0, 50 mM
Isopropanol (V/V) 15%

Buffer QF (Elution buffer)

NaCl 1.25 M
Tris.Cl, pH 8.5, 50 mM
Isopropanol (V/V) 15%

DD-EP Buffer

Sodium phosphate, pH 6.4, 10 mM
50 mM sucrose

DD-Cure Buffer

Sodium phosphate, pH 6.4, 10 mM
Sucrose 50 mM
MgCl₂ 5 mM
CaCl₂ 0.5 mM

Soerensen phosphate buffer

Na₂HPO₄ 0.356 g/l
KH₂PO₄ 1.99 g/l

Cure buffer

MgCl₂ 2 mM
CaCl₂ 2 mM

Bonner's solution

NaCl 0.6 g/l
KCl 0.75 g/l
CaCl₂ 0.3 g/l

2.2 Competent Cells

Competent cells were prepared by diluting an overnight bacterial-culture to 1:50 and letting them grow until an optical density of 0.3 – 0.4. The cells were incubated on ice for 15 minutes. Sterile falcon tubes were pre-chilled and the cells were centrifuged for 10 min., at 3000 rpm, at 4° C. The cell-pellet was re-suspended in 1/3 of the original volume in ice-cold buffer A and left on ice for 15min. Cells were spun again for 10 min, at 3000 rpm, in 4° C. The obtained pellet was further re-suspended in 1/12 of the original volume in ice-cold buffer B, and left on ice for at least 15 min. Finally 100 µl aliquots were flash frozen in liquid nitrogen. The buffers used in the above procedure were all sterilized by filtration.

2.3 Transformation of Plasmid DNA into Competent Cells

An aliquot of competent cells were thawed on ice for 20 min, 50-150 ng/µl of plasmid DNA was added to this aliquot. After gentle tapping of the micro centrifuge tube the mixture

was incubated for 10 min on ice. Cells were heated to 90 sec at 42° C, and immediately transferred to ice and incubated for 20 min. After which 900 µL of LB media were added and shaken at 200 rpm at 37° C for an hour in a table top shaker. This 1mL culture was spun at 2200 g using a table top centrifuge. 850 µL of the media was removed and the remaining pellet was re-suspended with remaining media in it and used to plate on the LB agar plates with corresponding antibiotics.

2.4 Plasmid DNA Isolation

Commercially available Qiagen kits were used for mini and maxi plasmid DNA isolations. A single colony from a freshly streaked plate was inoculated in LB medium containing the appropriate selective antibiotic. Cells were harvested by centrifugation at 6000 g for 15 min at 4° C. The obtained bacterial pellet was resuspended in buffer P1. After adding buffer P2 and vigorous mixing, the lysate was incubated for 5 min at room temperature. Prechilled buffer P3 was added and the resuspension was incubated for 20 more min at room temperature. Cartridges were used to clear the lysate; the obtained supernatant was allowed to pass through Qiagen columns which were equilibrated with buffer QBT, under gravity flow. The Qiagen-tip column was washed with buffer QC and the DNA was eluted with buffer QF, DNA was precipitated using 0.7 volumes of isopropanol and immediately centrifuged at 5000 g for 60 min at 4° C. The obtained DNA pellet was washed with 70% ethanol. Finally the pellet was air-dried and dissolved carefully in 10 mM Tris.Cl, pH 8.5.

2.5 *D. discoideum* Growth on Plates and in Shaking Culture

D. discoideum cells can be grown on tissue culture Petri dishes or in shaking culture at a constant temperature of 20 °C. The cells are cultured in HL5-C axenic medium containing 10 U/ml of penicillin/ streptomycin to prevent bacterial growth and the appropriate concentration of G418 (10-20µg/ml) in order to maintain the selection pressure on transformed cells. Untransformed wild type cells (AX2) or AX3 ORF⁺ cells are grown without G418. Transformed cells harboring a pDX vector with a *neo*^R cassette are grown in the presence of 10 to 20 µg/ml G418. The concentration depends on the particular construct expressed. Cells producing the dynaminA protein grow in the presence of 20 µg/ml G418 while cells producing Myosin2-DymAGTPase fusion grow with 10 µg/ml G418. For large-scale production, the cells were grown in flasks in shaking culture. The flasks were filled to no more than half their nominal volume with medium and shaken at 180 rpm. Wild type cells and

the transformants used in this work grow to a density of about 1×10^7 cells/ml with a doubling time of roughly 12 hrs. Cells are diluted when or before they reach 1×10^7 cells/ml, an exchange of the medium is not necessary. Upon dilution, the cell density should not drop below 5×10^5 cells/ml. On plates cells are grown until they are confluent and then washed off with medium. Alternatively, cells could be washed with Bonner's solution while adherent on the plate and then washed off with Bonner's for downstream processing. Fresh medium was added and the remaining cells continue growing. Plates can be stored at 4°C for several weeks without exchanging the medium. A confluent 9 cm Petri dish contains about 1×10^7 cells.

2.6 *D. discoideum* Electroporation

Cells were harvested at a density of 3×10^6 cells/ml by centrifugation at 1,000 g for 5 min, with a pre-chilled 15 ml centrifuge tubes. The cell pellet was washed with Soerensen phosphate buffer once. Cells were washed twice with cold DD-EP (*D. discoideum* electroporation) buffer and re-suspend in the same buffer at 1×10^7 cells/ml {if it is ORF+ cells, then it should be resuspended at $5-8 \times 10^6$ cells/ml}. In the meantime a 4mm electroporation cuvette was pre-chilled. 20-35 μg of plasmid DNA were mixed in 0.8 ml of cell suspension in a microfuge tube, and then this mixture was transferred into the 0.4 cm electroporation cuvette and chilled further for 5 min on ice. After a gentle tapping of the cuvette and drying the outer surface with a tissue, electroporation procedure was done immediately with the preset protocol for *D. discoideum* with a voltage set of 1200 Volts, a pulse length of 1 ms, the total number of pulses not exceeding 2, and an interval between two pulses of 5s. Bio-Rad Gene Pulser Xcell was used throughout this work for the electroporation of *D. discoideum*. The cuvette was immediately returned to ice. After 5 to 10 min cells were transferred to a Petri dish filled with 12 ml HL5-C medium. Alternatively cells can be first "cured" by mixing with 0.5 volumes of Cure Buffer in a well of a 24-well plate. The plate is shaken at 100 rpm for 15 min at 21°C . Next the whole mixture is transferred to a petri dish containing 12 ml medium. Cells were allowed to recover for 12 to 24 hours before applying selection for transformants.

2.7 Preparation and Cryo-Conservation of *D. discoideum* Spores

Cells are collected from liquid plate or suspension culture. Cells grown to a density of less than or equal to 5×10^6 cells/ml works best. They were washed in MES buffer and re-suspended at 2×10^8 cells/ml. 300 μ l of this suspension were spreaded on a MES-agar plate. Plates were dried until there was only a thin film of liquid left (the amount of liquid has a big effect on spore formation). The plates are incubated upside down for 48 hrs before harvesting the spores by tapping the inverted plate smartly on the benchtop. Spores from 3 plates are re-suspending in 1 ml 10 % glycerol and 100 μ l aliquots are frozen by putting them into the -80 °C freezer. The spores are stored at -80 °C.

Vegetative *D. discoideum* cells can be stored frozen without the need to make spores. Cells are washed with cold Bonner's Standard Solution and re-suspended at high density ($>10^8$ cell/ml) in HL5-C medium containing 10 % DMSO. Aliquots of the suspension are put for 2 hrs in a -20 °C freezer. Slow cooling is essential and a towel wrapped around the box containing the tubes may help slowing down the cooling and provide insulation in the following transfer to a -80 °C freezer. The cells are stored at -80 °C. The thawing process should be quick (e.g. warming the tubes on the hand palm) and are transferred immediately to a Petri dish with fresh medium. Once the cells have attached (after about 30 min), the medium is exchanged to get rid of DMSO.

2.8 Polymerase Chain Reaction (PCR)

The polymerase chain reaction allows the amplification of specific DNA sequences *in vitro*. Two oligonucleotides flanking the sequence of interest are used as primers for DNA polymerisation, one on each strand. The template double strands are heat denatured (95 °C) and then the primers present in excess are allowed to anneal to the template strands in a sequence specific manner at a temperature about 5-10 K below their melting temperature T_m . For the extension heat stable DNA polymerases from thermophilic organisms are used that are not inactivated during the denaturation. The DNA polymerisation is carried out at a temperature optimal for enzyme activity (72 °C). During multiple cycles the target sequence is amplified exponentially. In this work the Finnzymes Phusion High-Fidelity DNA polymerase was used.

The following reaction mixture was used for all PCR reactions presented in this work:

5x buffer (HF)	5.0 μ l
dNTPs (10 mM)	1.0 μ l
Primer (100 μ M)	0.5 μ l
Template DNA	20-100 ng
H ₂ O	40 μ l
Phusion High-Fidelity DNA polymerase	1.0 μ l

The following times and temperatures for denaturation, annealing and extension were used throughout except when necessary to optimize for some constructs.

Table 4: PCR cycle scheme

Initial Denaturation	98 °C	3 min	1cycle
Denaturation	95 °C	30 s	25cycle
Annealing	68 °C	30 s	
Elongation	72 °C	4 min	
Elongation	72 °C	10 min	1cycle

2.9 Restriction Enzyme Mediated Digestion of DNA

Sequence specific cleavage of DNA is carried out by use of restriction endonucleases. For analytical purposes about 200 ng of DNA are cut in a total volume of 10 μ l. In preparative restriction digests, 2-5 μ g of DNA are cut in a total volume of 50 μ l. Buffer conditions and temperature are used according to the manufacturers (Fermentas, NEB) instructions and the amount of enzyme added should not exceed 1/10 of the total volume to ensure a low glycerol concentration. Digestion is usually carried out with several units of enzyme per μ g of DNA for 3-4 hrs.

2.10 Separation of DNA-Fragments on Agarose Gels

DNA fragments can be separated according to their size by agarose gel electrophoresis. The concentration of the agarose dissolved in TAE-buffer depends on the size of the fragments to be separated but 1.4 % gels have been used throughout this work. The DNA

sample is mixed with 1/5 volume of 6x sample buffer. A voltage of 75 V is applied to minigels (6.5×10 cm) for about one hour. In the gel the DNA is visualized under UV light after staining with ethidium bromide, an intercalating agent that becomes fluorescent upon binding DNA.

2.11 Purification of DNA from PCR Reactions and Agarose Gels

Fragmented DNA intended for cloning is separated on an agarose minigel using broad wells for the larger amounts (usually 50-100 μ l). On each side of the broad well, a small aliquot of the digest is run in a normal sized well. The lanes on the side of the preparative lane are cut and stained with ethidium bromide, while the preparative lane itself is not, in order to avoid DNA damage. The position of the DNA band of interest is marked with a scalpel on the side-lanes under UV-light. The gel is reconstituted and the band of interest is excised from the preparative lane. The DNA is extracted from the excised gel slices using the QIAquick Gel Extraction Kit (QIAGEN). The purity and the amount of recovered DNA are checked on an analytical agarose gel prior to the use in ligation.

2.12 Ligation of DNA Fragments

DNA fragments that have complementary 5' or 3' overhangs or blunt ends that can be joined covalently using T4 DNA-ligase. The fragments are mixed with 2 μ l 10x ligase buffer and 1 μ l ligase (5 WeissU/ μ l; Fermentas) in a total volume of 20 μ l. A molar ratio of 3-10 insert/vector is used. Ligations were carried out for 2 hrs at room temperature. In some cases ligations were also carried out overnight at 16 °C.

2.13 SDS Polyacrylamide Gel Electrophoresis (SDS-PAGE)

Proteins can be separated by their molecular weight on SDS polyacrylamide gels. Depending on the size of the proteins, gels with 10 % to 15 % polyacrylamide are used. Minigels with a size of about 6×8 cm and 10 to 14 wells are used. The protein sample is mixed with an equal volume of 2x sample buffer and boiled for 5 min. 10-12 μ l of this mixture are loaded per lane. The gel is run with 180 V, 40 mA for 55 mins. For two gels, the current value is doubled. The gels are stained with Coomassie staining solution for 30 mins and destained for 15 min.

10x SDS running buffer (stock solution)

Tris	30 g/l
Glycine	144 g/l
SDS	10 g/l

2x sample buffer

Tris, pH 6.8	100 mM
SDS	4 %
β -mercapto-ethanol	2 %
Glycerol	20 %
Bromophenol blue	0.2 g

Coomassie stain

Coomassie brilliant blue R250	2.0 g
Coomassie brilliant blue G250	0.5 g
Methanol	50 ml
Ethanol	450 ml
Dissolve Coomassie; add	
Glacial acetic acid	100 ml
H ₂ O	400 ml

Destain

Ethanol	5.0 %
Acetic acid	7.5 %

2.14 Western Blotting***5x Transfer buffer***

Glycine	960 mM
Tris, pH 8.3	125 mM
Adjust volume to 1 l	

TBS

Tris, pH7.6	74 mM
NaCl	150 mM
Adjust volume to 1 l	

TBST

TBS + 0.5% Tween

Proteins can be transferred to a membrane by electrophoresis. The bound protein is then specifically detected using an enzyme linked antibody and an enzymatic reaction. A

semidry blotting machine is used for the transfer. The gel and the membrane (Whatman[®], PROTRAN[®] Nitrocellulose Transfer membrane) are briefly equilibrated in Transfer buffer. The blot is assembled by sandwiching 2 Gel-Blotting-paper 6 × 8.5cm (Whatman[®], Schleicher & Schuell[®]), the gel, the membrane and 2 Gel-Blotting-paper from bottom to top order. All components should be pre-wetted and there must be no air bubbles between gel and membrane. The sandwich is placed in the middle of the blotter machine and the voltage is applied such that the anode is at the side of the membrane. The transfer is done at room temperature at 12 volts for 1.5hr.

For specific detection, the membrane is incubated with an antibody directed against the protein of interest (primary antibody), washed and then incubated with an enzyme linked secondary antibody directed against the Fc part of antibodies from the species in which the primary antibody was raised. First, the membrane is blocked in 10ml TBS buffer with 5% skimmed milk powder from Roth[®] for 2 hr at room temperature. The membrane is then washed twice for 10mins each with TBST. Then the membrane is incubated with the primary antibody, which was prepared in 10ml TBS plus 3% milk powder, in case of mouse- anti-Penta-histidine a 1:5000 dilution and in case of rabbit-anti- DymA a 1:2000 dilution was used. The membrane is incubated in blocking solution containing an appropriate dilution of the primary antibody at 4 °C over night on a shaker. The membrane is washed 3 times for 10 min with TBST. The incubation with the secondary antibody (e.g. 1:10,000 of horse radish peroxidase conjugated antibody) in TBST is done for 1.5 hr at room temperature and the membrane is again washed 3 times for 10 min in TBST.

For detection, the Super signal[®] West Dura Extended Duration Substrate (Thermo Scientific) is used. Equal volumes of the two reagents are mixed and a total volume of about 0.6 ml per cm² of membrane is used. After 5 min incubation under low light or dark, the membrane is dried on a Whatman paper. Bio Rad Chemidoc equipped with CCD camera is used in chemi-luminescence mode to detect the signal.

2.15 Analytical Protein Preparations

LB50

Tris, pH 8.0	50.0 mM
EDTA	2.0 mM
EGTA	0.2 mM
NaCl	50.0 mM

The medium from a confluent 9 cm Petri dish of *D. discoideum* is removed and the cells are washed on the plate with Bonner's solution. The cells are then harvested in 1 ml of Bonner's, transferred to a 1.5 ml reaction tube and centrifuged at 3,000 rpm in a benchtop centrifuge. The supernatant is removed and the cells are lysed for 10 min at room temperature by addition of 1 ml of LB₅₀ containing protease inhibitors and 0.5 % Triton[®] X-100. The tubes are centrifuged for 30 min at full speed at 4° C. The supernatant is discarded. An aliquot can be saved for SDS-PAGE or western-blot. Protein is solubilized by homogenizing the pellet with 70 µl of LB₃₀₀ containing 10 mM of the appropriate nucleotide (ATP for myosin, GTP for dynamin) using a Roth[®] plastic pistil. After 20 min of centrifugation at full speed the supernatant and the pellet are analyzed by SDS-PAGE.

2.16 Purification of DynaminA

10-15 l of HDX cells are grown to a density of about 5×10^6 cells/ml to 1×10^7 cells/ml with 10 µg/ml of G418 (10 l culture at 8×10^6 cell/ml yield about 70 g of cells). The cells are harvested by centrifugation for 8 min at 1,000 g in a Beckmann J6 centrifuge. All followings steps and centrifugations are performed in the cold room, at 4 °C or on ice. The cells are washed once with cold PBS and centrifuged for 8 min at 1,000 g as before. The weight of the resulting cell pellet is determined (about 70 g from 10 l at 8×10^6 cells/ml). The pellet is resuspended in 10 cell volumes of LB₅₀ plus protease inhibitors and the cells are lysed by the addition of another 10 cell volumes of LB₅₀ containing protease inhibitors and 1 % Triton[®] X-100. After 30 min on ice, the completeness of lysis is checked under the microscope. The lysate is centrifuged at 30,000 g for 1 hr (e.g. in a Beckman JA-14 rotor). The supernatant is discarded, an aliquot saved for SDS-PAGE. The pellet is washed without resuspension with lysis buffer containing protease inhibitors and centrifuged for another 5 min. The pellet is extracted in 2 cell volumes of LB₃₀₀ containing protease inhibitors, 12 mM MgCl₂ and 10 mM GTP using a Dounce homogenizer with tight pistil. The extract is centrifuged at 20,000 g for 20 min (e.g. in a Beckman JA-25.50 rotor). The supernatant is dialyzed against 2 x 2 l of LB₅₀ containing 5 mM benzamidine (for 3hr and overnight). The dialyzed solution is centrifuged at 3,000 g for 15 min. A column (16 mm diameter) containing 30 ml of DEAE Fractogel (Merck) is equilibrated with LB₅₀ containing 5 mM benzamidine. The supernatant is loaded onto the column with a flow rate of 3 ml/min and washed with the equilibration buffer until the baseline of UV absorption is stable. The protein is eluted with a linear gradient from 0 to 30 % LB₅₀₀ over 5 column volumes. Dynamin A elutes early at a conductivity of about 11 mS/cm, while actin elutes later at a conductivity of about 13 –14 mS/cm. The fractions

containing dynamin but no actin are pooled and the resulting NaCl concentration is estimated. The pooled fractions are brought to 40 mM NaCl, rebound to an 8 ml DEAE column and step eluted with lysis buffer containing 100 mM NaCl for concentration. Protein concentrations of up to 8 mg/ml can be reached this way. Sucrose is added to a final concentration of 3 % (w/v) and small aliquots are flash frozen in liquid nitrogen and stored at -80°C .

2.17 Purification of DynaminA Domains Fused to Myosin II Motor Domain of *D. discoideum*

Cells are grown, harvested and lysed as described above (purification of dynaminA) but LB₀ is used instead of LB₅₀. The first pellet is washed with extraction buffer containing PMSF and centrifuged for another 5 min. The pellet is extracted in 2 cell volumes of extraction buffer containing protease inhibitors, 10 mM ATP and 2 mM GTP using a Dounce homogenizer with tight pistil. The extract is centrifuged at 20.000 g for 20 min (e.g. in a Beckman JA-25.50 rotor). The supernatant is then applied with a flow rate of 2 ml/min to an immobilized affinity chromatography (IMAC), the NiNTA column (e.g. Pharmacia XK16/20, 30 ml bed volume) equilibrated with low salt buffer. The column is washed with a flow rate of 3 ml/min with 10 column volumes (CV) of low salt buffer, with 10 CV of high salt buffer and with 10 CV of low salt buffer with 40 mM imidazole (8 % imidazole). The fusion protein is eluted with a gradient from 8 % to 100 % imidazole buffer over 5 CV and fractions of 3 ml are collected. The peak fractions are pooled and dialyzed over night against storage buffer. The protein is then concentrated using 20 ml Viva spin concentrators with 50 kDa cutoff (Vivascience). Depending on purity, the protein can be further purified over a preparative Superdex 200 gel filtration equilibrated in storage buffer. Alternatively it can be flash frozen in liquid nitrogen directly after adding sucrose to a final concentration of 3 % (w/v).

Extraction buffer

Hepes, pH 7.3	50 mM
K acetate	30 mM
NaCl	300 mM
Mg acetate	10 mM
β -mercapto-ethanol	7 mM

Low salt buffer

Hepes, pH 7.3	50 mM
K acetate	30 mM
Benzamidine	5 mM

High salt buffer

Hepes, pH 7.3	50 mM
K acetate	300 mM
Benzamidine	5 mM

Imidazole buffer

Imidazole, pH 7.3	500 mM
Benzamidine	5 mM

Storage buffer

Tris, pH 8.0	20 mM
MgCl ₂	1 mM
DTT	5 mM

2.18 GST-Amphiphysin1-SH3 Domain Purification***Lysis buffer***

Tris-HCl, pH 7.5	20 mM
NaCl	200 mM
Triton	0.1%

Wash1 buffer

Phosphate buffered saline (PBS)	
DTT	1.0 mM
NaCl	0.5 mM

Wash2 buffer

Tris-HCl, pH 7.5	20 mM
NaCl	200 mM
DTT	1 mM
PMSF	1 mM

Wash3 buffer

Tris-HCl, pH 8.0	50 mM
NaCl	150 mM
DTT	1 mM

Plasmid DNA was kindly provided by Dr. Thomas Reubold. Transformation of the plasmid was directly done in expression cells (*E. coli* BL21). Overnight primary culture was used to inoculate 6 l secondary culture. Cells were grown at 37°C until the cell density

reached up to 0.8 OD₆₀₀. 0.3 mM IPTG was used for induction. Cells were allowed to grow overnight at room temperature. Cells were harvested at 4,000 rpm for 15 min. Cells were washed once with ice cold PBS. 0.5 mM PMSF, 4 Roche[®] protease cocktail tablets and 10 mg of lysozyme per gram of cell were added along with lysis buffer. For about 45 min cells were slowly rocked in cold room. Cells were sonicated for 8 min with 2 min interval for each pulse of 1 min. Cells were centrifuged for 45 min, at 15,000 rpm using JLA16.250 rotor. In meantime *Glutathione Sepharose 4B* From GE Healthcare (10 mL bed volume) was washed with distilled water and PBS. The supernatant was allowed for batch binding with the beads for approximately 20 min with slow rocking. At very slow rate by gravity flow the supernatant was collected. Three wash step purification was carried out with following buffers; 50 mL of wash1 buffer, 25 mL of wash2 buffer and finally with 25 mL of wash3 buffer. The protein was finally eluted with wash3 buffer with 10 mM Glutathione reduced (15mL). The fractions were checked by SDS PAGE. The peak fractions were pooled, concentrated and flash frozen using liquid nitrogen.

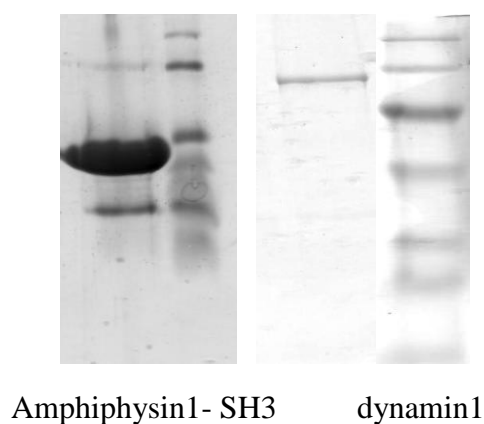


Figure 1: Gel picture showing, on the left amphiphysin1-SH3 domain and on the right dynamain1 purified using SH3 domain as affinity tag. Dynamain purified using this strategy was used for all the biochemical experiments.

2.19 Purification of Dynamain1

Lysis buffer

Hepes, pH 7.5	50 mM
NaCl	160 mM
KCl	30 mM
DTT	2 mM
EGTA	1 mM
EDTA	1 mM
Benzamidine	5 mM

Elution buffer

MES, pH 6.8	50 mM
NaCl	1.2 M
EGTA	1 mM
MgCl ₂	5 mM
DTT	2 mM

In this purification method, the knowledge that dynamin1 interacts with amphiphysin-SH3 domain was exploited to purify dynamin1 almost to purity of 95%. The vector, pFastBac-HTb which carries dynamin1 gene between the restriction sites BamHI and SalI is transformed into DH10BAC *E. coli* for bacmid preparation. The transformed DH10BAC cells were plated onto LB agar plates containing kanamycin 50 µg/mL, gentamicin 7 µg/mL, tetracycline 10 µg/mL, X-gal 100 µg/mL and IPTG 40 µg/mL. Following blue-white colony screening after 48 hrs, the positive white colonies were streaked again and incubated at 37 °C for 16 hr. Bacmid was prepared from this positive clone, and was used to transfect Sf9 cells using Cellfectin-reagent[®]. Hands on Invitrogen[®] protocol was used for transfection. After optimizing the amount of bacmids to use and cell density to use during transfection, P0 virus stocks were produced and for the P1 viral stock production P0 was used. Protein production at P1 stage was checked by lysing the cells and running SDS-PAGE. Further culture was scaled up to 6 l by infecting them with P1 viral stock. Times for harvesting cells were analyzed by time point experiment to check the protein production. Cells were harvested cells between 65 - 69 hrs after infection with P1 viral stock.

Cells after harvesting at appropriate time, was spun down at 2500 rpm for 6min. The obtained pellet was washed with cold PBS. Lysis buffer of volume 50 mL for pellet obtained from 1 l culture was used. Protease inhibitors TAME, TPCK, Leupeptin, PMSF were added to 1x from the stock of 100x. The pellet was re-suspended and kept in ice box and 50 mL more of the lysis buffer with protease inhibitors and 1% triton was added. The re-suspended cells

were rocked in an ice box for 45 min. After sonication of the cell for 2 min the suspension was spun at 15,000 rpm for 45 min using a JLA 16.250 rotor. In the meantime *Glutathione Sepharose 4B* from GE Healthcare[®] was washed with cold distilled water, PBS and lysis buffer at 3,000 g for 6 min for each. 250-500 µg of GST-Amphiphysin-SH3 protein was allowed for batch binding to the beads for 20 min. The supernatant from the Sf9 cells after centrifugation was mixed with the GST-Amphiphysin-SH3 incubated beads. The protein-protein complex was allowed for 20 min incubation in the cold room in a rocker at low speed. Glutathione Sepharose beads - GST-Amphiphysin-SH3-Supernatant was poured into a glass column and allowed to flow under gravity. Three wash steps were included before eluting the protein, wash1 was with PBS, wash2 was with lysis buffer with PMSF and other protease inhibitors, wash3 with lysis buffer alone. Finally the dynamin1 was eluted with 5 mL of elution buffer. Using SDS PAGE the samples were analyzed for purity. 95% pure protein was obtained. Protein was buffer exchanged with lysis buffer with 5 mM MgCl₂ using vivaspin20 concentrator from Sartorius[®].

2.20 Purification of Dynamin Related Protein1

Lysis buffer

HEPES, pH 7.5	50 mM
NaCl	300 mM
Benzamidine	5 mM
β-mercaptoethanol	7 mM
1mg/mL of lysis buffer Lysozyme	
PMSF	5 mM
Triton	1%

GPC buffer

HEPES, pH 7.4	50 mM
NaCl	100 mM
Benzamidine	5 mM
DTT	2 mM
MgCl ₂	5 mM

Drp1 expressing Rosetta[®] pLysS BL21 (DE3) cells were grown till the OD₆₀₀ of 1.1, and then the culture was induced with 0.5 mM IPTG, after induction cells were grown at room temperature for 9 hrs. Cells were harvested at 4200 rpm, for 20 min, the pellet was washed once with ice cold lysis buffer without protease inhibitors. 40 mL lysis buffer for one

liter of cell culture and a total volume of 240 ml of lysis buffer was used to resuspend the pellet. Complete, EDTA-free Protease inhibitor cocktail tablets in Easypack[®] used according to the manufacturer's protocol along with 40 µg of RNase was added and incubated for 20 min in ice with slow stirring in cold room followed by sonication for 15 min with 1 min interval for every one minute of sonication. The lysate was centrifuged at 13,000 rpm for 30 min using a JLA16.250 rotor. The supernatant was filtered using 0.22 µm syringe filters and loaded onto a NiNTA column which was washed with 5CV of lysis buffer with no additives. Supernatant was loaded at a flow rate of 2 mL per min. The column was washed with lysis buffer containing 20 mM Imidazole, pH 8.0 until absorbance measured at 280 nm has returned to base-line level. Bound protein was eluted in a gradient of 90 ml total volume starting with 20 mM imidazole to 500 mM imidazole, at the flow rate of 1 ml/min. Drp1 containing fractions were identified by SDS-PAGE and peak fractions were pooled and concentrated with 50 kDa cutoff Vivaspın20.

A Hiload[™] 26/60, Superdex[™] 200, Prep grade prepacked gel filtration column was used to further purify the protein. The column was equilibrated with 2 CV of GPC buffer. 7.8 mL loop was washed twice with GPC buffer. The concentrated protein was injected into the loop. Flow rate was maintained with keeping the pressure of the column under 0.5 MPa. Using a fractionation collector the eluted sample was collected and was analyzed with PAGE. Peak fractions were pooled, concentrated and aliquots of 50 µL were stored at -80°C. The obtained protein was 95% pure and was suitable for crystallization, kinetic and biochemical analysis.

2.21 Purification of Minimal Construct GG1 (dynamin1) and GGA (dynaminA)

The minimal construct was purified as maltose binding protein as fusion partner. The GG1 comprises of 6-320 residues of GTPase domain cloned between EcoRI, XbaI and 726-750 residues of C-terminal GTPase effector domain cloned between XbaI, HindIII similarly the GGA comprises of 2-316 residues of GTPase domain cloned between EcoRI, XbaI and 815-848 residues of C-terminal GTPase effector domain cloned between XbaI, HindIII both the constructs in pMALC2X vector from New England Biolabs (NEB).

MBPHK200

Hepes, pH 7.5	20 mM
KCl	200 mM
EDTA	1 mM
DTT	1 mM

MBPHK200+

Hepes, pH 7.5	20 mM
KCl	200 mM
EDTA	1 mM
DTT	1 mM
PMSF	10 mM
Roche Complete protease inhibitor cocktail	
Lysozyme 1mg/mL	

MBPHK25

Hepes, pH 7.5	20 mM
KCl	25 mM
EDTA	1 mM
DTT	1 mM

MBPHCBK100

Hepes, pH 7.5	20 mM
KCl	100 mM
EDTA	1 mM
DTT	1 mM

GFC buffer

Hepes, pH 7.5	20 mM
KCl	150 mM
MgCl ₂	4 mM
EGTA	2 mM
DTT	1 mM

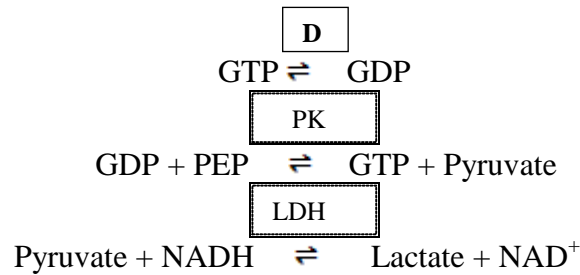
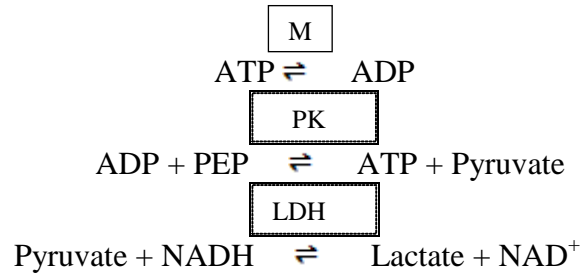
BL21 (DE3) bacterial cells carrying respective the construct with ampicillin as selection marker were used. An overnight primary culture was used to inoculate a 6 l secondary culture. Cells were grown at 37°C until the cell density reached up to 0.8 OD₆₀₀ using terrific broth (TB media). 0.3 mM IPTG was used for induction. Cells were allowed to grow for 6 hr at 30°C. Cells were harvested at 4000 rpm for 15 min. Cells were washed once with ice cold PBS. Cell pellet was further washed with MBPHK200 buffer. 20 ml of MBPHK200+ buffer per gram of cells *was* used to re-suspend the obtained pellet and the cell suspension were slowly rocked in cold room for 45 min. Cells were sonicated for 8 min with

2 min interval for each pulse of 1 min . Cells were centrifuged for 45 min, at 10,000 rpm using JLA16.250 rotor at 4°C. The lysate was further diluted with 30 ml MBPHK200 buffer. Amylose resin high flow from NEB was packed in a column and sequentially washed with filter sterile Millipore water and equilibrated with 3CV MBPHK200 buffer. The supernatant was passed through the column at 1 ml/min rate and washed with 5CV low salt MBPHK25 buffer. The protein was finally eluted with 10 mM Maltose. SDS PAGE was run to check the fractions. The peak fractions were collected and concentrated; further purified with Superdex 75 pre-packed gel filtration column using the GFC buffer, and the eluted protein was concentrated and frozen at -80°C.

2.22 Steady-State Kinetics

Steady state ATPase/GTPase activity assay, was performed using the PK/LDH - linked ATPase assay system. NADH oxidation was followed using an absorbance change with excitation at 340 nm. The assay was performed at 25° C in a buffer containing 25 mM HEPES, pH 7.5, 25 mM KCl and 5 mM MgCl₂, buffer condition vary for dynamins and dynamin-related proteins. Proteins to be investigated were added to a cuvette containing 0.5 mM DTT, 0.2 mM NADH, 0.5 mM phosphoenolpyruvate (PEP), 0.02 mg/mL lactate dehydrogenase (LDH), and 0.05 mg/mL pyruvate kinase (PK). Actin activation of myosin ATPase activity was measured by adding actin to the enzyme solution, finally 1 mM ATP or GTP according to the experiment, was added to this reaction mix to initiate the reaction, the change in NADH absorbance was recorded for periods of up to 900 s to 1800 s. **Table 5** shows the solubility of the psychotropic drugs that has been used in the inhibition of dynamin and dynamin related protein1 GTPase activity. The stock solutions were prepared and stored in -80 °C. The working solutions were diluted with 30 mM Tris for the assay.

Equation 1: Steady-state ATPase/GTPase assay. A coupled assay system reaction scheme and equation to calculate the activity.



$$\begin{array}{l}
 \Delta A = \epsilon_{\text{NADH}} * \Delta [\text{NADH}] * d \\
 \Delta [\text{NADH}] * = \Delta A / \epsilon_{\text{NADH}} * d \\
 \text{ATPase/GTPase} = \frac{-\Delta A}{60s * \epsilon * d * c}
 \end{array}$$

M.....Myosin

D.....Dynamin

ATP.....Adenosine-5'-triphosphate

ADP.....Adenosine diphosphate

GTP.....Guanosine-5'-triphosphate

GDP.....Guanosine diphosphate

PEP.....Phosphoenolpyruvate

NADH.....Nicotinamide adenine dinucleotide

ΔAChange in Absorbance (Oxidation of NADH to NAD^+)

ϵ_{NADH} 6220 $\text{M}^{-1}\text{cm}^{-1}$ (molar extinction coefficient for NADH at 340 nm)

d.....Path length (0.27cm)

c.....Concentration of the protein (μM)

Table 5: Summary of psychotropic drug's molecular weight and solubility

Name of the psychotropic drug	Molecular weight	solubility
Chlorpromazine	355.33	50 mg/mL in water
Clomipramine	351.33	25 mg/mL in water
Maprotiline	313.86	50 mg/mL in water
Fluoxetine	345.8	DMSO
Paroxetine	374.83	DMSO
Sertraline	342.69	DMSO >20 mg/mL
Fluvoxamine	434.41	DMSO

2.23 Stopped Flow Kinetics

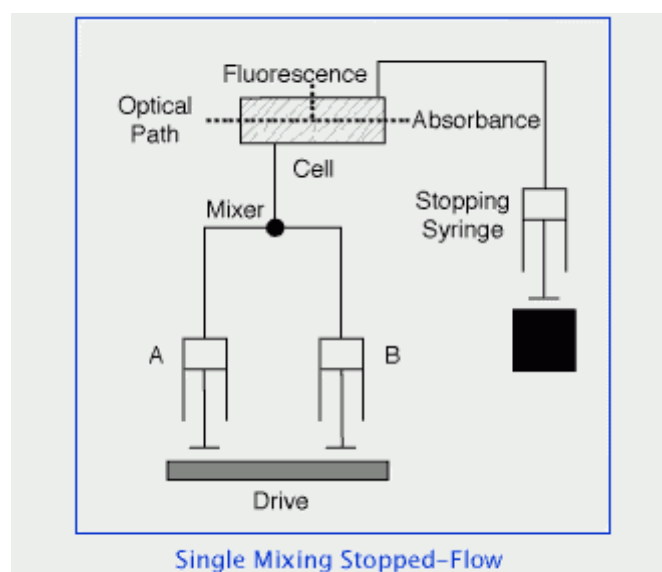


Figure 2: Sketch diagram of a single mixing stopped flow instrument.

Stopped flow techniques were performed to study the chemical kinetics of solutions. Two reactant solutions were mixed rapidly with constant volumes. The reactions can be monitored, followed as a function of time. The readout is change in absorbance or

fluorescence, binding of nucleotide to proteins was studied with mant-analogues of ATP/GTP and ADP/GDP. The mant-analogues were excited directly at 365nm and the emitted light was detected after passage through a KV389 cut-off filter. Data analysis was carried out using the Kinetic studio 1.08 software. The **Fig. 2** is the single mixing sketch of the stopped flow apparatus which was used in this work to study transient kinetics (www.hitechsci.com/techniques/stoppedflow).

2.24 *In-vitro* Motility Assay

2.24.1 Buffers

Assay buffer (AB)

Imidazol pH 7.4	25 mM
KCl	25 mM
MgCl ₂	4 mM
EGTA*	1 mM
DTT *	10 mM

*Freshly added

Buffer I

BSA/AB	0.5 mg/ml BSA in AB
--------	---------------------

Buffer II

Glucose §	5 mg/ml
Glucose oxidase §	0.1 mg/ml
Catalase§	0.02 mg/ml

§20µl of each stock solutions in 1 ml of buffer I

ATP Stock Solution

ATP	2 mM in buffer I
-----	------------------

Stock solutions stored at -20 °C

2.24.2 Actin Labelling

Rabbit skeletal actin was labelled with TRITC-Phalloidin. 2µM F-actin was sheared by pipetting up and down in buffer I. Dilute this actin 100 times in the same buffer and incubated with phalloidin on ice over night with gentle rocking.

2.24.3 Flow Cell Construction

Nitrocellulose solution is prepared in 1% amyloacetate. The micro centrifuge tube containing the solution is tightly sealed with para film and incubated in room temperature. Distilled water is taken in a 2 l beaker. Using 20 μ l pipette carefully the surface of the water was layered with a drop of nitrocellulose solution slowly. 18mm square coverslips are coated with a nitrocellulose film that is formed on a clean water surface. Remove the coverslips and keep in a clean tray to drip of the water, once the coverslip is ready prepare the glass slide. Place two parallel glue band about 10 mm apart onto the slide which by itself acts as spacers and creates a channel between them once the cover slip is placed, the coated side of the coverslip is faced inside. Store the flow cells at 4 °C.

2.24.4 Assay Procedure

Once the flow cell is prepared, the steps mentioned below were followed

1. Add 7 to 8 μ L of 0.025 mg/ml HIS antibody and incubate the flow cell for 5 min
2. Add 30 to 50 μ L of Assay Buffer(AB)
3. Add 7 to 8 μ L of myosin with 2R repeat of interest, in our case (we used myosin2-765-2R construct) and incubate the flow cell for 4 min
4. Wash once with buffer I
5. Add 10 μ L of Unlabeled actin (2 μ M) and incubate it for 2 min
6. Add 30 to 50 μ L of buffer III (ATP)
7. Add 30 to 50 μ L of Assay Buffer (AB) and wash the flow cell once
8. Add 30 to 50 μ L of Assay Buffer (AB) and wash once
9. Add 10 μ l of labeled actin and incubate it for 2 min
10. Add 30 to 50 μ L of Buffer II
11. Mount it for visualizations
12. Initiate the reaction with bufferII containing ATP
13. Mount the flow cell for recordings

2.24.5 Hardware and Software

The movement of actin filaments over the myosin-decorated nitrocellulose surface was determined with an Olympus IX70 microscope equipped with an 60x oil-immersion objective (PLAPO/TIRF) with temperature of 30°C enclosed in a box. The pixel size was defined by the reaction setup: When a camera-binning of 2x2, a microscopic magnification of 1.5 together with a 60-fold objective magnification was used, calibration with an object micrometre resulted in a pixel size of 0.144 μM . TRITC-fluorescence was excited at a wavelength of 545 nm and the fluorescence emission was detected at a wavelength of 570 nm. The corresponding filters were implemented in the microscope. Cell^R software for microscope control and data acquisition are used, Hamamatsu 1394 Orca-ERA CCD-camera for imaging, DiaTrack 3.01 is used for image processing and data analysis. Final histograms and graphs were prepared using Origin8G-8.0.63.988 SR6 software.

2.25 Microscale Thermophoresis

MST is a technique, which detects changes in the hydration shell of molecules and measures enzyme activities and bio molecules interactions under close to native conditions. Infrared lasers are used to produce precise microscale temperature gradients within thin glass capillaries that are filled with buffer of choice, in our study the buffer was 25mM HEPES pH 7.5, 100mM KCl, 5mM MgCl₂, and 1mM DTT. The small molecules of interest triiodophenol, pentabromophenol and tribromophenol were prepared in 90% DMSO as 100 mM stock solution, Myosin VI was labeled according to the manufacturer's protocol except for the buffer of choice. The labeled protein was kept at constant 118 nM concentration. The small molecules (TIP, PBPh, and TBP) with the starting concentration of 200 μM were serially diluted to yield a final concentration of 0.00305 nM (16 times). Four readings at different laser powers and heating the reaction mixture up to 30 sec and cooling for 5 s gave a thermophoresis curve, from which K_D value of the small molecule for the myosin VI was estimated. This is a recent biophysical method, which requires very less protein, highly efficient, less time consuming and can be useful for applications like protein-protein interaction, protein-lipid, protein-small molecule effector, protein-DNA interactions (Wienken et al., 2010).

2.26 Live Cell Total Internal Reflection Fluorescence (TIRF) Microscopy

The HeLa cell line used in this study was maintained at 37 °C in Dulbecco's Modified Eagle Medium (DMEM; Invitrogen, UK) supplemented with 10% fetal calf serum (FCS), 2 mM L-glutamine, and penicillin/streptomycin (Sigma-Aldrich, UK). To maintain selection for cells containing the relevant pQCXIP-S1-eGFP-FM4-FCS-hGH construct, this medium was also supplemented with puromycin (1.66 µg/mL).

For siRNA knockdown of myosin VI, we used a double knockdown protocol in which cells were transfected with a SMARTpool collection of four independent siRNA primers on days one and three using Oligofectamine (Invitrogen, UK) according to the manufacturer's instructions. Before siRNA knockdown, cells were grown to 70 percent confluence in a six well tray. For each knockdown, siRNA primers were diluted in Optimem I and transfected into individual wells of the six well tray at a final concentration of 90 nM. Efficiently depleted cells were imaged on day five.

For live cell Total Internal Reflection Fluorescence (TIRF) microscopy studies, cells were grown on 25-mm round coverslips (VWR International, UK) and imaged at 37° C in CO₂-independent medium (Invitrogen, UK). Imaging was conducted on a Zeiss TIRF 3 microscope (Carl Zeiss, Inc., UK) with a 488 nm argon laser line. Images were acquired with a 100x lens, Hamamatsu Photonics EM-CCD digital camera (Hamamatsu Photonics, Japan), and AxioVision Imaging Software (Carl Zeiss, Inc., UK). Samples were imaged in five minute intervals at maximum speed (approximately 4 frames per second) at points 25, 32, 39, 46, and 53 minutes after the addition of 1 µM AP21998.

2.27 Mass Spectrometry

Drp1 after phosphorylation by Cdk2/cyclinA, was loaded onto an SDS gel **Fig. 3**. The samples were treated with cystein alkylating agent, acrylamide at room temperature for 30 min, prior to loading to SDS gel. The sample has been digested using trypsin; the phosphopeptides were isolated and concentrated using TiO₂ (Titanium dioxide) beads. This work was done in collaboration with Prof. Andreas Pich, Mass spectrometry laboratory, Hannover Medical School.

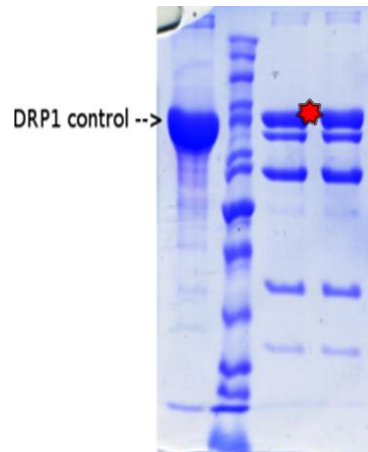


Figure 3: The protein sample sent for mass spectrometry analysis. The samples marked as red star on the gel indicates the Drp1 sample treated with Cdk2/CycA complex in the reaction mixture.

2.28 Crystallization of Proteins and Crystal Handling

2.28.1 X-Ray Diffraction

X-ray diffraction from crystalline solids occurs as a result of the interaction of X-rays with the electron charge distribution in the crystal lattice. The ordered nature of the electron charge distribution, whereby most of the electrons are distributed around atomic nuclei which are regularly arranged with translational periodicity, means that superposition of the scattered X-ray amplitudes will give rise to regions of constructive and destructive interference producing a diffraction pattern (Hiltner & Krieger, 1969; Marchesini et al, 2003).

The diffraction maxima are some times individually considered to be the result of diffraction of the incident X-ray beam of Wavelength (λ) from crystal lattice planes, having miller indices $h k l$ and spacing d_{hkl} . Diffraction occurs at an angle of incidence equal to the Bragg angle θ_B , i.e. Bragg's law is obeyed:

$$I = 2d_{hkl} \sin q_B$$

The way in which the separate scattered or diffracted rays combine to form an image depends on three factors associated with each ray: (a) the direction of the ray, (b) the amplitude and (c) the phases. In X-ray crystallography, the diffracted beams are separately observed and their intensities measured as the spots on an X-ray film or by direct quantum counting in a diffractometer (detector). By identifying the Miller indices (hkl) of the crystal plane-giving rise to each diffracted beam, the direction of the beam is specified. From the measured intensity of the beam its amplitude can be deduced by a simple relation, where the amplitude of the wave $|F_{hkl}|$ is proportional to the square root of the intensity measured on the detector. So the direction and the amplitudes information about each beam are known, but unfortunately there is no direct method available yet for observing the phases of each diffracted beams, which is the third necessary piece of information needed before mathematical recombination (Fourier calculations) is possible to produce an image of the structure. This constitutes what is known as the phase problem in crystallography (Taylor, 2003).

The solution of a crystal structure therefore consists of applying some technique for obtaining the approximate phases of at least some of the X-ray reflections (Molecular Replacement, Multiple Isomorphous Replacement, Single Anomalous Dispersion, Multiple Anomalous Dispersion and so on), and the process of structure refinement is one in which the knowledge of phases is extended to all reflections and is made as accurate as possible for all reflections. Apart from the direct methods of obtaining some initial phases, both the solution and refinement processes depend on the ability to calculate structure factors for a proposed approximate arrangement of some or all of the atoms in the crystal structure. It is possible to calculate simultaneously both the amplitude $|F_{hkl}|$ and phase α_{hkl} of each beam that would be diffracted by the proposed structure. Since the phases cannot be compared with any observable quantities, the validity of the proposed structure must be tested by comparison of the calculated values of the amplitudes of the structure factor F_c with the observed amplitudes $|F_0|$. This is represented by a *reliability index* or *R factor*:

$$R_{\text{factor}} = \frac{\sum |F_o| - |F_c|}{\sum |F_o|}$$

Electron density at a position (xyz) in the unit cell of a crystal is the summation of all the hkl planes, i.e. electron density at $(xyz) =$ the sum of contributions to the point (xyz) of waves scattered from plane (hkl) whose amplitude depends on the number of electrons in the plane, added with the correct relative phase relationship or, mathematically,

$$r(x, y, z) = \frac{1}{V} \sum_{hkl} \hat{a}_{hkl} |F_{hkl}| \exp(i a_{hkl}) \exp(-2\pi i (hx + ky + lz))$$

Where, V is the volume of the unit cell and α_{hkl} is the phase associated with the structure-factor amplitude $|F_{hkl}|$.

In this thesis, *D. discoideum* myosin II•carbazole complexes diffracted from 2.8 Å to 3.5 Å on Bruker proteum X8 rotating anode.

2.28.2 Hanging and Sitting Drop Vapor Diffusion

In the hanging and/or sitting drop vapor diffusion method, a small drop consisting of protein- and reservoir solution is equilibrated against a large volume of reservoir solution containing the precipitating agent. During the equilibration process between drop and reservoir, liquid is diffusing through the gas phase out of the drop into the reservoir. Thereby the concentration of protein and precipitating agent is slowly increased in the drop, leading to super saturation and ideally to conditions favorable for crystallization. Drops consisting of each 2 µl of protein and 2 µl of reservoir solution are equilibrated against 750 µl of reservoir solution in 24-well Limbro[®] plates (MP Biomedicals). The rim of each well is greased with vacuum grease from GE Bayer Silicones[™]. Cover slip 22 mm Thick Circles from Hampton Research[™] with drops of protein and reservoir is placed onto the well in hanging drop fashion. During screening or optimization of initial crystallization conditions plain cover slips from Jena Bioscience[™] are used. In the hanging drop method, the drop is placed on the coverslip so that it is hanging above the reservoir solution. In the sitting drop method the drop is placed on a micro bridge that is placed into the well.

2.28.3 Cryo-Protection of Crystals

During this work most of the data collection was carried out with cryo-cooled crystals, which are kept at 100 K by a stream of liquid nitrogen. Special care has to be taken during the process of freezing the crystals, as their diffraction quality can be impaired during freezing. Usually it is necessary to transfer the crystal to a solution containing a cryo-protectant prior to freezing in order to avoid the formation of ice crystals. The choice of the cryo-protectant can influence the diffraction quality of frozen crystals. A variety of cryo-protectants should be tested, namely sugars, alcohols, and low molecular weight PEGs. In an experiment to screen, mother liquor is mixed with various concentrations of the cryo-protectant. Then the minimal concentration of cryo-protectant that prevents the formation of ice-crystals is determined by forming a film using a MiTeGen micro mount nylon-loop and this cryo-protected mother liquor is completely soaked into a bath of liquid nitrogen followed by visual inspection of the frozen liquid film. The liquid film should not become opaque. The liquid film can be checked for ice rings in the x-ray beam. Then the behavior of the crystals in the cryo-protected mother liquor is examined under the light microscope, in order to sort out cryo-protectants that damage the crystals. In a final step, the diffraction properties of crystals mounted with various cryo-protectants are determined. Twenty five percent ethylene glycol I turned out to be a good cryo-protectant for all crystals produced during this work (with exception of the crystals of full-length dynamin3,). Usually, the concentration of the precipitating agent was slightly increased over that of the well-solution in the solution for cryo-protection. Optimal soak times have to be determined experimentally. In this work soaking times between 3 to 5 mins were used. When incorporating small molecules, reservoir and cryo-solutions containing the small molecules of interest were gradually diluted in four steps and the fifth step was 100% cryo-solution with small molecule. In each step, the crystal was soaked 3 min and finally the crystal was scooped up using a micromount loops and gently immersed in liquid nitrogen. The frozen crystals were stored in a magnetic cryo vials from Molecular Dimensions limitedTM.

2.28.4 Crystal Mounting for Data Collection

All data was collected under cryogenic conditions using an Oxford cryo-stream to cool the crystal during data collection. While mounting crystals for data collection, they need to be transferred from their storage containment to the goniometer without thawing. Crystal cap tubes are unscrewed while submersed in liquid nitrogen in a table top isotherm using a crystal

wand (Hampton) to hold the cap and using tweezers to hold the tube. A cryo-tongue (Hampton) is cooled in liquid nitrogen and used to transfer the crystal-cap with the crystal mounted in the loop from the table top isotherm to the goniometer.

2.28.5 Data Collection and Processing

Five test shots separated by a 90° rotation are taken to assess crystal quality. Data is collected using the oscillation method. The rotation angle is 0.5 or 1.0°, depending on the data quality obtained from the particular crystal. The important parameter that governs the data collection strategies are: unit cell of the crystal, orientation of the crystal's longest axis with respect to the incident X-ray beam and the crystal mosaicity. The exposure time has a role in improving data quality, but care must be taken not to destroy the crystal with very long exposure until or unless the crystal is stable. The detector used and its sensitivity to record the diffracted x-ray beam play crucial roles in data quality at high resolution. Data collection strategy, image handling, temperature maintenance were set by using the PROTEUM2 from BRUKER AXS, Integration of the data was performed using SAINT and SADABS was used to scale the data. Data reduction and quality were checked by using XPREP (Sheldrick GM).

The goal of data collection is to obtain data with completeness close to 100 %. Whenever long exposure time is used in order to obtain high resolution reflections care has to be taken that low-resolution spots are not saturated. The data is cut at an R_{merged}^F of about 40 % or an R_{meas} of about 30 % or I/σ cut-off 2. XDS -**X-ray Detector Software** (Kabsch, 1993) is used for data processing of data obtained from a single crystal monochromatic diffraction; the data is processed using the following three input scripts namely XDS.INP, XSCALE.INP and XDSCONV.INP

2.28.6 Structure Solution, Refinement and Model Building

The software packages CNS, CCP4, COOT (Brunger *et al.*, 1998; Murshudov *et al.*, 1996; Potterton *et al.*, 2003; Pottertonagin *et al.*, 2004; Emsley) were used during structure solution, refinement and model building. CNS was also used for model preparation for molecular replacement (MR); in most cases the default settings of the provided input files were used. MR phases and CNS model were used in automated model building using Arp/wARP, which is used for phase improvement and interpretation of electron density. Additional phase information that came from Arp /wARP was used and refined with refmac.

2.28.7 Simulated Annealing

During model preparation for molecular replacement, simulated annealing was performed to minimize the model structure, Torsion angle dynamics was used for this purpose. With 200 minimization cycles to regularize geometry preceded the torsion angle molecular dynamics. The slow cool protocol was used with the starting temperature of 3000 K and the drop in temperature per cycle was set to 25 K. finally after 100 cycles of minimization, the coordinates were used in for initial model building and phase improvement.

2.28.8 Model Building, Structure Interpretation and Figure Preparations

The molecular model is built into the electron density using the program Coot whenever necessary in case if automated model building fails to work. The model after simulated annealing and the structure factor files prepared from XDS were used in Arp/wARP, the refinement and model building were done hand in hand using reftmac for refinement and Coot for electron density interpretation. The structure was viewed in Coot or using the PyMol Schrodinger, LLC[®]. Figures were prepared using PyMol, and measurements of hydrogen bond length, electrostatic surface representation are calculated using Coot.

2.28.9 Data Processing Software and Modules

Table 6: Software used and the versions

Programs/Software suite/Modules	Version
CCP4 suite	6.0.2
CCP4 interface	1.4.4.2
Arp/wARP	7.0
Refmac5	5.5.0109
CNS_Solve	1.2
PyMol	1.2r3pre
COOT	0.6.1-pre-1
XDS	Version May 10,2010
Autodock	4.0
MGL tools	1.5.4
GOLD suite	V5.0
AutodockVina	1.1.1

CHAPTER 3

Results

3.1 Functional Characterization of Dynamin Related Protein1 (Drp1)

Dynamin related proteins (Drps) compose a diverse family of proteins that self-assemble in a GTP-dependent manner to assist remodeling of cellular membranes. The molecular mechanism by which Drps mediate membrane remodeling events and the specific role of their GTPase cycle is still not fully understood. Drp possess unique kinetic properties even though they are the members of the GTPase superfamily. Drp have relatively low affinity for guanine nucleotides but have high rates of GTP turnover and, under favorable conditions they self-assemble. Here, in the following studies I have used continuous, coupled steady-state assay that overcomes the limitations of the fixed time point assays. This can be used for the kinetic analysis of Drp GTPase activity under unassembled and assembled conditions (Ingerman and Nunnari, 2005).

3.1.1 Ionic Strength Dependence and Cooperativity of Drp1 GTPase Activity

Steady-state GTPase activity of Drp1 were performed with an NADH/PK coupled enzyme assay under standard assay condition (25 mM HEPES, 50 mM NaCl, 1 mM DTT, 5 mM MgCl₂). **Fig. 1** shows the dependence of the GTPase on Drp1 concentration over a range of 0-40 μ M. The rate of GTP hydrolysis increases in a sigmoidal manner indicating a cooperative behaviour (**Fig. 1**, open triangle). Data points were fit with a Hill equation yielding a K_D value of $22.57 \pm 5.18 \mu$ M and a Hill-coefficient $n = 2.99 \pm 1.78$. Interestingly, at high salt conditions (300 mM NaCl) the GTPase activity of Drp1 remained constant irrespective of the protein concentrations (**Fig. 1**, black circles) showing that the cooperative nature of the Drp1-Drp1 interaction is reduced by salt. This is in agreement with earlier work on dynamins demonstrating the ionic basis of the interaction between dynamin molecules. The cooperative behaviour has been demonstrated earlier for dynamin1 (Binns et al., 1999; Binns et al., 2000).

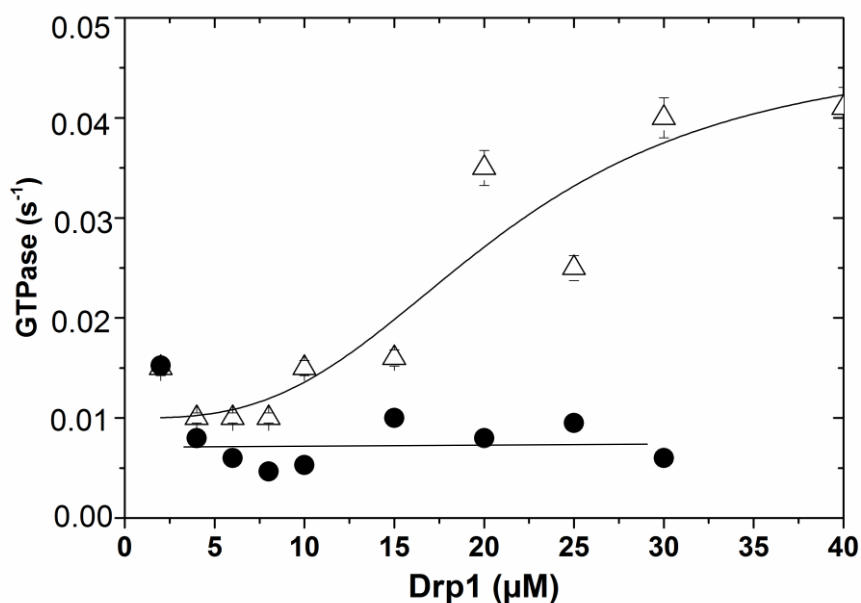


Figure 1: Steady-state GTPase activity of Drp1. GTPase activity as a function of Drp1 concentration at low (black) and high (triangle) ionic strengths. The open triangles indicate 50 mM NaCl (low) concentration, whereas the black circle represents 150 mM NaCl (high) concentration. The rate of GTPase hydrolysis of Drp1 from separate steady-state measurement is 0.07 s^{-1} (values mentioned are normalized with protein concentrations; here and elsewhere in this work) which is very low compared to classical human dynamin1 which has the GTP hydrolysis rate of 0.7 s^{-1} ten times higher. A saturating amount of GTP concentration of 1 mM was used in the steady-state GTPase assays in the reaction mix.

3.1.2 Transient Kinetic Characterization of Drp1 Interactions with Nucleotides

Stopped-flow techniques in combination with a spectrometer, which is calibrated to detect changes in fluorescence signal intensity at a defined wavelength over a fixed time, can be used to study enzyme mechanisms on a milliseconds scale. After two solutions are mixed the change in conformation upon substrate binding can be correlated to the intrinsic tryptophan. But in the case of Drp1, GTP analogs which are fluorescent nucleotides were used as Drp1's substrate since there is no detectable intrinsic fluorescence change detected. The binding of mantd-guanosine nucleotides to Drp1 was investigated under pseudo-first-order conditions. Binding of GTP and GDP to Drp1 was studied with mant-analogues of GTP and GDP. The mant-analogues were excited directly at 365 nm and the emitted light was detected after passage through a KV389 cut-off filter. MantdGTP, mantdGDP binding and mantdGTP, mantGTP- γ -S,

mantdGDP release kinetics at 1 μM Drp1 concentration and range of nucleotide analog concentrations were titrated and the curves were fitted with single exponential fit. A very simple enzymatic scheme was modeled and K_1 (μM^{-1}) and k_{+2} (s^{-1}) were determined. The enzymatic mechanism was followed as shown in the scheme 1.



Scheme 1: Enzymatic reaction scheme for Drp1 with its substrate mant nucleotides (Binns et al., 2000).

3.1.2.1 GTP Binding to Drp1

The binding of fluorescent nucleotide analogues to Drp1 was investigated by monitoring mant-fluorescence at different concentrations of nucleotide. **Fig. 2a** shows the change in fluorescence upon mixing 70 μM mantdGTP with 2 μM Drp1. The change in fluorescence follows a single exponential curve with rate constants (k_{obs}) **Fig. 2c**. There are several possible mechanisms of binding of mantdGTP to Drp1 that could give rise to this type of behavior. These are described previously (Bagshaw, 1977; Bagshaw et al., 1974; Bagshaw and Trentham, 1974) in interpreting their results of the binding of ATP to myosin subfragment1. The one possibility considered here is that the hyperbolic behavior arises from the binding of mantdGTP to Drp1 being a two-step process in which there is a rapid equilibrium to form a collision complex, followed by an isomerization of this complex in a process which reports the change of fluorescence intensity.

In the mantdGTP binding to Drp1 study, it was observed that upon mixing 2 μM Drp1 with 70 μM mantdGTP an increase in fluorescence intensity of 2% was observed that could be well fitted to a single exponential with a rate constant k_{obs} of $15.2 \pm 0.39 \text{ s}^{-1}$. The dependence of the observed rate constant of binding of mantdGTP to Drp1 was investigated over the range of 5-150 μM mantdGTP. As the concentration of mantdGTP increased, the background fluorescence signal also increased with a reduction in the signal from the binding reaction. Therefore, measurements could not be made above this concentration. The estimated $1/K_1$ which is dissociation equilibrium constant for mantdGTP binding to Drp1 is $76.9 \pm 4.30 \mu\text{M}$ and rate constant k_{+2} is $15.2 \pm 0.39 \text{ s}^{-1}$ and the estimated k_{-2} from plotting initial rate constant was determined to be $10.95 \pm 1.35 \text{ s}^{-1}$. In comparison to the classical dynamin2 from previously published data, the affinity of mantdGTP to Drp1 is higher than the affinity of mantdGTP to

dynmain2 which is $91 \mu\text{M}$ and the k_{+2} or the rate of isomerization complex to the collision complex is ~ 18 times lesser for Drp1 in comparison to dynamin2.

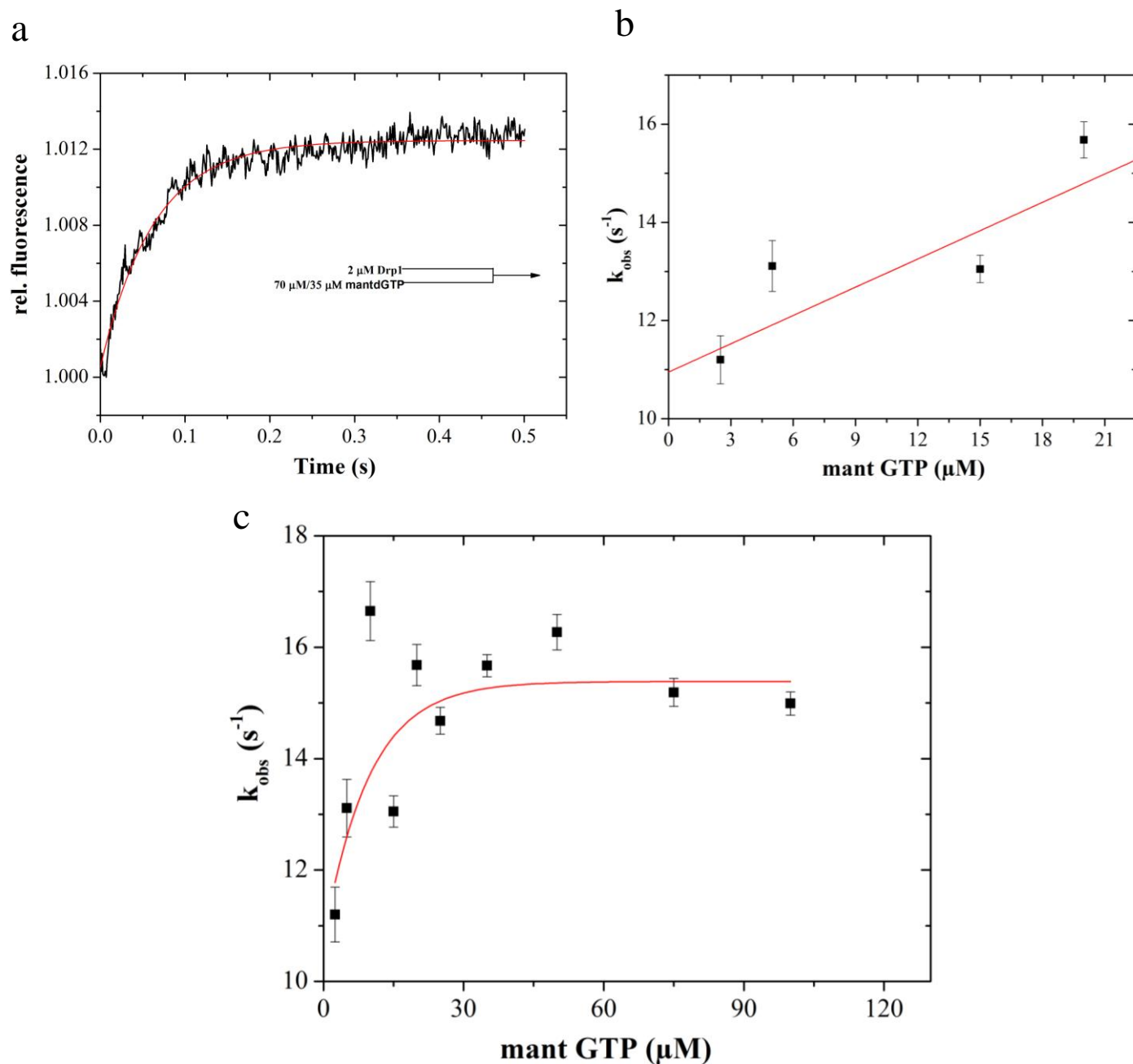


Figure 2: (a) Stopped-flow fluorescence record of the fluorescence change upon mixing $2 \mu\text{M}$ Drp1 with $70 \mu\text{M}$ mantdGTP. Transient shown is the average of four to six consecutive shots in the stopped-flow apparatus. (b) Rate of mantdGTP-binding to Drp1. Dependence of the observed rate constant of fluorescence change on mantdGTP-concentration. The second order rate constant (K_1k_{+2}) $0.19 \pm 0.09 \mu\text{M}^{-1}\text{s}^{-1}$ were obtained from the slope. (c) Dependence of the observed rate constant of the binding of mantGTP to Drp1 on nucleotide concentration from $1 - 150 \mu\text{M}$. The experiments were performed at $23 \text{ }^\circ\text{C}$; statistical analysis and model fitting were carried out using the Kinetic studio 1.08 software and Origin8.

3.1.2.2 GDP Binding to Drp1

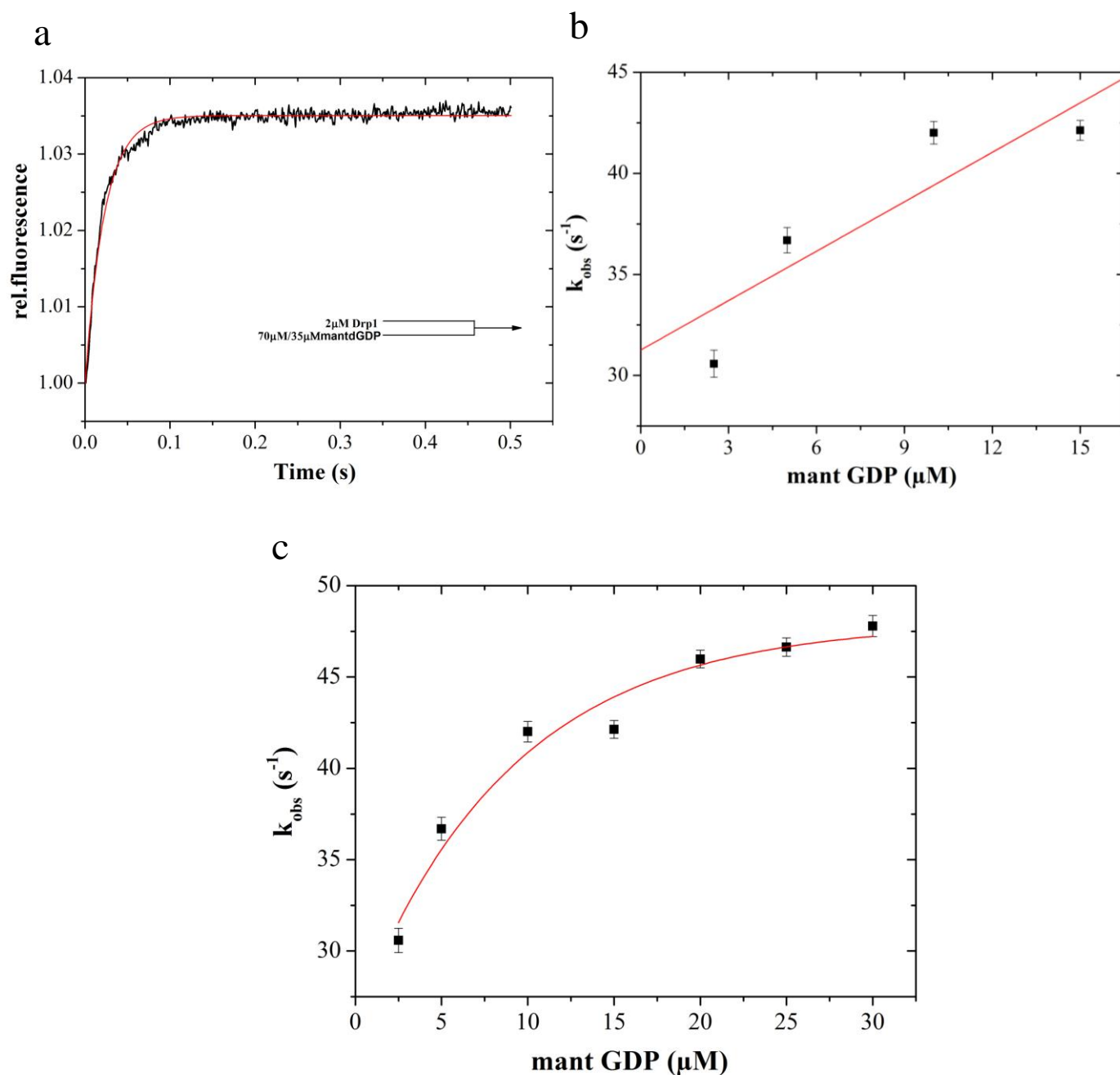


Figure 3: (a) Stopped-flow fluorescence record of the fluorescence change upon mixing 2 μM Drp1 with 70 μM mantdGDP. Transient shown is the average of four to six consecutive shots in the stopped-flow apparatus. (b) Rate of mantdGDP-binding to Drp1. Dependence of the observed rate constant of fluorescence change on mantdGTP-concentration. The second order rate constant (K_1k_{+2}) $0.82 \pm 0.29 \mu\text{M}^{-1}\text{s}^{-1}$ were obtained from the slope. (c) Dependence of the observed rate constant of the binding of mantGTP to Drp1 on nucleotide concentration from 0 – 30 μM . The experiments were performed at 23 $^\circ\text{C}$; statistical analysis and model fitting were carried out using the Kinetic studio 1.08 software and Origin8.

Similar binding measurements were made with mantdGDP. Again an exponential increase in fluorescence was observed as it was for mantdGTP, but this was faster and of higher amplitude than that observed for mantdGTP. For example, at 35 μ M mantdGDP, the increase in fluorescence was 4% (**Fig. 3a**). The increase in signal to noise ratio with respect to the increase in mantdGDP concentration limited measurements of mantdGDP binding to Drp1 to the range of 2.5- 35 μ M. The observed rate constant of this process was shown to be exponentially dependent on mantdGDP concentration (**Fig. 3c**). This is the expected behavior of a two-step binding process.

The maximum observed rate constant k_{+2} was $48.10 \pm 1.65 \text{ s}^{-1}$, and the estimated $1/K_1$ for GDP binding is $58.8 \pm 5.71 \text{ }\mu\text{M}^{-1}$. On the basis of the slope of the line in **Fig. 3b**, the apparent second order binding constant K_1k_{+2} is $0.82 \pm 0.29 \text{ }\mu\text{M}^{-1}\text{s}^{-1}$. The intercept gives k_{-2} 31.25 ± 3.11 which is a estimation of *off* rate value for mantdGDP to Drp1. However, the concentration range at which the reaction could be studied was more limited than that of mantdGTP, and it cannot be excluded that mantdGDP, like mantdGTP, also binds to Drp1 by a more complex mechanism. In a comparative study with dynamin2 mantdGDP binding, Drp1 has 3 times lesser affinity for mantdGDP. But in both Drp1 and dynamin2, the affinity for mantdGDP is higher than affinity for mantdGTP.

3.1.2.3 Nucleotide Dissociation Kinetics of Drp1

To understand and gain more information about the dissociation of mantd-nucleotides from Drp1, a solution containing Drp1 with mantd-nucleotide was rapidly mixed with a large excess of GTP. **Fig. 4a** shows that on mixing a solution of 1 μ M Drp1, 2 μ M mantdGTP with a solution of 500 μ M GTP, there was a 4% decrease in fluorescence. This could be fitted to a single exponential with a rate constant of $6.61 \pm 0.18 \text{ s}^{-1}$, the displacement of mantGTP- γ -S with 500 μ M GTP yielded a rate constant of $8.02 \pm 0.12 \text{ s}^{-1}$ **Fig. 4b** and there was a 10% decrease in fluorescence. The displacement of mantdGDP with a solution of 500 μ M GDP **Fig. 5a** was also fitted to a single exponential with a rate constant of $31.22 \pm 0.34 \text{ s}^{-1}$ and the decrease in fluorescence was $\sim 10\%$.

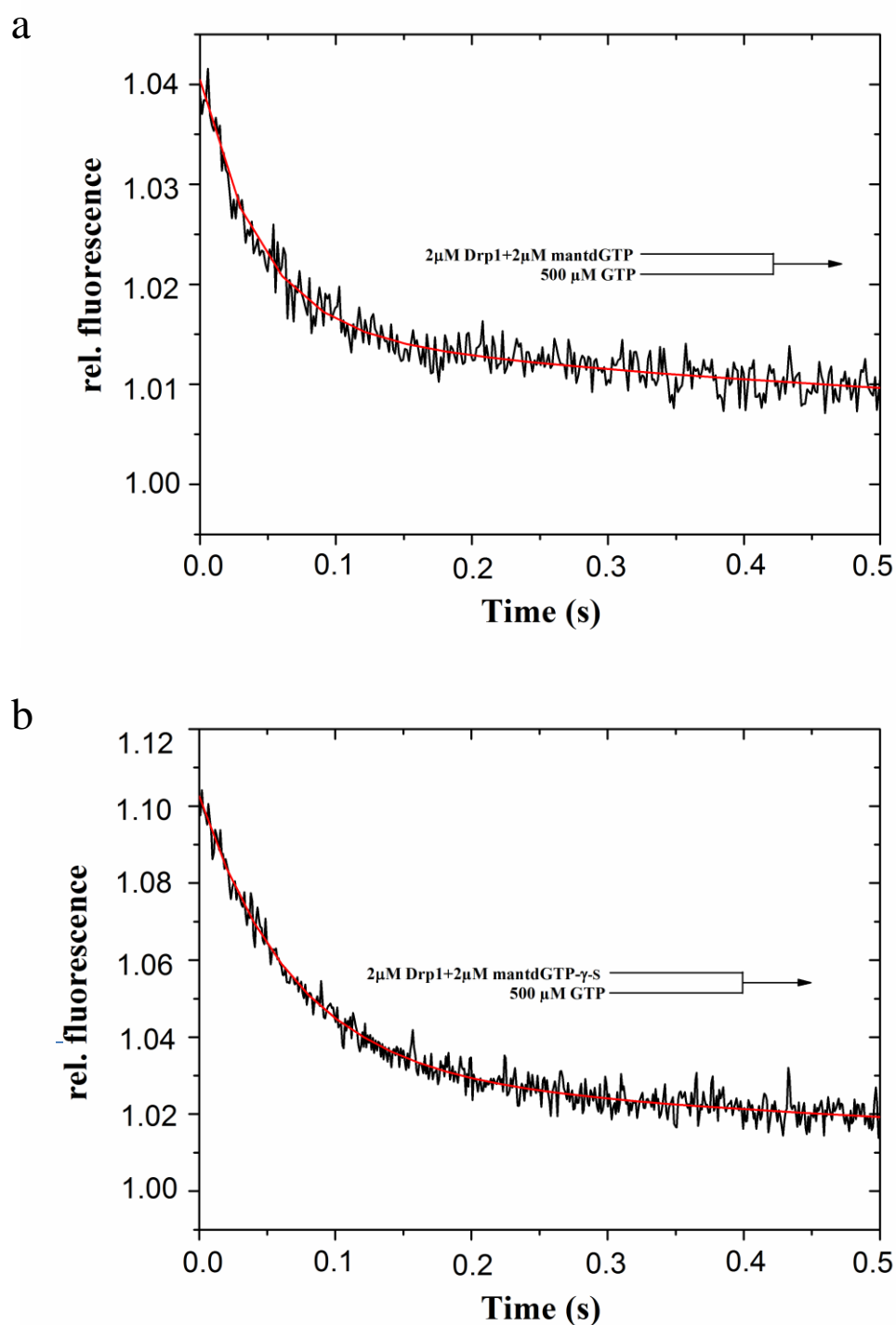


Figure 4: Stopped-flow fluorescence record of the displacement of mantdGTP from Drp1. (a) One syringe contained 2 μ M Drp1, 2 μ M mantdGTP, and the other syringe contained 500 μ M GTP. The plot is for a fit to a single exponential with a rate constant of $6.61 \pm 0.18 \text{ s}^{-1}$ (b) One syringe contained 2 μ M Drp1, 2 μ M mantdGTP- γ -S, and the other contained 500 μ M GTP. The line is a fit to a single exponential with a rate constant of $8.02 \pm 0.12 \text{ s}^{-1}$. The data represent six reactions averaged.

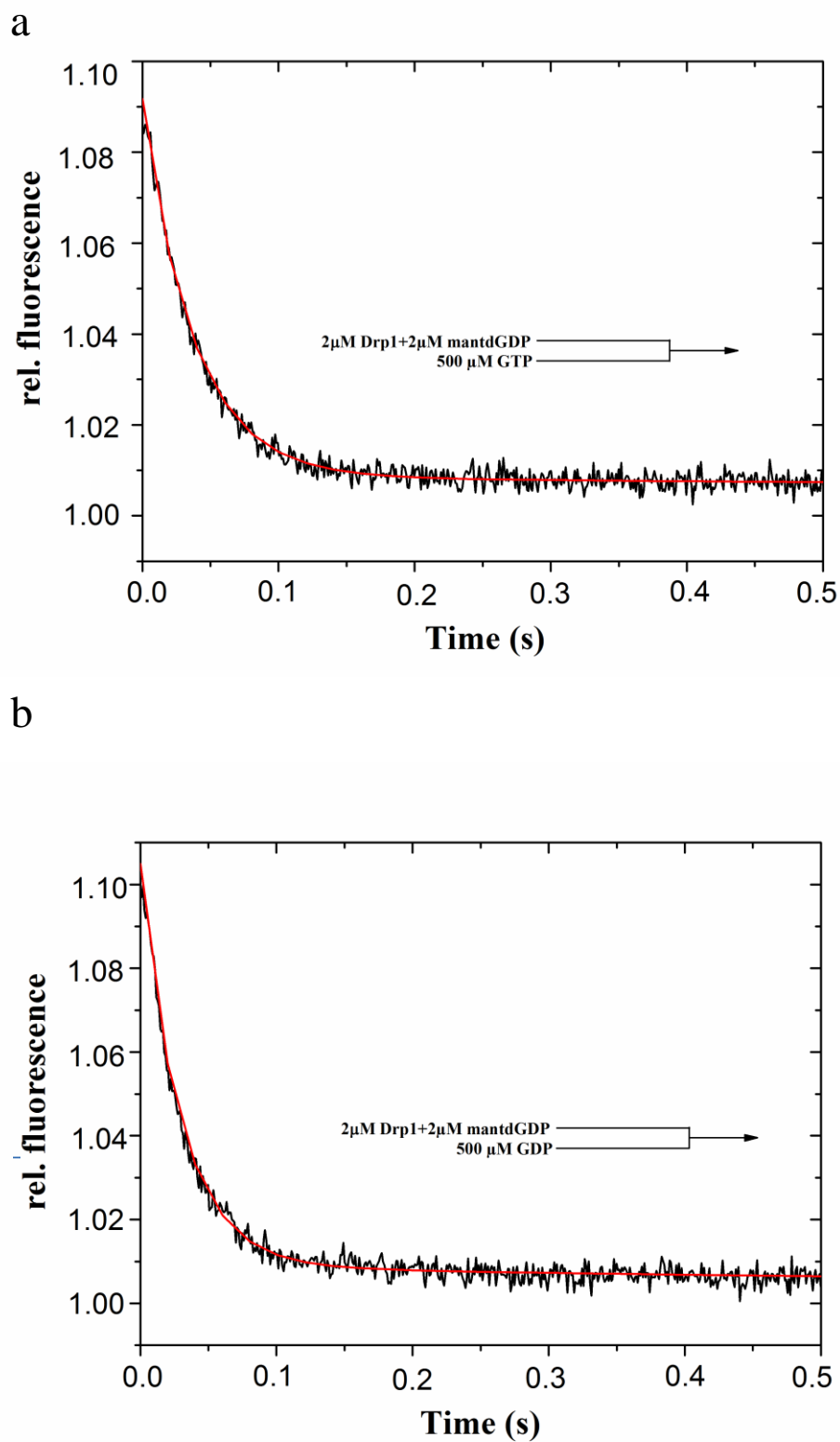


Figure 5: Stopped-flow fluorescence record of the displacement of mantdGDP from Drp1. (c) One syringe contained 2 μ M Drp1, 2 μ M mantdGDP, and the other syringe contained 500 μ M GTP. The plot is for a fit to a single exponential with a rate constant of $26.78 \pm 0.33 \text{ s}^{-1}$ (d) One syringe contained 2 μ M Drp1, 2 μ M mantdGDP, and the other contained 500 μ M GDP. The line is a fit to a single exponential with a rate constant of $31.22 \pm 0.34 \text{ s}^{-1}$. The data represent six reactions averaged.

In comparison to that of dynamin2 mantd-nucleotides release, Drp1 has ~5.7 time higher mantdGTP release rate and ~1.7 time higher release rate for mantdGDP. Where dynamin2 has a rate constant of 1.4 s^{-1} for mantdGTP release and $18.2 \pm 1.3 \text{ s}^{-1}$ for mantdGDP release.

3.1.2.4 Summary of Nucleotide Binding and Nucleotide Dissociation Kinetics

Interactions of Drp1 with mantdGTP and mantdGDP have been shown as two-step process. The data have been interpreted in terms of an initial rapidly reversible process with an equilibrium constant K_1 (mantdGTP) of $1.2 \times 10^4 \text{ M}^{-1}$ followed by an isomerization of the Drp1-mantdGTP complex with a rate constant of $15.2 \pm 0.39 \text{ s}^{-1}$. This results in an apparent second-order binding constant of $0.19 \pm 0.09 \times 10^6 \text{ M}^{-1} \text{ s}^{-1}$. However, other mechanisms are also possible i.e. an isomerization of the Drp1 prior to binding mantdGTP or two distinct modes of mantdGTP binding to Drp1 resulting in an equilibrium mixture of both complexes. Unlike dynamin2, Drp1 shows two-step process for mantdGDP binding with an equilibrium constant K_1 (mantdGDP) of $1.7 \times 10^4 \text{ M}^{-1}$ followed by an isomerization of the Drp1-mantdGDP complex with a rate constant of $47.99 \pm 1.65 \text{ s}^{-1}$. Dissociation of mantdGTP and mantdGDP from Drp1 shows complex behavior.

Table 7: Summary of kinetic data of Drp1 in comparison to dynamin2 kinetics.

Nucleotide	$1/K_1$ (μM)	$K_1 k_{+2}$ ($\mu\text{M}^{-1} \text{s}^{-1}$)	k_{+2} (s^{-1})	k_{off} (s^{-1}) (intercept)	k_{off} (s^{-1})
Drp1					
mantdGTP	76.9 ± 4.30	0.19 ± 0.09	15.2 ± 0.39	10.95 ± 1.35	8.02 ± 0.12
mantdGDP	58.8 ± 5.71	0.82 ± 0.29	47.99 ± 1.65	31.25 ± 3.11	31.22 ± 0.34
Dynamin2*					
mantdGTP	91.0	3.0	280	-	3.1 ± 0.3
mantdGDP	19.4	3.3	-	64	88 ± 15

Since mantdGTP exists as a single isomer, any speculation on biphasic behavior could be ruled out for Drp1. From the above study, it was found that the association rate constant of mantdGDP is higher than for the mantdGTP. Also, the above study was done in a salt

concentration where Drp1 could not self-assemble which means the GED activation of GTPase is not likely to take place, thus this is only the basal GTPase characterization.

3.2 Mdivi-1 and Sertraline Binding Properties to Drp1

Sertraline (**Fig. 6**) is a selective serotonin reuptake inhibitor. To keep the extracellular serotonin level, and to prevent it from binding to pre-synaptic receptors, sertraline is used as an antagonist against agonist serotonin. It is a FDA (Food and Drug Administrations) approved drug in the treatment of panic disorder, obsessive-compulsive disorder, depression and bulimia. The pathway by which sertraline is metabolized remains unclear. But it has been shown to be de-aminated by monoamine oxidases, a protein which is found on the outer membrane of the mitochondria.

Whereas, mdivi-1 **Fig. 6** is a direct mitochondrial division attenuator and also attenuates apoptosis indirectly (Cassidy-Stone et al., 2008; Tanaka and Youle, 2008). It seems to interact specifically with Dnm1, a yeast orthologous of human Drp1. The mechanism of action of this drug is also unclear. But it has been shown that the basal GTP hydrolysis of Dnm1 is not affected by mdivi-1. The attenuation effect of mdivi-1 on division and apoptosis is speculated to be through the inhibition of assembly of Dnm1 around mitochondria.

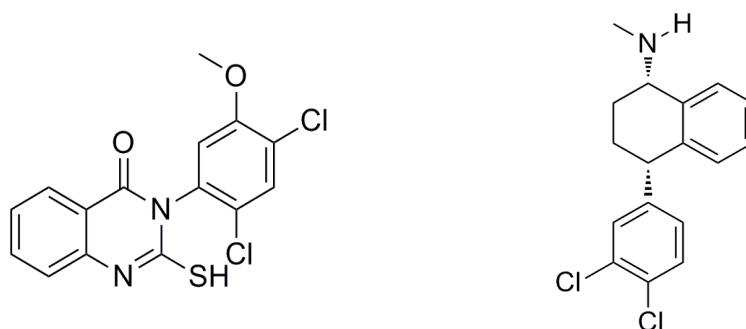


Figure 6: Chemical structures of mdivi-1 and sertraline.

Thus we characterized the affinity of sertraline and mdivi-1 for Drp1. The binding of sertraline changed the fluorescence intensity of labeled Drp1 in microscale thermophoresis experiment in concentration dependent manner. The K_D value obtained after the fit was $0.914 \mu\text{M}$ for sertraline to Drp1, whereas the K_D value of mdivi-1 for Drp1 is $0.26 \mu\text{M}$ **Fig. 7**. Thus both sertraline and mdivi-1 influences the fluorescence property of the labeled Drp1 implying that they can interact with Drp1 even at sub-micro molar concentrations.

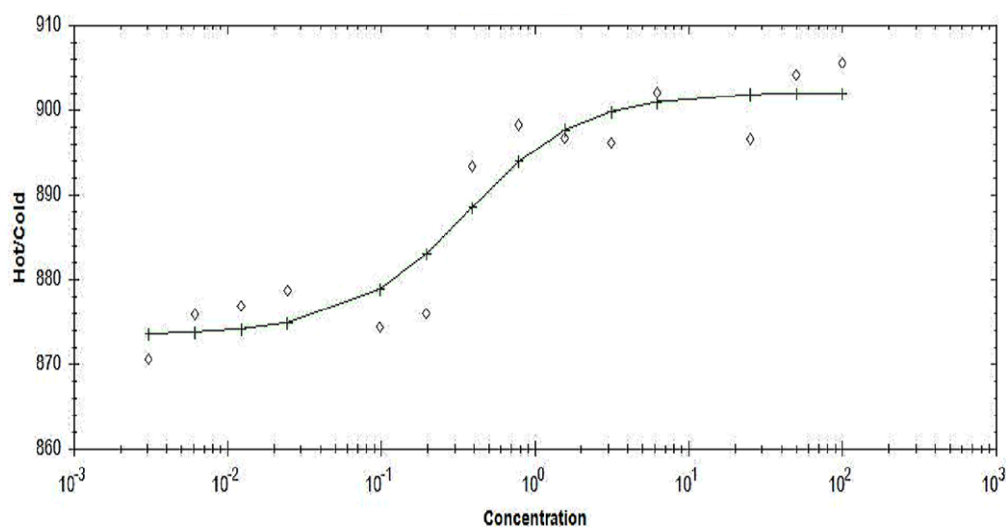
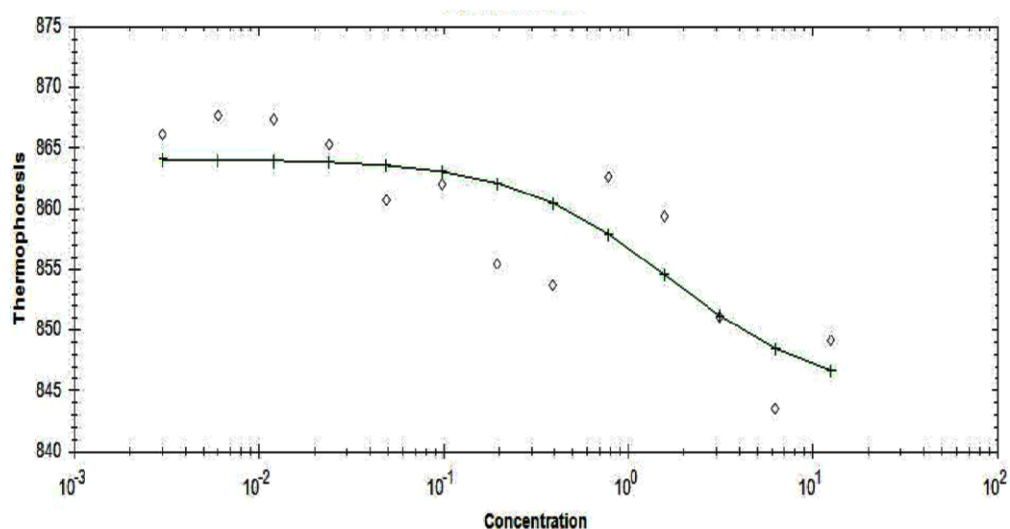
a**b**

Figure 7: Graphs showing the thermophoresis and hot/cold effect upon binding of sertraline and mdiv1 in microscale thermophoresis experiment. The data is fitted to the fluorescence change due to hot/cold effect and thermophoresis effect. The y-axis represents the change in fluorescence, whereas the x-axis represents the concentration range of the sertraline and mdiv1. The affinity of the effectors mdivi-1 and sertraline for Drp1 is obtained from the fitting of the K_D equation.

3.3 Assembly Properties of Drp1 Studied by Dynamic Light Scattering

GTPase activity of classical dynamin increases as a function of dynamin concentration (Tuma and Collins, 1994), this finding suggests that dynamin self-association is an important feature in the regulation of its enzymatic activity. The cooperative nature of the dynamin-

dynamain interaction is influenced by salt, implying that the ionic basis of this interaction and its importance. At low salt concentration (25-50 mM NaCl) dynamain self-assembles into large, sedimentable structures composed of rings and stacks of interconnected rings (Hinshaw and Schmid, 1995). Owing to this idea, and to check whether Drp1 possess similar properties we conducted series of experiments.

3.3.1 Salt Dependence of Drp1 Self-Assembly

To monitor the state of isolated Drp1 and to examine the assembly property at a given salt condition dynamic light scattering (DLS) method was used. The mass and intensity distribution profile for Drp1 under different salt conditions were analyzed. DLS yields the hydrodynamic radius of a species in solution and thus reflects the state of association at a given condition. Viscotek 802 DLS machine equipped with OmniSize acquisition and control software was used, sample volumes of 15 to 20 μL were very carefully pipetted into a quartz sample cell. Each time the sample cell was washed thoroughly with 2% SDS followed by filtered distilled water. This was done to avoid noise from dust particle during the course of the measurement. The experiment was performed at 22°C.

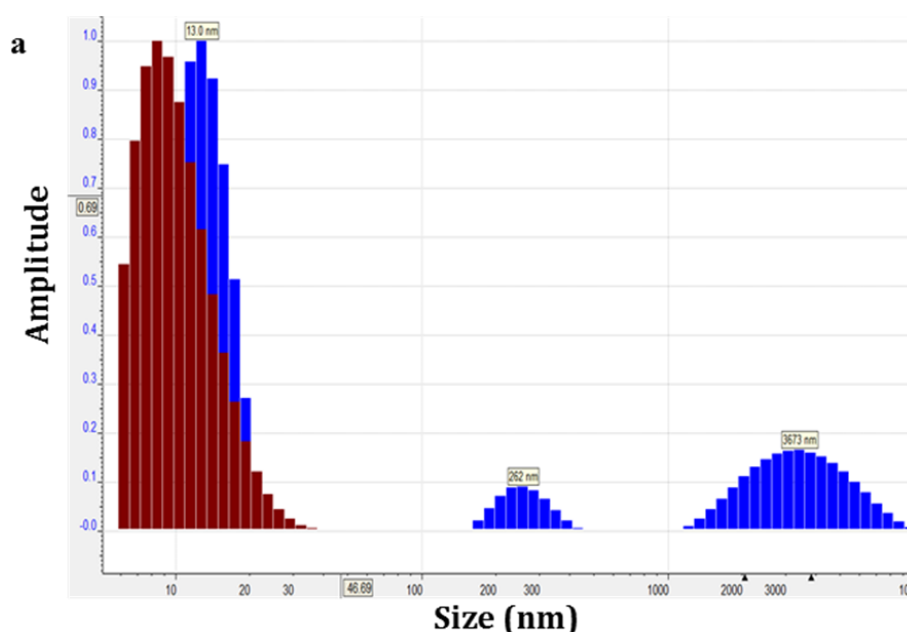


Figure 8a: Histogram of distribution of hydrodynamic radii (Rh) obtained from ‘protein as mass model and with intensity distribution’ of data from dynamic light scattering experiments. (a) Drp1 self-assembles at 50 mM NaCl salt condition in blue histogram where the peaks represents 12.27, 271.62 and 3673.17 nm of Rh with 72.2%, 4.5% and 23.4% area respectively. Drp1 dissociates at 300mM NaCl salt condition in brown histogram, with 10.51 nm Rh with 100% area.

Isolated Drp1 at two different ionic strengths, 50 mM and 300 mM NaCl were investigated. All the readings were measured at pH 7.6, at concentration 20 μ M yielded uniformly a hydrodynamic radius for the major species of Drp1 assemblies. The intensity distribution is measured directly and this information is sufficient when analyzing nearly spherical particles, like in this case we directly measured the intensity distribution over 4 s and averaged the experiment after 75 runs. Mass distribution is obtained from the raw intensity data obtained, assuming protein model and feeding in an appropriate shape factor. In this case we used default shape factor for protein. The Drp1 at low ionic strength yielded 3 prominent peaks, with a major peak of 72% area had an estimated Rh of 12.27 ± 2.73 nm, corresponding to molecular weight of 1237.67 kD, which is \sim 14 mers **Fig. 8a**. The summary of the results has been shown under the **Table 6**, whereas Drp1-Drp1 associations are perturbed under high salt condition **Fig. 8b**. In which single peak was obtained with Rh of 10.51 nm with calculated molecular weight of 857 kD, which is \sim 10mer.

3.3.2 Influence of Sertraline and Mdivi-1 on Drp1 Self-Assembly

To test whether these small molecule effectors, has any effect on the ionic strength induced assembly of Drp1, the DLS experiment was performed in the presence of mdivi-1 and sertraline.

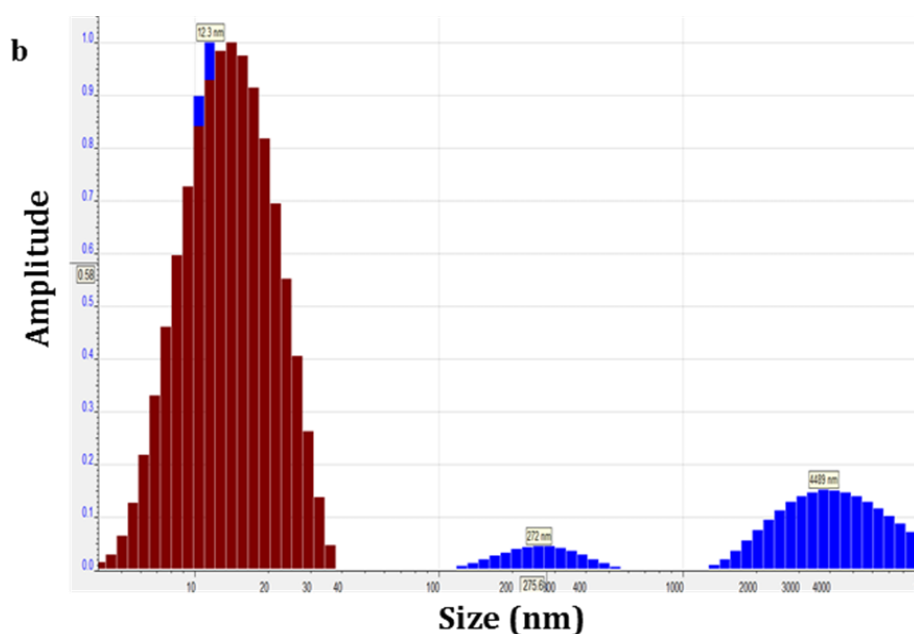


Figure 8b: Histogram of distribution of hydrodynamic radii (Rh) obtained from ‘protein as mass model and with intensity distribution’ of data from dynamic light scattering experiments. (b) Drp1 self-assembles at 50 mM NaCl salt condition in blue histogram where the peaks represent 12.27, 271.62 and 3673.17 nm of Rh with 72.2%, 4.5% and 23.4% area respectively. Drp1 dissociates in the presence of 20 μ M sertraline brown histogram, with 10.44 nm Rh with 100% area.

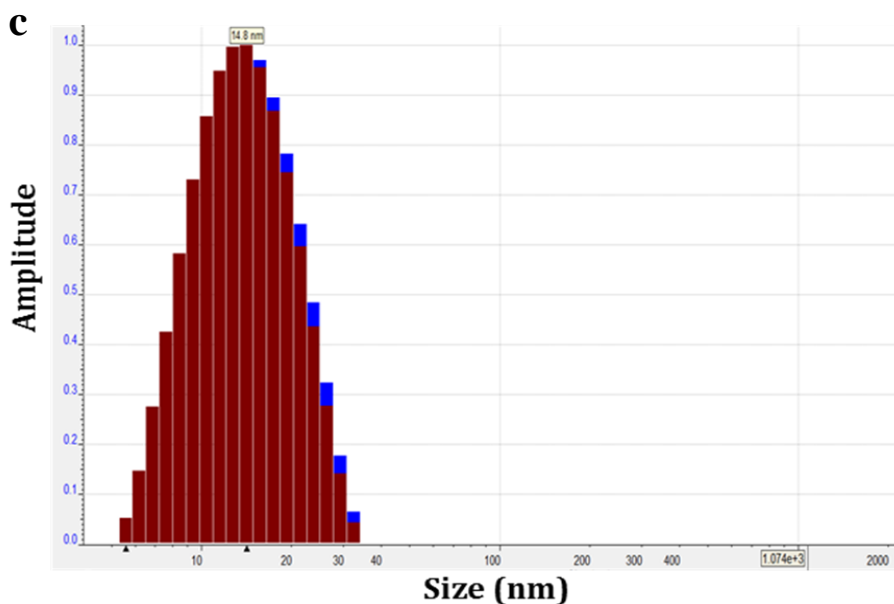


Figure 8c: Histogram of distribution of hydrodynamic radii (Rh) obtained from ‘protein as mass model and with intensity as distribution type’ of data from dynamic light scattering experiments. (d) Drp1 dissociates in the presence of both sertraline (blue) and mdivi-1 (brown) mimicking the high salt condition, with 14.81 nm Rh (intensity distribution type) equivalent to ~10.4 nm in the mass distribution type with 100% area.

Addition of mdivi1 or sertraline in the low salt condition buffer resulted in the peak distribution similar to that of high salt distribution profile **Fig. 8c** which means the small molecule effectors have an influence on the Drp1-Drp1 self-assembly.

3.3.3 Effect of Sertraline on GTP- γ -S Induced Drp1 Self-Assembly

Next, sertraline’s influence on GTP- γ -S induced Drp1 self-assembly has been tested. The size of the particle corresponding to the peak obtained in the presence of non-hydrolysable GTP analogue and in the presence of sertraline was 18.4 nm. But only in the presence of GTP- γ -S the peak obtained has hydrodynamic radius ~19.1 nm **Fig. 8d**. Thus it might be that sertraline could not compete with GTP- γ -S induced Drp1 self-assembly, but restricts from forming huge oligomers.

Thus the results from dynamic light scattering experiments provided the strong evidence that, Drp1 self assembles to higher order of oligomers under low ionic strength and GTP- γ -S. But under high salt or in the presence of sertraline and mdivi-1 the self-assembly is restricted or prevented.

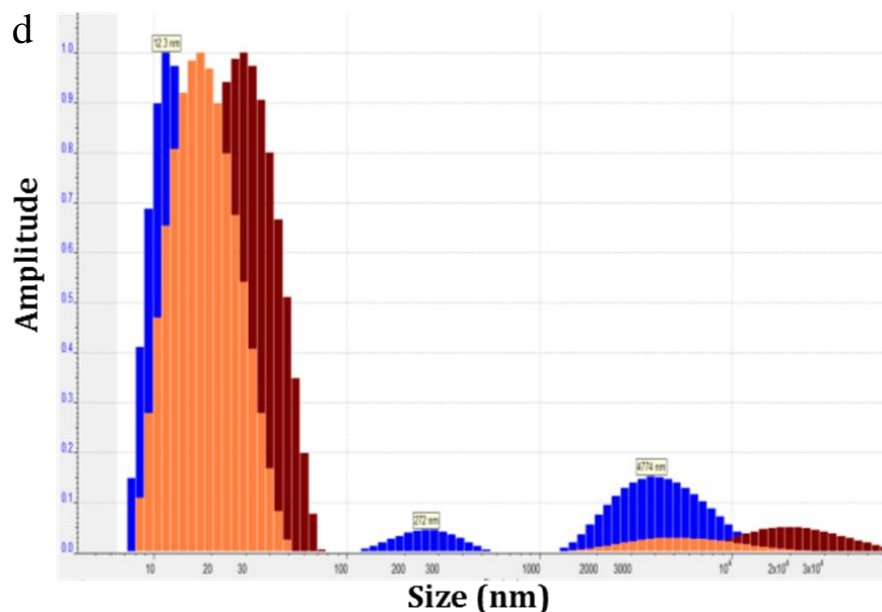


Figure 8d: Histogram of distribution of hydrodynamic radii (Rh) obtained from ‘protein as mass model and with intensity as distribution type’ of data from dynamic light scattering experiments. (c) Drp1 self-associates at 50 mM NaCl salt condition in blue histogram. GTP- γ -S induces Drp1 self-assembly to higher orders shown in orange histogram. Sertraline could not reverse the effect induced by GTP- γ -S Drp1 assembly shown in brown histogram.

Table 8: Summary of dynamic light scattering results

NaCl condition + 20 μ M Drp1	GTP- γ -S nucleotide analog	Sertraline	Mdivi-1	No. of peaks	Hydrodynamic radii (nm)
300 mM	-	-	-	1	10.51
50 mM	-	-	-	3	11, 213, 2806
50 mM	-	20 μ M	-	1	10.44
50 mM	100 μ M	-	-	2	19.6
50 mM	100 μ M	100 μ M	-	1 to 3	18.4
50 mM	-		20 μ M	1	10.8

3.4 Assembly Properties of Drp1 Studied by Analytical Ultra-Centrifugation (AUC)

3.4.1 Concentration Dependence of Oligomer Formation

Sedimentation velocity experiment was performed at protein concentrations of 2.8, 11.2 and 33.5 μM Drp1 under 25 mM Hepes pH 7.5, 100 mM NaCl, 5 mM MgCl₂ buffer condition. As can be seen from **Fig. 9** the protein undergoes a concentration dependent oligomerization reaction. Even at the lowest concentration used the sample displays a two distribution profile peaks. The peak with the highest s -value occurs at 19.1 S, with respect to the standard sedimentation coefficient $s_{(20, w)}$ to 20.0 S of a smooth compact spherical protein molecule in water at 20 °C. The highest oligomers formed must be at least hexamers (not tetramers as expected). Since a smooth compact spherical, minimum-hydrated tetramer of Drp1 is expected to sediment with an $s_{(20, w)}$ of 16.5 S.

Additionally, it has to be taken into account that the oligomerization reaction seems to be fast and that a reaction boundary is observed. Therefore, at higher protein concentration, Drp1 might sediment with an even higher sedimentation coefficient.

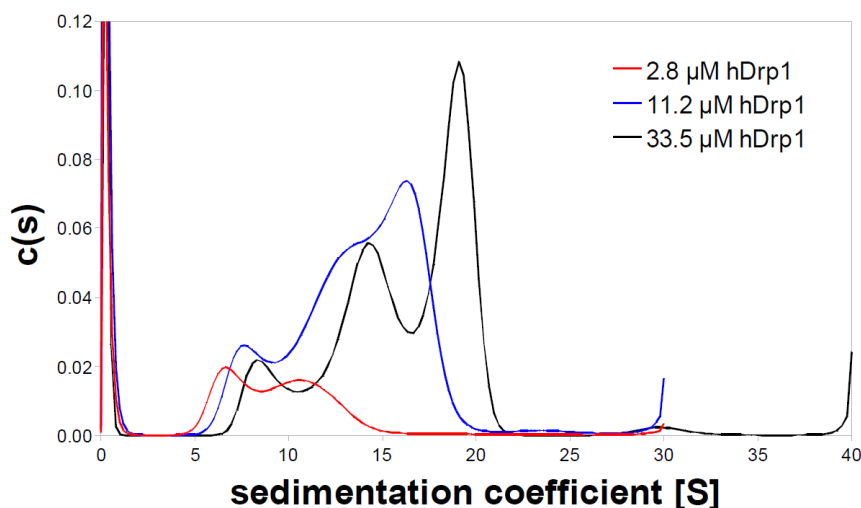


Figure 9: $c(s)$ distributions for three different concentrations of Drp1.

The peak with the smallest s -value occurs at 6.6 S, this corresponds to an $s_{(20, w)}$ of 7.0 S.

Since the $s_{(20, w)}$ of monomeric, spherical and unhydrated Drp1 is expected to be 6.5 S, this peak might at least represent dimers, or a fast equilibrium between monomers and dimers.

3.4.2 Influence of GTP- γ -S on Drp1 Oligomerization

The experiment at a concentration of 11.2 μ M Drp1 was repeated in the presence of 100 μ M GTP- γ -S with and without 20 μ M sertraline. As can be seen from the $c(s)$ -distribution in **Fig. 10**, the shift due to GTP- γ -S to higher s -values is not pronounced, therefore the formation of higher oligomers can be ruled out at the salt concentration used for this experiment. The addition of sertraline has no influence on the sedimentation velocity. It has been shown with the DLS that sertraline could not reverse the GTP- γ -S induced effect at 50 mM NaCl. The buffer used in AUC experiment has the salt concentration of 100 mM NaCl, higher than in the buffer used in the dynamic light scattering experiment. This may explain why Drp1 in the presence of sertraline or GTP- γ -S has shown no significant shift in its sedimentation coefficient.

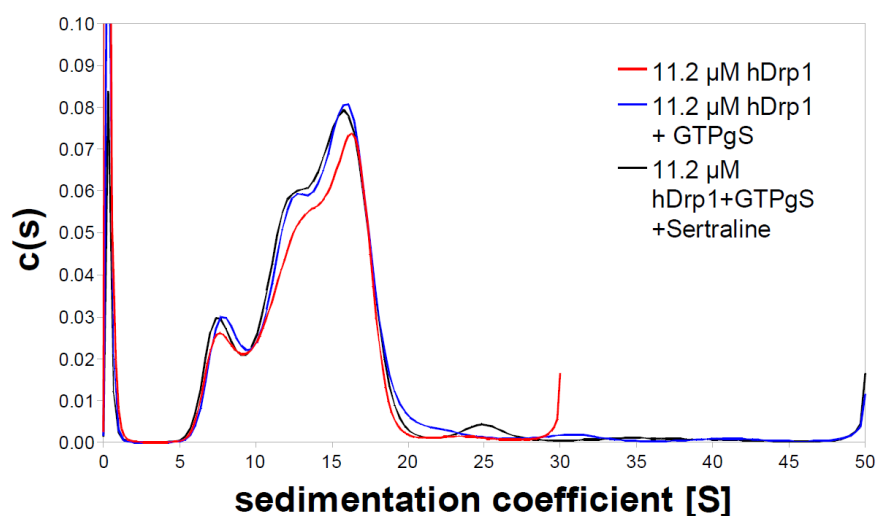


Figure 10: Influence of GTP- γ -S and Sertraline on the sedimentation behavior of Drp1.

3.4.3 Influence of GDP on Drp1 Self-Assembly

The experiment at a concentration of 11.2 μ M Drp1 was repeated in the presence of 100 μ M GDP with and without 20 μ M Sertraline. As can be seen in **Fig. 11**, GDP does not shift the $c(s)$ -distribution to higher s -values, therefore the formation of higher oligomers can be ruled out even in this case also. However, a shift to smaller s -values is observed, this might be due to a

conformational change of Drp1 in the presence of GDP. The addition of sertraline seems to have no influence on the sedimentation velocity.

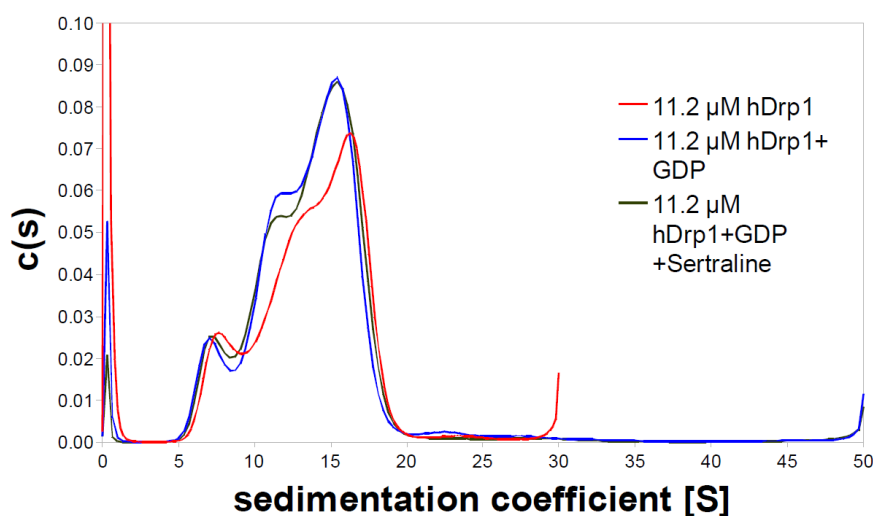


Figure 11: Influence of GDP and Sertraline on the sedimentation behavior of Drp1.

3.4.4 Influence of GTP- γ -S and GDP on Drp1 Self-assembly

Whereas both GTP γ S and GDP do not induce the formation of higher oligomers under these conditions, a shift of the $c(s)$ distribution to lower s -values is observed. This might either be due to dissociation of Drp1 oligomers or, more probably, due to a conformational change of Drp1 in the presence of nucleotide. This effect is more pronounced in the presence of GDP **Fig. 12**.

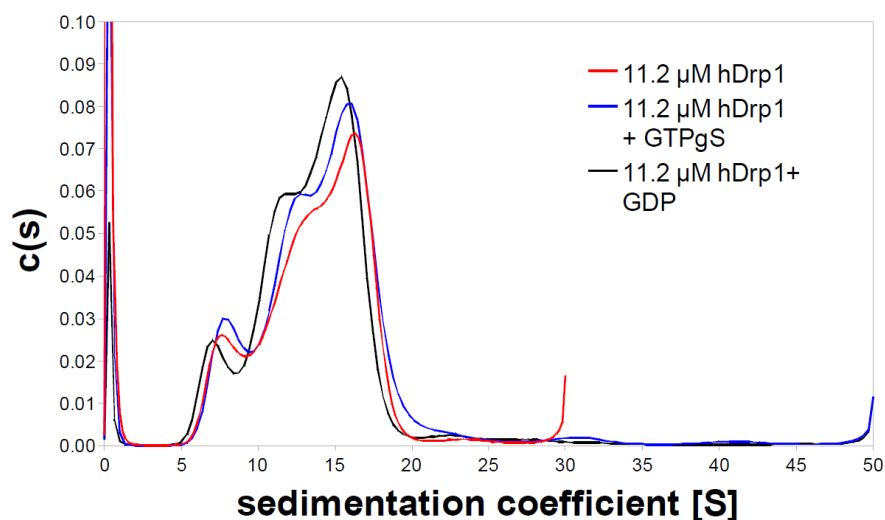


Figure 12: Comparison of the influence of GTP- γ -S and GDP on the sedimentation of Drp1.

To check whether the AUC (analytical ultra-centrifuge) run resulted in degradation of the protein, 5 μ g of each sample after the run were applied on an SDS gel **Fig. 13**. Since no degradation could be observed, the occurrence of several species in the sedimentation velocity run is not due to degradation of Drp1.

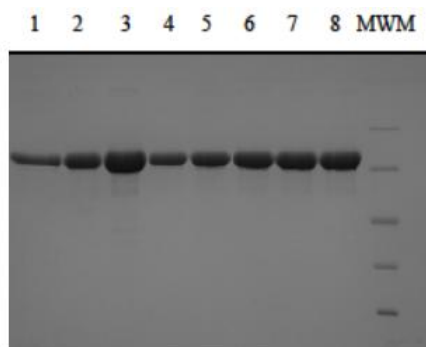


Figure 13: 10% SDS PAGE of the samples after analytical ultracentrifuge (AUC) run. Aliquots corresponding to amounts of 5 μ g were applied onto the gel. Lane 4: Drp1 stock solution, lane 1-3 and lane 5-8: aliquots of the samples from cell 1 to 7 from AUC.

3.5 Drp1 Acts as Substrate of the Cdk2/CyclinA Complex

To investigate whether Drp1 is a substrate for Cdk2/CyclinA complex, and to examine whether the complex can phosphorylate Drp1, a steady-state ATPase assay system was used. In this assay release of ADP upon Cdk2/CyclinA catalyzed reaction is used by PK/LDH enzyme system and the NADH oxidation was followed by the absorbance change. The detail of the assay system is explained in the materials and methods. As a positive control, histone H1 is used as the substrate for cdk2/CyclinA complex. As a negative control, the phosphorylation of the substrates, histone H1 and Drp1 were analyzed in the presence and absence of p27. p27 is a 27 kDa protein which is a potent inhibitor of Cdk2/cyclinA kinase activity. The decrease in absorbance from 0.6 to 0.1 was observed for over 3500 s, the reaction reached the saturation point between 3500 s to 4500 s. The assay was initiated with 1 mM ATP concentration in the reaction mix. The assay was performed under standard buffer conditions containing 50 mM HEPES pH 7.3, 150 mM NaCl, 10 mM MgCl₂, 2 mM DTT.

The slope of the fit doesn't seem to vary between the various Drp1 concentrations significantly (**Fig. 14**). The relative increase in the ATP hydrolysis between the reactions in the absence of p27 and to the reaction in the presence of p27 is significantly high **Fig. 15**. The

results from the steady state ATPase assay indicate that Cdk2/CyclinA phosphorylates Drp1 similar to histone H1 whereas p27 inhibits its phosphorylation.

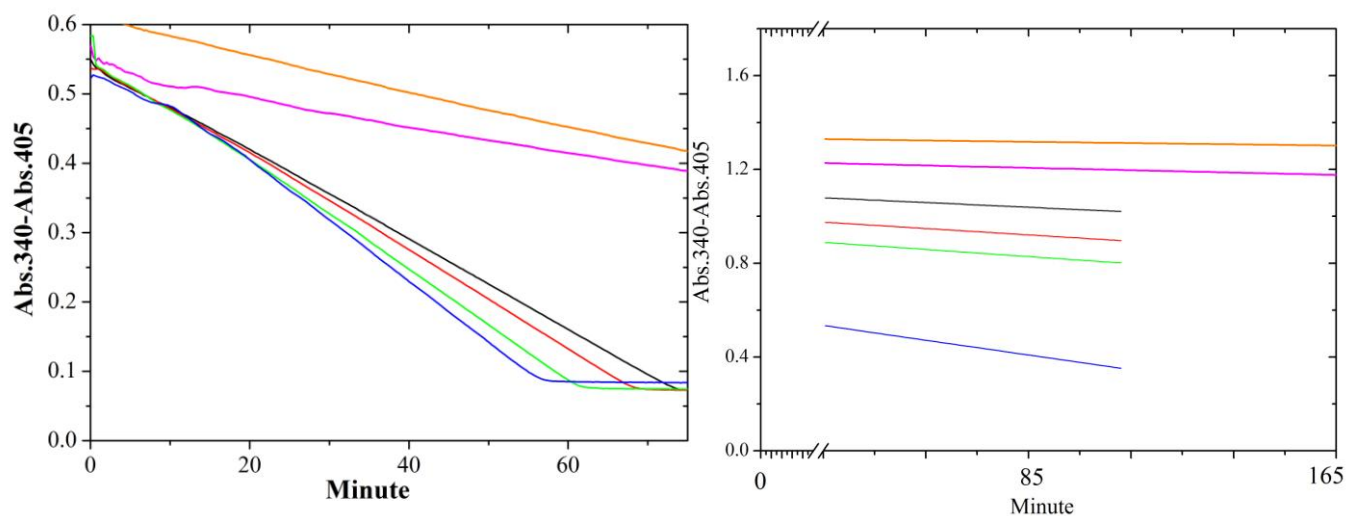


Figure 14: Steady-state ATPase assay to determine the ATPase activity of Cdk2/CyclinA complex. The assay in the presence of histone H1 in black serves as positive control. The assay in the presence p27/histoneH1/Cdk2/CyclinA (orange) and p27/Drp1 or dynamin1/Cdk2/CyclinA (magenta) serves as negative control. The Drp1 phosphorylation was indirectly measured from the slope of the decrease in 340 nm absorption of NADH. The assay was performed in the presence of Drp1 as substrate (left), dynamin1 (right) as substrate for Cdk2/CyclinA complex at three different concentrations of Drp1 and dynamin1 correspondingly, 0.5 μ M in red, 4 μ M in green and 20 μ M in blue.

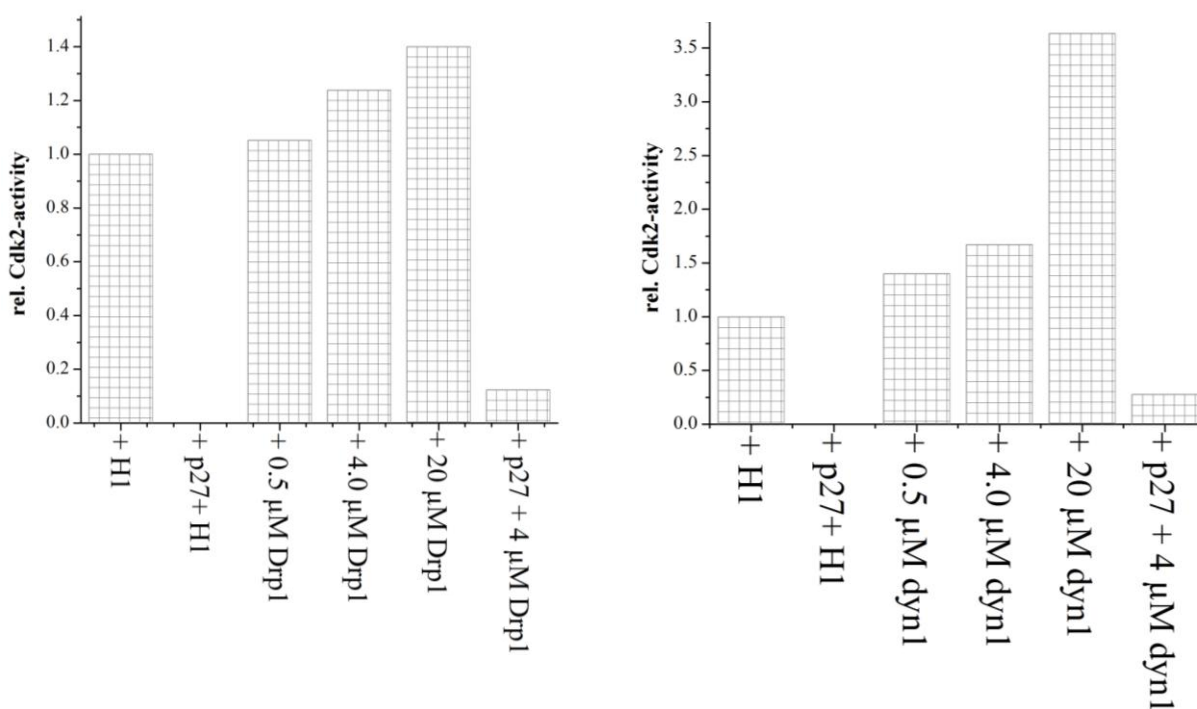


Figure 15: Cdk2/CyclinA phosphorylation activity of histone H1 as substrate and in comparison to that of Drp1 (left), dynamin1 (right) as their substrates.

Table 8: Summary of Cdk2/CyclinA ATPase activity in the presence of Drp1 as substrate

Cdk2/CyclinA +	Activity (s⁻¹)
p27 + Histone1	0.005
p27 + Drp1	0.004
Histone1	0.010
Drp1	0.070

3.5.1 Mass Spectrometry Analysis of Drp1 Phosphorylation

Since it was observed that Cdk2/CyclinA phosphorylates Drp1, quantitative profiling of phosphorylated Drp1 to identify the site of phosphorylation mass spectrometry analysis was undertaken. For this purpose Drp1 was incubated with Cdk2/cyclinA complex in the presence of ATP. The sample protein was loaded on a SDS gel. The samples were treated with acrylamide at room temperature for 30 minutes, prior to loading to SDS gel.

The samples were first digested using trypsin. Following which the obtained peptides from experiment were subjected to strong-cation exchange chromatography and elutes were collected, and enriched for phosphopeptides with TiO₂. Enriched elutes were recombined by fraction and analyzed using mass spectrometer

However, in some MS spectra the information obtained revealed more than one phosphate group but it is possible that the PO₄⁻-group is localized at different amino acids. This might be due to different parallel phosphorylation or an artifact caused by the database search. The results from mass spectrometry identified a unique phosphorylation site. In the peptides 1, 3 and 4, **S548** and in the peptide 5, **S616** were unambiguously identified as the site of phosphorylation. The results are summarized in the table below.

Table 9: Peptide mass finger printing

Peptide Fragments	Peptide
⁵³⁶ VPSALAPASQEP <u>S</u> PAASAEADGKLIQDSR ⁵³⁶ VPSALAPASQEP <u>S</u> PAASAEADGKLIQDSR ⁵³⁶ VPSALAPASQEP <u>S</u> PAASAEADGK	peptides 1,3,4
⁶⁰⁷ SKPIPIMP <u>A</u> S <u>P</u> QKGHAVNLLDVPVVAR	peptide 5
⁵³¹ DKSSKVP <u>S</u> ALAPASQEPSPAASAEADGK ⁵³¹ DK <u>S</u> SKVPSALAPASQEPSPAASAEADGK ⁵³¹ DK <u>S</u> SKVPSALAPASQEPSPAASAEADGK	peptide 2
³⁹ <u>S</u> SVLESLVGR	peptide 6
³⁹ <u>S</u> SVLESLVGR	peptide 7

The interesting result is that the neuronal Drp1 (isoform 1) is the only Drp1, that has the additional region of amino acid residues spanning from 533-569, whereas this region is absent in all other isoform of Drps. The S616 is a known phosphorylation site and is phosphorylated by Cdk1/CyclinB complex and has been shown to tubulate mitochondria during cell starvation. Our results show that Drp1 is one of the substrate for Cdk2. The [S/T]P motif is the minimum sequence required for Cdks to recognize their substrate and this is the motif of Drp1 S548. But the consequence of this phosphorylation during cell cycle is not known yet and will be an interesting topic to study.

3.5.2 FRET-Based Displacement Experiments of the CyclinA/p27 Complex by Drp1 and Dynamin1

To analyze whether Drp1 could displace the protein-protein interactions between cyclinA-p27, fluorescence resonance energy transfer (FRET) experiment was performed. In this experiment CFP and YFP were the FRET pairs. The FRET pairs, the CFP was tagged to cyclinA and YFP was tagged to p27. The FRET signal is decreased upon the displacement of

cyclinA to p27 by Drp1. The assumption here is that , if the substrates either Drp1 or dynamin1 competes with cyclinA-p27 interactions, then with addition of excess of substrates it is also possible to displace the interaction between cyclinA and p27. The assay was performed under 40 mM Tris pH 7.5, 150 mM NaCl, 5 mM MgSO₄, 5 mM DTT buffer condition. The fraction of bound YFP-p27 was calculated as follows:

$$\text{FRET_Signal } (J) = \text{Emission } 527 / \text{Emission } 485$$

$$\text{Fraction of bound YFP-p27} = \frac{(J_{\text{sample}} - J_{\text{low concentration}})}{(J_{\text{high concentration}} - J_{\text{low concentration}})}$$

Equation 2: Calculation of the fraction of bound YFP-p27 to the Drp1 and dynamin1

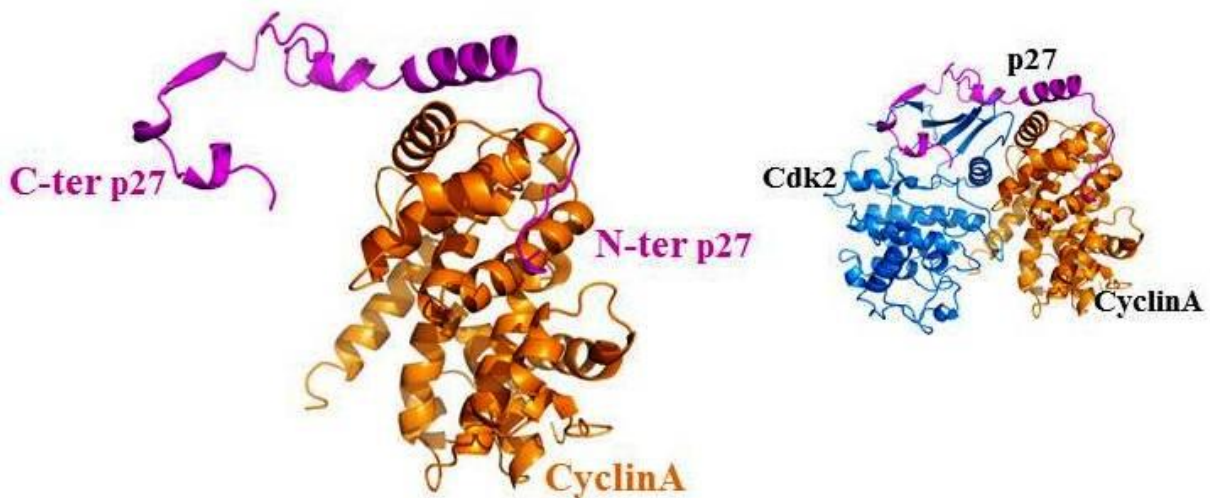


Figure 16: Cartoon representation of CyclinA/p27 complex. This is one of the experimental p27-cyclinA interactions proved by x-ray crystallography. CyclinA is shown in orange, p27 is shown in magenta. The cartoon in the right is the Cdk2/cyclinA/p27 complex structure; coordinates are obtained from the PDB id: 1jsu.

The fraction of p27 bound to cyclinA remains unchanged with increasing protein concentrations of Drp1. The readouts of the emission at 485 nm (for CFP) and 527 nm (for YFP) after excitation at 430 nm are recorded using Fluoroskan Ascent plate reader. The FRET signal remains stable during incubation of Drp1 with the complex, which means the p27-cyclinA is not

perturbed by Drp1. The results of the FRET-titration indicate that the p27 - cyclinA interaction can be displaced by an excess of dynamin1 but not of Drp1 **Fig. 17**. Thus, it can be assumed that dynamin1 is recognized by cyclinA facilitating the phosphorylation of dynamin1 by Cdk2, while the Cdk2 inhibitor, p27 blocks this recognition by cyclinA. But it cannot be excluded here that dynamin1 competes with cyclinA for binding to p27. On the other hand, Drp1 interaction does not interfere with the interaction between p27-cyclinA interactions. The above work was done in collaboration with Gunnar Weninger, methodological advice for the FRET studies and proteins (Cdk2, CyclinA, p27) were kindly provided by the collaborator.

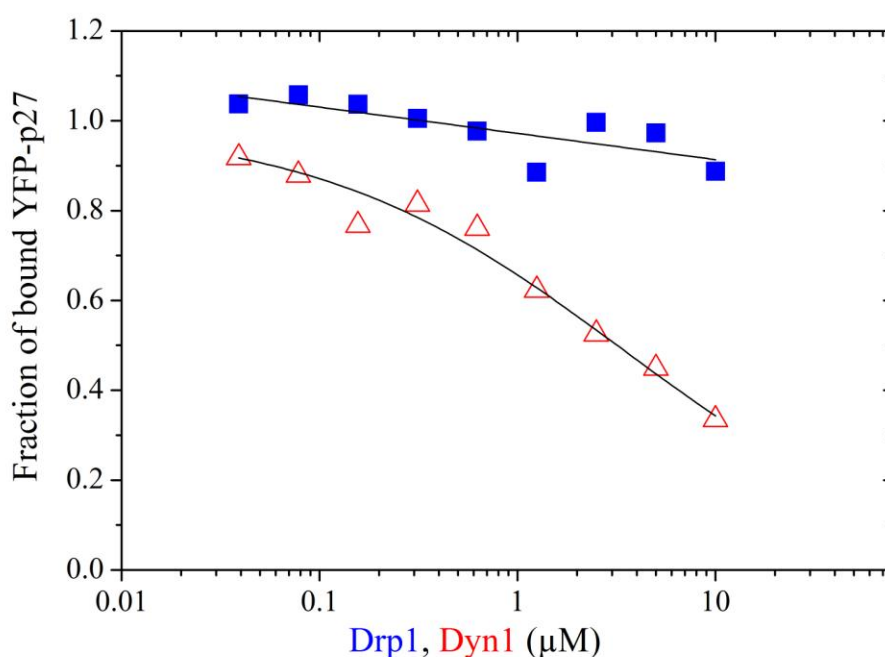


Figure 17: The FRET-signal decreases with increasing amounts of added dynamin1 (open triangle) and with increasing incubation time. Whereas Drp1 (closed squares) binds to the p27-CyclinA complex like dynamin1. But dynamin1 displaces one of the fret pair unlike Drp1. The plot is the representation of Drp1 and dynamin1 at various concentrations. The fraction of p27 bound to CFP-CyclinA from the formula given above.

3.6 Binding Affinity of Drp1 for Cardiolipin and the Influence of Nucleotides on Drp1-Cardiolipin Interaction

Mitochondrial lipids such as cardiolipin play a major role in mitochondrial fusion and fission process. Proteins that are involved in membrane remodeling to initiate fusion or fission process first have to alter the lipid environment. Hence it is necessary to study the protein-

lipid interactions to understand the remodeling processes. It has been shown that mitoPLD, a fusion implicated protein interacts with cardiolipin. Since fusion and fission are highly dynamic process, we wanted to quantify the Drp1-cardiolipin interaction.

To study the Drp1 interaction with cardiolipins and its interaction in the presence of nucleotides, microscale thermophoresis method was used. This method detects the changes in the hydration shell of molecules upon binding to their substrate close to native conditions. Infrared lasers were used to produce precise microscale temperature gradients with in thin glass capillaries that are filled with buffer of choice. The nucleotides like ATP, GTP- γ -S were also titrated in the presence of cardiolipin with labeled Drp1. The K_D for cardiolipin was obtained in an individual experiment. Once affinity value for cardiolipin is obtained, Drp1 was titrated with non-hydrolysable GTP analog and ATP in the absence of cardiolipin. And the experiments were performed and analyzed to see how ATP and GTP- γ -S could alter the affinity of Drp1 to cardiolipin. These experiments yielded the lipid affinity in the presence and absence of nucleotides for Drp1 **Fig. 18**. Three readings at different laser powers, if translated in terms of increase in temperature it could be from 2° to 8°C temperature rise from room temperature was measured. K_D values were calculated either from thermophoresis, temperature jump or from the combination of both the effects. Heating the reaction mixture up to 30sec and cooling for 5 s gave a determination curve; from which K_D values were estimated. Results are summarized in the **Table 10**.

Table 10: Summary of cardiolipin affinity to Drp1 in the presence of nucleotides

	Complex	K_D (μM)
Labeled Drp1 (230 nM)	a. Cardiolipin	7.21
	b. Cardiolipin + ATP	0.14
	c. Cardiolipin+ GTP- γ -S	1.50

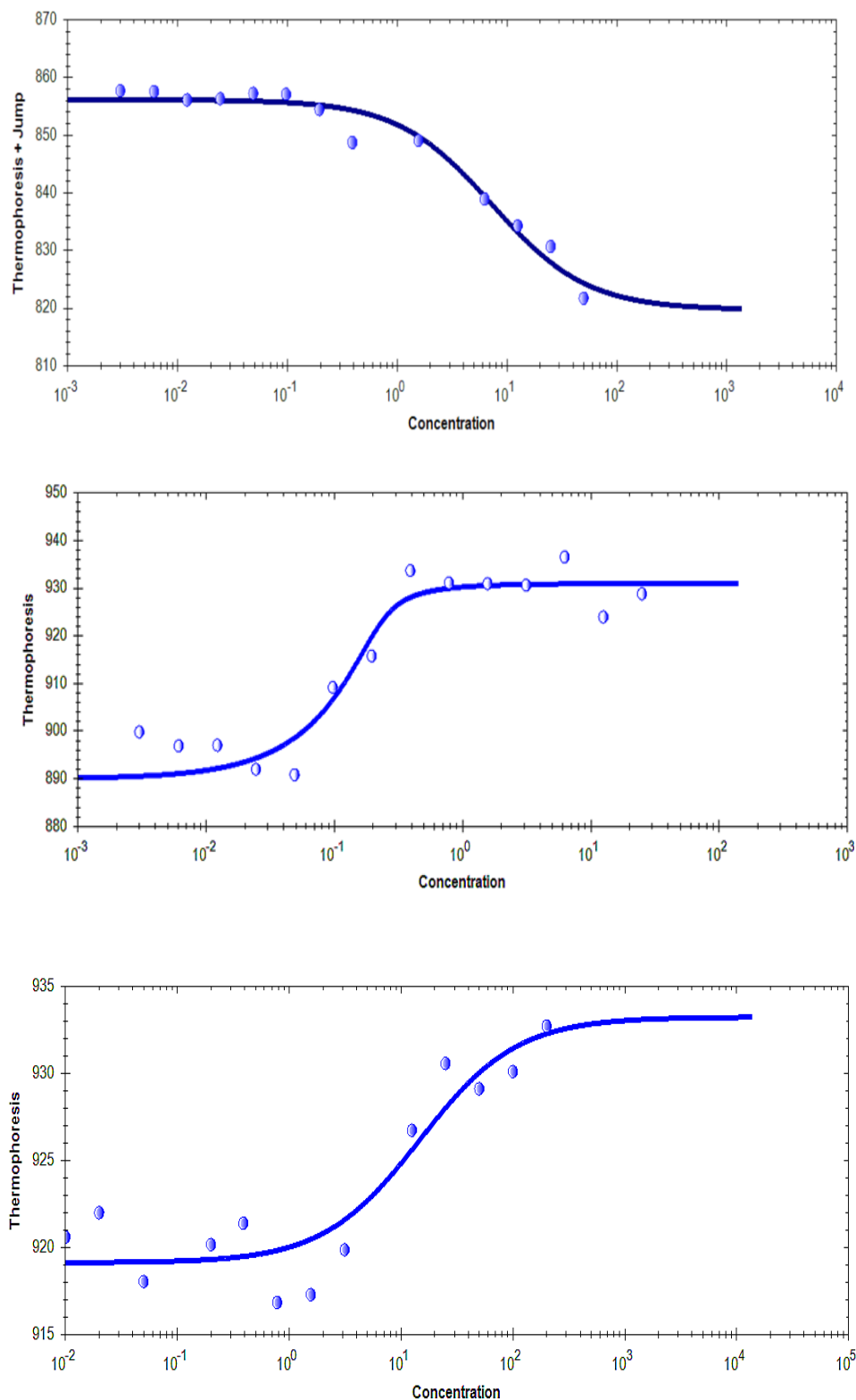


Figure 18: Alexa 647, a fluorescence marker labelled Drp1 titrated with (a) Cardioliipin, where the fluorescence intensity change was observed due to thermophoresis and temperature jump effect was fitted to obtain the affinity value of carioliipin for Drp1 (b) Cardioliipin and ATP, where the fluorescence intensity change due to thermophoresis effect was fitted to obtain the affinity value of cardioliipin for Drp1 (c) Cardioliipin and GTP- γ -S, where the fluorescence intensity change due to thermophoresis effect was fiited to obtain the affinity value of cardioliipin for Drp1.

3.7 Homology Modeling and Structural Analysis of the Drp1 GTPase Domain in Complex with Nucleotides and Cardiolipin

The sequence similarity between human Drp1 (isoform 1) and dynaminA of *D. discoideum* was 79.5% for their GTPase domain **Fig. 19**. Based on x-ray crystallographically solved dynaminA structure, Drp1 structure was homology modeled. This core of the GTPase domain and the helices around the core β -sheets were structurally well conserved except for a few inserts in Drp1 **Fig. 21**.

```

humdrp1 MEALIPVINKLQDVFNITVGADIIQLPQIVVVGTSQSSGKSSVLESIVGRDLLPRGTGIVTR 60
DymA    MDQLIPVINKLQDVFNITLGSPLDLPQIVVVGTSQSSGKSSVLENIVGRDFLPRGSGIVTR 60
      * : *****:***:*** :*****:*****. :****:****:*****

humdrp1 RPLILQLVHVTQEDKRKTTGEEENGVEAEWQKFLHTKNKLYTDFDEIRQEIENETERISG 120
DymA    RPLILQLTHLPIAD-----DGSQTQEWGEFLHKPNDFYDFSEIRREIIRDTRMTG 112
      *****. *:.*          :* :::***:***.*.: : **.***:**. :*:*:**

humdrp1 NNKGVSEPEIHLKIFSPNVNLTLLVDLPGMTKVPVGDQPKDIELQIRELILRFISNPNSI 180
DymA    KNKGISAQPINLKIYSPHVNLTLLVDLPGITKVPVGDQPTDIEQQIRRMVMAYIKKQNAI 172
      :***:* . :**:***:***:******:*****.*****. ::: :* . : *:*

humdrp1 ILAVTAANTDMATSEALKISREVDPPGRRTLAVITKLDLMDAGTDAMDVLMGRVIPVKLG 240
DymA    IVAVTPANTDLANSDALQLAKEVDPEGKRTIGVITKLDLMDKGTDAMEVLTGRVIPLTLG 232
      *:***.*****:*.*:***:~::~*****:~::~.*****:*****:*****:~**

humdrp1 IIGVNRSQLDINNKKSVTDSIRDEYAFLOKQ--YPSLANNGTKYLARTLNRLMHHIR 298
DymA    FIGVINRSQEDIIAKKSIRESLKSEILYFKNHPIYKSIANRSGTAYLSKTLNKLMLFHIR 292
      :***:*****: :*~::~* :~::~* **:***.***:*:***:***.***

humdrp1 DC----- 300
DymA    DTLPLDKV 300

```

Figure 19: Sequence alignment of the GTPase domain of Drp1 and dynaminA. The sequences are 61.7 % identical and 79.5 % similar. The alignment is based on Needleman-Wunsh method lit.

Our preliminary modeling and computational analysis showed that R247 residue in Drp1 which is equivalent to R239 in dynaminA GTPase domain sequence of *D. discoideum* is important in coordinating the nucleotide in the active site of dynaminA structure **Fig. 20**. Drp1 R247E mutant expressing cells formed elongated mitochondrial tubules and significantly decreased BAX oligomerization. This has further experimentally confirmed by other groups in a recent study (Montessuit et al., 2010). Our modelling studies on the R239 of dynaminA and its importance in interaction with the ATP similar to that of R239 interaction

with GTP as in the crystal structure of dynaminA explained how ATP can accommodate into the active site of the dynaminA GTPase domain. Docking studies were performed using GOLD program, and docking was performed in the presence of GTP and ATP in an individual run and the grid was centred on K208 of dynaminA crystal structure.

The GTPase domain of *D. discoideum* dynaminA clearly showed the importance of R239 in coordinating with the GDP ribose oxygen. Our docking experiment proved that this residue is also important for ATP coordination too. This coordination is mediated with the backbone carbonyl atom of the arginine.

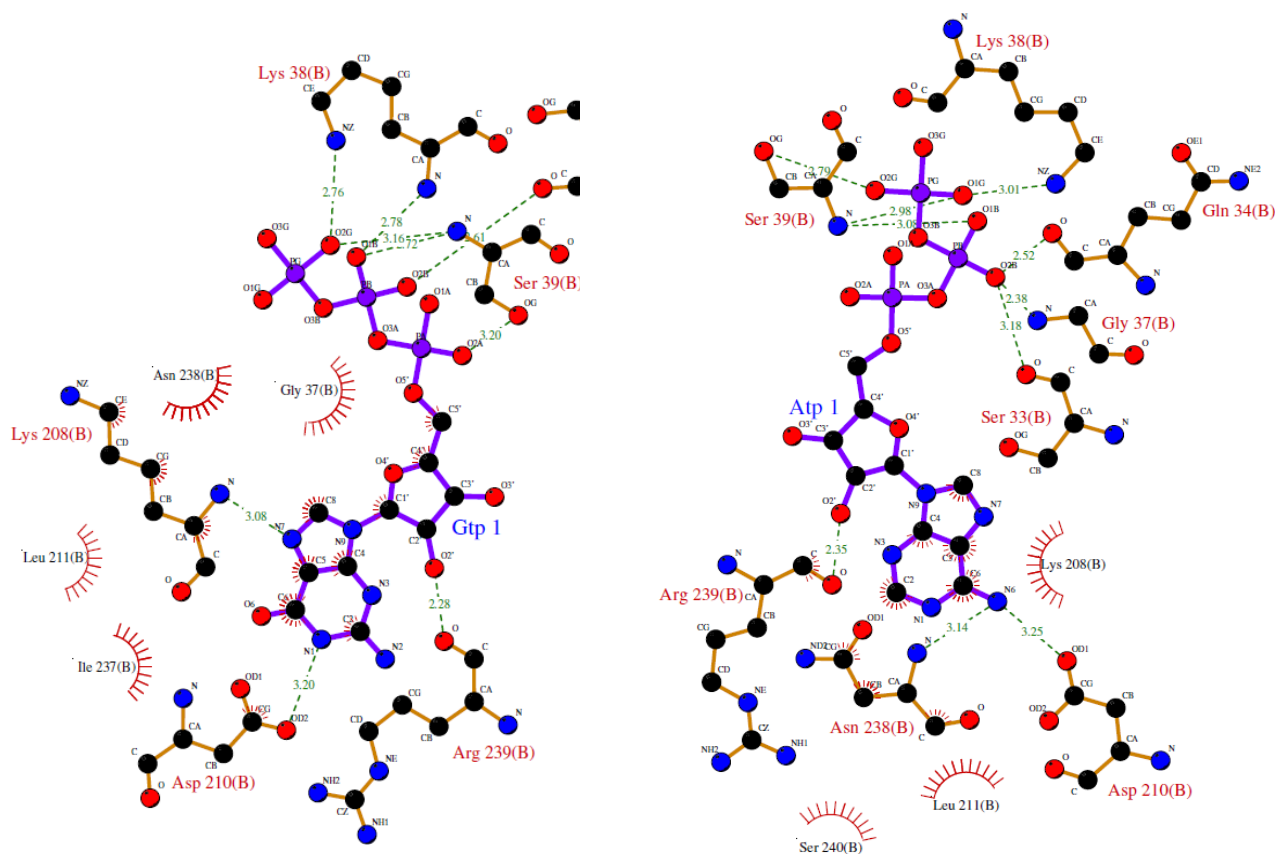


Figure 20: Ligplot comparing the interacting amino acids of *D. discoideum* dynaminA with GTP (left) and ATP in the nucleotide binding pocket (right). The figure shows the interaction of the ribose with arginine 239, the equivalent amino acid residue to arginine 247 in Drp1.

In another individual docking experiment with 2 phosphate head group containing cardiolipins and with Drp1 GTPase domain homology model as target confirmed the importance

of R247, i.e. the arginine to cardiolipin interaction might take place between the phosphate head group and the backbone carbonyl group. It was shown that the binding of ATP to Drp1 stabilizes the quaternary structures **Fig. 22**. But extensive molecular dynamics calculations in the presence of waters are needed to understand the detailed interactions especially when studying with charged lipid molecules that have resonance structure. This would help in assessing particular interaction when the head group of cardiolipins gets tucked in due to proton availability from the water group. Cardiolipins has a resonance structure in bilayers and other conformations in solution (Kates et al., 1993). Cardiolipin binding to Drp1 is important and has been shown that cardiolipin containing liposomes is required for tBid assisted Drp1 induced Bax oligomerization.

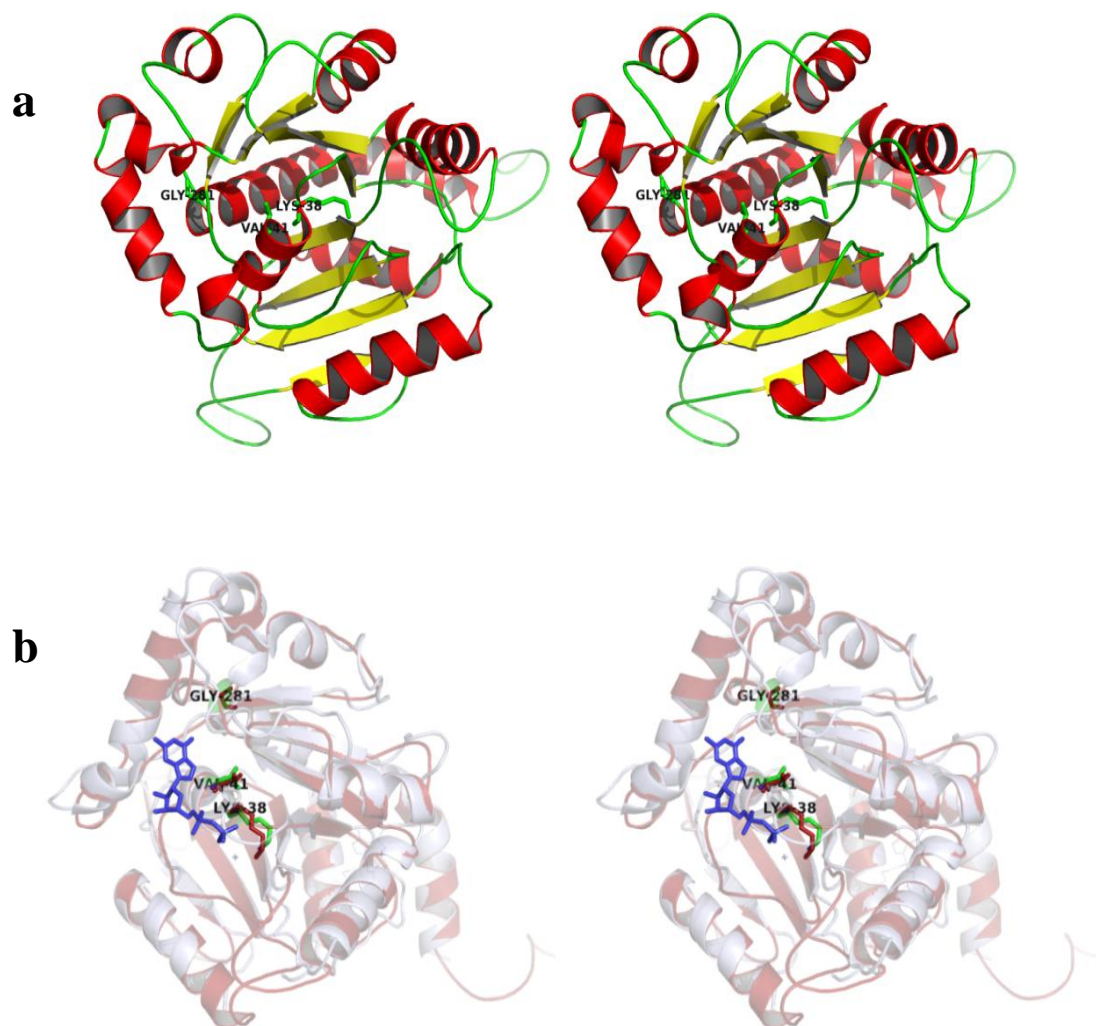


Figure 21: (a, b) Homology models of Drp1 GTPase domain based on multiple structure alignment. (a) Stereo view of Drp1 GTPase domain and labeled with the residues implied in dominant negative phenotype (b) superimposed stereo view of modeled Drp1 and dynaminA GTPase domain from the pdb id:1jx2.

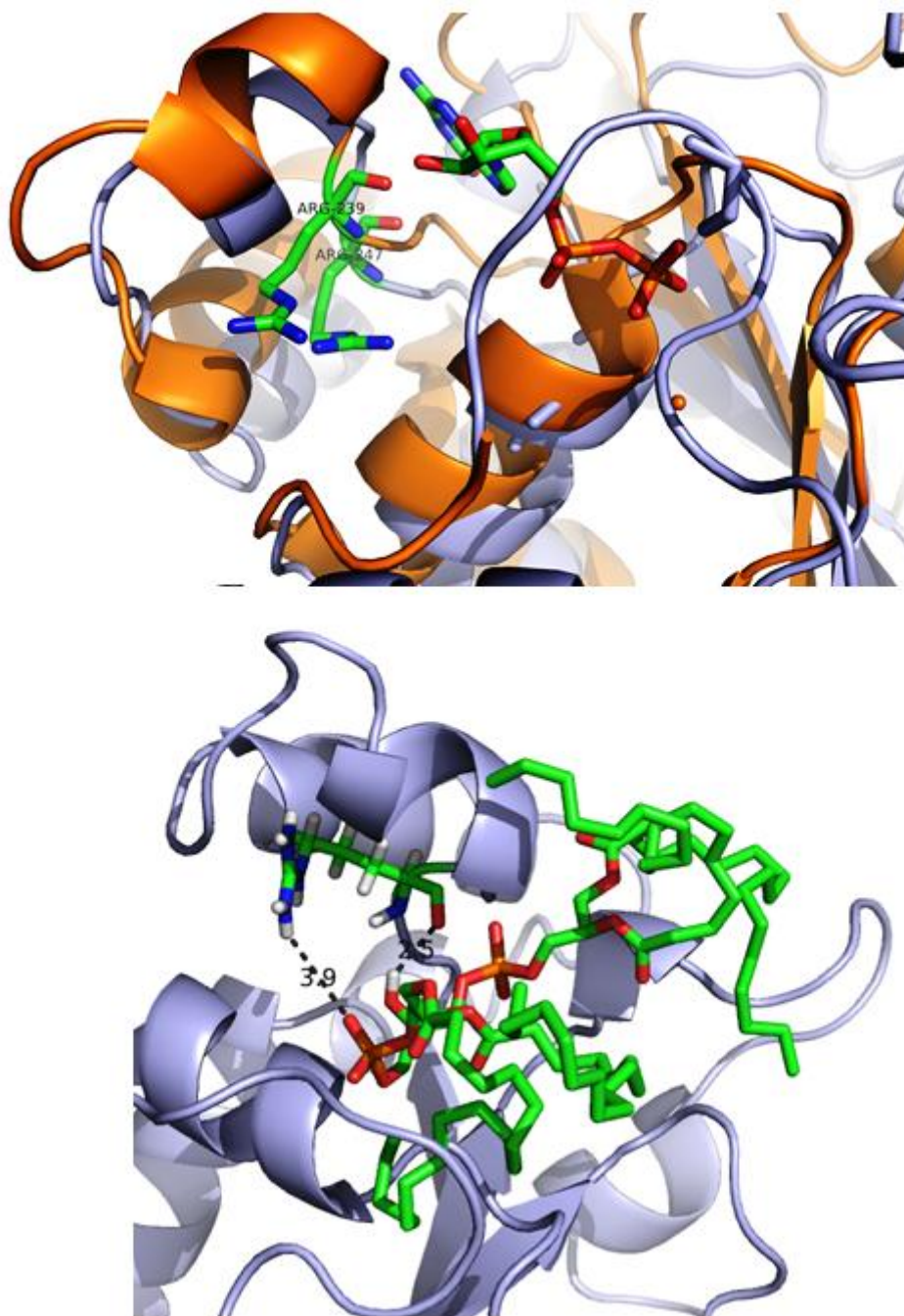


Figure 22: (top) Superimposed cartoons of experimentally solved dynaminA GTPase domain (pdb id: 1jwy) structure in orange with homology modeled Drp1 in blue. R247, R239, GDP are shown as sticks (bottom) cartoon representation of Drp1 homology model in blue. The docking of cardiolipin on the modeled Drp1 GTPase domain shows the possibility of R247 interaction with the head group of the cardiolipin.

3.8 Crystallization Experiments of Drp1

Crystal structure of Drp1 and derivation of functions from the 3-dimensional structure would provide evidence about the existing theories on mitochondrial fission, interactions with cardiolipins, assembly stimulated GTP hydrolysis, force generation coupled to conformational changes, interactions with regulatory molecules such as cyclinA. To achieve this aim, complete range of commercially available crystallization trials has been screened to crystallize Drp1. Drp1 full length, Drp1 full length with sertraline, Drp1 full length with ADP meta-vanadate, Drp1 in complex with Cdk2/cyclinA complex were a few crystallization projects that has been focused during this thesis work. Until now the attempts to obtain diffractable crystals were rate limiting. Comparable mutant constructs of Drp1 to dynamin3 mutant constructs of monomer, has also been made and is in the pipeline to crystallize.

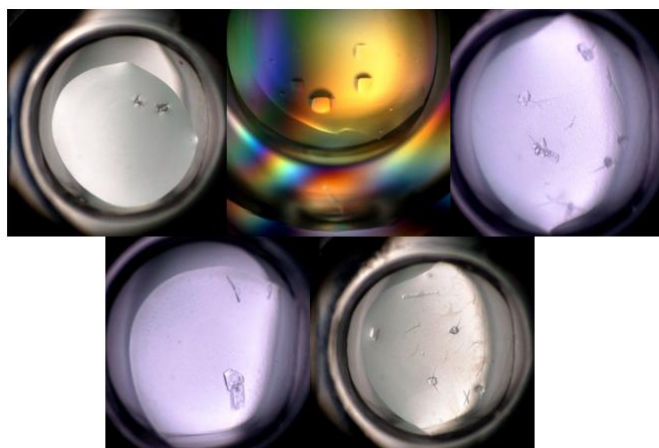


Figure 23: Crystals obtained from the commercially available crystallization screenings with Drp1.

The I481 of dynamin3 equivalent is I489 of Drp1 is mutated to D and H687, F688 of dynamin3 equivalent is H672, and L673 of Drp1 is mutated to D, S respectively. These monomer constructs are in the pipeline to produce diffractable crystals.

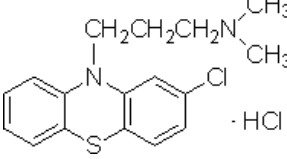
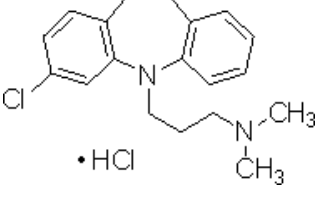
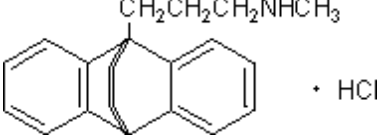
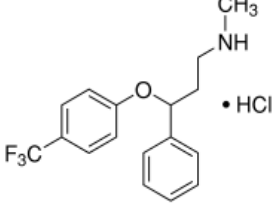
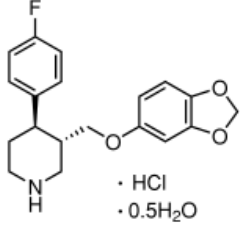
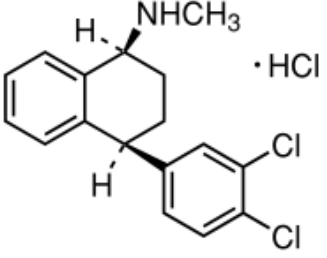
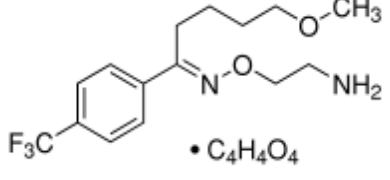
3.9 Use of Psychotropic Drugs as Potential Dynamin and Drp1 Modulators

Psychotropic drugs modulate the level of brain monoamines and neurotransmitters (Preziosi, 1977). Previously it has been shown that selective serotonin reuptake inhibitor (SSRI), is a mixed-type inhibitor of dynamin1 with respect to both GTP and l- α -phosphatidyl-l-serine *in vitro*, implicating its role in the regulation of neurotransmitter transport by modulating synaptic vesicle endocytosis (Otomo, 2008 ; Takahashi, 2010). The mechanism of action might be through the inhibition of dynamin1 GTPase activity. Selected psychotropic drugs (see introduction) were used for the study of their modulating effects on dynamin and Drp1. Chlorpromazine, sertraline have been shown to inhibit the GTPase activity of dynamin1. This study focused on the modulation of GTPase activity of neuron specific, neuron enriched dynamin1, and Drp1 isoform1 by the psychotropic drugs. To obtain the affinity, and to test their specificity and potency by the pharmacologically active compounds such as sertraline, fluvoxamine, and chlorpromazine for dynamin1 and Drp1, steady-state kinetics and microscale thermophoresis were performed. The following are a few drugs used for the study:

- Chlorpromazine - antipsychotic-phenothiazin class
- Clomipramine - antidepressant-tricyclic
- Maprotiline - antidepressant-tetracyclic
- Fluoxetine - antidepressant
- Paroxetine - antidepressant
- Sertraline - antidepressant
- Fluvoxamine – antidepressant

The drug molecules were prepared either in water or DMSO as stocks. The solubility of the compounds are summarized in the material and methods chapter, and from this stock, the compounds were further dissolved in 30 mM Tris-buffer for performing the assays. Sertraline and fluvoxamine had an effect on dynamin1 and Drp1's GTPase activity, other drugs had no or very high IC_{50} value for dynamin1.

Table 11: Psychotropic drugs and their molecular structures

Psychotropic Drugs	Chemical Structure
Chlorpromazine	
Clomipramine	
Maprotiline	
Fluoxetine	
Paroxetine	
Sertraline	
Fluvoxamine	

3.9.1 Fluvoxamine and Sertraline are Potent Inhibitors of Drp1 and Dynamin1 GTPase Activity

Fluvoxamine seems to inhibit dynamin1 full length protein **Fig. 24b**, but not the minimal construct (GG1) **Fig. 25b** which consist of the GTPase domain and C-terminal GED. We can speculate that fluvoxamine might bind to PH domain or middle domain of dynamin1 thereby inhibiting the dynamin1 GTPase activity, but sertraline on the other hand seems to have different IC_{50} values for the full length dynamin1 and GG1 proteins. The lower IC_{50} value for GG1 means, sertraline preferentially could influence the GTPase activity via binding to GED binding groove in the N-terminal GTPase domain. Recent GG1 structure in complex with $GDP \cdot AlF_4^-$ (Chappie et al., 2010), provides structural detail about the GED binding and its influence on stimulated GTP hydrolysis rate. Both fluvoxamine and sertraline drugs have been used in the treatment of antidepressant (Takahashi et al., 2009), antipsychotic. But the mechanism of action is not clear for these drugs; except for the fact that drugs like chlorpromazine is well known endocytosis inhibitor (Otomo et al., 2008). Understanding the mechanism of action of these drugs by inhibiting dynamin1's GTPase activity is important, for this purpose the full length proteins that were produced recombinantly in Sf9 cells in case of dynamin1 and in *E. coli* in case of Drp1 were used. The minimal construct which has GTPase domain and C-terminal GED (GTPase effector domain) of dynamin1 also recombinantly produced in *E. coli* and used in the assay system. Other than steady-state kinetics, the compounds that had an effect on GTPase activity with the dynamin1 full length, GG1 and Drp1 have been used in screening with crystallization conditions to obtain crystals.

In case of Drp1, sertraline however unable to compete GTP binding site or in other words sertraline is unable to inhibit GTP dependent polymerisation of the protein (from dynamic light scattering and analytical ultracentrifuge data). The mechanism, how sertraline inhibits Drp1's stimulated GTPase activity can be speculated i.e. sertraline may bind to the GED binding site and thereby inhibits the GED induced GTPase activity (inhibition of assembly stimulated GTPase activity). In summary, the compounds efficiency to perturb GTPase activity of the GG1, dynamin1 and Drp1, using kinetic, biophysical and cell biological experiments gave us insight into the importance of sertraline. The IC_{50} of sertraline for Drp1 is 8 μM **Fig. 26**, kinetic data in an ionic dependent manner also showed that sertraline inhibited the assembly stimulated GTPase activity of Drp1. From the above studies

and the results derived from them showed that sertraline and fluvoxamine can be used as modulators or as an effector for dynamin1 and Drp1.

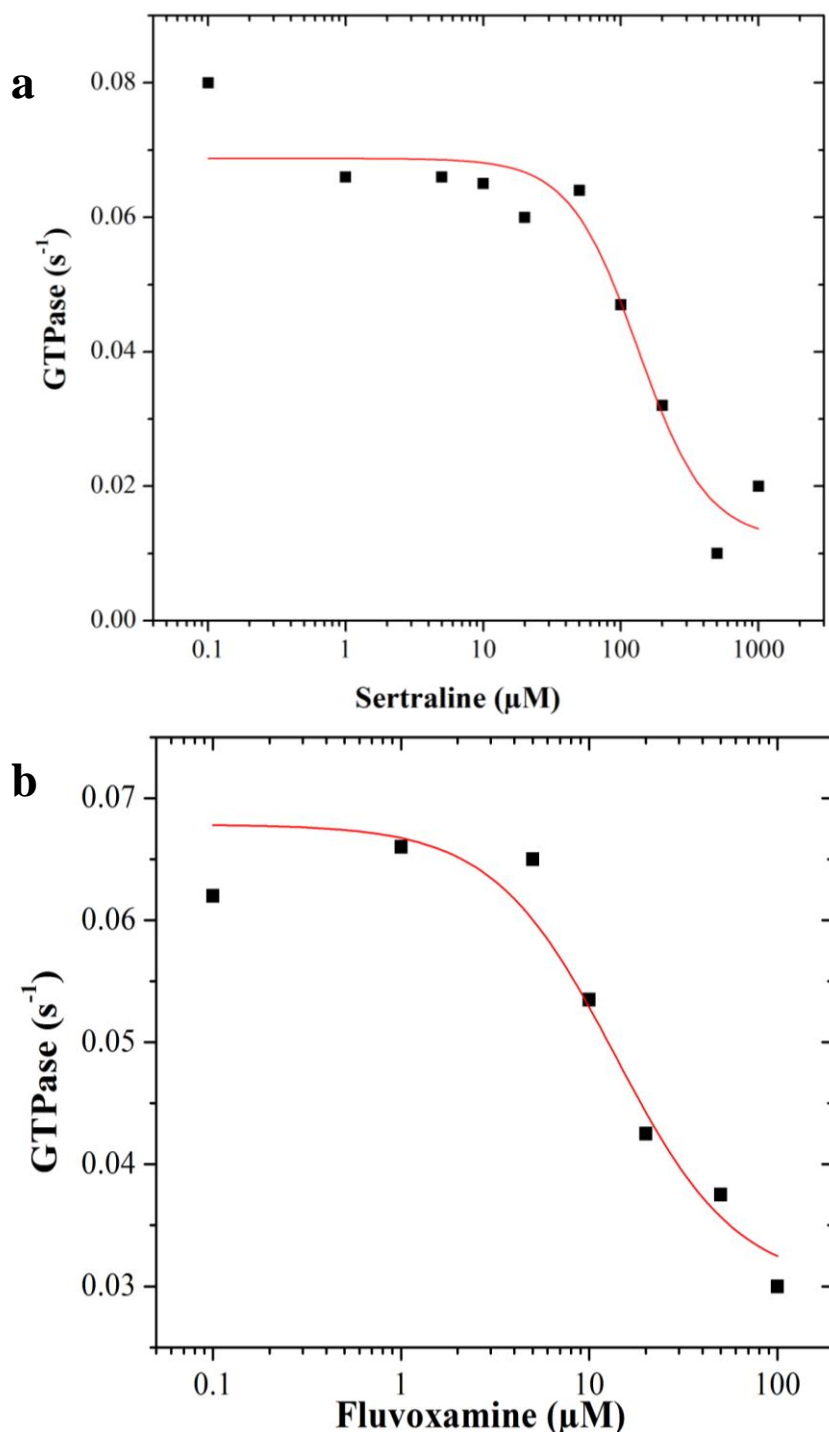


Figure 24: (a) Steady-state GTPase hydrolysis activity of dynamin1 in the presence of sertraline and (b) fluvoxamine. IC_{50} of sertraline for dynamin1 full length is 71 to 130 μM and IC_{50} of fluvoxamine for dynamin1 full length is 14 μM . The concentration range for sertraline is 0.1 μM – 1000 μM , and 0.1 μM – 100 μM for fluvoxamine were used in the assay.

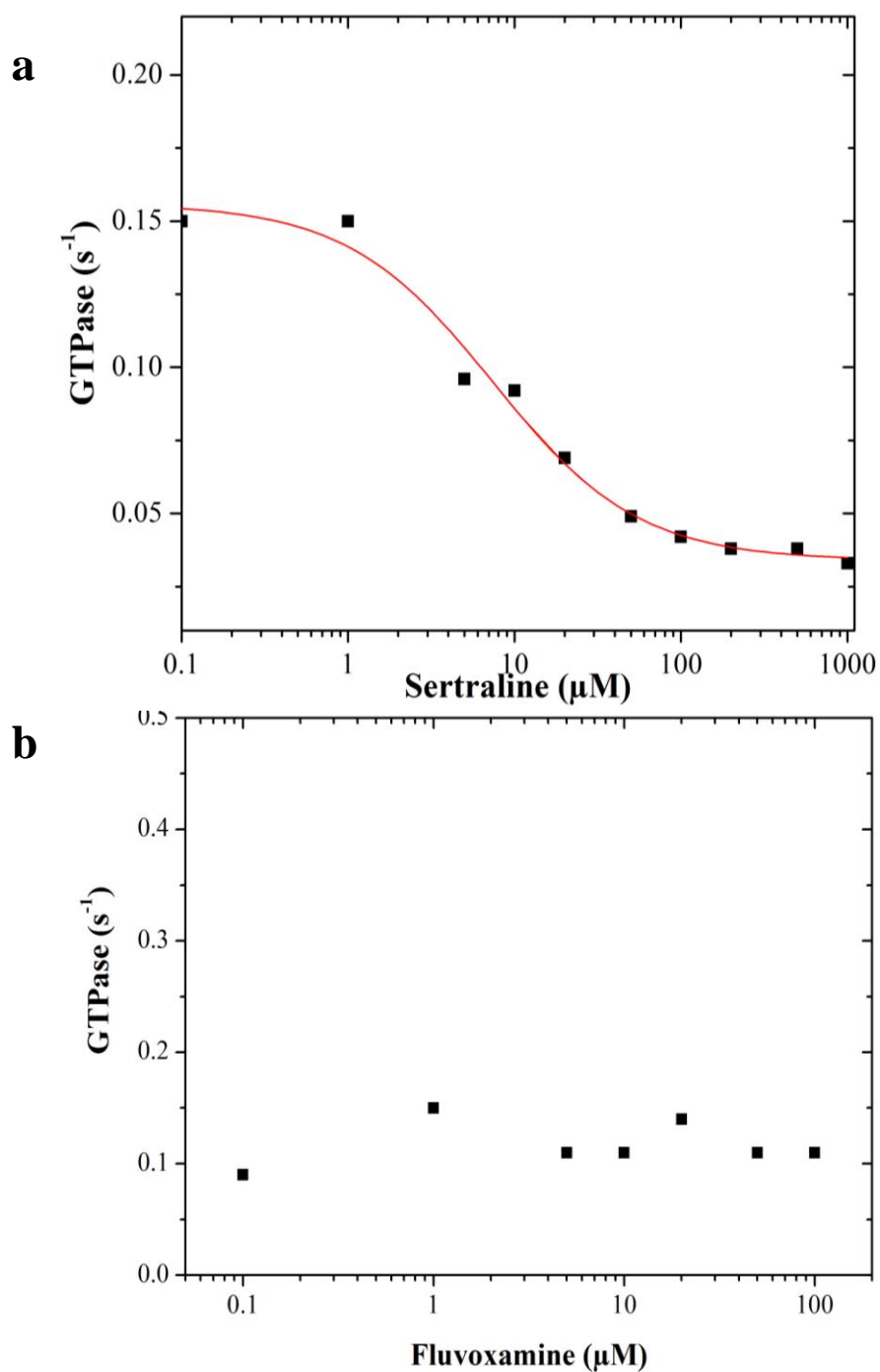


Figure 25: Plots showing the steady-state GTPase hydrolysis inhibition activity of dynamin1 minimal construct (GG1) which has the GTPase domain and c-terminal GED domain. (a) Sertraline and (b) Fluvoxamine. The sertraline had an effect on the GTPase hydrolysis rate of GG1; IC_{50} of sertraline is $8.1 \mu\text{M}$ for the dynamin1 minimal construct almost no inhibition is observed with fluvoxamine on GTPase hydrolysis activity.

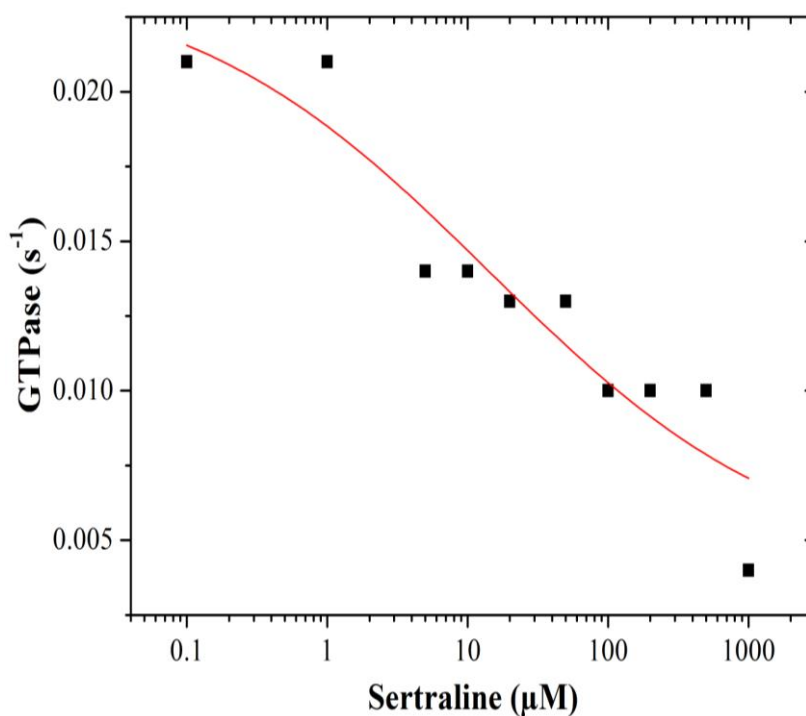


Figure 26: Inhibition of Drp1 GTPase activity by sertraline.

3.9.2 Engineering, Production, and Crystallization of Genetically Modified Dynamin1 Constructs for High Resolution Structure Determination

3.9.2.1 Engineering of Various Full-Length and Truncated Dynamin1 Constructs

The c-terminal PRD domain of dynamin1, have been modified to histidine arginine rich (HRD) domain **Fig. 27**. For this purpose the c-terminal have been synthetically made and inserted at the c-terminal of dynamin1. We were interested in perturbing the intrinsic disorder by changing the propensity for secondary structural elements that has been predicted by domain prediction plot **Fig. 28a**. We optimized the protein sequence at the proline/arginine rich domain, and we were able to clone this construct in pFastHtb, express and purify them from sf9 cells produced with baculo virus system, but the expression level became the rate limiting for further experimental analysis. Replacement caused 6% variation with the original

full length sequence and reduced the disordered propensity significantly; we calculated the disordered propensity of the sequence using a web based tool **Fig. 27**.

```

10      20      30      40      50      60
PRD;   VSTPMPPVDDSWLQVQVSPAGRRSPTSSPTQRRAPAVPPARPGSRGPAPGPPPAGSAL
      : : : : : : : : : : : : : : : : : : : : : : : : : : : : : : : : : :
HRD;   VETPMHHVDDSWLQVQVSPAGRRNHNEEHPEQRRAPAVHHARPGERGHAHGPHHAGEAL
      10      20      30      40      50      60

      70      80      90      100     110
PRD;   GGAPPVPSRPGASPDFFGPPPQVPSRPNRAPPGVPSRSGQASPSRPESPRPPFDL
      : : : : : : : : : : : : : : : : : : : : : : : : : : : : : : : : : :
HRD;   GGAHHVHERHGAEPDHFQVPEPHNRAHHGVHEREGQASHERHEEHRHPPFDL
      70      80      90      100     110

```

Figure 27: Sequence comparison of PRD and modified HRD (histidine - arginine rich domain) domains.

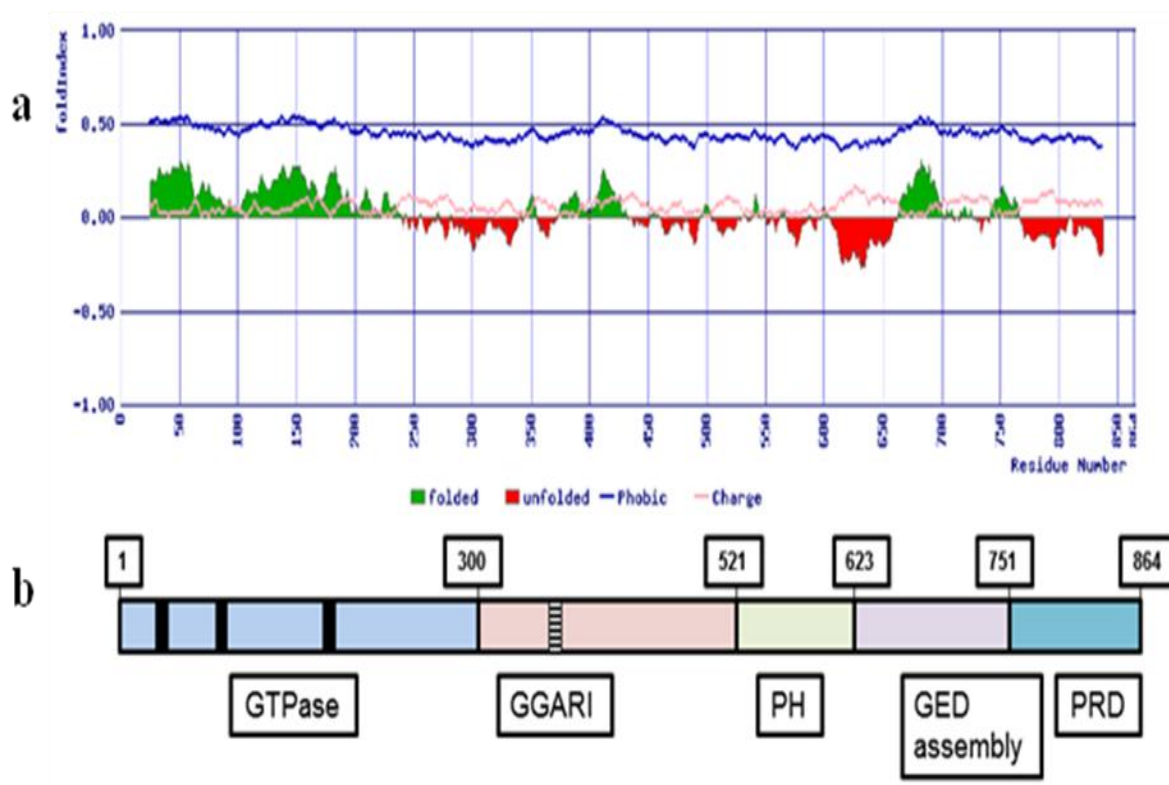


Figure 28: (a) Fold index plot, where the area under green represents the ordered region and the area under red represents the intrinsically disordered region of the protein sequence (bip.weizmann.ac.il/fldbin/index). (b) Represents the domain organization of human dynamin1 and its sequence annotation.

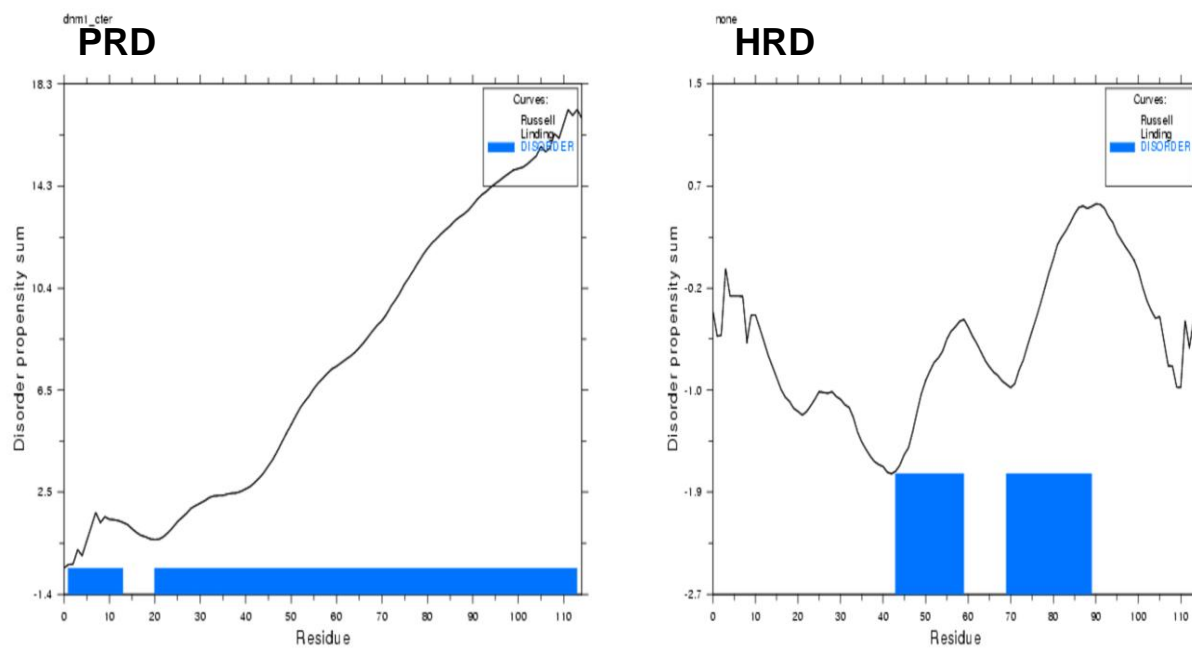


Figure 29: (a) Domain prediction plot for wild type dynamin1 proline rich domain (PRD) (b) Domain prediction plot after rational insertion of histidines at the PRD of the dynamin1 sequence (<http://globplot.embl.de/>). The blue histogram represents the disorderness over the predicted PRD of the human dynamin1.

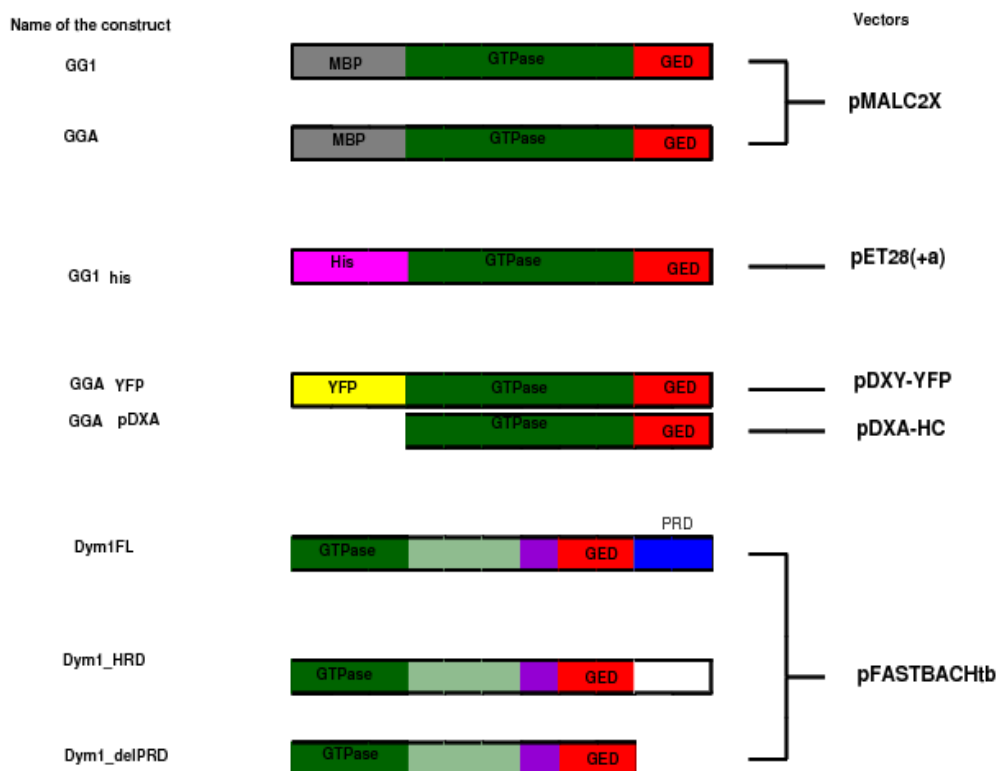


Figure 30: (a) Dynamin1 constructs prepared during the course of this work and their domain organizations.

We were also interested in understanding the mechanism of known endocytosis inhibitor like chlorpromazine; we also found that fluvoxamine another drug like molecule could inhibit full length dynamin and not the minimal construct. The minimal constructs were designed with the aim to prove the indirect influence of GTPase effector domain (GED) on dynamin's basal and assembly stimulated GTP hydrolysis. The minimal construct was purified as maltose binding protein as fusion partner. The GG1 comprises of 6-320 residues of GTPase domain cloned between EcoRI, XbaI and 726-750 residues of C-terminal GTPase effector domain cloned between XbaI ,HindIII similarly the GGA comprises of 2-316 residues of GTPase domain cloned between EcoRI, XbaI and 815-848 residues of C-terminal GTPase effector domain cloned between XbaI ,HindIII both the constructs in pMALC2X vector.

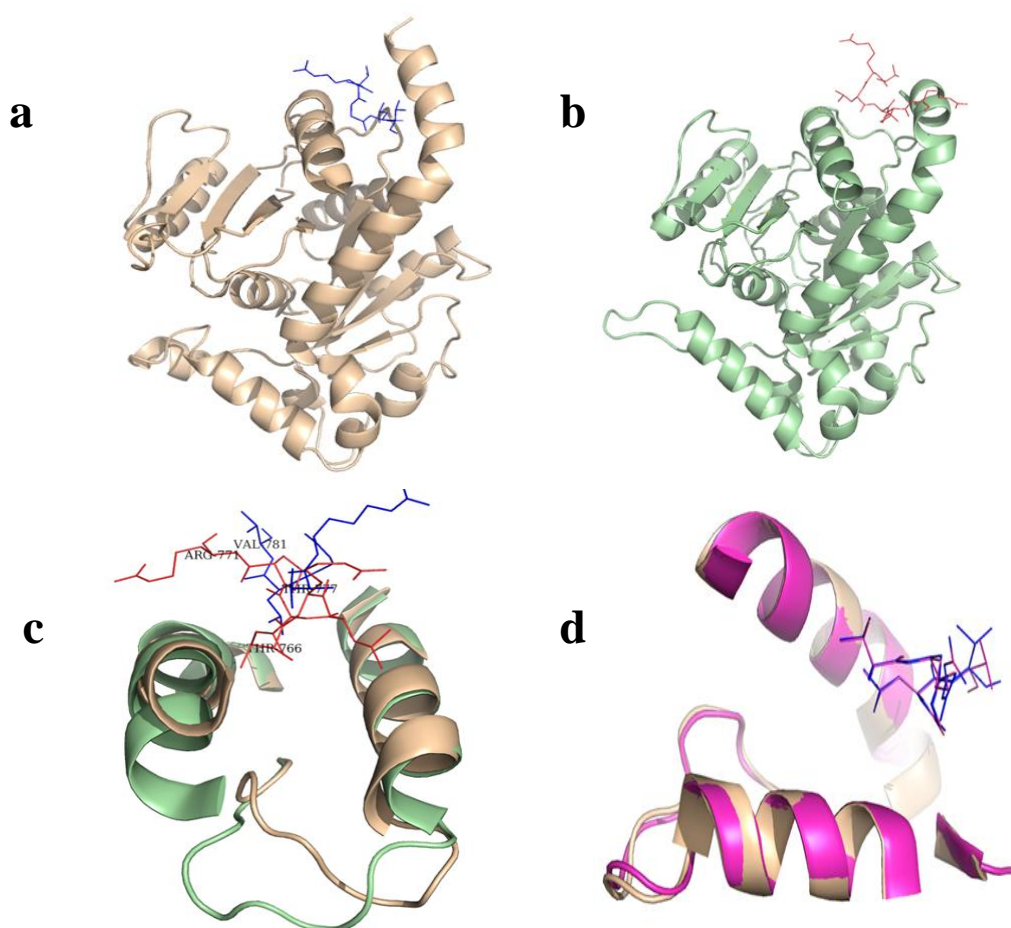


Figure 31: Dynamin GTPase domains in cartoon representation and c-terminal myosin helix in line representation (a) pdb id: 1jx2, dymA GTPase domain in brown and c-terminal myosin helix in blue (b) pdb id: 2aka, dnm1 GTPase domain in green and c-terminal myosin helix in in red (c) superpose of the hydrophobic groove, suspected GED binding pocket (d) superpose of 1jx2-GDPfree form in brown and 1jwy-GDP bound form in pink.

The minimal constructs we rationalised were inferred from the myosin II-dynaminaA GTPase domain structure (*pdb id: 1jx2*, Hartmut Niemann) and myosin II-dynamina1 GTPase domain structure (*pdb id: 2aka*, Hartmut Niemann) **Fig. 31a,b,c,d**. The knowledge and the model obtained from *hGBP* (human guanylate binding protein, Prakash *et al.*, 2000) also assisted in preparing the constructs, The hydrophobic groove where the myosin helix binds to the GTPase domain in both the structure are similar, except for the groove area, dynaminaA GTPase domain has compact and smaller groove area compared to the rat Dnm1 GTPase domain **Table 12**. We are not sure about the difference, why almost three times more basal GTPase activity for myosin II-dnm1 fusion than myosin II-dymA fusion protein. It might be this hydrophobic pocket which influence the GED binding might have influence during GTP binding or transition state but not in GDP bound state because no major conformational difference has been observed with GDP bound and GDP free state structure in dymA GTPase domain except for the Q34 flip in the G1 motif **Fig. 32**.

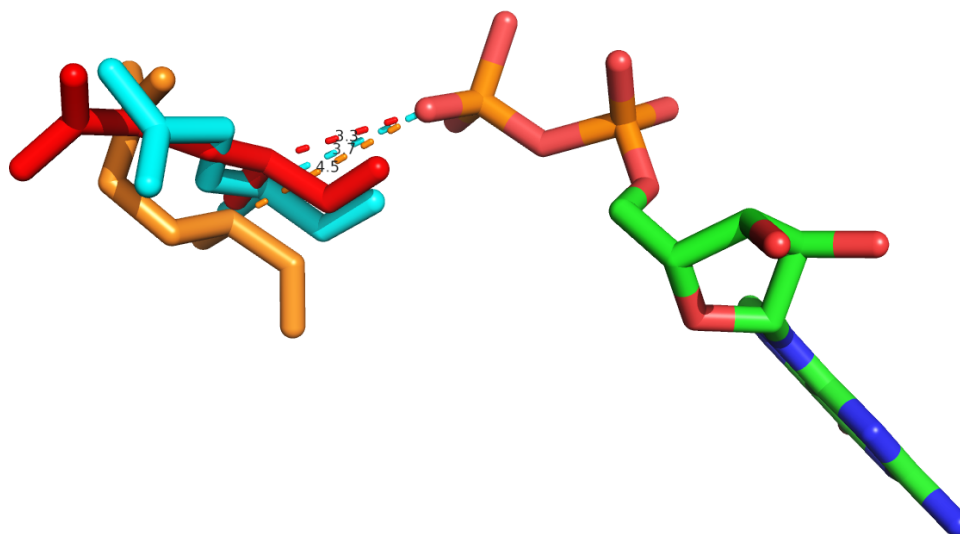


Figure 32: Gln34 in orange is GDP bound dynaminaA GTPase domain structure whereas Gln in red is unbound form; in cyan is Gln40 is dnm1GTPase domain GDP free form. Both Gln and GDP are shown in sticks.

A simple Kyte-Doolittle hydrophathy index observation shows that higher the hydrophathy lesser the GTPase activity. TRGLV is 2.4 (myosin II-dynaminaA fusion); RTLVP is -3.3 (myosin II-dnm1 fusion); DEMLRMYHALKEALSIIIGDINTTTV is 2.8 (c terminal GED in GG1 construct). The values for individual amino acids are taken from ExPASy server. We further measured the GTPase activity of all necessary constructs and screened complete set of

commercially available crystallisation conditions for dynamin1 full length, dynamin3- Δ PRD, MBP-GG1 proteins. **Table 12** summarizes the basal GTPase activity of some of the constructs we prepared.

3.9.2.2 GTPase Activity Test of Various Dynamin1 Constructs

The basal GTPase activity of a range of constructs were measured under standard steady-state assay condition 25 mM HEPES pH7.3, 150 mM NaCl/KCl, 5mM MgCl₂, and 0.5 mM DTT. The measured GTPase activity provided the basis for cross validation of the dynamin activities that has been measured with the presence of inhibitors and modulators. The summary of the measured GTPase activities have been shown in the table below.

Table 12: Basal GTPase activity of various dynamin, dynamin fusion and myosin proteins used in this thesis

Dynamin Constructs	Basal GTPase s⁻¹
DynaminA Full length (<i>D. discoideum</i>)	0.112 \pm 0.020
Myosin II-dynaminA fusion (<i>D. discoideum</i>)	0.119 \pm 0.030
Myosin II-dynamin1 fusion (<i>R. norvegicus</i>)	0.610 \pm 0.070
Maltose binding protein-GG1fusion (<i>H.sapiens</i>)	0.210 \pm 0.020
Dynamin related protein1 (<i>H. sapiens</i>)	0.070 \pm 0.006
Dynamin1 full length (<i>H. sapiens</i>)	0.270 \pm 0.040
Myosin II motor domain (<i>D. discoideum</i>)	0.018 \pm 0.003

3.9.2.3 SH3-Domain Mediated Binding of Amphiphysin1 to Dynamin1

Neuronal amphiphysin1 is a 125 kDa dynamin1 binding protein involved in clathrin mediated endocytosis in neurons. The mechanism how it regulates the binding of dynamin1 is not clear. Amphiphysin1 heterodimer with amphiphysin2 assist dynamin1 interaction with clathrin coat and membranes. We quantified the affinity of amphiphysin1-SH3 domain with microscale thermophoresis **Fig. 33**, dynamin1 was labeled with NT-647 dye from the manufacturer. SH3 domain was serially diluted and titrated. The thermophoresis effect against concentration curve yielded the affinity of 270 nM. The SH3 domain of amphiphysin1 commonly recognizes PXXP motifs, and it binds to specific site from 833–838 of dynamin1 which has the amino acid sequence PSRPNR. Since the SH3 domain of amphiphysin1 has nanomolar affinity for dynamin1, it is used as a affinity tag during the purification of dynamin1.

To examine whether SH3 domain's interaction has influence on dynamin1 GTPase activity, the steady-state kinetics was performed in the presence of the SH3 domain at 150 mM NaCl salt condition, but we could not observe any significant change or no difference at all.

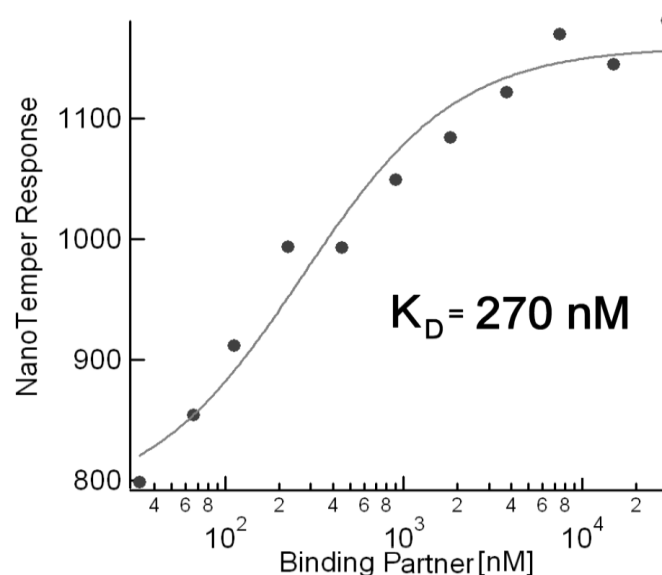


Figure 33: Response curve from microscale thermophoresis experiment. The nano temper response for labeled dynamin1 that was titrated against amphiphysin1-SH3 domain. The K_D value obtained from the fit is 270 nM. Thermophoresis effect is the nano-temper response in the graph.

The GTPase hydrolysis rate has no significant difference as observed 2.2 min^{-1} and 3.7 min^{-1} for without and with SH3 domain respectively. This might be obvious. Because the protein – protein interaction domain has an adapter role than that of effector role to act like a GED. From our results we can say that, SH3 domain has no role in stimulating GTPase hydrolysis activity of dynamin1 or to intervene in the basal GTPase hydrolysis activity.

4. Small Molecule Effectors of Myosin Motor Activity

4.1 Structure-Based Identification of Myosin VI Specific Inhibitors

In this work halogenated carbazoles and phenols were studied as potential modulators of myosin motor activity. Small molecule effectors of motor proteins that are cell permeable, specific, hold potential as therapeutic drugs and as cell biological tools. Upon identification of such small molecule effectors; optimization and several rounds of refinement using pharmacokinetics procedures, the effector molecules can be used as drug candidates targeting myosin, one of the important motor proteins within the cell for a specific therapeutic purpose.

Unconventional class-6 myosins are exclusively expressed in higher eukaryotes and encoded by a single gene (MYO6) (Sellers, 2000). In contrast to all other myosins studied so far, myosin VI was shown to traffic towards the pointed end of polarized actin filaments. These property origins from a structurally unique, class-specific insertion within the catalytic motor domain, redirecting the lever arm around 120° relative to that of plus-end directed myosins (Bahloul, 2004; Bryant, 2007; Chevreux, 2005; De La Cruz, 2001; Liao, 2009; Menetrey, 2005; Mukherjea, 2009; Park, 2007). In agreement with the directionality of the F-actin, it was shown that myosin VI participates in a multitude of fundamental physiological processes involving endocytosis, secretion, the intracellular transport of organelles and vesicles as well as normal and cancerous cell migration (Aschenbrenner, 2003; Dunn, 2006; Geisbrecht, 2002; Hasson, 2003; Mermall, 1994; Yoshida, 2004).

Thus, myosin VI is an interesting therapeutic target. Selective inhibitors are postulated to have medicinal relevance. Despite the potential of myosin VI as drug target, inhibitors of the actomyosin ATPase activity were not identified. Already known allosteric small-molecule inhibitors with selectivity for class-1, -2, and -5 myosins do not exhibit potency against

myosin VI. This might in be in particularly due to the differences in the structural and kinetic features of the myosin VI motor domain, showing the rationale for the design of new inhibitor scaffolds.

One of the allosteric binding pockets in myosin is located 16 Å away from the active site. This pocket is surrounded by strut-loop, cm-loop, loop-2, loop-4 and helix-loop-helix. This collectively forms the actin binding region on myosins. The difference in the allosteric binding pocket between the structural models of *D. discoideum* myosin II (*pdb id: 2jhr*) and *S. scrofa* myosin VI (*pdb id: 2v26*) lies in the cavity size or the volume of the allosteric binding pocket. The difference is brought about by the sequence in this potential binding pocket. H430 and D433 are the equivalent residues for R428 and L431 in comparison to the sequence of *D. discoideum* myosin II. The allosteric binding pocket shown in the **Fig. 34** is the preferred binding site for most of the small molecule inhibitors tested by us (Fedorov et al., 2009; Martin et al., 2009; Preller et al.). K265, A424, R428, L431 are the major interacting amino acid residues with the small molecule effectors known so far. Whereas K232, T426, H430, D433 are the corresponding residues in myosin VI.

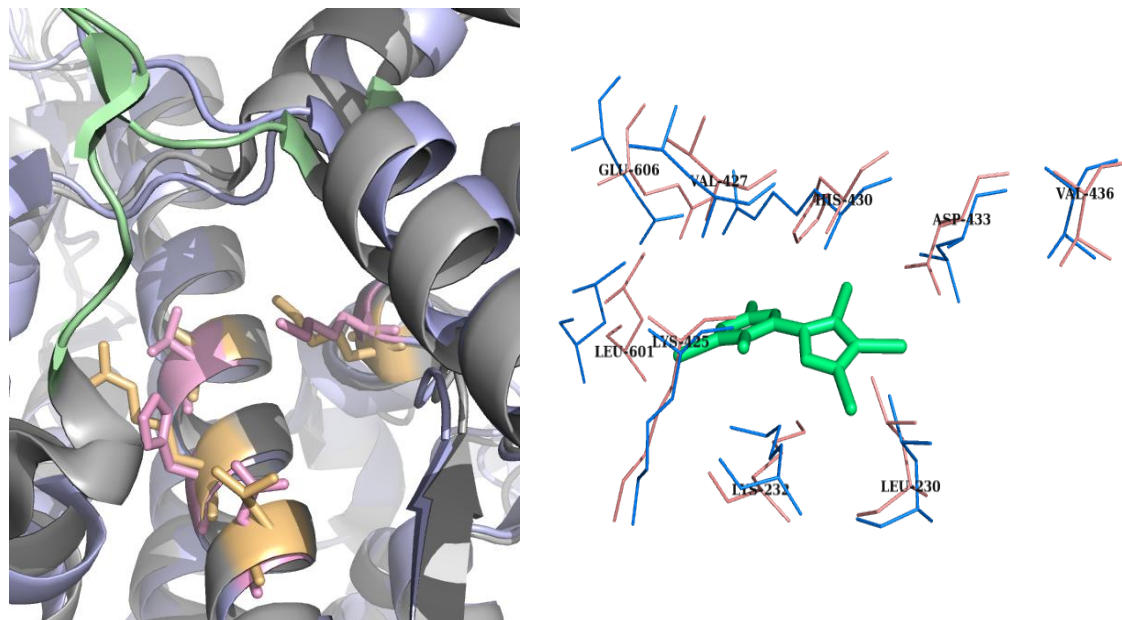


Figure 34: Comparison of Allosteric Binding Site of *D. discoideum* Myosin II and *S. scrofa* Myosin VI Motor Domain (a) Potential allosteric binding pocket of myosin II, shown as a structural comparison at the allosteric pocket with myosin VI. Amino acid residues in stick representation (Pink = myosin VI; orange = myosin II). (b) Close-up view of the pentabromopseudilin (green stick model) binding site in *D. discoideum* myosin II. The side chains in line representation, superimposed with myosin VI (blue) side chains with myosin II (orange).

This project started with understanding and comparing well characterized allosteric binding pockets, and screening a set of compounds, testing them in *in-vitro* assays, to see the influence of the compounds on the basal and actin-activated ATP hydrolysis activity. *In-vivo* assay like vesicle fusion assay combined with live cell TIRF imaging was also performed using the small ligand AP21998 induced vesicle fusion system (Jaiswal, 2009). Initial protein-small molecule interaction studies were performed *in-silico*.

All the phenols for investigations were drawn using JME editor, and the 2-dimensional sketch coordinates were supplied to the GlycoBioChem - PRODRG2 (<http://davapc1.bioch.dundee.ac.uk/prodrg/>) server for minimization. The output from the server produced mol2 format files. The resulting mol2 files were again supplied to autodock for ligand preparations. This includes protonation and energy minimization of the ligands. The output PDBQT files of the ligands were used in autodock vina, in targeted docking mode. The receptor, i.e. myosin VI coordinate file was prepared using autodock MGL tools (<http://mgl.scripps.edu/>), the grid center and grid size were also obtained from autodock. Finally, using a self-written PBS script file autodock vina was executed. The following configuration file is in the materials and methods section.

Table 13: Polyhalogenated phenols and their calculated free energies of binding

Phenols	Molecular formula	Calculated energies (predicted free energy of binding) <i>kcal/mol</i>
2,4,6-Triiodophenol (TIP)	C ₆ H ₃ O ₁ I ₃	-5.6
Pentabromophenol (PBPh)	C ₆ H ₁ O ₁ Br ₅	-5.4
3,5-Bis(trifluoromethyl)phenol (TFMP)	C ₈ H ₄ O ₁ F ₆	-7.6
3,4,5-Trimethoxyphenol (TMP)	C ₉ H ₁₂ O ₄	-5.4
2,4,6-Tribromophenol (TBP)	C ₆ H ₃ O ₁ Br ₃	-5.8

The docking study provided different poses for the phenols in the allosteric binding pocket. They were ranked from one to five; **Fig. 35** shows the preferred binding pose of the individual phenols that were top ranked from the docking studies. Following the docking

experiments, the microscale thermophoresis technique was used to determine the affinity of the compounds for myosin VI.

The low molecular weight effectors used in the above docking studies resulted in different free energy of binding. The halogen bonding and the hydrophobic interactions vary with their substituents. 3,5-Bis(trifluoromethyl)phenol has the least predicted free energy whereas pentabromophenol and 3,4,5-Trimethoxyphenol has the highest calculated free energies.

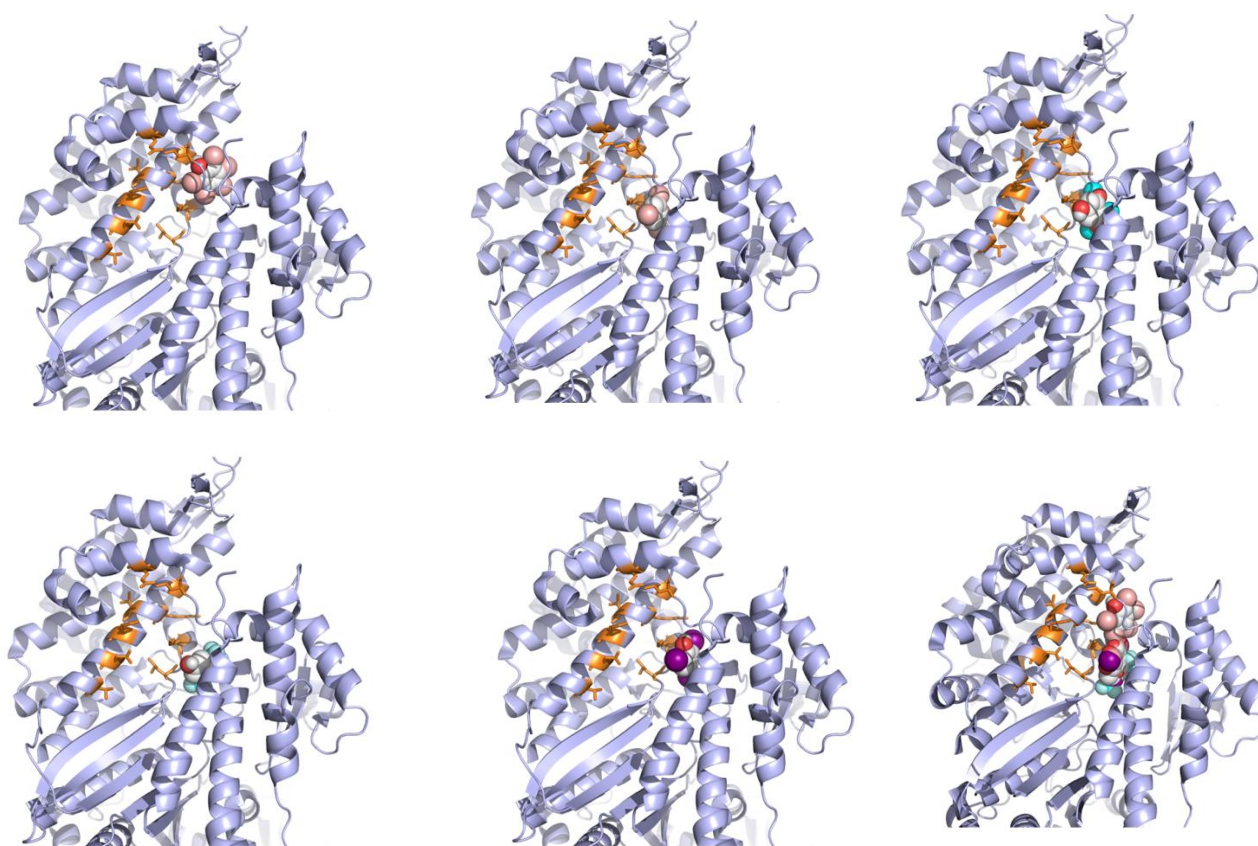


Figure 35: Myosin VI models showing the docking results with (a) Pentabromophenol (b) 2,4,6-Tribromophenol; (c) 3,4,5-Trimethoxyphenol; (d) 3,5-Bis(trifluoromethyl)phenol; (e) 2,4,6-Triiodophenol; (f) model showing cleft occupied by all the phenols.

4.1.1 Functional Characterization of Myosin VI Specific Inhibitors

In the present study, we describe the effect of polyhalogenated phenol derivatives on the *in vitro* steady-state ATPase activity and *in vivo* function of human myosin VI. The basic understanding of the enzymology allowed us to specifically test small molecule effectors on their inhibitory activity. Our data indicates that the myosin ATPase activity can be specifically targeted by the bioactive small-molecule inhibitors 2,4,6-Triiodophenol (TIP, also known as Bobel-24 or AM-24) and 2,3,4,5,6-Pentabromophenol (PBPh), leading to a decrease of the catalytic activity of myosin VI *in vitro*. *In-vivo*, treatment of live cells with TIP and PBPh leads to a phenotype that is comparable with a myosin VI knockdown, indicating a selective blockade of the myosin motor function.

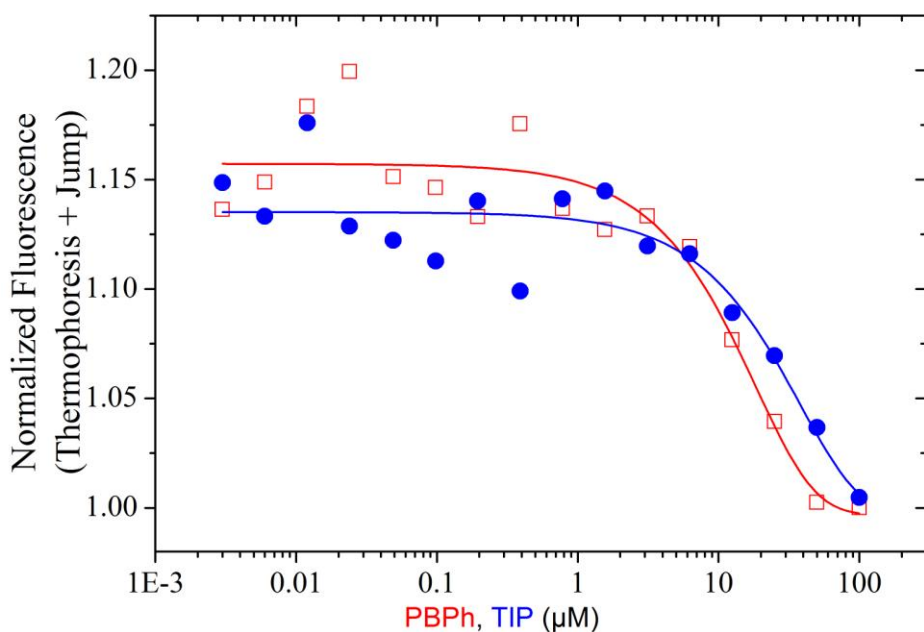


Figure 36: Microscale thermophoresis plot, fitted to the fluorescence intensity change obtained from the thermophoresis effect. The change in thermophoresis movement of labeled myosin VI upon binding to pentabromophenol (green) and triiodophenol (blue) is measured as the change in fluorescence intensity. K_D represents the affinity value of the phenols to myosin VI.

The results obtained gave the order of affinity of the compounds to myosin VI as follows: Pentabromophenol > 2,4,6-triiodophenol with the values of 44, and 61 μM respectively **Fig. 36**. TMP, TFMP, and TBP had produced no significant change in the fluorescence intensity.

4.1.2 Inhibition of Myosin VI ATPase Activity by PBPh and TIP

After the preliminary phenol-myosin VI interaction studies, steady state kinetic experiments were performed to test the influence of the compounds on the myosin ATP hydrolysis activity. The small molecule effector TIP display a biphasic behavior with 37% initial inhibition at $0.8 \pm 0.5 \mu\text{M}$ and 63% inhibition at $37 \pm 2.6 \mu\text{M}$ concentrations. Whereas PBPh decreased the maximum rate of actin activated ATPase rate of myosin VI at $13.7 \mu\text{M}$ concentration. **Fig. 37** shows the ATP hydrolysis rate inhibition by myosin VI by both TIP and PBPh.

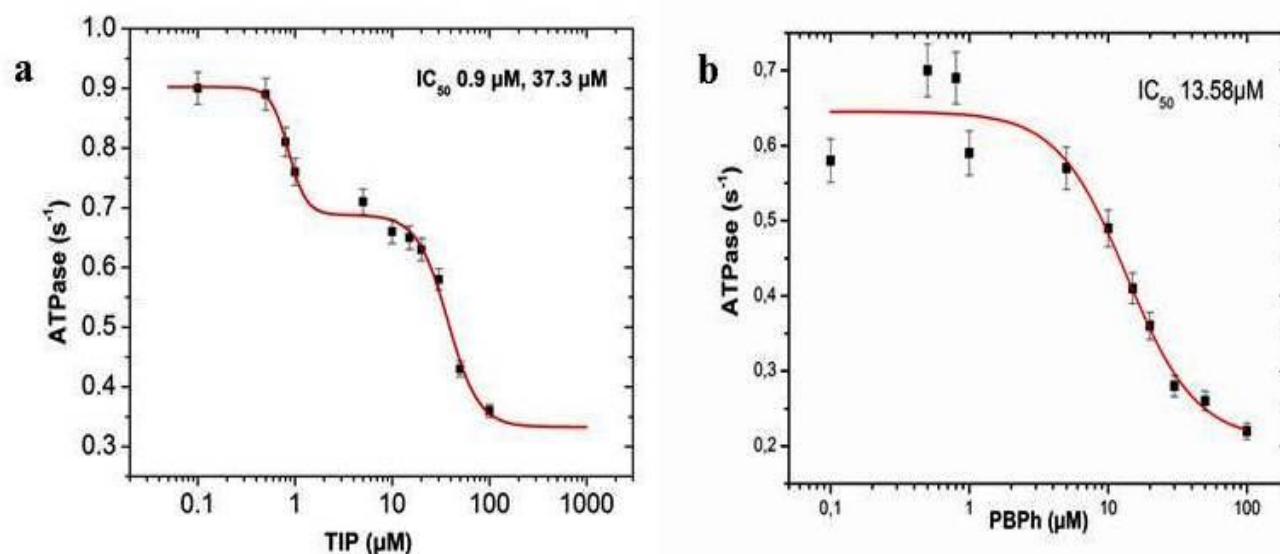


Figure 37: Steady-state ATPase activity. Chemical inhibition of the actin-activated steady-state ATPase activity of myosin VI by TIP and PBPh results in an IC₅₀ value of $7.9 \pm 1.9 \mu\text{M}$ and 13.7 ± 2.67 . Steady-state ATP hydrolysis activity of myosin VI in the presence of 0.1-100 μM of the inhibitors.

The characteristics of the two curves upon fitting the ATPase steady-state assay data are different for TIP and PBPh. TIP has more gradual slope than PBPh, which has steep fall. The other phenols 3,5-Bis(trifluoromethyl)phenol; 3,4,5-Trimethoxyphenol, and 3,4,5-Tribromophenol either had no or had effect at higher concentrations of the compounds on Myosin VI ATP hydrolysis activity. From the binding and activity assays, it could be inferred that TIP and PBPh can bind and modulate the myosin VI motor activity. Particularly the specificity of TIP was tested for myosin VI. Myosin I, myosin II and β -cardiac myosin ATPase hydrolysis activity was not perturbed by the TIP. The table below summarizes the TIP's activity on other classes of myosin.

Table 14: Specificity of TIP for myosin VI and its influence on other myosins ATPase activity

Myosin Isoforms	Basal ATPase activity (s^{-1})	Actin activated ATPase activity (s^{-1})	Inhibition
HMM	0.03	-	n.a
Myosin IB	0.07	0.7	Triiodophenol / inhibition at above 50 μ M
Myosin ID	0.04	1.2	Triiodophenol / no inhibition
Myosin IIC	0.02	1.19	Triiodophenol / no inhibition
β -cardiac myosin	0.034	-	Triiododphenol / no inhibition

4.1.3 Inhibition of Myosin VI Cellular Function by Halogenated Phenols

TFMP, TMP, and TBP have no effect on actin-activated ATP hydrolysis activity of myosin VI. So, as to confirm the specific inhibitory effect of PBPh and TIP in *in-vivo*, vesicle fusion assay was done and TIRF mode in microscopy was used for visualization. In this experiment HeLa cells were treated by the compounds of interest. Treatment of

cells with 2,4,6-Triiodophenol or 2,3,4,5,6-Pentabromophenol reduces the number of exocytic fusion events at the plasma membrane *in vivo* **Fig. 38**.

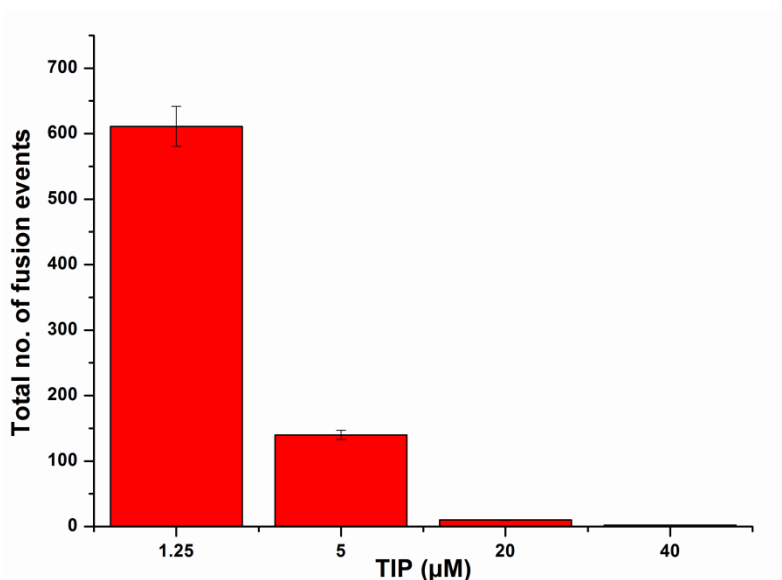


Figure 38: Representative graph of fusion assay: HeLa cells treated with different triiodophenol concentration (1.25, 5, 20 and 40 μM). The exocytic fusion of vesicles to plasma membrane is inhibited by triiodophenol.

TIRF microscopy was used to study and quantify the total number of fusion events at the base of sets of ten cells treated with AP21998 and either TIP or PBPh and monitored at specific, five minute intervals between 25 and 60 minutes after this treatment. The results showed that treatment with increasing concentrations of TIP (0.2 μM, 1 μM, 3 μM, 5 μM, 25 μM) results in correspondingly stronger decreases in the number of fusion events at the plasma membrane, as compared with mock cells (23%, 46%, 67%, 85%, and 100% decreases, respectively). Similarly, treatment with increasing concentrations of PBPh (0.2 μM, 1 μM, 3 μM, 5 μM, 25 μM) results in correspondingly stronger decreases in the number of fusion events (34%, 44%, 72%, 92%, and 100% decreases, respectively).

The moderate, 46% or 44% decreases in the number of fusion events after treatment of cells with 1 μM TIP or PBPh are comparable to the 42% decrease in fusion

events seen after a knockdown of myosin VI with a SMARTpool collection of four independent siRNA primers. In addition to this quantitative similarity to myosin VI knockdown cells, there are qualitative similarities in the appearance and distribution of vesicles at the base of cells treated with TIP or PBPh and myosin VI knockdown cells. As a negative control, cells treated with 25 μM TBP were monitored in a similar manner and found to have no significant deviation from mock cells in the number of secretory fusion events at the plasma membrane **Fig. 39**.

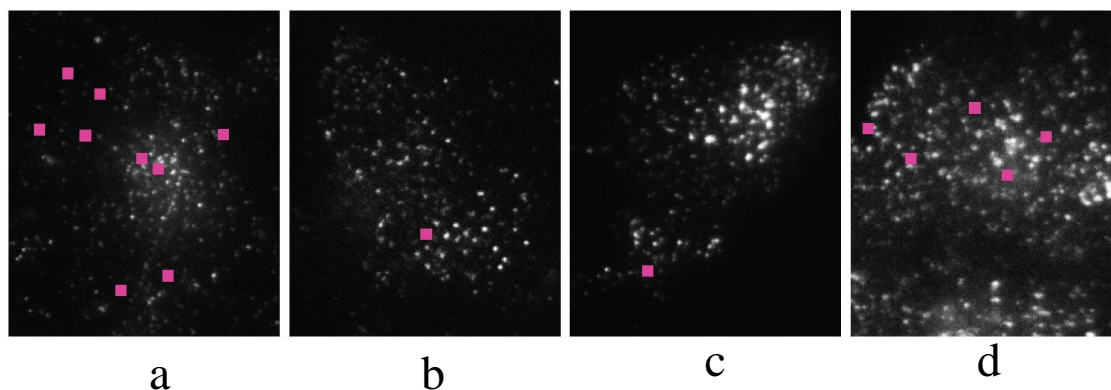


Figure 39: Total number of vesicle fusion events at the plasma membrane. From left to right, sample images of the TIRF field at the base of a mock cell (a), a cell treated with 5 μM 2,4,6-Triiodophenol (b), a cell treated with 5 μM 2,3,4,5,6-Pentabromophenol (c), and a cell in which myosin VI has been knocked down by siRNA transfection (d). Pink squares mark the approximate locations of fusion events over the course of a 5 second movie.

The selection of the lead compounds that only differ in the modifications of the phenol-ring and the unique inhibitor scaffold that does not resemble any other myosin inhibitor described so far are the structural requirements for the selective myosin VI inhibition. The predicted binding mode within the known pseudilin binding site indicates an allosteric mechanism underlying the chemical inhibition. In summary, both closely related organo-halogenic compounds exhibit very similar interaction profiles with myosin VI, indicating that the phenolic scaffold is a good lead. Fine-tuning and optimization of the compounds could lead to the generation of potent, highly selective myosin VI inhibitors with therapeutic potential as well as useful tool compounds. The results are summarized in the table.

Table 15: Summary of myosin VI specific inhibitors TIP and PBPh.

Parameter	Assay	TIP	PBPh
$\Delta G_{\text{bind,free}}$ (kcal/mol)	Docking	-5.6	-5.4
K_D (μM)	Thermophoresis	61 ± 3.0	44 ± 3.83
IC_{50} (μM)	NADH assay	0.8 ± 0.5 and 37 ± 2.6	13.7 ± 2.67
IC_{50} (μM)	Live cell imaging	1.6 ± 0.6	1.5 ± 1.9

4.2 Carbazoles as Modulators of Myosin Motor Activity

Carbazoles are aromatic heterocyclic organic compound. They have a tricyclic structure, consisting of two six-membered benzene ring fused on either side of a five-membered nitrogen-containing ring **Fig. 40**. The compound's structure is an indole structure but in which a second benzene ring is fused to the five-membered ring at the 2-3 position of indole (equivalent to the 4a-8a double bond in carbazole). Graebe and Glazer were the first to isolate carbazoles from coal tar in 1872 (Knolker and Reddy, 2008). In 1965, Chakraborty, (Chakraborty et al., 1995a; Chakraborty et al., 1995b; Chakraborty and Roy, 1991, 2003; Chakraborty et al., 2009) described the isolation and antibiotic properties of carbazole alkaloids from *Murraya koenigii* Spreng. Most of the carbazole alkaloids have been isolated from the taxonomically related higher plants of the genus *Murraya*, *Glycosmis*, and *Clausena* from the family Rutaceae. Further natural sources of carbazole alkaloids are *streptomyces*, blue-green algae *hyella caespitose*, *aspergillus*, *actinomadura* and the ascidian *didemnum granulatum* species.

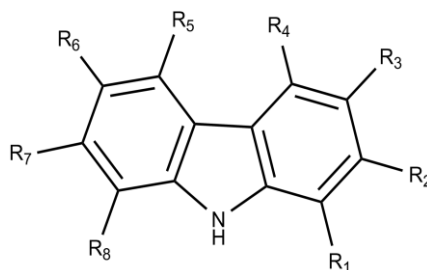
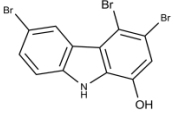
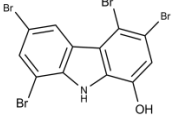
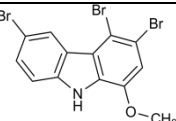
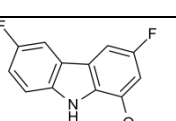
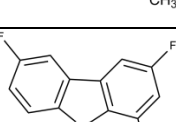
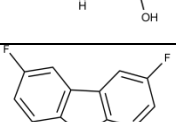
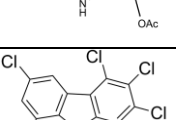
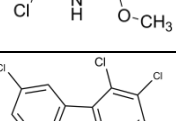
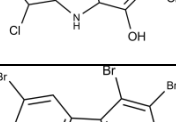
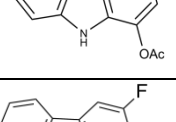
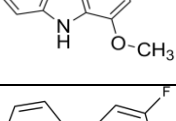
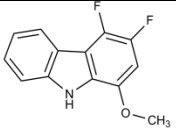
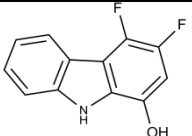
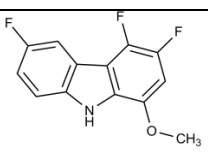
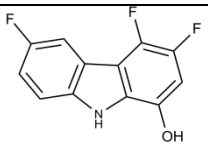
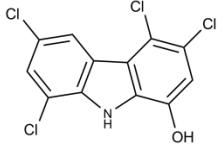
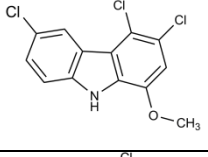
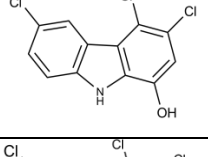
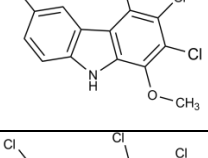
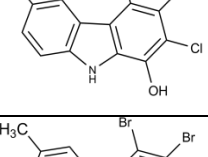
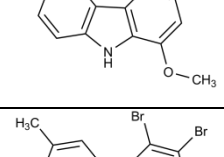
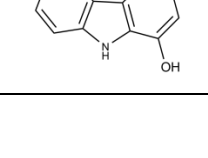


Figure 40: Chemical structures of carbazoles

Table 16: List of Carbazole compounds used for molecular modeling and kinetic studies

KIN.No.	Molecular Structure	Molecular Formula	Molecular Weight (kDa)
79		$C_{12}H_6Br_3NO$	419.8941
80		$C_{12}H_5Br_4NO$	498.7902
81		$C_{13}H_8Br_3NO$	433.921
82		$C_{13}H_9F_2NO$	233.213
83		$C_{12}H_7F_2NO$	219.187
84		$C_{14}H_9F_2NO_2$	261.224
85		$C_{13}H_6Cl_4NO$	369.458
86		$C_{12}H_4Cl_4NO$	355.431
87		$C_{14}H_8Br_3NO_2$	461.931
88		$C_{13}H_{10}F_2NO$	215.223
89		$C_{12}H_8F_2NO$	201.196

90		$C_{13}H_9F_2NO$	233.214
91		$C_{12}H_7F_2NO$	219.187
92		$C_{13}H_8F_3NO$	251.204
93		$C_{12}H_6F_3NO$	237.177
95		$C_{12}H_5Cl_4NO$	320.986
96		$C_{13}H_8Cl_3NO$	300.568
97		$C_{12}H_6Cl_3NO$	286.541
98		$C_{13}H_7Cl_4NO$	335.013
99		$C_{12}H_5Cl_4NO$	320.986
100		$C_{14}H_{11}Br_2NO$	369.051
101		$C_{13}H_9Br_2NO$	355.025

Carbazole derivatives are well known for their various pharmacological activities, including anti-HIV, anticancer, antibacterial and antifungal activities (Arakawa et al., 1999; Barta et al., 2009; Hu et al., 2007; Hu et al., 2006; Okumura et al., 2006). Natural and synthetic carbazoles represent an important and heterogeneous class of anticancer agents. Natural carbazole alkaloids in spite of its many biological activities displays also cytotoxicity against varieties of tumor cell lines. Many carbazole derivatives have been tested for cytotoxic activity, some of them have also entered clinical trials, but only a few have been approved for the treatment of cancer so far, since the clinical application of many carbazoles has encountered problems like severe side effects or multidrug resistance. So, it is necessary to screen diversified carbazole molecules on various biological targets. We tested the listed carbazoles with myosin as target.

So, considering the fact that, myosin II motor domain of the slime mold *D. discoideum* represent as excellent model proteins, as they can be produced in recombinant form in sufficient quantities for detailed kinetic and crystallographic studies. Investigation of the effect of different carbazole derivatives on the basal and actin-activated ATPase activity of class-2, class-5, and class-1 myosins and crystallization experiments with myosin II in complex with $Mg \cdot ADP \cdot VO_3$ and several carbazole compounds were also carried out in this work. Depending on the substitution pattern of the respective carbazoles, the results showed differences in myosin class specific effects, including inhibition as well as activation of myosin and actomyosin ATPase activity.

4.2.1 Free Energy Calculations of Carbazoles Binding to Myosins Using a Molecular Mechanics Approach

Modeling tools, like molecular graphics tools (MGL) package for input data preparation and docking programs like autodock vina with efficient algorithms can provide the theoretical binding scores for the small molecules upon binding to the receptors. In this section results obtained from using myosins from different classes as receptors and halogenated carbazoles as ligands is presented. The simple schematic flowchart in **Fig. 41** represents the experimental scheme that has been used during the molecular docking studies.

The results obtained from autodock vina were used as a starting point to get an idea about the preference of carbazoles for particular myosin isoforms, for example myosin II from *D. discoideum* has preference of KIN86 which is a penta-chlorinated 1-OH carbazole over KIN79 which is a brominated 1-OH carbazole. Similarly, myosin IXb homology models of *C. elegans*, *R. novergicus* and myosin Vb of *D. discoideum* were also used for the docking studies.

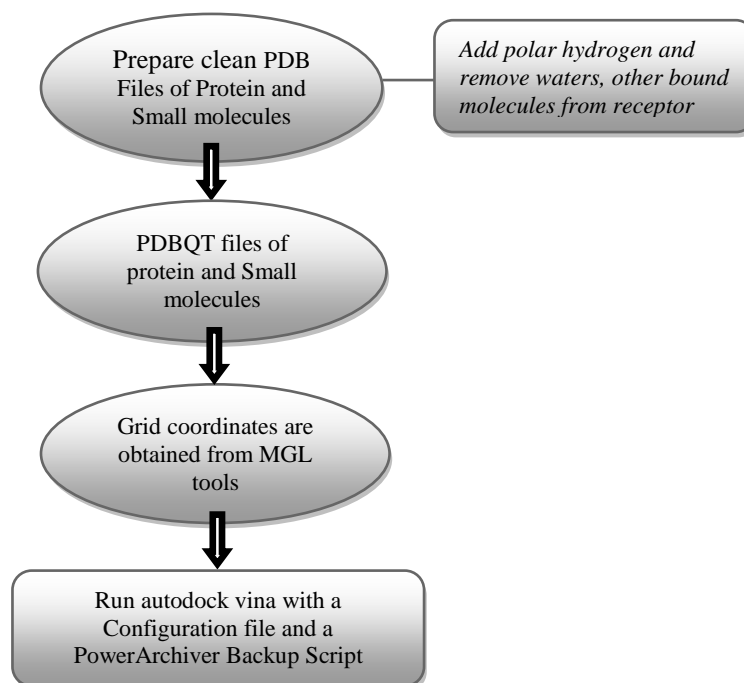


Figure 41: Flowchart for docking of myosin models with carbazoles using autodock- vina

The table below summarizes the docking results of some of the myosin isoforms with carbazoles. The predicted binding values are in *kcal/mol*. KIN83 which is fluorinated at R₃ and R₆ position has the highest calculated free energy value for myosin IXb of *R. novergicus*. The variation of the sequence of myosin IXb of *R. novergicus* to myosin IXb of *C. elegans* at serine drastically changes the preference from fluorinated to chlorinated carbazoles. The united atom scoring function in autodock vina allows the degrees of freedom only to polar hydrogens but not to any hydroxyl groups in the docking site. This

might have an internal steric constraints when an allosteric pocket has -OH group containing amino acid side chains. Moreover the ten-fold increase in exhaustiveness parameter from 8 to 80 has improved and increased the probability of finding the minima in the energy landscape.

Table 17: Summary of molecular docking results of carbazoles on various myosin classes

Myosin motor domain used as receptors	Organism to which the myosin belongs to	Calculated free energy values in kcal/mol	Substituted functional groups	Availability of experimental data
Myosin IXb	<i>C. elegans</i>	1. KIN86 -7.9 2. KIN99 -7.6 3. KIN101 -7.5 4. KIN79 -7.4	5Cl,1OH 4Cl,1OH 2Br,1Me,1OH 3Br,1OH	Yes
Myosin IXb	<i>R. norvegicus</i>	1. KIN83 -8.2 2. KIN93 -8.2 3. KIN89 -8.1 4. KIN99 -8.0	2Fl,1OH 3Fl,1OH 1Fl,1OH 4Cl,1OH	No
Myosin Vb_0K	<i>D. discoideum</i>	1. KIN93 -8.0 2. KIN91 -7.9 3. KIN83 -7.7 4. KIN89 -7.5	3Fl,1OH 2Fl,1OH 2Fl,1OH 1Fl,1OH	No
Myosin Vb_6k	<i>D. discoideum</i>	1. KIN101 -6.9 2. KIN93 -6.9 3. KIN97 -6.9 4. KIN86 -6.9	2Br,1OH 3Fl,1OH 3Cl,1OH 5Cl,1OH	No
Myosin II	<i>D. discoideum</i>	1.KIN86 -8.1 2.KIN99 -7.8 3.KIN84 -7.7 4.KIN93 -7.7	5Cl,1OH 4Cl,1OH 2F,1OAc 3Fl,1OH	Yes

Mostly the carbazoles with high affinity values docked between the upper and lower 50kDa cleft in the myosin structure. They bind to the similar allosteric site where pentabromopseudilin binds. The mechanism of inhibition of selected carbazoles has been

investigated by systematic kinetics study of several myosin classes and in particular myosin II isoforms. Blind docking and site specific (target based) docking simulations on various myosins guided us through the modeling assisted drug discovery (MADD). Modeling programs like Modeller was very helpful in using multiple structures to generate homology models. Thus, to prepare and validate the homology models of myosin IXb and myosin V MODELLER was used **Fig. 42**. Homology models of myosin IXb and myosin Vb were built using MODELLER. This modeling program is a script based command line module. With user assisted inputs, one can efficiently generate a model containing all non-hydrogen atoms. Also, MODELLER implements comparative protein structure modeling by satisfaction of spatial restraints, so the user has an opportunity to do loop optimization, multiple alignments of protein sequences and/or structures. These two important steps have been used in preparing the models in this work.

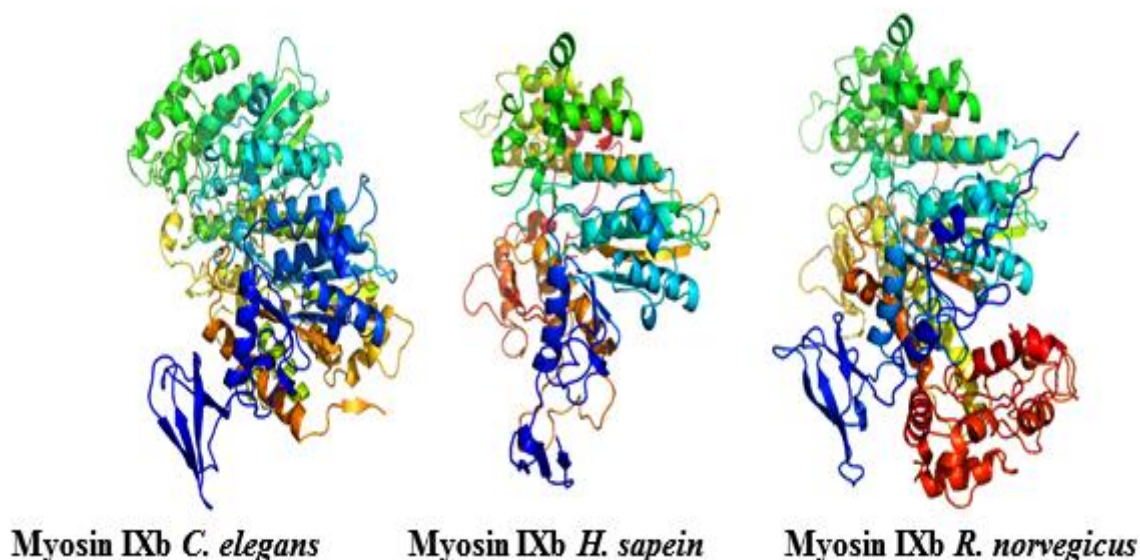


Figure 42: Homology models of Myosin IXb, prepared using MODELER, these models were used in docking studies with carbazoles

Table 18: Comparison of amino acids around the allosteric binding site of *D. discoideum* myosin II with different myosin isoforms. Color coded according to residue property.

Myo II <i>D. discoideum</i>	LYS 265 K	ALA424 A	ALA420 A	ASP590 D	ALA618 A	ARG428 R	ILE617 I	LEU431 L
Myo V <i>D. discoideum</i>	K	F	S	D	F	M	K	D
Myo IXb <i>H. sapiens</i>	K	S	S	D	A	A	V	D
Myo IXb <i>R. norvegicus</i>	K	S	S	D	A	A	V	D
Myo IXb <i>C. elegans</i>	K	C	A	D	A	S	V	H
Myo XI <i>N. Tabacum</i>	R	V	A	D	E	R	E	D

Myosin II of *D. discoideum* and myosin IXb of *C. elegans* had preference for penta-chlorinated carbazole, whereas myosin Vb of *D. discoideum* and myosin IXb of *R. norvegicus* had preference for fluorinated carbazoles **Fig. 43, 44**. Preference of the halogen substituted carbazoles might be due to the variation in the hydrophobicity in the allosteric binding pockets of various myosins. The table above shows a close comparison of amino acids around the known allosteric binding pocket of myosin II of *D. discoideum* to other myosins.

To identify the binding site for 2,3,4,6,8-pentachloro-9H-carbazol-1-ol (KIN86), the penta-chlorinated carbazole as the candidate compound was crystallized with the *D. discoideum* myosin II motor domain complexed with Mg^{2+} .ADP.VO₃. The structure was solved by molecular replacement using the structure of *D. discoideum* myosinII.ADP.VO₃ complex as a starting model (pdb id: 2JJ9) and refined to 2.7 Å resolution (the final values of R_{work} and R_{free} are 20% and 28% respectively). Crystallization of other carbazoles like 3,4-dibromo-6-methyl-9H-carbazol-1-ol (KIN101), KIN79 with the *D. discoideum* myosin II motor domain and other myosin isoforms are in progress but could not be completed within the time frame of this work.

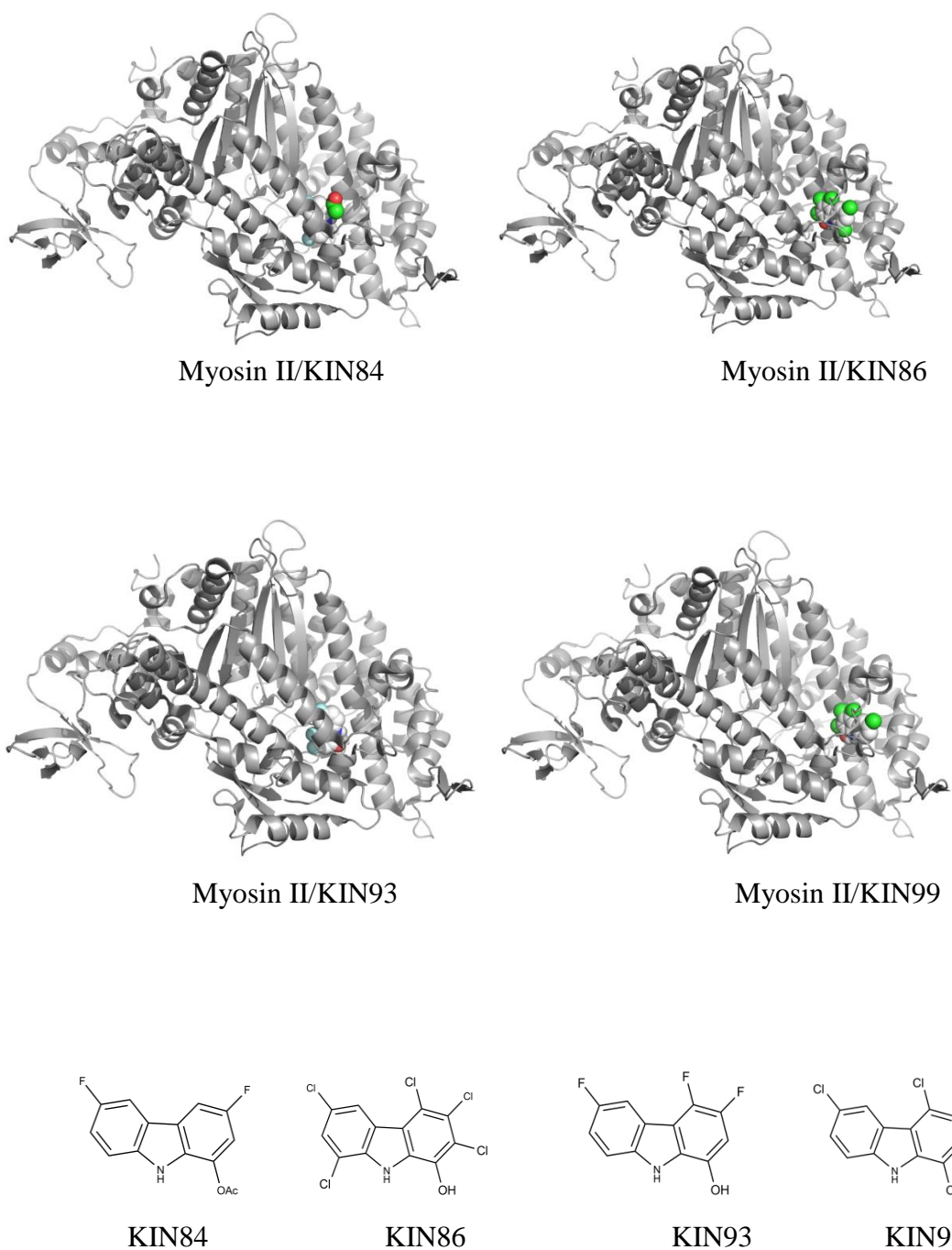
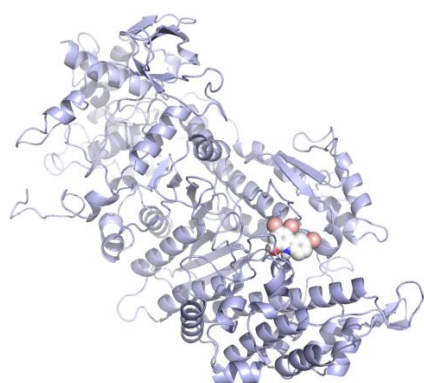


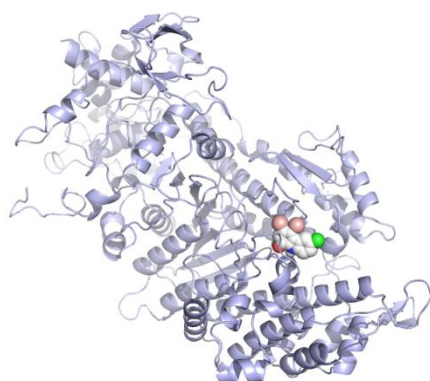
Figure 43: Docking results of chlorinated and fluorinated carbazoles to myosin II motor domain of *D. discoideum*.



Myosin IXb/KIN79



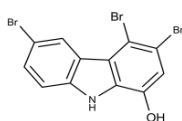
Myosin IXb/KIN86



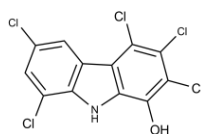
Myosin IXb/KIN99



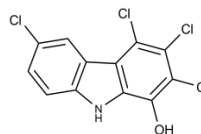
Myosin IXb/KIN101



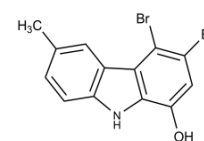
KIN79



KIN86



KIN99



KIN101

Figure 44: Docking results of brominated and chlorinated carbazoles to myosin IXb of *C. elegans*.

4.2.2 Inhibiting Potency of Pre-Selected Carbazoles on Myosin ATPase Activity

Steady-state ATPase assays could further confirm the modeling data. KIN101, one of the top ranked small molecule effector from docking results which has Br at R₃, R₄ and CH₃

at R₆ positions had modulating effect on myosin IXb's actin-activated ATPase activity in an individual activity assay. KIN101 is a potentially inhibitor compared to other KINs. Whereas, KIN79 is specific to myosin Ib (**Fig. 45**). R₃, R₄ and R₆ positions of KIN79 were substituted with bromines. Myosin II from *D. discoideum* had a preference for range of carbazole compounds with different affinity values. KIN86 was selected, as it was the top scored molecule for myosin II from the docking studies. R₂, R₃, R₄, R₆, and R₈ positions were substituted with chlorines. Crystals of myosin II in complex with KIN86 were used for soaking experiment, and the complex structure gave us insight in the binding mode of carbazoles to myosins.

Table 19: Summary of KIN79 effect on actin-activated ATPase activity of myosin isoforms

KIN79	Actin-activated ATP hydrolysis activity
parameters	IC₅₀ (μM) k_{min} (s⁻¹)
<i>D. d</i> Myosin II	40.5 ± 1.7 0.03
<i>D. d</i> Myosin Vb	26.9 ± 16.9 0.24
<i>O. c</i> Myosin II HMM	171.5 ± 1.75 0.09
<i>D. d</i> Myosin Ib	4.2 ± 2.1 0.03

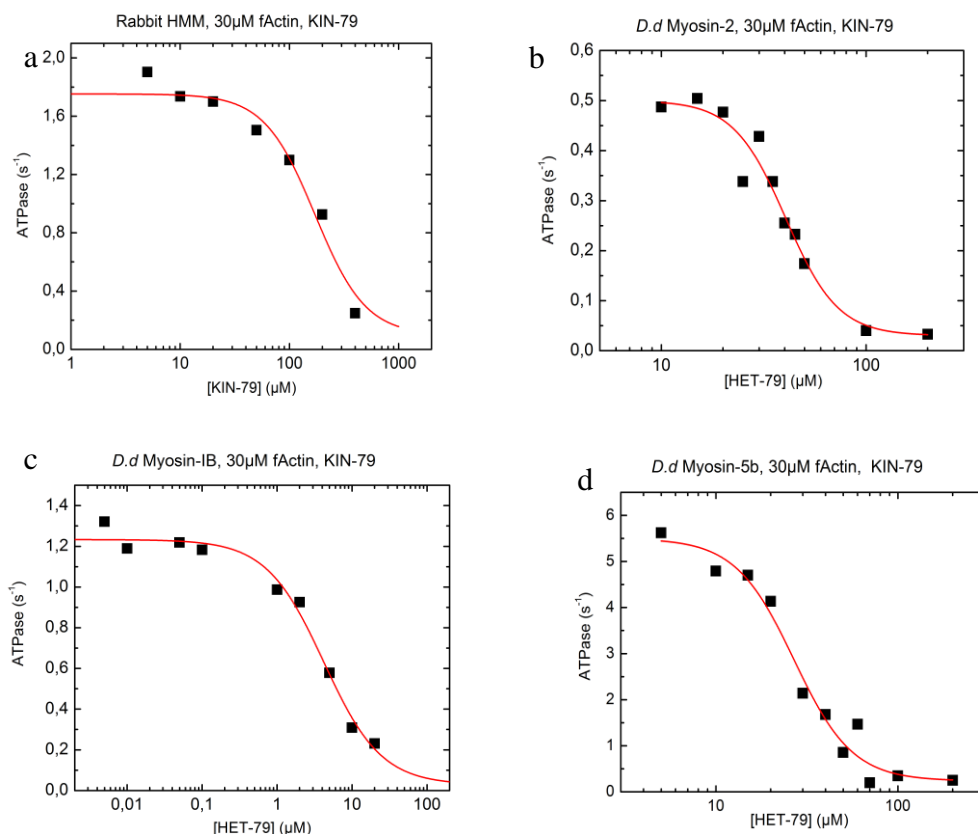


Figure 45: Steady state ATPase activity of myosin II, myosin V, myosin Ib and HMM. (a,b,c,d) Actin-activated ATPase activity of different myosin isoforms in the presence of KIN79 (e) Normalized ATPase rate shows KIN79 specificity for *D. discoideum* myosin Ib in violet curve. The inserted table gives the IC₅₀ values for respective myosins for KIN79.

The actin-activated ATPase activity of myosin Vb from *D. discoideum* is reduced by 3,4,6,-tribromo-1-hydroxycarbazole (KIN79) with an IC₅₀ value of 26 μM. This compound additionally inhibits myosin II of *D. discoideum* with IC₅₀ of 40 μM. KIN79 is a most potent compound for myosin Ib of *D. discoideum* with IC₅₀ of 4.2 μM. In contrast, 2,3,4,6,8-pentachloro-1OH-carbazole (KIN86) exhibits the opposite effect by activating actin-activated ATPase activity of myosin II of *D. discoideum*, but has an inhibitory effect on HMM up to the concentrations of 10 μM and 8 μM, respectively.

From the modeling, kinetic and structural data, It could be shown that 3,4,6-tribromophenol-9H-carbazol-1-ol (KIN79) is an inhibitor with low IC₅₀ of 4.2 μM for myosin Ib. But, 2,3,4,6,8-pentachloro-9H-carbazol-1-ol(KIN86) is an activator of actin-activated ATPase rate of myosin II of *D. discoideum*. Thus the results obtained shows that halogenated

carbazoles can be used as allosteric inhibitors and activators to perturb the activity of myosins.

KIN86 is a chlorinated carbazole which activates actin-activated ATPase rate for *D. discoideum* myosin II but inhibits rabbit skeletal heavy meromyosin (HMM). Steady state kinetics can clearly show the inhibition and activation of actin-activated ATPase rate of various classes of myosins as shown in **Fig. 46**. Increase in the actin filament movement is clearly seen in *in-vitro* motility analysis; narrow distribution from 400 trajectories signifies the data quality.

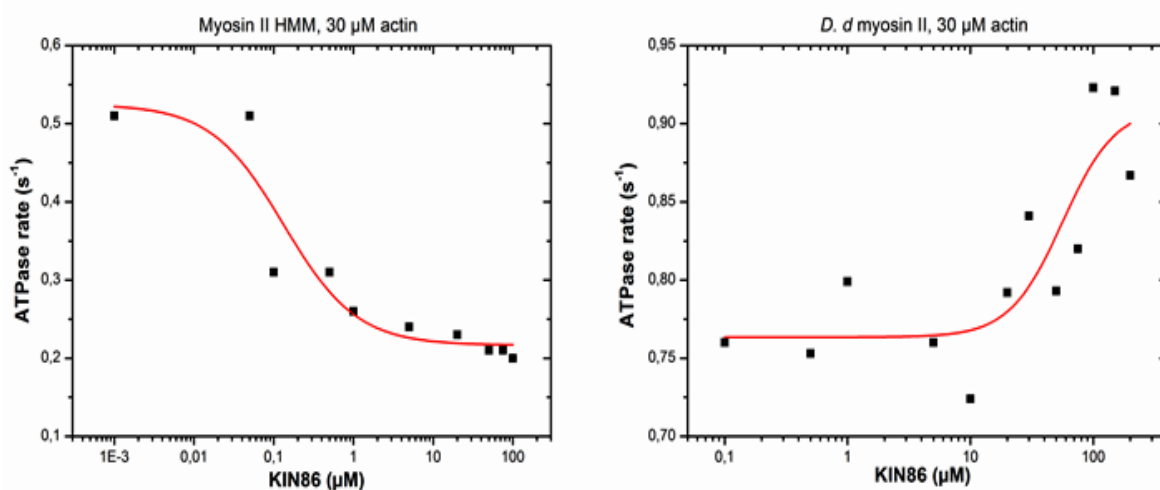


Figure 46: Steady state ATPase activity of myosin II, in the presence of KIN86 with concentration ranging from 0.1-100 μM . On the left, inhibition of the actin-activated ATPase rate in the case of rabbit HMM. The fit on the right shows KIN86 activating the actin-activated ATPase rate in the case of myosin II. The assay was performed in the presence of 30 μM of actin.

In agreement with the steady-state kinetics data, KIN86 mediated activation of *D. discoideum* myosin II in the *in-vitro* motility assay also **Fig. 47**. The histograms show the average sliding velocity of rhodamine-phalloidin-labeled actin filaments in the absence and presence of 5 μM KIN86. *D. discoideum* myosin II moves actin filaments with an average velocity of $0.76 \pm 0.15 \mu\text{m s}^{-1}$, addition of 5 μM KIN86 in the same flow cell increases the average sliding velocity to $1.08 \pm 0.16 \mu\text{m s}^{-1}$.

Activation of *Dd* myosin-2 actin filament movement by 5 μ M KIN-86

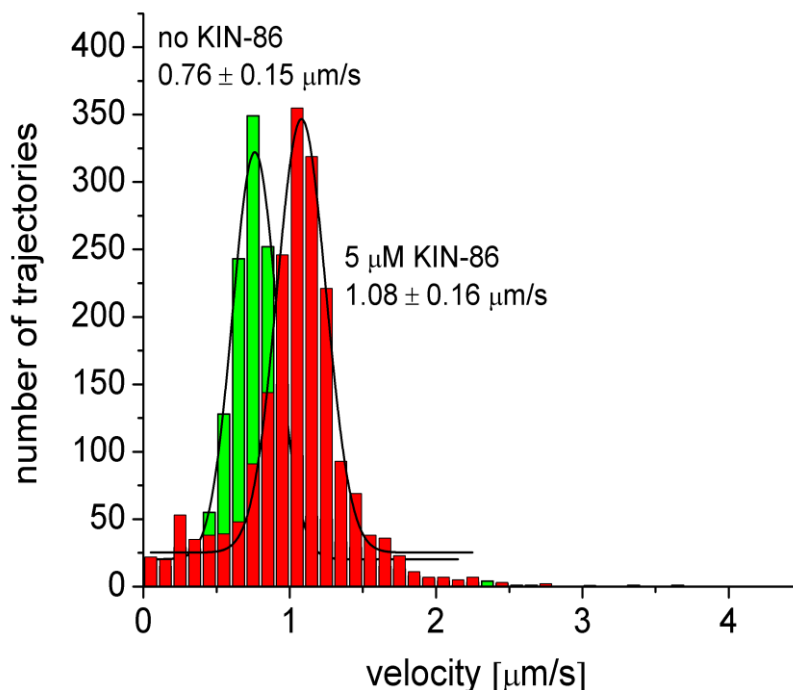


Figure 47: KIN86-mediated activation of *D. discoideum* myosin II in the *in vitro* motility assay. Increase in the actin filament movement in in-vitro motility analysis indicated KIN86 can act as activator and inhibitor for different myosins.

4.3 Crystal Structure of the Myosin II Motor Domain in Complex with 2,3,4,6,8-pentachlorododecahydro-1*H*-carbazol-1-ol (KIN86)

4.3.1 Structural Characterization of the KIN86 Binding Site

Primary screens of carbazole derivatives were performed with myosins as target biological system in the *in-vitro* assays. The phenomenon of interest for this study were myosin ATPase activation, inhibition of actin activated ATPases and inhibition of active tension generation. Elucidating these points would provide a clue about the properties of myosin intermediate states and help understanding the mechanisms underlying the muscle contraction.

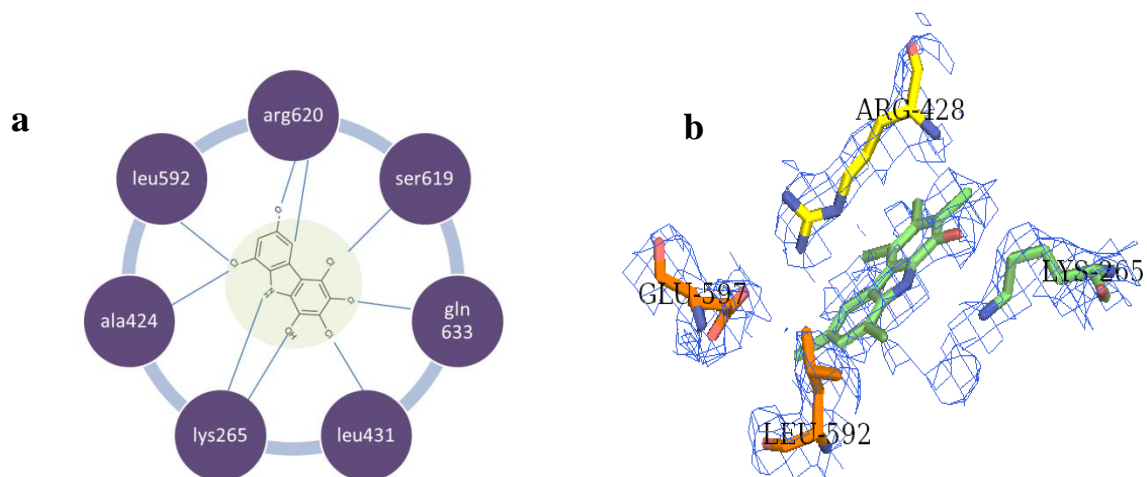


Figure 48: (a) KIN86 binding site and interacting residues, (b) 2F₀-F_c density map of the KIN86 binding site.

The myosin II motor domain structure of *D. discoideum* solved in complex with KIN86 had the overall fold of the motor domain to already reported myosin II motor domain structures. The meta-vanadate ion shows tetrahedral interaction, and the distance between the vanadium atom and the β - γ -bridging oxygen is 2.1 Å. The meta-vanadate thus fully replaces the position of the γ -phosphate. Therefore, the nucleotide *meta*-vanadate complex at the active site resembles ATP. The electron density for KIN86 is unambiguous **Fig. 48b** and shows the inhibitor to bind in a pocket close to actin binding residues and located 18.9Å away from the nucleotide-binding site. The experimentally observed conformation of KIN86 is planar in agreement with Hückel's rule, with extra two electrons coming from the unshared pair in sp² hybrid orbitals on nitrogen atom. The translational and rotational displacement of the molecule by itself varies from one carbazoles to the other, which is evident from our docking data. Upon binding of KIN86, the changes brought about in the main chain compared to the pdb structure 2JJ9, which is the myosin II structure with no small molecule effector is almost negligible. The calculated r.m.s.d is approximately 0.332 Å up to amino acid 648. Mostly, the small molecules influence the side chains along the relay pathway between the nucleotide binding pocket and the allosteric binding site (Chinthlapudi et al., 2011).

Structural analysis showed that the carbazole-derivatives bind to the same site as pentabromopseudilin **Fig. 48a**, at the tip of the myosin motor domain, near actin-binding region. Thus, halogenated 1-OH-carbazoles emerge as promising lead compounds for the

development of myosin-directed therapeutic drugs. In conclusion all the results show how small effector molecules affect energetic coupling and thereby myosin motor functions.

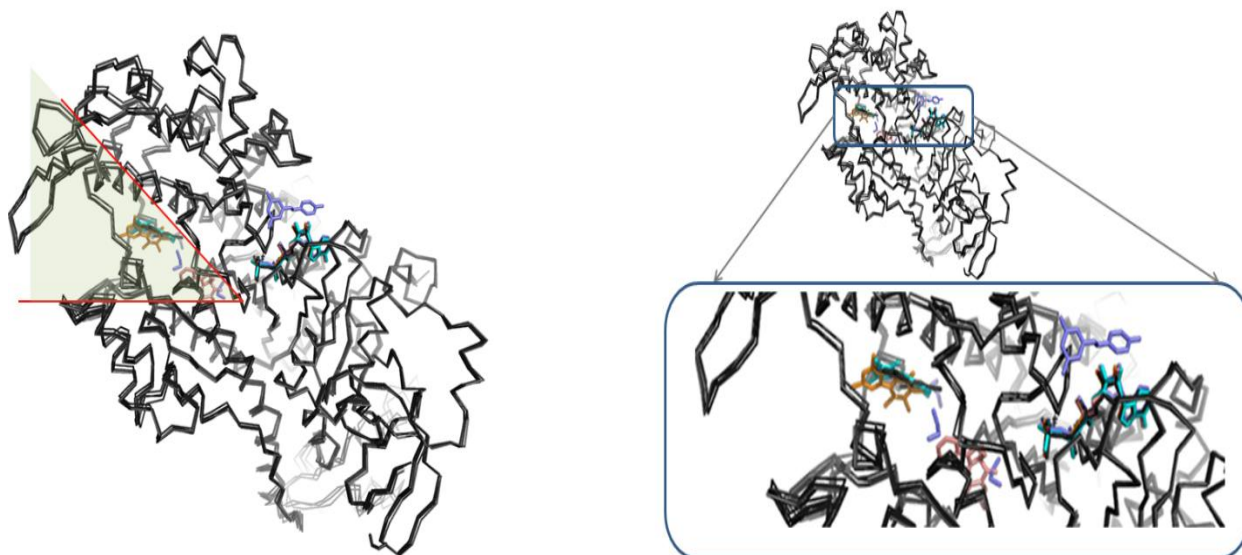


Figure 49: A close up view of superimposed myosin II pdb coordinates of structure with small molecule effectors. On the left is the side view of the actin binding cleft marked in red line whereas in the right, the cleft highlighted and enlarged in box, the actin binding interface where effectors molecules are observed in crystal structures of 2JHR, 2X9H, 2XO8, 3MNP, 3MJX.

The inner face of this KIN86 binding pocket is formed by helix13 and helix 21 and loop 2, which are connected by a helix-loop-helix motif that covers part of the cleft and U50 kDa in a lid-like fashion as similar to PBP binding mode. The myosin motor domain does not undergo any major conformational change upon binding of KIN86, except for local changes directly involved in the coordination of the effector molecule. The interactions of the small molecule modulators like tribromodichloropseudilin; pentachloropseudilin; pentabromopseudilin and with the basic residue corresponding to K265 in myosin II are conserved among the known complex structures and this is also the case with the KIN86 carbazole. Except blebbistatin, all the other allosteric modulators, are approximately 16 to 18 Å away from the catalytic site **Fig. 49**. In the resulting conformation K265 appears to be closer to K423 compared to the uncomplexed structure. The relay pathway is shown in the **Fig. 50**.

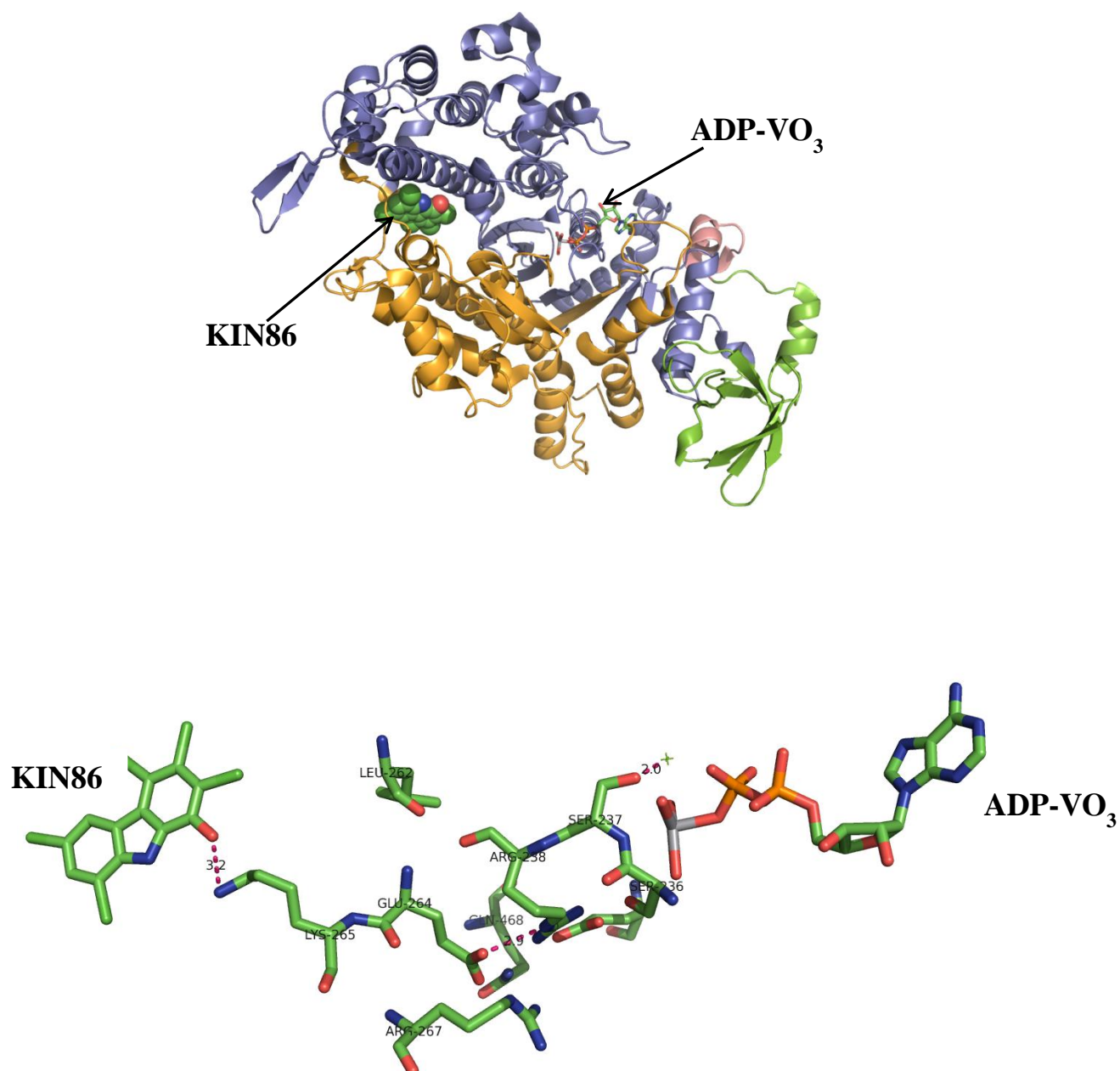


Figure 50: (Top) Overall view of the myosin motor domain in cartoon representation. KIN86 is shown in spheres mode and nucleotide in stick representation. Blue, upper 50-kDa domain; orange, lower 50-kDa domain; green, SH3-like domain. (Below) Schematic illustration of the relay pathway connecting the allosteric pocket and the nucleotide binding site in the presence of KIN86-myosin II.ADP.VO₃.Mg²⁺ motor domain structure.

Table 20: Data collection and refinement statistics

Space group	C2221
Cell dimensions a, b, c (Å)	89.2 1446.6 153.7
Resolution (Å)	20.0-2.7
Rmerge (%) <I/σI>2.4	0.40
Completeness	100
Redundancy	5
Refinement	
Resolution	20.0-2.7
Rwork/Rfree (%)	20/28
No of reflections working /test set	26158/1377
No.Atoms	
Proteins	5483
Ligands/ions	51
Water	198
Average B-Factors (Å ²)	38

4.3.2 B-Factor Analysis of the X-ray Structures of the Myosin II Motor Domain in Complex with Different Inhibitors

In the structure presented in this work, the waters were added to the protein and refined using CNS and Refmac. During the process of model validation of the final refined structures, some waters were removed using the distance criteria in COOT. The following B-factor plots show comparison between the myosin II structures without (PDB id: 2JJ9) and with ligand (PDB id: 2X9H, 2JHR).

The physical meaning of the B-factors depends on the resolution of the data obtained. In the case of the presented structural details, the low B-factors for the residues around the KIN86 binding site K265, A420, A424, R428, L431, D590, I617, A618 might represent the degree of confidence of the atomic position. The KIN86 almost freezes all the residues except I617 compared to the pentabromopseudilin at the allosteric binding pocket in the myosin structure. But in comparison with uncomplexed myosin structure 2JJ9, both KIN86 and pentabromopseudilin bound structures 2X9H and 2JHR respectively reduced the dynamics of the allosteric pocket. Restricting the flexibility of the side chains might perturb the relay pathway between the allosteric binding pocket and the nucleotide pocket. This brings about the alteration in the kinetic properties of myosin for their nucleotide hydrolysis, which again is coupled with the affinity of myosin to actin. Thus B-factors play an important role in describing the protein's intrinsic disorder and indicate the changes after and before small molecule effectors binds to it.

The thermal fluctuations of atoms from their mean position can be calculated and used as an indicator for the dynamics of a polypeptide or functional protein. The backbone atoms and side chains are constantly in thermal motion; displacements of atoms from their mean positions indicate the degree of protein flexibility. Upon binding to the substrates the intrinsic flexibility of myosin may vary, and this is evident from the results presented above. Myosins have the allosteric site, which change its conformation upon substrate binding or product release to allow actin to dissociate or to bind. The B-factor analysis can help revealing the dynamic properties of the allosteric site and thus facilitate in defining a descriptor during the development of new myosin effectors based on the scaffold. The changes in overall myosin three-dimensional structure are subtle even upon small molecule effector binding to its allosteric site. The r.m.s.d of the backbone C- α atom between complexed and uncomplexed

structures are minimum as mentioned before. But, the noticeable wobbling of side chains along the relay path i.e. the communication pathway between the allosteric and active sites implies the effectiveness in interactions and the perturbation of the energetic couplings between acto-myosin complexes brought about by the KIN86.

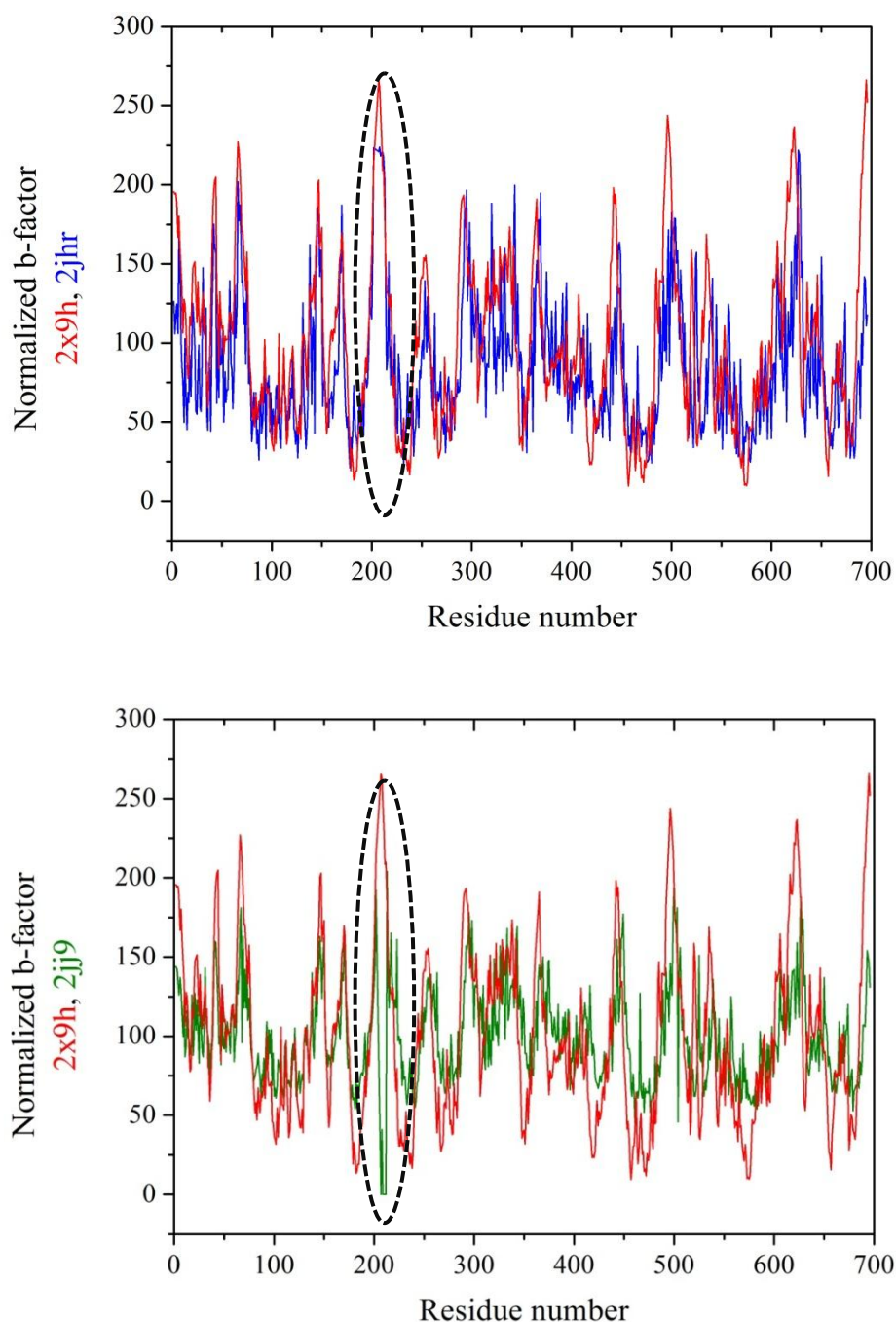


Figure 51: B-factor plots: Normalized B-factor between 2x9h in red (myosin II/KIN86), 2jhr in blue (myosin II/pentabromopseudilin) and 2jj9 in green (myosin II/no inhibitor). For example there is clear difference in the normalized B-factor values around 207-212 residues dotted circle which is a loop1 region.

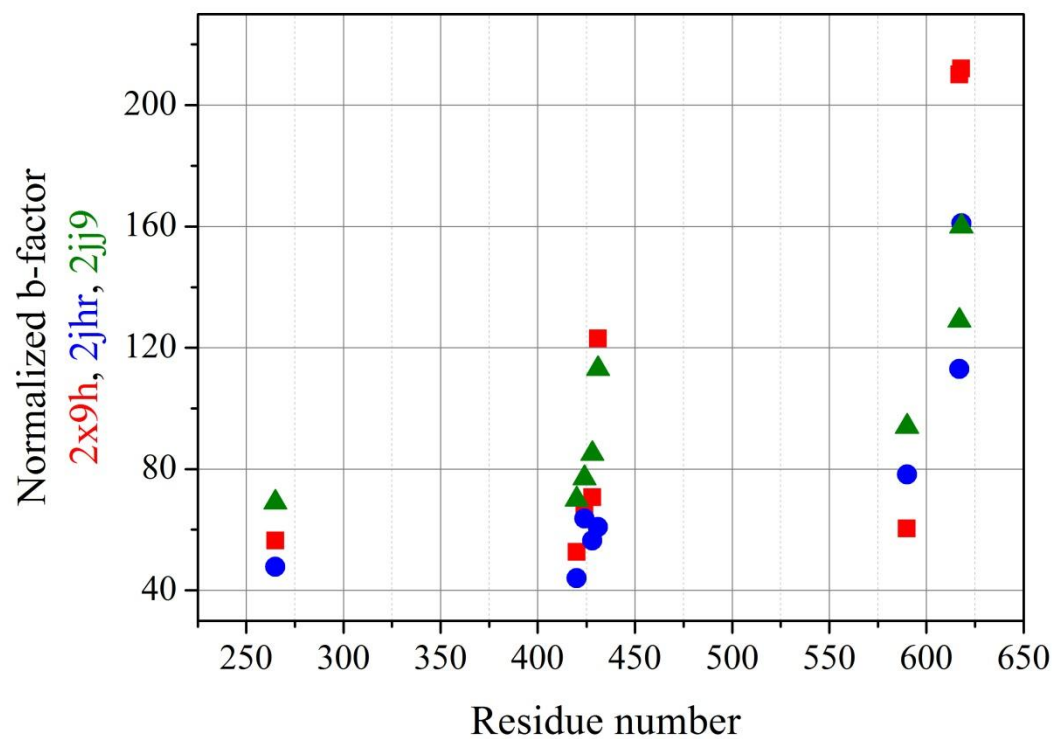


Figure 52: B-factor plots: Normalized B-factor between 2x9h in red square (myosin II/KIN86), 2jhr in blue circle (myosin II/pentabromopseudilin) and 2jj9 in green triangle (myosin II/no inhibitor), The plot highlights the normalized B-factors of the residues K265,A420,A424,R428,L431,D590,I617,A618 which forms the allosteric binding site of KIN86.

The careful understanding of B-factors, not only provide the insight about the protein flexibility, but also might tell about the conserved waters, that may be important for hydrogen bonding either with the protein or with the bound ligands. During the processes like, defining the quantitative structure active relationship (QSAR) studies of similar ligands with the proteins, the initial step is to pose the ligands on to the available X-ray co-crystal structure and keep the conserved waters. So, B-factor analysis assists and gives an idea about the water molecules that's necessary during QSAR studies.

Discussion

5.1 The Combinatorial Approach

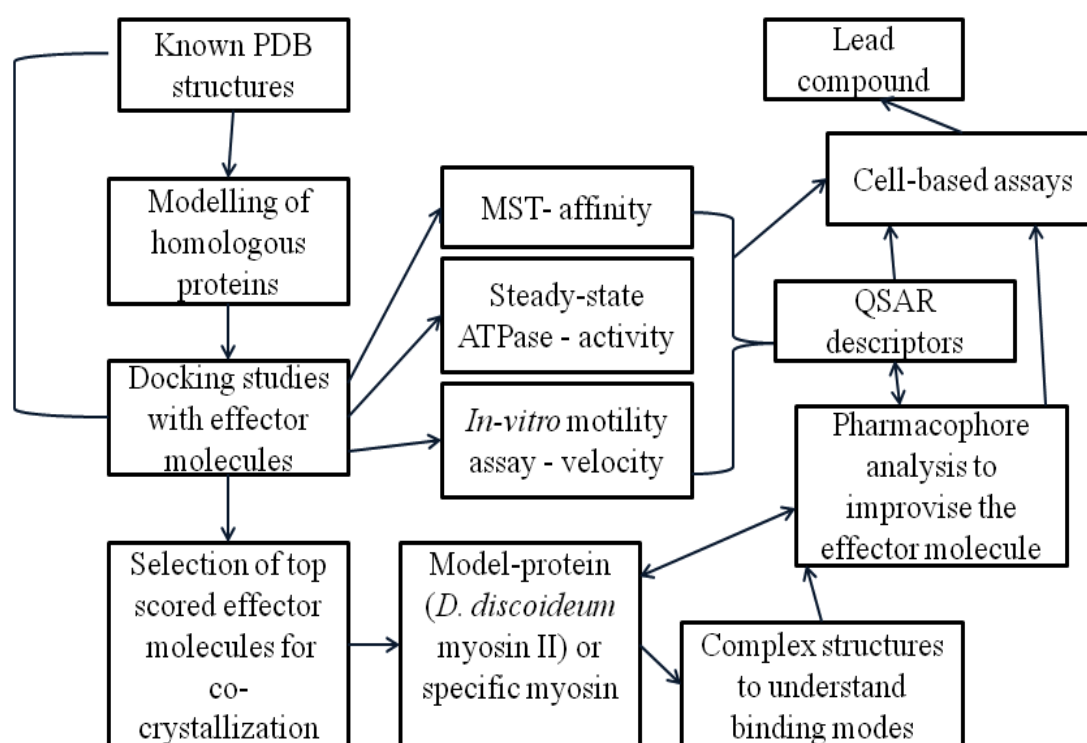


Figure D1: Scheme used in my work to identify the small molecule modulators of myosin, dynamin1 and Drp1.

5.1.1 Psychotropic Drugs as Potent Effectors of Dynamin1 and Drp1

Dynamin and dynamin related proteins are interesting pharmacological targets among the proteins involved in endocytosis, vesicle sorting and mitochondrial division. The structural and functional differences between the classical dynamin and non-classical dynamin provides for the development of selective and potent modulators that can be used as novel treatments for the diseases associated with endocytosis and mitochondrial division. The semi-carbazone compound dynasore inhibits dynamin and Drp1 GTPase activity with ~15 and 80 μM respectively (Nankoe, 2006; Macia, 2006). Since there is a need for specific compounds to modulate various dynamins and dynamin related proteins, it is important to screen different class of small molecules. Particularly psychotropic drugs which act on the

receptors of the post synaptic neurons to control the level of neurotransmitters in the brain have been implicated in the treatment of depression, anxiety and other psychotic states. The recycling of the vesicles containing neurotransmitters within pre-synaptic neuron and uptake of the neurotransmitter bound receptors on the post-synaptic neurons are mediated by dynamin. Neuroleptic drug chlorpromazine inhibits Low-Density-Lipoprotein receptor recycling, implying that psychotropic drugs can interfere with endocytosis (Wang, 19). Since it has been shown that inhibitors of dynamin1 could have potential use as anti-psychotic drugs, a few psychotropic drugs that are approved by FDA and that are used in psychological illness were investigated on knowledge based screening of drugs. Mechanism of action of these drugs for particular psychotic states vary upon which particular receptor is being blocked in the neurons. Sertraline, the Drp1's anti-assembly agent found in our study, belongs to the class of drugs called selective serotonin reuptake inhibitor (SSRI). It is a derivative of 1-naphthylamine and works by increasing the serotonin level at brain by blocking serotonin reuptake, thus affecting the receptor numbers and distribution in the brain (Koe, 1983). There are some studies indicating that psychotropic drugs may also work through intercalation in membrane phospholipids (Oruch, 2010). As a proof of concept, the psychotropic drug fluvoxamine here in our study is speculated to bind to the lipid binding domain of dynamin1.

Classical serotonin (5-HT) transmission between neurons is shown in the **Fig. D1**. Therefore, Chlorpromazine, sertraline and fluvoxamine which are generic drugs are tested for their effect on the GTPase activity of dynamin1, dynamin related protein1 and minimal dynamin1 (GG) proteins. Sertraline was used to test for its effects on self-assembly stimulated Drp1 GTPase activity and dynamin1 GTPase activity. The IC_{50} values of two selective serotonin reuptake inhibitors i.e. sertraline and fluvoxamine were 70 and 14 μ M for dynamin1 full length protein, respectively. IC_{50} of sertraline for Drp1 was between 15 to 30 μ M and for the minimal dynamin1 the IC_{50} was 8 μ M. From the results, it's clear that sertraline is a mixed type of inhibitor i.e. dynamin1 minimal construct (GG1) which has no middle domain and PH domain has lower IC_{50} value than the dynamin1 full-length, whereas Drp1 which has no PH domain can be also influenced by the sertraline for its assembly induced GTP activity. The kinetic analysis revealed that fluvoxamine is a non-competitive inhibitor of dynamin1 GTPase with respect to GTP. Fluvoxamine has no effect on GG1 or Drp1, indicating that it binds to PH domain. Structurally fluvoxamine is similar to phosphoinositide with a head and a tail group. Our results indicate that sertraline and fluvoxamine inhibit dynamin1 GTPase activity

and could be potential modulators of dynamins. Thus, sertraline and other psychotropic drugs expanded our understanding of the biological space for dynamin and dynamin related proteins.

Thus, ‘‘Understanding risk factors of diseases and the way they have to be treated for mental illness patients are important’’.

5.1.1.1 Characterization of Sertraline as a New Allosteric Inhibitor of Drp1 Self-Assembly

Drp1 like classical dynamin1 also has ionic strength dependent GTP hydrolysis activity, i.e. at low ionic strength concentration, GTP hydrolysis activity of Drp1 increases with the increase in protein concentrations. Whereas, there is no significant change of the basal GTP hydrolysis activity of Drp1 at high ionic strength concentration that has been observed at the similar protein concentrations range to that of the concentration range in low ionic strength. This increase in the hydrolysis activity can be linked to the assembly stimulated effect of the Drp1. Particularly sertraline, a newly identified small molecule modulator of Drp1 seems to convert assembly competent population of Drp1 to incompetent conformation. Thereby inhibiting the assembly stimulated GTP hydrolysis activity of Drp1. Mass distribution profile from DLS at low ionic strength had three different peaks with three different apparent hydrodynamic radiuses (R_h). Whereas, in case of high ionic strength a single peak was obtained, implying the mono-dispersity of the protein at this ionic strength. But, the presence of the psychotropic drug sertraline, Drp1 seems to reverse the effect on Drp1’s propensity to form polymers. Upon addition of sertraline at low ionic condition, a single peak was obtained as similar to that of high ionic condition. This suggests that, sertraline can act as an anti-polymerization agent for Drp1. Analytical ultracentrifuge (AU) data shows the influence of GTP- γ -S and GDP on Drp1 assembly property. In comparison to GTP- γ -S, GDP shifts the s -values implying that it might induce conformational change of Drp1. But in the presence of sertraline Drp1 had no effect on GDP induced sedimentation coefficient shift. Thus, sertraline might have a role as anti-polymerization agent and act as an inhibitor of assembly stimulated GTPase activity of Drp1 but not a direct inhibitor of basal GTPase activity of Drp1. Also, the binding efficiency of Drp1 for GDP is higher than that of GTP. This can be correlated to, why GDP could possibly induce significant conformational change and there by shifting the s -value in the AUC experiment.

5.1.1.1.1 Drp1 Acts as a Substrate of Cdk2/CyclinA

The fraction of Drp1 that is found around mitochondria is about 3% of the total protein (Smirnova et al, 2001). There has to be a mechanism of how Drp1 is regulated from cytoplasmic pool to the mitochondrial outer membrane during programmed cell death (PCD). Thus the steps like (i) recruitment of Drp1 by adapter proteins, (ii) Drp1 nucleation, (iii) assembly stimulated GTP hydrolysis and (iv) disassembly from the scaffold lipid membranes, should be highly regulated. Understanding the interaction partners and the modifications of Drp1 post translationally helps in resolving and dissecting the steps mentioned above. Previous studies have shown that, phosphorylation of Ser616 by Cdk1/CyclinB (Chang et al, 2007), Ser637 by protein kinase A (PKA) and also by Ca^{2+} /calmodulin-dependent protein kinase I α (CaMKI α) (Han et al, 2008), other modifications such as, sumoylation of Drp1 and its role for the Bax/Bak association (Wasiak et al, 2007) all have physiological importance for post translationally modified Drp1. Even some other studies have shown that Drp1 in *Xenopus* specifically bind to cyclinA (Funokoshi et al, 1999). Some of our own studies on the interaction between Drp1 and cyclin dependent kinase (Cdk2) indicated that Drp1 is being phosphorylated by Cdk2. In which, S548 is identified as one of the amino acid as phosphorylation site in Drp1. We also showed that Drp1 does not compete for p27 binding site in the CycA/p27 complex, but instead binds to cyclinA. Combining the steady-state kinetics and FRET data it can be inferred that Drp1 can bind to cyclinA and still can be inhibited from getting phosphorylated. There might my other regulatory or adaptor proteins to signal the Cdk2 to phosphorylate Drp1 or to inhibit p27 from binding to Cdk2/CycA complex so as to get Drp1 phosphorylated. But the current study could not provide enough evidence about other interacting partners or signaling proteins. Thus Drp1 is one of the substrate for Cdk2/CyclinA complex, and a new phosphorylation site in Drp1 was identified. However, the physiological relevance for this phosphorylation event is not clear at the moment. But S548A and S548D mutant Drp1 construct can be used to study the biochemical and cell biological analysis; this will prove the importance of the newly identified phosphorylation site. Furthermore screening of crystallization conditions to co-crystallize the non-ubiquitinated CyclinA-Drp1 fulllength was also set up during the course of this work. This will give an insight into the protein-protein interactions and their regulatory mechanism on Drp1 during mitosis, where Cdks plays an important role.

5.1.1.1.2 ATP Increases Drp1 Binding Affinity to Mitochondrial Lipids

When normal cells are exposed to toxic substances or irradiation, they undergo necrosis. During necrosis, mitochondrial swelling, DNA fragmentation and membrane rupture take place which results in severe inflammation around the damaged cells. In contrast to necrosis, apoptosis also called programmed cell death (PCD) takes place during tissue proliferation to remove unwanted cells. Apoptosis is necessary during development of organs like brain, limbs and also PCD is crucial process in peripheral nerve fiber formation. Inhibition of apoptosis leads to cancer or deregulation in neuron growth, leading to neurodegenerative diseases. In another intriguing study of lipid-protein interaction; it was found that, cardiolipin, the lipid enriched on mitochondrial membrane, could bind to Drp1 and this interaction is enhanced by ATP. But we could not confirm the importance of ATP on Drp1-cardiolipin's interaction and its physiological role.

Cardiolipins are phospholipids, with two pK values, the low pK₁ (1.04) and high pK₂(>8.0) (Kate et al., 1993). The mammalian cardiolipins have four polyunsaturated chains, with two phosphate head groups. It is the only lipid produced in mitochondria and is absent from the cytosol until cell death. During apoptosis (Gonzalvez et al., 2008; Schug, 2009; Schug and Gottlieb, 2009) when cells commit suicide, the mitochondria has to be destructed. This is because mitochondria are the power house of the cell. Contact sites in mitochondria are enriched with cardiolipins (Kerr et al., 1972), the tbid protein which carries the apoptotic stimuli targets and remodels the contact sites on mitochondria and assist for Bax oligomerization (Epand et al., 2002a; Epand et al., 2002b) and thus leading to the cells to apoptosis and emphasize the importance of cardiolipins. Taffazin gene is one more factor that assists in remodeling cardiolipins, malfunction of taffazin has (Bione et al., 1996; Bione et al., 1994; Bione et al., 1995; Bione et al., 1993) been implicated in many diseases including Barth's syndrome. The chain length of cardiolipin has a very important consequence in its biological and biochemical role. The dissections of cardiolipin's role in cell death, mitochondrial fissioning and ATP synthesis are crucial. Results from our studies provide us some hint on the local environment of mitochondria and Drp1's affinity for mitochondrial membrane.

5.1.1.2 Molecular Engineering of Optimized Dynamin Constructs for Structure Determination and Functional Studies

It has been shown that I697A has significant influence on assembly of dynamin1 into multimers (see **Fig. 28b** for domain organization). Studies have also shown purified GED alone tend to (to form multimers) oligomerize in vitro (>600kda) (Chugh et al., 2006; Chugh et al., 2007). Peptides from 654-681 residues and 712-740 residues in dynamin1 have tendencies to aggregate into tetramer, hexamer respectively (Okamoto et al., 1997; Okamoto et al., 1999). The functional importance of GED might be, that it acts allosterically, may contribute one of its arginine to the catalytic center but this possibility can be ruled out, because similar entry routes are blocked in rat dynamin1 (Reubold et al., 2005). GED may interact and stabilize switch II and with accumulating evidence it might be that GED is not a classical GAP (GTPase activating protein). Dynamins which are the large GTPase family of proteins, for which there is new structures available now, (Chappie et al., 2010; Chappie et al., 2009). Many approaches can be followed so as to obtain the three dimensional conformation of the full length protein. Site directed mutagenesis or creating mutants from the knowledge of homologous proteins or using scaffold proteins are some of the ways to obtain enough soluble form of proteins. Thus our GG1, GGA minimal constructs and mutants constructs to obtain the dimeric form of dynamin1, dynamin3, dynamin related protein1 have gave us an insight of how high molecular weight oligomerizing proteins can be studied systematically.

5.1.2 Small Molecule Effectors of Myosin

Myosins play fundamental roles in a wide range of physiological functions within every human cell. Muscle contraction, cell migration, intracellular transport, endocytosis, and protein secretion are some of the roles of myosin in muscle and non muscle cells. Non-muscle myosin IIa and IIb as well as myosin Va were shown to play a major role in cancer cells, providing essential functions in cell migration and metastasis (Carmona-Fontaine et al., 2008a; Carmona-Fontaine et al., 2008b; Choi et al., 2008; Giannone et al., 2007; Gupton et al., 2005). Alterations in cell motility are a prerequisite for cancer cells to migrate from the primary site into surrounding tissues to disseminate and to metastasize. The inhibition of myosin II has been shown to strongly affect migration due to loss of motile activity and

cohesive forces, a prerequisite for invasive cancer cell migration. Recently, it was shown that myosin VI and optineurin are important in the regulation of fusion pores formed between secretory vesicles and the plasma membrane during the final stages of secretion (Bond et al., 2011). Polarized trafficking of vesicle-bound membrane proteins in neurons is mediated and directed by myosin VI, which results in enrichment of surface proteins in axons (Tommy et al., 2011). The importance of myosin VI in sound transduction (in auditory system) and balance has been well documented (Ahmed et al., 2003; Coling et al., 1997; Duncan et al., 2006; Friedman et al., 1999; Hilgert et al., 2008; Melchionda et al., 2001; Mohiddin et al., 2004; Sato, 2006; Schultz et al., 2005; Seiler et al., 2004). Known inhibitors of myosins such as blebbistatin, BDM (2,3-butanedione monoxime), and BTS (N-benzyl-p-toluol-sulfonamide) are unspecificity, toxic, and have side effects. Hence using such compounds as therapeutic applications in cancer treatment pose a severe restrictions.

As mentioned in the beginning of the discussion, high resolution X-ray structures of protein-inhibitor complexes and their biochemical, biophysical, and cell biological characterization are prerequisite to identify potent, specific and non-toxic inhibitors. Crystal structure analyses led to the identification of a carbazole binding sites in the myosin motor domain. The sites show a considerable amino acid sequence variance between individual myosin isoforms, which allows the development of highly selective myosin inhibitors. Such as myosin VI allosteric binding cavity volume is small in compared with that of myosin II, and this explains why small scaffolds like phenols have an inhibitory effect on myosin VI. But X-ray structures are necessary to define the changes that alter the myosin VI motor activity.

5.1.2.1 Mechanism and Specificity of Myosin Inhibition by Halogenated Carbazoles and Phenols

Myosin effectors are useful tool in order to dissect the functional role of myosin *in vivo* and *in vitro*. Myosin is considered as an attractive drug target for the treatment of diseases like familial hypertrophic cardiomyopathy, cancer, deafness and distal arthrogryposis. Mutational studies revealed that the disruption of communication between active site and lever arm in myosin II *D. discoideum* results in the blockage of motor activity, improper fruiting-body formation, cytokinesis and growth of *D. discoideum* cells in suspension (Tsiavaliaris et al., 2002). Mutation in loop2 of myosin V, which is a surface loop in the actin binding region, alters the myosin affinity for actin, thereby decreasing the

processivity of myosin V (Christopher et al., 2004). Thus, actin-activated ATPase and *in-vitro* motility are mostly affected due to changing the charge distribution or hydrophobicity of loop2, cardiomyopathy loop and strut loop (Naoya sasaki et al., 2002). The strut loop which is a connector between upper and lower 50 kda domain depends on its length and plasticity, can also be perturbed by small molecule modulators, which could further lead to alteration in subdomain interactions with actin.

Small molecules can be used to bring about the parallel effects in comparison to the mutagenesis experiments. This further increases the degree of confidence in understanding the manipulation and fine tuning of the motor activity of myosins. Hence, the intricate communication pathways by comparing the mutagenesis experiments and available X-ray crystallographic models of complex structures along with kinetics data can be a valuable tool in designing potent and class specific and isoform specific myosin inhibitors. Therefore, studying the effects of small molecule compounds like carbazoles and phenols on myosin function is a promising way to develop new drugs for therapeutic application in cancer treatment and other myosin related diseases. Infection of the host cells by protozoa

P. falciparum and *T. Gondii* movement in the host cell is myosin mediated, in such cases myosin of the protozoa can also be one of the target for treatment of diseases like malaria, and toxoplasmosis. The fundamental principle in understanding a disease is to understand the molecular components involved in causing that disease. Once the pathway is established, the next step is to understand the mechanisms at molecular level. It is at this stage, a small molecule can be used to probe the enzymatic activity either to act as an agonist or antagonist. The small molecules can be a biomarker in which case imaging is possible to track down the localization of the enzymes involved or a drug like molecule can be used in which, it helps to activate or inhibit the enzyme activity or a pharmacological chaperone can be used to assist the target protein in regaining the functions that has been lost due to mutations or misfolding.

Both carbazoles and phenols that were screened and tested had an effect on the enzymatic activity of myosin. So, series of halogenated carbazoles were screened and tested on the different myosin classes to check their potency and specificity. The effect of different carbazole derivatives and phenols on the basal and actin-activated ATPase activity of class-2,

class-5, and class-1 myosins were studied. KIN79, a penta-brominated carbazole was identified as one of the specific inhibitor with low IC_{50} of 4.2 μ M for myosin Ib.

Despite the great success in identifying selective inhibitors of myosin classes-1, -2 and -5, small molecule effectors specifically targeting class-6 myosins have not been described yet. The identification of myosin VI effects are one of the focus of recent research, since myosin VI and its binding partners participate in signaling and transport processes that have been linked to inflammatory processes, apoptosis, and the metastatic spreading of cancer cells. Myosin VI has been also shown to reduce the directed migration of cells towards a growth factor stimulus (Margarita et al, 2010). The loss of MYO6 expression might cause shaker/waltzer behavior and deafness. Along with myosin VI, myosin VIIA and myosin XV are the causative agents for hearing loss, Usher syndrome type1B (Friedman et al., 1999).

In the present study, phenolic effectors scaffold was chosen as potential lead to specifically target myosin VI. Previously studies have shown halogenated phenols to act as selective antineoplastic agents. TIP was shown to possess antitumor effect on leukemia cells and human pancreatic cell lines by inducing Bcl2- and caspase-independent lysosomal and mitochondrial cell death. Furthermore, the inhibition profile of TIP revealed the compound to function as leukotriene B4 synthesis inhibitor and anti-inflammatory drug.

We show TIP and PBPh to selectively inhibit human myosin VI motor function *in vitro* and *in vivo*. We subsequently provide evidence for a direct interaction of TIP and PBPh with myosin motor domain in a thermophoretic assay, indicating moderate binding affinities in the low micromolar range. Through analyzing the effect of the iodinated phenole derivative on a specific, myosin VI dependent exocytic pathway, our data shows a concentration-dependent reduction of fusion events of exocytic particles at the plasma membrane of HeLa cells after TIP and PBPh-treatment. In agreement with the observation that TIP inhibits, but does not abolish exocytic fusion events is the moderate reduction of the steady-state myosin ATPase activity in response to TIP exposure. The obtained IC_{50} values obtained from steady-state ATPase data and the *in vivo* data obtained from live cell imaging are in good agreement and indicate a higher responsiveness of the myosin motor in a cellular background than in the *in vitro* assay.

Co-crystal structure of myosin II motor domain from *D. discoideum* with carbazole

KIN86 (focus of this thesis) was solved. The ADP meta vanadate stabilized crystal structure provided insight about the binding mode of a planar small molecule like carbazoles. Carbazole derivatives are well known for their various pharmacological activities, including anti-HIV, anticancer, antibacterial and antifungal activities (Arakawa et al., 1999; Barta et al., 2009; Hu et al., 2007; Hu et al., 2006; Okumura et al., 2006). Natural and synthetic carbazoles represent an important and heterogeneous class of anticancer agents. Carbazole alkaloids in spite of its many biological activities displays also cytotoxicity against varieties of tumor cell lines. Many carbazole derivatives have been tested for cytotoxic activity, some of them have entered clinical trials, but only very few have been approved for the treatment of cancer so far, since the clinical application of many carbazoles has encountered problems like severe side effects or multidrug resistance. Due to their polycyclic, planar and aromatic structure carbazoles are predestined for intercalation into DNA and therefore DNA remains one of the main targets for cytotoxic carbazoles.

The allosteric binding pocket accommodated the KIN86 with both dispersion and non-covalent interactions. Structural analysis shows that the carbazole-derivative KIN86 binds to the similar site as pentabromopseudilin, at the tip of the myosin motor domain, near actin binding residues. From the crystal structure we can speculate how small effector molecules affect the energetic coupling and thereby myosin motor functions. The communication pathway between the allosteric site and the active sites are conserved among the various classes of myosin. The polarity and hydrophobicity of the allosteric cleft combined with various halogen substitutions of the carbazoles that binds to this cleft brings about the specificity and the potency for different carbazoles. From the results, these compounds were further classified into activators and inhibitors according to the effect they have on actin-activated ATP hydrolysis activity of myosins. Thus, by establishing the communication pathway with which the small molecule effectors can modulate the association of myosin to actin and thereby the cross bridge cycle give clear picture about the chemo-mechanics of the motor proteins.

The structural information obtained for chicken fast skeletal muscle myosin II (Rayment et al., 1993), *D. discoideum* myosin II (Fisher et al., 1995a; Fisher et al., 1995b), Chicken smooth-muscle myosin II (Dominguez et al., 1998), Scallop striated myosin II (Houdusse et al., 1999) and Pig myosin VI (Menetrey et al., 2007) served in modeling other class of myosins and in modeling myosins from the same class from different species. These

validated models were used in our docking studies. With the aid of molecular docking methods the binding mode of the different class of compounds has been identified. Calculated affinity values that were obtained using the molecular docking were used as a guide to select compounds for further co-crystallization procedures. In further quantitative studies, the correlation between bioactivity and structures of variably substituted carbazoles and phenols can be systematically analyzed by quantitative structure activity relationship methods. The readouts from the steady-state ATPase kinetics i.e. the IC_{50} or AC_{50} values, *in-vitro* motility assay i.e. sliding velocities, and the affinity values obtained using microscale thermophoresis can be used as meaningful descriptors during such systematic analysis on the correlation studies of bioactivity and small molecule structures. QSAR studies thus provide a systematic analysis of chemical libraries of similar classes of small molecules. This further narrow down the time required during the process of drug discovery pipeline.

5.2 Outlook

Understanding of motor proteins–small molecule effectors interactions has increased rapidly, particularly through the combination of chemical synthesis, mutagenesis of proteins, biophysical techniques such as microscale thermophoresis, dynamic light scattering, and analytical ultracentrifuge and structural technique like X-ray crystallography. Thus enabling to obtain highly selective effectors of specific dynamin and myosin isoforms which have a wide range of potential therapeutic application in the treatment of diseases including epilepsy, Alzheimer's, Parkinson's, cancer, deafness and malaria. Our results show that psychotropic drugs, halogenated carbazoles and phenols can thus be used as scaffold to design compounds that induces specific functional changes in the motor-activity of myosin, dynamin and Drp1.

References

- Ahmed, Z.M., Morell, R.J., Riazuddin, S., Gropman, A., Shaukat, S., Ahmad, M.M., Mohiddin, S.A., Fananapazir, L., Caruso, R.C., Husnain, T., *et al.* (2003). Mutations of MYO6 are associated with recessive deafness, DFNB37. *American journal of human genetics* 72, 1315-1322.
- Alexander, C., Votruba, M., Pesch, U.E., Thiselton, D.L., Mayer, S., Moore, A., Rodriguez, M., Kellner, U., Leo-Kottler, B., Auburger, G., *et al.* (2000). OPA1, encoding a dynamin-related GTPase, is mutated in autosomal dominant optic atrophy linked to chromosome 3q28. *Nature genetics* 26, 211-215.
- Altschuler, Y., Barbas, S.M., Terlecky, L.J., Tang, K., Hardy, S., Mostov, K.E., and Schmid, S.L. (1998). Redundant and distinct functions for dynamin-1 and dynamin-2 isoforms. *The Journal of cell biology* 143, 1871-1881.
- Anderson, S.L., Carton, J.M., Lou, J., Xing, L., and Rubin, B.Y. (1999). Interferon-induced guanylate binding protein-1 (GBP-1) mediates an antiviral effect against vesicular stomatitis virus and encephalomyocarditis virus. *Virology* 256, 8-14.
- Antoine, J.C., Absi, L., Honnorat, J., Boulesteix, J.M., de Brouker, T., Vial, C., Butler, M., De Camilli, P., and Michel, D. (1999). Anti-amphiphysin antibodies are associated with various paraneoplastic neurological syndromes and tumors. *Archives of neurology* 56, 172-177.
- Arakawa, H., Morita, M., Kodera, T., Okura, A., Ohkubo, M., Morishima, H., and Nishimura, S. (1999). In vivo anti-tumor activity of a novel indolocarbazole compound, J-107088, on murine and human tumors transplanted into mice. *Jpn J Cancer Res* 90, 1163-1170.
- Baaske, P., Wienken, C.J., Reineck, P., Duhr, S., and Braun, D. (2010). Optical thermophoresis for quantifying the buffer dependence of aptamer binding. *Angewandte Chemie (International ed)* 49, 2238-2241.
- Banks, G.T., and Fisher, E.M. (2008). Cytoplasmic dynein could be key to understanding neurodegeneration. *Genome biology* 9, 214.
- Barta, T.E., Barabasz, A.F., Foley, B.E., Geng, L., Hall, S.E., Hanson, G.J., Jenks, M., Ma, W., Rice, J.W., and Veal, J. (2009). Novel carbazole and acyl-indole antimetabolites. *Bioorganic & medicinal chemistry letters* 19, 3078-3080.
- Bauerfeind, R., David, C., Grabs, D., McPherson, P.S., Nemoto, Y., Slepnev, V.I., Takei, K., and De Camilli, P. (1998). Recycling of synaptic vesicles. *Advances in pharmacology (San Diego, Calif)* 42, 253-257.
- Bement, W.M., Hasson, T., Wirth, J.A., Cheney, R.E., and Mooseker, M.S. (1994a). Identification and overlapping expression of multiple unconventional myosin genes in vertebrate cell types. *Proceedings of the National Academy of Sciences of the United States of America* 91, 6549-6553.
- Bement, W.M., Wirth, J.A., and Mooseker, M.S. (1994b). Cloning and mRNA expression of human unconventional myosin-IC. A homologue of amoeboid myosins-I with a single IQ motif and an SH3 domain. *Journal of molecular biology* 243, 356-363.
- Bensen, E.S., Costaguta, G., and Payne, G.S. (2000). Synthetic genetic interactions with temperature-sensitive clathrin in *Saccharomyces cerevisiae*. Roles for synaptojanin-like Inp53p and dynamin-related Vps1p in clathrin-dependent protein sorting at the trans-Golgi network. *Genetics* 154, 83-97.
- Berg, J.S., Derfler, B.H., Pennisi, C.M., Corey, D.P., and Cheney, R.E. (2000). Myosin-X, a novel myosin with pleckstrin homology domains, associates with regions of dynamic actin. *Journal of cell science* 113 Pt 19, 3439-3451.
- Binns, D.D., Barylko, B., Grichine, N., Atkinson, M.A., Helms, M.K., Jameson, D.M., Eccleston, J.F., and Albanesi, J.P. (1999). Correlation between self-association modes and GTPase activation of dynamin. *Journal of protein chemistry* 18, 277-290.

- Bione, S., D'Adamo, P., Maestrini, E., Gedeon, A.K., Bolhuis, P.A., and Toniolo, D. (1996). A novel X-linked gene, G4.5, is responsible for Barth syndrome. *Nature genetics* 12, 385-389.
- Bione, S., Maestrini, E., Rivella, S., Mancini, M., Regis, S., Romeo, G., and Toniolo, D. (1994). Identification of a novel X-linked gene responsible for Emery-Dreifuss muscular dystrophy. *Nature genetics* 8, 323-327.
- Bione, S., Small, K., Aksmanovic, V.M., D'Urso, M., Ciccodicola, A., Merlini, L., Morandi, L., Kress, W., Yates, J.R., Warren, S.T., and et al. (1995). Identification of new mutations in the Emery-Dreifuss muscular dystrophy gene and evidence for genetic heterogeneity of the disease. *Human molecular genetics* 4, 1859-1863.
- Bione, S., Tamanini, F., Maestrini, E., Tribioli, C., Poustka, A., Torri, G., Rivella, S., and Toniolo, D. (1993). Transcriptional organization of a 450-kb region of the human X chromosome in Xq28. *Proceedings of the National Academy of Sciences of the United States of America* 90, 10977-10981.
- Bleazard, W., McCaffery, J.M., King, E.J., Bale, S., Mozdy, A., Tieu, Q., Nunnari, J., and Shaw, J.M. (1999). The dynamin-related GTPase Dnm1 regulates mitochondrial fission in yeast. *Nature cell biology* 1, 298-304.
- Bond, L.M., Peden, A.A., Kendrick-Jones, J., Sellers, J.R., and Buss, F. (2011). Myosin VI and its binding partner optineurin are involved in secretory vesicle fusion at the plasma membrane. *Molecular biology of the cell* 22, 54-65.
- Bos, T.J. (1992). Oncogenes and cell growth. *Advances in experimental medicine and biology* 321, 45-49; discussion 51.
- Bourne, H.R., and Stryer, L. (1992). G proteins. The target sets the tempo. *Nature* 358, 541-543.
- Brown, J., and Bridgman, P.C. (2003a). Role of myosin II in axon outgrowth. *J Histochem Cytochem* 51, 421-428.
- Brown, M.E., and Bridgman, P.C. (2003b). Retrograde flow rate is increased in growth cones from myosin IIB knockout mice. *Journal of cell science* 116, 1087-1094.
- Campuzano, S., and Modolell, J. (1980). Hydrolysis of GTP on elongation factor Tu.ribosome complexes promoted by 2'(3')-O-L-phenylalanyladenosine. *Proceedings of the National Academy of Sciences of the United States of America* 77, 905-909.
- Cao, H., Garcia, F., and McNiven, M.A. (1998). Differential distribution of dynamin isoforms in mammalian cells. *Molecular biology of the cell* 9, 2595-2609.
- Carmona-Fontaine, C., Matthews, H., and Mayor, R. (2008a). Directional cell migration in vivo: Wnt at the crest. *Cell adhesion & migration* 2, 240-242.
- Carmona-Fontaine, C., Matthews, H.K., Kuriyama, S., Moreno, M., Dunn, G.A., Parsons, M., Stern, C.D., and Mayor, R. (2008b). Contact inhibition of locomotion in vivo controls neural crest directional migration. *Nature* 456, 957-961.
- Cassidy-Stone, A., Chipuk, J.E., Ingerman, E., Song, C., Yoo, C., Kuwana, T., Kurth, M.J., Shaw, J.T., Hinshaw, J.E., Green, D.R., and Nunnari, J. (2008). Chemical inhibition of the mitochondrial division dynamin reveals its role in Bax/Bak-dependent mitochondrial outer membrane permeabilization. *Developmental cell* 14, 193-204.
- Chakraborty, A., Chowdhury, B.K., and Bhattacharyya, P. (1995a). Clausenol and clausenine-two carbazole alkaloids from *Clausena anisata*. *Phytochemistry* 40, 295-298.
- Chakraborty, A., Saha, C., Podder, G., Chowdhury, B.K., and Bhattacharyya, P. (1995b). Carbazole alkaloid with antimicrobial activity from *Clausena heptaphylla*. *Phytochemistry* 38, 787-789.
- Chakraborty, D.P., and Roy, S. (1991). Carbazole alkaloids. III. Fortschritte der Chemie organischer Naturstoffe. *Progress in the chemistry of organic natural products* 57, 71-152.
- Chakraborty, D.P., and Roy, S. (2003). Carbazole alkaloids. IV. Fortschritte der Chemie organischer Naturstoffe. *Progress in the chemistry of organic natural products* 85, 125-230.

- Chakraborty, M., Saha, S., and Mukhopadhyay, S. (2009). Murrayakoeninol--a new carbazole alkaloid from *Murraya koenigii* (Linn) Spreng. *Natural product communications* 4, 355-358.
- Chappie, J.S., Acharya, S., Leonard, M., Schmid, S.L., and Dyda, F. (2010). G domain dimerization controls dynamin's assembly-stimulated GTPase activity. *Nature* 465, 435-440.
- Chappie, J.S., Acharya, S., Liu, Y.W., Leonard, M., Pucadyil, T.J., and Schmid, S.L. (2009). An intramolecular signaling element that modulates dynamin function in vitro and in vivo. *Molecular biology of the cell* 20, 3561-3571.
- Chen, M.S., Obar, R.A., Schroeder, C.C., Austin, T.W., Poodry, C.A., Wadsworth, S.C., and Vallee, R.B. (1991). Multiple forms of dynamin are encoded by shibire, a *Drosophila* gene involved in endocytosis. *Nature* 351, 583-586.
- Chinthalapudi, K., Taft, M.H., Martin, R., Heissler, S.M., Preller, M., Hartmann, F.K., Brandstaetter, H., Kendrick-Jones, J., Tsiavaliaris, G., Gutzeit, H.O., *et al.* (2011). Mechanism and Specificity of Pentachloropseudilin-mediated Inhibition of Myosin Motor Activity. *The Journal of biological chemistry* 286, 29700-29708.
- Choi, C.K., Vicente-Manzanares, M., Zareno, J., Whitmore, L.A., Mogilner, A., and Horwitz, A.R. (2008). Actin and alpha-actinin orchestrate the assembly and maturation of nascent adhesions in a myosin II motor-independent manner. *Nature cell biology* 10, 1039-1050.
- Chrzanowska-Wodnicka, M., and Burridge, K. (1992). Rho, rac and the actin cytoskeleton. *Bioessays* 14, 777-778.
- Chugh, J., Chatterjee, A., Kumar, A., Mishra, R.K., Mittal, R., and Hosur, R.V. (2006). Structural characterization of the large soluble oligomers of the GTPase effector domain of dynamin. *The FEBS journal* 273, 388-397.
- Chugh, J., Sharma, S., and Hosur, R.V. (2007). Pockets of short-range transient order and restricted topological heterogeneity in the guanidine-denatured state ensemble of GED of dynamin. *Biochemistry* 46, 11819-11832.
- Clark, S.G., Shurland, D.L., Meyerowitz, E.M., Bargmann, C.I., and van der Blik, A.M. (1997). A dynamin GTPase mutation causes a rapid and reversible temperature-inducible locomotion defect in *C. elegans*. *Proceedings of the National Academy of Sciences of the United States of America* 94, 10438-10443.
- Coling, D.E., Espreafico, E.M., and Kachar, B. (1997). Cellular distribution of myosin-V in the guinea pig cochlea. *Journal of neurocytology* 26, 113-120.
- Cooke, R. (1995). The actomyosin engine. *Faseb J* 9, 636-642.
- Damke, H., Baba, T., Warnock, D.E., and Schmid, S.L. (1994). Induction of mutant dynamin specifically blocks endocytic coated vesicle formation. *The Journal of cell biology* 127, 915-934.
- Damke, H., Binns, D.D., Ueda, H., Schmid, S.L., and Baba, T. (2001a). Dynamin GTPase domain mutants block endocytic vesicle formation at morphologically distinct stages. *Molecular biology of the cell* 12, 2578-2589.
- Damke, H., Muhlberg, A.B., Sever, S., Sholly, S., Warnock, D.E., and Schmid, S.L. (2001b). Expression, purification, and functional assays for self-association of dynamin-1. *Methods in enzymology* 329, 447-457.
- David-Pfeuty, T., Simon, C., and Pantaloni, D. (1979). Effect of antimetabolic drugs on tubulin GTPase activity and self-assembly. *The Journal of biological chemistry* 254, 11696-11702.
- David, C., McPherson, P.S., Mundigl, O., and de Camilli, P. (1996). A role of amphiphysin in synaptic vesicle endocytosis suggested by its binding to dynamin in nerve terminals. *Proceedings of the National Academy of Sciences of the United States of America* 93, 331-335.
- Delettre, C., Griffoin, J.M., Kaplan, J., Dollfus, H., Lorenz, B., Faivre, L., Lenaers, G., Belenguer, P., and Hamel, C.P. (2001). Mutation spectrum and splicing variants in the OPA1 gene. *Human genetics* 109, 584-591.

- Delettre, C., Lenaers, G., Griffoin, J.M., Gigarel, N., Lorenzo, C., Belenguer, P., Pelloquin, L., Grosgeorge, J., Turc-Carel, C., Perret, E., *et al.* (2000). Nuclear gene OPA1, encoding a mitochondrial dynamin-related protein, is mutated in dominant optic atrophy. *Nature genetics* 26, 207-210.
- Dobrowolski, J.M., Carruthers, V.B., and Sibley, L.D. (1997). Participation of myosin in gliding motility and host cell invasion by *Toxoplasma gondii*. *Molecular microbiology* 26, 163-173.
- Dominguez, R., Freyzon, Y., Trybus, K.M., and Cohen, C. (1998). Crystal structure of a vertebrate smooth muscle myosin motor domain and its complex with the essential light chain: visualization of the pre-power stroke state. *Cell* 94, 559-571.
- Duncan, L.J., Mangiardi, D.A., Matsui, J.I., Anderson, J.K., McLaughlin-Williamson, K., and Cotanche, D.A. (2006). Differential expression of unconventional myosins in apoptotic and regenerating chick hair cells confirms two regeneration mechanisms. *The Journal of comparative neurology* 499, 691-701.
- Ellis, S., and Mellor, H. (2000). Regulation of endocytic traffic by rho family GTPases. *Trends in cell biology* 10, 85-88.
- Eband, R.F., Martinou, J.C., Montessuit, S., and Eband, R.M. (2002a). Membrane perturbations induced by the apoptotic Bax protein. *The Biochemical journal* 367, 849-855.
- Eband, R.F., Martinou, J.C., Montessuit, S., Eband, R.M., and Yip, C.M. (2002b). Direct evidence for membrane pore formation by the apoptotic protein Bax. *Biochemical and biophysical research communications* 298, 744-749.
- Farsad, K., Ringstad, N., Takei, K., Floyd, S.R., Rose, K., and De Camilli, P. (2001). Generation of high curvature membranes mediated by direct endophilin bilayer interactions. *The Journal of cell biology* 155, 193-200.
- Fedorov, R., Bohl, M., Tsiavaliaris, G., Hartmann, F.K., Taft, M.H., Baruch, P., Brenner, B., Martin, R., Knolker, H.J., Gutzeit, H.O., and Manstein, D.J. (2009). The mechanism of pentabromopseudilin inhibition of myosin motor activity. *Nature structural & molecular biology* 16, 80-88.
- Fish, K.N., Schmid, S.L., and Damke, H. (2000). Evidence that dynamin-2 functions as a signal-transducing GTPase. *The Journal of cell biology* 150, 145-154.
- Fisher, A.J., Smith, C.A., Thoden, J., Smith, R., Sutoh, K., Holden, H.M., and Rayment, I. (1995a). Structural studies of myosin:nucleotide complexes: a revised model for the molecular basis of muscle contraction. *Biophysical journal* 68, 19S-26S; discussion 27S-28S.
- Fisher, A.J., Smith, C.A., Thoden, J.B., Smith, R., Sutoh, K., Holden, H.M., and Rayment, I. (1995b). X-ray structures of the myosin motor domain of *Dictyostelium discoideum* complexed with MgADP.BeFx and MgADP.AlF₄. *Biochemistry* 34, 8960-8972.
- Foth (2006). New insights into myosin evolution and classification. *Proceedings of the National Academy of Sciences of the United States of America* 103, 3681-3686.
- Frank, S., Gaume, B., Bergmann-Leitner, E.S., Leitner, W.W., Robert, E.G., Catez, F., Smith, C.L., and Youle, R.J. (2001). The role of dynamin-related protein 1, a mediator of mitochondrial fission, in apoptosis. *Developmental cell* 1, 515-525.
- Friedman, T.B., Sellers, J.R., and Avraham, K.B. (1999). Unconventional myosins and the genetics of hearing loss. *American journal of medical genetics* 89, 147-157.
- Fujimoto, M., Arimura, S., Mano, S., Kondo, M., Saito, C., Ueda, T., Nakazono, M., Nakano, A., Nishimura, M., and Tsutsumi, N. (2009). Arabidopsis dynamin-related proteins DRP3A and DRP3B are functionally redundant in mitochondrial fission, but have distinct roles in peroxisomal fission. *Plant J* 58, 388-400.
- Gammie, A.E., Kurihara, L.J., Vallee, R.B., and Rose, M.D. (1995). DNMI1, a dynamin-related gene, participates in endosomal trafficking in yeast. *The Journal of cell biology* 130, 553-566.

- Gao, H., Kadirjan-Kalbach, D., Froehlich, J.E., and Osteryoung, K.W. (2003). ARC5, a cytosolic dynamin-like protein from plants, is part of the chloroplast division machinery. *Proceedings of the National Academy of Sciences of the United States of America* *100*, 4328-4333.
- Geeves, M.A., Fedorov, R., and Manstein, D.J. (2005). Molecular mechanism of actomyosin-based motility. *Cell Mol Life Sci* *62*, 1462-1477.
- Geeves, M.A., and Holmes, K.C. (1999). Structural mechanism of muscle contraction. *Annual review of biochemistry* *68*, 687-728.
- Geeves, M.A., and Holmes, K.C. (2005). The molecular mechanism of muscle contraction. *Advances in protein chemistry* *71*, 161-193.
- Giannone, G., Dubin-Thaler, B.J., Rossier, O., Cai, Y., Chaga, O., Jiang, G., Beaver, W., Dobreiner, H.G., Freund, Y., Borisy, G., and Sheetz, M.P. (2007). Lamellipodial actin mechanically links myosin activity with adhesion-site formation. *Cell* *128*, 561-575.
- Gonzalvez, F., Schug, Z.T., Houtkooper, R.H., MacKenzie, E.D., Brooks, D.G., Wanders, R.J., Petit, P.X., Vaz, F.M., and Gottlieb, E. (2008). Cardiolipin provides an essential activating platform for caspase-8 on mitochondria. *The Journal of cell biology* *183*, 681-696.
- Gray, N.W., Fourgeaud, L., Huang, B., Chen, J., Cao, H., Oswald, B.J., Hemar, A., and McNiven, M.A. (2003). Dynamin 3 is a component of the postsynapse, where it interacts with mGluR5 and Homer. *Curr Biol* *13*, 510-515.
- Gray, N.W., Kruchten, A.E., Chen, J., and McNiven, M.A. (2005). A dynamin-3 spliced variant modulates the actin/cortactin-dependent morphogenesis of dendritic spines. *Journal of cell science* *118*, 1279-1290.
- Gu, X., and Verma, D.P. (1996). Phragmoplastin, a dynamin-like protein associated with cell plate formation in plants. *The EMBO journal* *15*, 695-704.
- Gupton, S.L., Anderson, K.L., Kole, T.P., Fischer, R.S., Ponti, A., Hitchcock-DeGregori, S.E., Danuser, G., Fowler, V.M., Wirtz, D., Hanein, D., and Waterman-Storer, C.M. (2005). Cell migration without a lamellipodium: translation of actin dynamics into cell movement mediated by tropomyosin. *The Journal of cell biology* *168*, 619-631.
- Haller, O., Frese, M., and Kochs, G. (1998). Mx proteins: mediators of innate resistance to RNA viruses. *Revue scientifique et technique (International Office of Epizootics)* *17*, 220-230.
- Heaslip, A.T., Dzierszynski, F., Stein, B., and Hu, K. TgMORN1 is a key organizer for the basal complex of *Toxoplasma gondii*. *PLoS pathogens* *6*, e1000754.
- Heaslip, A.T., Leung, J.M., Carey, K.L., Catti, F., Warshaw, D.M., Westwood, N.J., Ballif, B.A., and Ward, G.E. A small-molecule inhibitor of *T. gondii* motility induces the posttranslational modification of myosin light chain-1 and inhibits myosin motor activity. *PLoS pathogens* *6*, e1000720.
- Henley, J.R., Krueger, E.W., Oswald, B.J., and McNiven, M.A. (1998). Dynamin-mediated internalization of caveolae. *The Journal of cell biology* *141*, 85-99.
- Higuchi, H., and Takemori, S. (1989). Butanedione monoxime suppresses contraction and ATPase activity of rabbit skeletal muscle. *Journal of biochemistry* *105*, 638-643.
- Hilgert, N., Topsakal, V., van Dinther, J., Offeciers, E., Van de Heyning, P., and Van Camp, G. (2008). A splice-site mutation and overexpression of MYO6 cause a similar phenotype in two families with autosomal dominant hearing loss. *Eur J Hum Genet* *16*, 593-602.
- Hill, E., van Der Kaay, J., Downes, C.P., and Smythe, E. (2001). The role of dynamin and its binding partners in coated pit invagination and scission. *The Journal of cell biology* *152*, 309-323.
- Hill, T., Odell, L.R., Edwards, J.K., Graham, M.E., McGeachie, A.B., Rusak, J., Quan, A., Abagyan, R., Scott, J.L., Robinson, P.J., and McCluskey, A. (2005). Small molecule inhibitors of dynamin I GTPase activity: development of dimeric tyrophostins. *Journal of medicinal chemistry* *48*, 7781-7788.

- Hill, T.A., Gordon, C.P., McGeachie, A.B., Venn-Brown, B., Odell, L.R., Chau, N., Quan, A., Mariana, A., Sakoff, J.A., Chircop, M., *et al.* (2009). Inhibition of dynamin mediated endocytosis by the dynoles--synthesis and functional activity of a family of indoles. *Journal of medicinal chemistry* *52*, 3762-3773.
- Hill, T.A., Odell, L.R., Quan, A., Abagyan, R., Ferguson, G., Robinson, P.J., and McCluskey, A. (2004). Long chain amines and long chain ammonium salts as novel inhibitors of dynamin GTPase activity. *Bioorganic & medicinal chemistry letters* *14*, 3275-3278.
- Hinshaw, J.E., and Schmid, S.L. (1995). Dynamin self-assembles into rings suggesting a mechanism for coated vesicle budding. *Nature* *374*, 190-192.
- Hirokawa, N., Niwa, S., and Tanaka, Y. (2010). Molecular motors in neurons: transport mechanisms and roles in brain function, development, and disease. *Neuron* *68*, 610-638.
- Hoepfner, D., van den Berg, M., Philippsen, P., Tabak, H.F., and Hettema, E.H. (2001). A role for Vps1p, actin, and the Myo2p motor in peroxisome abundance and inheritance in *Saccharomyces cerevisiae*. *The Journal of cell biology* *155*, 979-990.
- Houdusse, A., Kalabokis, V.N., Himmel, D., Szent-Gyorgyi, A.G., and Cohen, C. (1999). Atomic structure of scallop myosin subfragment S1 complexed with MgADP: a novel conformation of the myosin head. *Cell* *97*, 459-470.
- Hu, L., Jiang, J.D., Qu, J., Li, Y., Jin, J., Li, Z.R., and Boykin, D.W. (2007). Novel potent antimitotic heterocyclic ketones: synthesis, antiproliferative activity, and structure-activity relationships. *Bioorganic & medicinal chemistry letters* *17*, 3613-3617.
- Hu, L., Li, Z.R., Li, Y., Qu, J., Ling, Y.H., Jiang, J.D., and Boykin, D.W. (2006). Synthesis and structure-activity relationships of carbazole sulfonamides as a novel class of antimitotic agents against solid tumors. *Journal of medicinal chemistry* *49*, 6273-6282.
- Imoto, M., Tachibana, I., and Urrutia, R. (1998). Identification and functional characterization of a novel human protein highly related to the yeast dynamin-like GTPase Vps1p. *Journal of cell science* *111 (Pt 10)*, 1341-1349.
- Ishihara, N., Nomura, M., Jofuku, A., Kato, H., Suzuki, S.O., Masuda, K., Otera, H., Nakanishi, Y., Nonaka, I., Goto, Y., *et al.* (2009). Mitochondrial fission factor Drp1 is essential for embryonic development and synapse formation in mice. *Nature cell biology* *11*, 958-966.
- Jones, B.A., and Fangman, W.L. (1992). Mitochondrial DNA maintenance in yeast requires a protein containing a region related to the GTP-binding domain of dynamin. *Genes & development* *6*, 380-389.
- Jones, S.M., Howell, K.E., Henley, J.R., Cao, H., and McNiven, M.A. (1998). Role of dynamin in the formation of transport vesicles from the trans-Golgi network. *Science (New York, N.Y)* *279*, 573-577.
- Kagawa, M., Sato, N., and Obinata, T. (2006). Effects of BTS (N-benzyl-p-toluene sulphonamide), an inhibitor for myosin-actin interaction, on myofibrillogenesis in skeletal muscle cells in culture. *Zoological science* *23*, 969-975.
- Kamitani, A., Yamada, H., Kinuta, M., Watanabe, M., Li, S.A., Matsukawa, T., McNiven, M., Kumon, H., and Takei, K. (2002). Distribution of dynamins in testis and their possible relation to spermatogenesis. *Biochemical and biophysical research communications* *294*, 261-267.
- Kang, S.G., Jin, J.B., Piao, H.L., Pih, K.T., Jang, H.J., Lim, J.H., and Hwang, I. (1998). Molecular cloning of an Arabidopsis cDNA encoding a dynamin-like protein that is localized to plastids. *Plant molecular biology* *38*, 437-447.
- Kasai, K., Shin, H.W., Shinotsuka, C., Murakami, K., and Nakayama, K. (1999). Dynamin II is involved in endocytosis but not in the formation of transport vesicles from the trans-Golgi network. *Journal of biochemistry* *125*, 780-789.
- Kates, M., Syz, J.Y., Gosser, D., and Haines, T.H. (1993). pH-dissociation characteristics of cardiolipin and its 2'-deoxy analogue. *Lipids* *28*, 877-882.

- Kerr, J.F., Wyllie, A.H., and Currie, A.R. (1972). Apoptosis: a basic biological phenomenon with wide-ranging implications in tissue kinetics. *British journal of cancer* 26, 239-257.
- Kim, Y.W., Park, D.S., Park, S.C., Kim, S.H., Cheong, G.W., and Hwang, I. (2001). Arabidopsis dynamin-like 2 that binds specifically to phosphatidylinositol 4-phosphate assembles into a high-molecular weight complex in vivo and in vitro. *Plant physiology* 127, 1243-1255.
- Klockow, B., Tichelaar, W., Madden, D.R., Niemann, H.H., Akiba, T., Hirose, K., and Manstein, D.J. (2002). The dynamin A ring complex: molecular organization and nucleotide-dependent conformational changes. *The EMBO journal* 21, 240-250.
- Knolker, H.J., and Reddy, K.R. (2008). Chemistry and biology of carbazole alkaloids. *The Alkaloids* 65, 1-410.
- Kochs, G., and Haller, O. (1999a). GTP-bound human MxA protein interacts with the nucleocapsids of Thogoto virus (Orthomyxoviridae). *The Journal of biological chemistry* 274, 4370-4376.
- Kochs, G., and Haller, O. (1999b). Interferon-induced human MxA GTPase blocks nuclear import of Thogoto virus nucleocapsids. *Proceedings of the National Academy of Sciences of the United States of America* 96, 2082-2086.
- Koenig, J.H., and Ikeda, K. (1989). Disappearance and reformation of synaptic vesicle membrane upon transmitter release observed under reversible blockage of membrane retrieval. *J Neurosci* 9, 3844-3860.
- Koenig, J.H., Kosaka, T., and Ikeda, K. (1989). The relationship between the number of synaptic vesicles and the amount of transmitter released. *J Neurosci* 9, 1937-1942.
- Kosaka, T., and Ikeda, K. (1983). Possible temperature-dependent blockage of synaptic vesicle recycling induced by a single gene mutation in *Drosophila*. *Journal of neurobiology* 14, 207-225.
- Labrousse, A.M., Shurland, D.L., and van der Blik, A.M. (1998). Contribution of the GTPase domain to the subcellular localization of dynamin in the nematode *Caenorhabditis elegans*. *Molecular biology of the cell* 9, 3227-3239.
- Labrousse, A.M., Zappaterra, M.D., Rube, D.A., and van der Blik, A.M. (1999). *C. elegans* dynamin-related protein DRP-1 controls severing of the mitochondrial outer membrane. *Molecular cell* 4, 815-826.
- Lad, P.M., Nielsen, T.B., Preston, M.S., and Rodbell, M. (1980). The role of the guanine nucleotide exchange reaction in the regulation of the beta-adrenergic receptor and in the actions of catecholamines and cholera toxin on adenylate cyclase in turkey erythrocyte membranes. *The Journal of biological chemistry* 255, 988-995.
- Lee, Y.H., Gallant, C., Guo, H., Li, Y., Wang, C.A., and Morgan, K.G. (2000). Regulation of vascular smooth muscle tone by N-terminal region of caldesmon. Possible role of tethering actin to myosin. *The Journal of biological chemistry* 275, 3213-3220.
- Leprince, C., Le Scolan, E., Meunier, B., Fraissier, V., Brandon, N., De Gunzburg, J., and Camonis, J. (2003). Sorting nexin 4 and amphiphysin 2, a new partnership between endocytosis and intracellular trafficking. *Journal of cell science* 116, 1937-1948.
- Leprince, C., Romero, F., Cussac, D., Vayssiere, B., Berger, R., Tavitian, A., and Camonis, J.H. (1997). A new member of the amphiphysin family connecting endocytosis and signal transduction pathways. *The Journal of biological chemistry* 272, 15101-15105.
- Lombardi, R., and Riezman, H. (2001). Rvs161p and Rvs167p, the two yeast amphiphysin homologs, function together in vivo. *The Journal of biological chemistry* 276, 6016-6022.
- Lopez, M.A., Pardo, P.S., Cox, G.A., and Boriek, A.M. (2008). Early mechanical dysfunction of the diaphragm in the muscular dystrophy with myositis (Ttnmdm) model. *American journal of physiology* 295, C1092-1102.
- Low, H.H., and Lowe, J. (2006). A bacterial dynamin-like protein. *Nature* 444, 766-769.

- Marks, B., Stowell, M.H., Vallis, Y., Mills, I.G., Gibson, A., Hopkins, C.R., and McMahon, H.T. (2001). GTPase activity of dynamin and resulting conformation change are essential for endocytosis. *Nature* *410*, 231-235.
- Martin, R., Jager, A., Bohl, M., Richter, S., Fedorov, R., Manstein, D.J., Gutzeit, H.O., and Knolker, H.J. (2009). Total synthesis of pentabromo- and pentachloropseudilin, and synthetic analogues--allosteric inhibitors of myosin ATPase. *Angewandte Chemie (International ed)* *48*, 8042-8046.
- Masaike, Y., Takagi, T., Hirota, M., Yamada, J., Ishihara, S., Yung, T.M., Inoue, T., Sawa, C., Sagara, H., Sakamoto, S., *et al.* (2007). Identification of dynamin-2-mediated endocytosis as a new target of osteoporosis drugs, bisphosphonates. *Molecular pharmacology* *77*, 262-269.
- McNiven, M.A., Cao, H., Pitts, K.R., and Yoon, Y. (2000a). The dynamin family of mechanoenzymes: pinching in new places. *Trends in biochemical sciences* *25*, 115-120.
- McNiven, M.A., Kim, L., Krueger, E.W., Orth, J.D., Cao, H., and Wong, T.W. (2000b). Regulated interactions between dynamin and the actin-binding protein cortactin modulate cell shape. *The Journal of cell biology* *151*, 187-198.
- McPherson, P.S., Garcia, E.P., Slepnev, V.I., David, C., Zhang, X., Grabs, D., Sossin, W.S., Bauerfeind, R., Nemoto, Y., and De Camilli, P. (1996). A presynaptic inositol-5-phosphatase. *Nature* *379*, 353-357.
- Mears, J.A., Lackner, L.L., Fang, S., Ingerman, E., Nunnari, J., and Hinshaw, J.E. (2010). Conformational changes in Dnm1 support a contractile mechanism for mitochondrial fission. *Nature structural & molecular biology* *18*, 20-26.
- Melchionda, S., Ahituv, N., Bisceglia, L., Sobe, T., Glaser, F., Rabionet, R., Arbones, M.L., Notarangelo, A., Di Iorio, E., Carella, M., *et al.* (2001). MYO6, the human homologue of the gene responsible for deafness in Snell's waltzer mice, is mutated in autosomal dominant nonsyndromic hearing loss. *American journal of human genetics* *69*, 635-640.
- Melen, K., Ronni, T., Broni, B., Krug, R.M., von Bonsdorff, C.H., and Julkunen, I. (1992). Interferon-induced Mx proteins form oligomers and contain a putative leucine zipper. *The Journal of biological chemistry* *267*, 25898-25907.
- Menetrey, J., Llinas, P., Mukherjea, M., Sweeney, H.L., and Houdusse, A. (2007). The structural basis for the large powerstroke of myosin VI. *Cell* *131*, 300-308.
- Miyagishima, S.Y., Nishida, K., and Kuroiwa, T. (2003). An evolutionary puzzle: chloroplast and mitochondrial division rings. *Trends in plant science* *8*, 432-438.
- Mohiddin, S.A., Ahmed, Z.M., Griffith, A.J., Tripodi, D., Friedman, T.B., Fananapazir, L., and Morell, R.J. (2004). Novel association of hypertrophic cardiomyopathy, sensorineural deafness, and a mutation in unconventional myosin VI (MYO6). *Journal of medical genetics* *41*, 309-314.
- Montessuit, S., Somasekharan, S.P., Terrones, O., Lucken-Ardjomande, S., Herzig, S., Schwarzenbacher, R., Manstein, D.J., Bossy-Wetzel, E., Basanez, G., Meda, P., and Martinou, J.C. (2010). Membrane remodeling induced by the dynamin-related protein Drp1 stimulates Bax oligomerization. *Cell* *142*, 889-901.
- Morgen, D.O. (1997). CYCLIN-DEPENDENT KINASES: Engines, Clocks, and Microprocessors. *Annual Review of Cell and Developmental Biology* *13*, 261-291.
- Muhlberg, A.B., Warnock, D.E., and Schmid, S.L. (1997). Domain structure and intramolecular regulation of dynamin GTPase. *The EMBO journal* *16*, 6676-6683.
- Nguyen, C., and Bibb, J.A. (2003). Cdk5 and the mystery of synaptic vesicle endocytosis. *The Journal of cell biology* *163*, 697-699.
- Nguyen, M.D., Mushynski, W.E., and Julien, J.P. (2002). Cycling at the interface between neurodevelopment and neurodegeneration. *Cell death and differentiation* *9*, 1294-1306.

- Nothwehr, S.F., Conibear, E., and Stevens, T.H. (1995). Golgi and vacuolar membrane proteins reach the vacuole in vps1 mutant yeast cells via the plasma membrane. *The Journal of cell biology* 129, 35-46.
- Obar, R.A., Collins, C.A., Hammarback, J.A., Shpetner, H.S., and Vallee, R.B. (1990). Molecular cloning of the microtubule-associated mechanochemical enzyme dynamin reveals homology with a new family of GTP-binding proteins. *Nature* 347, 256-261.
- Odell, L.R., Howan, D., Gordon, C.P., Robertson, M.J., Chau, N., Mariana, A., Whiting, A.E., Abagyan, R., Daniel, J.A., Gorgani, N.N., *et al.* (2010). The pthaladyns: GTP competitive inhibitors of dynamin I and II GTPase derived from virtual screening. *Journal of medicinal chemistry* 53, 5267-5280.
- Okamoto, P.M., Herskovits, J.S., and Vallee, R.B. (1997). Role of the basic, proline-rich region of dynamin in Src homology 3 domain binding and endocytosis. *The Journal of biological chemistry* 272, 11629-11635.
- Okamoto, P.M., Tripet, B., Litowski, J., Hodges, R.S., and Vallee, R.B. (1999). Multiple distinct coiled-coils are involved in dynamin self-assembly. *The Journal of biological chemistry* 274, 10277-10286.
- Okumura, H., Nakazawa, J., Tsuganezawa, K., Usui, T., Osada, H., Matsumoto, T., Tanaka, A., and Yokoyama, S. (2006). Phenothiazine and carbazole-related compounds inhibit mitotic kinesin Eg5 and trigger apoptosis in transformed culture cells. *Toxicology letters* 166, 44-52.
- Olichon, A., Baricault, L., Gas, N., Guillou, E., Valette, A., Belenguer, P., and Lenaers, G. (2003). Loss of OPA1 perturbs the mitochondrial inner membrane structure and integrity, leading to cytochrome c release and apoptosis. *The Journal of biological chemistry* 278, 7743-7746.
- Oliver, T.N., Berg, J.S., and Cheney, R.E. (1999). Tails of unconventional myosins. *Cell Mol Life Sci* 56, 243-257.
- Otomo, M., Takahashi, K., Miyoshi, H., Osada, K., Nakashima, H., and Yamaguchi, N. (2008). Some selective serotonin reuptake inhibitors inhibit dynamin I guanosine triphosphatase (GTPase). *Biological & pharmaceutical bulletin* 31, 1489-1495.
- Otsuga, D., Keegan, B.R., Brisch, E., Thatcher, J.W., Hermann, G.J., Bleazard, W., and Shaw, J.M. (1998). The dynamin-related GTPase, Dnm1p, controls mitochondrial morphology in yeast. *The Journal of cell biology* 143, 333-349.
- Otsuka, A., Abe, T., Watanabe, M., Yagisawa, H., Takei, K., and Yamada, H. (2009). Dynamin 2 is required for actin assembly in phagocytosis in Sertoli cells. *Biochemical and biophysical research communications* 378, 478-482.
- Park, J.M., Cho, J.H., Kang, S.G., Jang, H.J., Pih, K.T., Piao, H.L., Cho, M.J., and Hwang, I. (1998). A dynamin-like protein in *Arabidopsis thaliana* is involved in biogenesis of thylakoid membranes. *The EMBO journal* 17, 859-867.
- Park, J.M., Kang, S.G., Pih, K.T., Jang, H.J., Piao, H.L., Yoon, H.W., Cho, M.J., and Hwang, I. (1997). A dynamin-like protein, ADL1, is present in membranes as a high-molecular-mass complex in *Arabidopsis thaliana*. *Plant physiology* 115, 763-771.
- Pavlovic, J., Schroder, A., Blank, A., Pitossi, F., and Staeheli, P. (1993). Mx proteins: GTPases involved in the interferon-induced antiviral state. *Ciba Foundation symposium* 176, 233-243; discussion 243-237.
- Pelloquin, L., Belenguer, P., Menon, Y., and Ducommun, B. (1998). Identification of a fission yeast dynamin-related protein involved in mitochondrial DNA maintenance. *Biochemical and biophysical research communications* 251, 720-726.
- Pelloquin, L., Belenguer, P., Menon, Y., Gas, N., and Ducommun, B. (1999a). Fission yeast Msp1 is a mitochondrial dynamin-related protein. *Journal of cell science* 112 (Pt 22), 4151-4161.
- Pelloquin, L., Ducommun, B., and Belenguer, P. (1999b). Interaction between the fission yeast nim1/cdr1 protein kinase and a dynamin-related protein. *FEBS letters* 443, 71-74.

- Phillips, G.R., Huang, J.K., Wang, Y., Tanaka, H., Shapiro, L., Zhang, W., Shan, W.S., Arndt, K., Frank, M., Gordon, R.E., *et al.* (2001). The presynaptic particle web: ultrastructure, composition, dissolution, and reconstitution. *Neuron* *32*, 63-77.
- Pitossi, F., Blank, A., Schroder, A., Schwarz, A., Hussi, P., Schwemmle, M., Pavlovic, J., and Staeheli, P. (1993). A functional GTP-binding motif is necessary for antiviral activity of Mx proteins. *Journal of virology* *67*, 6726-6732.
- Pitts, K.R., Yoon, Y., Krueger, E.W., and McNiven, M.A. (1999). The dynamin-like protein DLP1 is essential for normal distribution and morphology of the endoplasmic reticulum and mitochondria in mammalian cells. *Molecular biology of the cell* *10*, 4403-4417.
- Pollard, T.D., Doberstein, S.K., and Zot, H.G. (1991). Myosin-I. *Annual review of physiology* *53*, 653-681.
- Poodry, C.A., and Edgar, L. (1979). Reversible alteration in the neuromuscular junctions of *Drosophila melanogaster* bearing a temperature-sensitive mutation, shibire. *The Journal of cell biology* *81*, 520-527.
- Post, P.L., Bokoch, G.M., and Mooseker, M.S. (1998). Human myosin-IXb is a mechanochemically active motor and a GAP for rho. *Journal of cell science* *111* (Pt 7), 941-950.
- Praefcke, G.J., Geyer, M., Schwemmle, M., Robert Kalbitzer, H., and Herrmann, C. (1999). Nucleotide-binding characteristics of human guanylate-binding protein 1 (hGBP1) and identification of the third GTP-binding motif. *Journal of molecular biology* *292*, 321-332.
- Prakash, B., Praefcke, G.J., Renault, L., Wittinghofer, A., and Herrmann, C. (2000a). Structure of human guanylate-binding protein 1 representing a unique class of GTP-binding proteins. *Nature* *403*, 567-571.
- Prakash, B., Renault, L., Praefcke, G.J., Herrmann, C., and Wittinghofer, A. (2000b). Triphosphate structure of guanylate-binding protein 1 and implications for nucleotide binding and GTPase mechanism. *The EMBO journal* *19*, 4555-4564.
- Preller, M., Chinthalapudi, K., Martin, R., Knolker, H.J., and Manstein, D.J. Inhibition of Myosin ATPase activity by halogenated pseudilins: a structure-activity study. *Journal of medicinal chemistry* *54*, 3675-3685.
- Ramamurthy, B., Yengo, C.M., Straight, A.F., Mitchison, T.J., and Sweeney, H.L. (2004). Kinetic mechanism of blebbistatin inhibition of nonmuscle myosin IIb. *Biochemistry* *43*, 14832-14839.
- Ramaswami, M., Krishnan, K.S., and Kelly, R.B. (1994). Intermediates in synaptic vesicle recycling revealed by optical imaging of *Drosophila* neuromuscular junctions. *Neuron* *13*, 363-375.
- Rayment, I., Holden, H.M., Whittaker, M., Yohn, C.B., Lorenz, M., Holmes, K.C., and Milligan, R.A. (1993). Structure of the actin-myosin complex and its implications for muscle contraction. *Science (New York, N.Y)* *261*, 58-65.
- Reems, J.A., Wang, W., Tsubata, K., Abdurrahman, N., Sundell, B., Tijssen, M.R., van der Schoot, E., Di Summa, F., Patel-Hett, S., Italiano, J., Jr., and Gilligan, D.M. (2008). Dynamin 3 participates in the growth and development of megakaryocytes. *Experimental hematology* *36*, 1714-1727.
- Rehberg, M., Praetner, M., Leite, C.F., Reichel, C.A., Bihari, P., Mildner, K., Duhr, S., Zeuschner, D., and Krombach, F. (2101). Quantum dots modulate leukocyte adhesion and transmigration depending on their surface modification. *Nano letters* *10*, 3656-3664.
- Reubold, T.F., Eschenburg, S., Becker, A., Kull, F.J., and Manstein, D.J. (2003). A structural model for actin-induced nucleotide release in myosin. *Nature structural biology* *10*, 826-830.
- Reubold, T.F., Eschenburg, S., Becker, A., Leonard, M., Schmid, S.L., Vallee, R.B., Kull, F.J., and Manstein, D.J. (2005). Crystal structure of the GTPase domain of rat dynamin 1. *Proceedings of the National Academy of Sciences of the United States of America* *102*, 13093-13098.

- Ridley, A.J. (2001). Rho family proteins: coordinating cell responses. *Trends in cell biology* 11, 471-477.
- Roberts, R., Lister, I., Schmitz, S., Walker, M., Veigel, C., Trinick, J., Buss, F., and Kendrick-Jones, J. (2004). Myosin VI: cellular functions and motor properties. *Philosophical transactions of the Royal Society of London* 359, 1931-1944.
- Robinson, P.J., Sontag, J.M., Liu, J.P., Fykse, E.M., Slaughter, C., McMahon, H., and Sudhof, T.C. (1993). Dynamin GTPase regulated by protein kinase C phosphorylation in nerve terminals. *Nature* 365, 163-166.
- Rosenblatt, J.E., del Carmen, R., and Wyatt, R.J. (1980). A high affinity GTP binding site in rat brain. *European journal of pharmacology* 64, 365-366.
- Rothman, J.H., Raymond, C.K., Gilbert, T., O'Hara, P.J., and Stevens, T.H. (1990). A putative GTP binding protein homologous to interferon-inducible Mx proteins performs an essential function in yeast protein sorting. *Cell* 61, 1063-1074.
- Saiz, A., Dalmau, J., Butler, M.H., Chen, Q., Delattre, J.Y., De Camilli, P., and Graus, F. (1999). Anti-amphiphysin I antibodies in patients with paraneoplastic neurological disorders associated with small cell lung carcinoma. *Journal of neurology, neurosurgery, and psychiatry* 66, 214-217.
- Sasaki, N., Ohkura, R., and Sutoh, K. (2002). Dictyostelium myosin II as a model to study the actin-myosin interactions during force generation. *Journal of muscle research and cell motility* 23, 697-702.
- Sasaki, N., Ohkura, R., and Sutoh, K. (2003). Dictyostelium myosin II mutations that uncouple the converter swing and ATP hydrolysis cycle. *Biochemistry* 42, 90-95.
- Sato, O. (2006). [Myosin VI: involvement in hereditary hearing loss]. *Seikagaku* 78, 45-50.
- Savoia, A., De Rocco, D., Panza, E., Bozzi, V., Scandellari, R., Loffredo, G., Mumford, A., Heller, P.G., Noris, P., De Groot, M.R., *et al.* Heavy chain myosin 9-related disease (MYH9 - RD): neutrophil inclusions of myosin-9 as a pathognomonic sign of the disorder. *Thrombosis and haemostasis* 103, 826-832.
- Savoia, A., Germeshausen, M., De Rocco, D., Henschel, B., Kratz, C.P., Kuhlen, M., Rath, B., Steuhl, K.P., Wermes, C., and Ballmaier, M. MYH9-related disease: Report on five German families and description of a novel mutation. *Annals of hematology* 89, 1057-1059.
- Schafer, D.A. (2002). Coupling actin dynamics and membrane dynamics during endocytosis. *Current opinion in cell biology* 14, 76-81.
- Schafer, D.A. (2004). Regulating actin dynamics at membranes: a focus on dynamin. *Traffic (Copenhagen, Denmark)* 5, 463-469.
- Schug, T.T. (2009). Awakening p53 in senescent cells using nutlin-3. *Aging* 1, 842-844.
- Schug, Z.T., and Gottlieb, E. (2009). Cardiolipin acts as a mitochondrial signalling platform to launch apoptosis. *Biochimica et biophysica acta* 1788, 2022-2031.
- Schultz, J.M., Yang, Y., Caride, A.J., Filoteo, A.G., Penheiter, A.R., Lagziel, A., Morell, R.J., Mohiddin, S.A., Fananapazir, L., Madeo, A.C., *et al.* (2005). Modification of human hearing loss by plasma-membrane calcium pump PMCA2. *The New England journal of medicine* 352, 1557-1564.
- Schumacher, B., and Staeheli, P. (1998). Domains mediating intramolecular folding and oligomerization of MxA GTPase. *The Journal of biological chemistry* 273, 28365-28370.
- Seiler, C., Ben-David, O., Sidi, S., Hendrich, O., Rusch, A., Burnside, B., Avraham, K.B., and Nicolson, T. (2004). Myosin VI is required for structural integrity of the apical surface of sensory hair cells in zebrafish. *Developmental biology* 272, 328-338.
- Sellers, J.R. (1999). Unphosphorylated crossbridges and latch: smooth muscle regulation revisited. *Journal of muscle research and cell motility* 20, 347-349.
- Sellers, J.R. (2000). Myosins: a diverse superfamily. *Biochimica et biophysica acta* 1496, 3-22.

- Sesaki, H., and Jensen, R.E. (1999). Division versus fusion: Dnm1p and Fzo1p antagonistically regulate mitochondrial shape. *The Journal of cell biology* 147, 699-706.
- Sever, S., Damke, H., and Schmid, S.L. (2000a). Dynamin:GTP controls the formation of constricted coated pits, the rate limiting step in clathrin-mediated endocytosis. *The Journal of cell biology* 150, 1137-1148.
- Sever, S., Damke, H., and Schmid, S.L. (2000b). Garrotes, springs, ratchets, and whips: putting dynamin models to the test. *Traffic (Copenhagen, Denmark)* 1, 385-392.
- Sever, S., Muhlberg, A.B., and Schmid, S.L. (1999). Impairment of dynamin's GAP domain stimulates receptor-mediated endocytosis. *Nature* 398, 481-486.
- Shepard, K.A., and Yaffe, M.P. (1999). The yeast dynamin-like protein, Mgm1p, functions on the mitochondrial outer membrane to mediate mitochondrial inheritance. *The Journal of cell biology* 144, 711-720.
- Shupliakov, O., Low, P., Grabs, D., Gad, H., Chen, H., David, C., Takei, K., De Camilli, P., and Brodin, L. (1997). Synaptic vesicle endocytosis impaired by disruption of dynamin-SH3 domain interactions. *Science (New York, N.Y)* 276, 259-263.
- Sivadon, P., Bauer, F., Aigle, M., and Crouzet, M. (1995). Actin cytoskeleton and budding pattern are altered in the yeast *rvs161* mutant: the *Rvs161* protein shares common domains with the brain protein amphiphysin. *Mol Gen Genet* 246, 485-495.
- Slebos, R.J., and Rodenhuis, S. (1992). The ras gene family in human non-small-cell lung cancer. *Journal of the National Cancer Institute*, 23-29.
- Slepnev, V.I., Ochoa, G.C., Butler, M.H., and De Camilli, P. (2000). Tandem arrangement of the clathrin and AP-2 binding domains in amphiphysin 1 and disruption of clathrin coat function by amphiphysin fragments comprising these sites. *The Journal of biological chemistry* 275, 17583-17589.
- Slepnev, V.I., Ochoa, G.C., Butler, M.H., Grabs, D., and De Camilli, P. (1998). Role of phosphorylation in regulation of the assembly of endocytic coat complexes. *Science (New York, N.Y)* 281, 821-824.
- Smirnova, E., Griparic, L., Shurland, D.L., and van der Blik, A.M. (2001). Dynamin-related protein Drp1 is required for mitochondrial division in mammalian cells. *Molecular biology of the cell* 12, 2245-2256.
- Smirnova, E., Shurland, D.L., Newman-Smith, E.D., Pishvae, B., and van der Blik, A.M. (1999). A model for dynamin self-assembly based on binding between three different protein domains. *The Journal of biological chemistry* 274, 14942-14947.
- Smirnova, E., Shurland, D.L., Ryazantsev, S.N., and van der Blik, A.M. (1998). A human dynamin-related protein controls the distribution of mitochondria. *The Journal of cell biology* 143, 351-358.
- Song, B.D., Leonard, M., and Schmid, S.L. (2004a). Dynamin GTPase domain mutants that differentially affect GTP binding, GTP hydrolysis, and clathrin-mediated endocytosis. *The Journal of biological chemistry* 279, 40431-40436.
- Song, B.D., and Schmid, S.L. (2003). A molecular motor or a regulator? Dynamin's in a class of its own. *Biochemistry* 42, 1369-1376.
- Song, B.D., Yasar, D., and Schmid, S.L. (2004b). An assembly-incompetent mutant establishes a requirement for dynamin self-assembly in clathrin-mediated endocytosis in vivo. *Molecular biology of the cell* 15, 2243-2252.
- Stowell, M.H., Marks, B., Wigge, P., and McMahon, H.T. (1999). Nucleotide-dependent conformational changes in dynamin: evidence for a mechanochemical molecular spring. *Nature cell biology* 1, 27-32.
- Sweitzer, S.M., and Hinshaw, J.E. (1998). Dynamin undergoes a GTP-dependent conformational change causing vesiculation. *Cell* 93, 1021-1029.

- Taguchi, N., Ishihara, N., Jofuku, A., Oka, T., and Mihara, K. (2007). Mitotic phosphorylation of dynamin-related GTPase Drp1 participates in mitochondrial fission. *The Journal of biological chemistry* 282, 11521-11529.
- Takahashi, K., Miyoshi, H., Otomo, M., Osada, K., Yamaguchi, N., and Nakashima, H. (2009). Suppression of dynamin GTPase activity by sertraline leads to inhibition of dynamin-dependent endocytosis. *Biochemical and biophysical research communications* 391, 382-387.
- Takei, K., McPherson, P.S., Schmid, S.L., and De Camilli, P. (1995). Tubular membrane invaginations coated by dynamin rings are induced by GTP-gamma S in nerve terminals. *Nature* 374, 186-190.
- Takei, K., Mundigl, O., Daniell, L., and De Camilli, P. (1996). The synaptic vesicle cycle: a single vesicle budding step involving clathrin and dynamin. *The Journal of cell biology* 133, 1237-1250.
- Takei, K., Slepnev, V.I., Haucke, V., and De Camilli, P. (1999). Functional partnership between amphiphysin and dynamin in clathrin-mediated endocytosis. *Nature cell biology* 1, 33-39.
- Tanabe, K., and Takei, K. (2009). Dynamic instability of microtubules requires dynamin 2 and is impaired in a Charcot-Marie-Tooth mutant. *The Journal of cell biology* 185, 939-948.
- Tanaka, A., and Youle, R.J. (2008). A chemical inhibitor of DRP1 uncouples mitochondrial fission and apoptosis. *Molecular cell* 29, 409-410.
- Tomizawa, K., Ohta, J., Matsushita, M., Moriwaki, A., Li, S.T., Takei, K., and Matsui, H. (2002). Cdk5/p35 regulates neurotransmitter release through phosphorylation and downregulation of P/Q-type voltage-dependent calcium channel activity. *J Neurosci* 22, 2590-2597.
- Tomizawa, K., Sunada, S., Lu, Y.F., Oda, Y., Kinuta, M., Ohshima, T., Saito, T., Wei, F.Y., Matsushita, M., Li, S.T., *et al.* (2003). Cophosphorylation of amphiphysin I and dynamin I by Cdk5 regulates clathrin-mediated endocytosis of synaptic vesicles. *The Journal of cell biology* 163, 813-824.
- Tsiavaliaris, G., Fujita-Becker, S., Batra, R., Levitsky, D.I., Kull, F.J., Gees, M.A., and Manstein, D.J. (2002). Mutations in the relay loop region result in dominant-negative inhibition of myosin II function in *Dictyostelium*. *EMBO reports* 3, 1099-1105.
- Tuma, P.L., and Collins, C.A. (1994). Activation of dynamin GTPase is a result of positive cooperativity. *The Journal of biological chemistry* 269, 30842-30847.
- Urrutia, R., Henley, J.R., Cook, T., and McNiven, M.A. (1997). The dynamins: redundant or distinct functions for an expanding family of related GTPases? *Proceedings of the National Academy of Sciences of the United States of America* 94, 377-384.
- van der Blik, A.M. (1999). Functional diversity in the dynamin family. *Trends in cell biology* 9, 96-102.
- van der Blik, A.M., and Meyerowitz, E.M. (1991). Dynamin-like protein encoded by the *Drosophila shibire* gene associated with vesicular traffic. *Nature* 351, 411-414.
- Veugelers, M., Bressan, M., McDermott, D.A., Weremowicz, S., Morton, C.C., Mabry, C.C., Lefavre, J.F., Zunamon, A., Destree, A., Chaudron, J.M., and Basson, C.T. (2004). Mutation of perinatal myosin heavy chain associated with a Carney complex variant. *The New England journal of medicine* 351, 460-469.
- Vizeacoumar, F.J., Vreden, W.N., Fagarasanu, M., Eitzen, G.A., Aitchison, J.D., and Rachubinski, R.A. (2006). The dynamin-like protein Vps1p of the yeast *Saccharomyces cerevisiae* associates with peroxisomes in a Pex19p-dependent manner. *The Journal of biological chemistry* 281, 12817-12823.
- Volchuk, A., Narine, S., Foster, L.J., Grabs, D., De Camilli, P., and Klip, A. (1998). Perturbation of dynamin II with an amphiphysin SH3 domain increases GLUT4 glucose transporters at the plasma membrane in 3T3-L1 adipocytes. Dynamin II participates in GLUT4 endocytosis. *The Journal of biological chemistry* 273, 8169-8176.

- Walsh, R., Rutland, C., Thomas, R., and Loughna, S. (2010a). Cardiomyopathy: a systematic review of disease-causing mutations in myosin heavy chain 7 and their phenotypic manifestations. *Cardiology* 115, 49-60.
- Walsh, V.L., Raviv, D., Dror, A.A., Shahin, H., Walsh, T., Kanaan, M.N., Avraham, K.B., and King, M.C. (2010b). A mouse model for human hearing loss DFNB30 due to loss of function of myosin IIIA. *Mamm Genome* 22, 170-177.
- Watanabe, M., Yumoto, M., Tanaka, H., Wang, H.H., Katayama, T., Yoshiyama, S., Black, J., Thatcher, S.E., and Kohama, K. (2010). Blebbistatin, a myosin II inhibitor, suppresses contraction and disrupts contractile filaments organization of skinned taenia cecum from guinea pig. *American journal of physiology* 298, C1118-1126.
- Waterham, H.R., Koster, J., van Roermund, C.W., Mooyer, P.A., Wanders, R.J., and Leonard, J.V. (2007). A lethal defect of mitochondrial and peroxisomal fission. *The New England journal of medicine* 356, 1736-1741.
- Wechsler-Reya, R., Elliott, K., Herlyn, M., and Prendergast, G.C. (1997a). The putative tumor suppressor BIN1 is a short-lived nuclear phosphoprotein, the localization of which is altered in malignant cells. *Cancer research* 57, 3258-3263.
- Wechsler-Reya, R., Sakamuro, D., Zhang, J., Duhadaway, J., and Prendergast, G.C. (1997b). Structural analysis of the human BIN1 gene. Evidence for tissue-specific transcriptional regulation and alternate RNA splicing. *The Journal of biological chemistry* 272, 31453-31458.
- Wechsler-Reya, R.J., and Barres, B.A. (1997). Retinal development: communication helps you see the light. *Curr Biol* 7, R433-436.
- Wells, A.L., Lin, A.W., Chen, L.Q., Safer, D., Cain, S.M., Hasson, T., Carragher, B.O., Milligan, R.A., and Sweeney, H.L. (1999). Myosin VI is an actin-based motor that moves backwards. *Nature* 401, 505-508.
- Wienke, D.C., Knetsch, M.L., Neuhaus, E.M., Reedy, M.C., and Manstein, D.J. (1999). Disruption of a dynamin homologue affects endocytosis, organelle morphology, and cytokinesis in *Dictyostelium discoideum*. *Molecular biology of the cell* 10, 225-243.
- Wienken, C.J., Baaske, P., Rothbauer, U., Braun, D., and Duhr, S. (2010). Protein-binding assays in biological liquids using microscale thermophoresis. *Nature communications* 1, 100.
- Wilsbach, K., and Payne, G.S. (1993). Vps1p, a member of the dynamin GTPase family, is necessary for Golgi membrane protein retention in *Saccharomyces cerevisiae*. *The EMBO journal* 12, 3049-3059.
- Wong, E.D., Wagner, J.A., Gorsich, S.W., McCaffery, J.M., Shaw, J.M., and Nunnari, J. (2000). The dynamin-related GTPase, Mgm1p, is an intermembrane space protein required for maintenance of fusion competent mitochondria. *The Journal of cell biology* 151, 341-352.
- Wylie, S.R., Wu, P.J., Patel, H., and Chantler, P.D. (1998). A conventional myosin motor drives neurite outgrowth. *Proceedings of the National Academy of Sciences of the United States of America* 95, 12967-12972.
- Yang, Z., Li, H., Chai, Z., Fullerton, M.J., Cao, Y., Toh, B.H., Funder, J.W., and Liu, J.P. (2001). Dynamin II regulates hormone secretion in neuroendocrine cells. *The Journal of biological chemistry* 276, 4251-4260.
- Yoo, J., Jeong, M.J., Cho, H.J., Oh, E.S., and Han, M.Y. (2005). Dynamin II interacts with syndecan-4, a regulator of focal adhesion and stress-fiber formation. *Biochemical and biophysical research communications* 328, 424-431.
- Yoon, B.I., Jung, S.Y., Hur, K., Lee, J.H., Joo, K.H., Lee, Y.S., and Kim, D.Y. (2000). Differentiation of hamster liver oval cell following *Clonorchis sinensis* infection. *The Journal of veterinary medical science / the Japanese Society of Veterinary Science* 62, 1303-1310.
- Yoon, Y., Pitts, K.R., Dahan, S., and McNiven, M.A. (1998). A novel dynamin-like protein associates with cytoplasmic vesicles and tubules of the endoplasmic reticulum in mammalian cells. *The Journal of cell biology* 140, 779-793.

- Yoon, Y., Pitts, K.R., and McNiven, M.A. (2001). Mammalian dynamin-like protein DLP1 tubulates membranes. *Molecular biology of the cell* *12*, 2894-2905.
- Yumura, S., and Uyeda, T.Q. (2003). Myosins and cell dynamics in cellular slime molds. *International review of cytology* *224*, 173-225.
- Zanna, C., Ghelli, A., Porcelli, A.M., Karbowski, M., Youle, R.J., Schimpf, S., Wissinger, B., Pinti, M., Cossarizza, A., Vidoni, S., *et al.* (2008). OPA1 mutations associated with dominant optic atrophy impair oxidative phosphorylation and mitochondrial fusion. *Brain* *131*, 352-367.
- Zhang, Z., Hong, Z., and Verma, D.P. (2000). Phragmoplastin polymerizes into spiral coiled structures via intermolecular interaction of two self-assembly domains. *The Journal of biological chemistry* *275*, 8779-8784.
- Zurcher, T., Pavlovic, J., and Staeheli, P. (1992a). Mechanism of human MxA protein action: variants with changed antiviral properties. *The EMBO journal* *11*, 1657-1661.
- Zurcher, T., Pavlovic, J., and Staeheli, P. (1992b). Mouse Mx2 protein inhibits vesicular stomatitis virus but not influenza virus. *Virology* *187*, 796-800.
- Zurcher, T., Pavlovic, J., and Staeheli, P. (1992c). Nuclear localization of mouse Mx1 protein is necessary for inhibition of influenza virus. *Journal of virology* *66*, 5059-5066.
- Bagshaw, C.R. (1977). The mechanism of adenosine triphosphate hydrolysis by myosin [proceedings]. *Biochemical Society transactions* *5*, 1272-1274.
- Bagshaw, C.R., Eccleston, J.F., Eckstein, F., Goody, R.S., Gutfreund, H., and Trentham, D.R. (1974). The magnesium ion-dependent adenosine triphosphatase of myosin. Two-step processes of adenosine triphosphate association and adenosine diphosphate dissociation. *The Biochemical journal* *141*, 351-364.
- Bagshaw, C.R., and Trentham, D.R. (1974). The characterization of myosin-product complexes and of product-release steps during the magnesium ion-dependent adenosine triphosphatase reaction. *The Biochemical journal* *141*, 331-349.
- Binns, D.D., Barylko, B., Grichine, N., Atkinson, M.A., Helms, M.K., Jameson, D.M., Eccleston, J.F., and Albanesi, J.P. (1999). Correlation between self-association modes and GTPase activation of dynamin. *Journal of protein chemistry* *18*, 277-290.
- Binns, D.D., Helms, M.K., Barylko, B., Davis, C.T., Jameson, D.M., Albanesi, J.P., and Eccleston, J.F. (2000). The mechanism of GTP hydrolysis by dynamin II: a transient kinetic study. *Biochemistry* *39*, 7188-7196.
- Hinshaw, J.E., and Schmid, S.L. (1995). Dynamin self-assembles into rings suggesting a mechanism for coated vesicle budding. *Nature* *374*, 190-192.
- Ingerman, E., and Nunnari, J. (2005). A continuous, regenerative coupled GTPase assay for dynamin-related proteins. *Methods in enzymology* *404*, 611-619.
- Tuma, P.L., and Collins, C.A. (1994). Activation of dynamin GTPase is a result of positive cooperativity. *The Journal of biological chemistry* *269*, 30842-30847.
- Wienken, C.J., Baaske, P., Rothbauer, U., Braun, D., and Duhr, S. (2010). Protein-binding assays in biological liquids using microscale thermophoresis. *Nature communications* *1*, 100.
- Alexander, C., Votruba, M., Pesch, U.E., Thiselton, D.L., Mayer, S., Moore, A., Rodriguez, M., Kellner, U., Leo-Kottler, B., Auburger, G., *et al.* (2000). OPA1, encoding a dynamin-related GTPase, is mutated in autosomal dominant optic atrophy linked to chromosome 3q28. *Nature genetics* *26*, 211-215.
- Altschuler, Y., Barbas, S.M., Terlecky, L.J., Tang, K., Hardy, S., Mostov, K.E., and Schmid, S.L. (1998). Redundant and distinct functions for dynamin-1 and dynamin-2 isoforms. *The Journal of cell biology* *143*, 1871-1881.
- Anderson, S.L., Carton, J.M., Lou, J., Xing, L., and Rubin, B.Y. (1999). Interferon-induced guanylate binding protein-1 (GBP-1) mediates an antiviral effect against vesicular stomatitis virus and encephalomyocarditis virus. *Virology* *256*, 8-14.

- Antoine, J.C., Absi, L., Honnorat, J., Boulesteix, J.M., de Brouker, T., Vial, C., Butler, M., De Camilli, P., and Michel, D. (1999). Anti-amphiphysin antibodies are associated with various paraneoplastic neurological syndromes and tumors. *Archives of neurology* 56, 172-177.
- Banks, G.T., and Fisher, E.M. (2008). Cytoplasmic dynein could be key to understanding neurodegeneration. *Genome biology* 9, 214.
- Bauerfeind, R., David, C., Grabs, D., McPherson, P.S., Nemoto, Y., Slepnev, V.I., Takei, K., and De Camilli, P. (1998). Recycling of synaptic vesicles. *Advances in pharmacology* (San Diego, Calif) 42, 253-257.
- Bement, W.M., Hasson, T., Wirth, J.A., Cheney, R.E., and Mooseker, M.S. (1994a). Identification and overlapping expression of multiple unconventional myosin genes in vertebrate cell types. *Proceedings of the National Academy of Sciences of the United States of America* 91, 6549-6553.
- Bement, W.M., Wirth, J.A., and Mooseker, M.S. (1994b). Cloning and mRNA expression of human unconventional myosin-IC. A homologue of amoeboid myosins-I with a single IQ motif and an SH3 domain. *Journal of molecular biology* 243, 356-363.
- Bensen, E.S., Costaguta, G., and Payne, G.S. (2000). Synthetic genetic interactions with temperature-sensitive clathrin in *Saccharomyces cerevisiae*. Roles for synaptojanin-like Inp53p and dynamin-related Vps1p in clathrin-dependent protein sorting at the trans-Golgi network. *Genetics* 154, 83-97.
- Berg, H.C. (2003). The rotary motor of bacterial flagella. *Annual review of biochemistry* 72, 19-54.
- Berg, J.S., Derfler, B.H., Pennisi, C.M., Corey, D.P., and Cheney, R.E. (2000). Myosin-X, a novel myosin with pleckstrin homology domains, associates with regions of dynamic actin. *Journal of cell science* 113 Pt 19, 3439-3451.
- Binns, D.D., Barylko, B., Grichine, N., Atkinson, M.A., Helms, M.K., Jameson, D.M., Eccleston, J.F., and Albanesi, J.P. (1999). Correlation between self-association modes and GTPase activation of dynamin. *Journal of protein chemistry* 18, 277-290.
- Bleazard, W., McCaffery, J.M., King, E.J., Bale, S., Mozdy, A., Tieu, Q., Nunnari, J., and Shaw, J.M. (1999). The dynamin-related GTPase Dnm1 regulates mitochondrial fission in yeast. *Nature cell biology* 1, 298-304.
- Bos, T.J. (1992). Oncogenes and cell growth. *Advances in experimental medicine and biology* 321, 45-49; discussion 51.
- Bourne, H.R., and Stryer, L. (1992). G proteins. The target sets the tempo. *Nature* 358, 541-543.
- Brown, J., and Bridgman, P.C. (2003a). Role of myosin II in axon outgrowth. *J Histochem Cytochem* 51, 421-428.
- Brown, M.E., and Bridgman, P.C. (2003b). Retrograde flow rate is increased in growth cones from myosin IIB knockout mice. *Journal of cell science* 116, 1087-1094.
- Campuzano, S., and Modolell, J. (1980). Hydrolysis of GTP on elongation factor Tu. ribosome complexes promoted by 2'(3')-O-L-phenylalanyl-adenosine. *Proceedings of the National Academy of Sciences of the United States of America* 77, 905-909.
- Cao, H., Garcia, F., and McNiven, M.A. (1998). Differential distribution of dynamin isoforms in mammalian cells. *Molecular biology of the cell* 9, 2595-2609.
- Chen, M.S., Obar, R.A., Schroeder, C.C., Austin, T.W., Poodry, C.A., Wadsworth, S.C., and Vallee, R.B. (1991). Multiple forms of dynamin are encoded by shibire, a *Drosophila* gene involved in endocytosis. *Nature* 351, 583-586.
- Chinthalapudi, K., Taft, M.H., Martin, R., Heissler, S.M., Preller, M., Hartmann, F.K., Brandstaetter, H., Kendrick-Jones, J., Tsiavalariis, G., Gutzeit, H.O., et al. (2011). Mechanism and Specificity of Pentachloropseudilin-mediated Inhibition of Myosin Motor Activity. *The Journal of biological chemistry* 286, 29700-29708.

- Chrzanowska-Wodnicka, M., and Burridge, K. (1992). Rho, rac and the actin cytoskeleton. *Bioessays* 14, 777-778.
- Clark, S.G., Shurland, D.L., Meyerowitz, E.M., Bargmann, C.I., and van der Blik, A.M. (1997). A dynamin GTPase mutation causes a rapid and reversible temperature-inducible locomotion defect in *C. elegans*. *Proceedings of the National Academy of Sciences of the United States of America* 94, 10438-10443.
- Cooke, R. (1995). The actomyosin engine. *Faseb J* 9, 636-642.
- Damke, H., Baba, T., Warnock, D.E., and Schmid, S.L. (1994). Induction of mutant dynamin specifically blocks endocytic coated vesicle formation. *The Journal of cell biology* 127, 915-934.
- Damke, H., Binns, D.D., Ueda, H., Schmid, S.L., and Baba, T. (2001a). Dynamin GTPase domain mutants block endocytic vesicle formation at morphologically distinct stages. *Molecular biology of the cell* 12, 2578-2589.
- Damke, H., Muhlberg, A.B., Sever, S., Sholly, S., Warnock, D.E., and Schmid, S.L. (2001b). Expression, purification, and functional assays for self-association of dynamin-1. *Methods in enzymology* 329, 447-457.
- David-Pfeuty, T., Simon, C., and Pantaloni, D. (1979). Effect of antimitotic drugs on tubulin GTPase activity and self-assembly. *The Journal of biological chemistry* 254, 11696-11702.
- David, C., McPherson, P.S., Mundigl, O., and de Camilli, P. (1996). A role of amphiphysin in synaptic vesicle endocytosis suggested by its binding to dynamin in nerve terminals. *Proceedings of the National Academy of Sciences of the United States of America* 93, 331-335.
- Delettre, C., Griffoin, J.M., Kaplan, J., Dollfus, H., Lorenz, B., Faivre, L., Lenaers, G., Belenguer, P., and Hamel, C.P. (2001). Mutation spectrum and splicing variants in the OPA1 gene. *Human genetics* 109, 584-591.
- Delettre, C., Lenaers, G., Griffoin, J.M., Gigarel, N., Lorenzo, C., Belenguer, P., Pelloquin, L., Grosgeorge, J., Turc-Carel, C., Perret, E., *et al.* (2000). Nuclear gene OPA1, encoding a mitochondrial dynamin-related protein, is mutated in dominant optic atrophy. *Nature genetics* 26, 207-210.
- Di Paolo, G., Sankaranarayanan, S., Wenk, M.R., Daniell, L., Perucco, E., Caldarone, B.J., Flavell, R., Picciotto, M.R., Ryan, T.A., Cremona, O., and De Camilli, P. (2002). Decreased synaptic vesicle recycling efficiency and cognitive deficits in amphiphysin 1 knockout mice. *Neuron* 33, 789-804.
- Dobrowolski, J.M., Carruthers, V.B., and Sibley, L.D. (1997). Participation of myosin in gliding motility and host cell invasion by *Toxoplasma gondii*. *Molecular microbiology* 26, 163-173.
- Ellis, S., and Mellor, H. (2000). Regulation of endocytic traffic by rho family GTPases. *Trends in cell biology* 10, 85-88.
- Endow, S.A. (1991). The emerging kinesin family of microtubule motor proteins. *Trends in biochemical sciences* 16, 221-225.
- Farsad, K., Ringstad, N., Takei, K., Floyd, S.R., Rose, K., and De Camilli, P. (2001). Generation of high curvature membranes mediated by direct endophilin bilayer interactions. *The Journal of cell biology* 155, 193-200.
- Fish, K.N., Schmid, S.L., and Damke, H. (2000). Evidence that dynamin-2 functions as a signal-transducing GTPase. *The Journal of cell biology* 150, 145-154.
- Foth (2006). New insights into myosin evolution and classification. *Proceedings of the National Academy of Sciences of the United States of America* 103, 3681-3686.
- Frank, S., Gaume, B., Bergmann-Leitner, E.S., Leitner, W.W., Robert, E.G., Catez, F., Smith, C.L., and Youle, R.J. (2001). The role of dynamin-related protein 1, a mediator of mitochondrial fission, in apoptosis. *Developmental cell* 1, 515-525.

- Fujimoto, M., Arimura, S., Mano, S., Kondo, M., Saito, C., Ueda, T., Nakazono, M., Nakano, A., Nishimura, M., and Tsutsumi, N. (2009). Arabidopsis dynamin-related proteins DRP3A and DRP3B are functionally redundant in mitochondrial fission, but have distinct roles in peroxisomal fission. *Plant J* 58, 388-400.
- Gammie, A.E., Kurihara, L.J., Vallee, R.B., and Rose, M.D. (1995). DNM1, a dynamin-related gene, participates in endosomal trafficking in yeast. *The Journal of cell biology* 130, 553-566.
- Gao, H., Kadirjan-Kalbach, D., Froehlich, J.E., and Osteryoung, K.W. (2003). ARC5, a cytosolic dynamin-like protein from plants, is part of the chloroplast division machinery. *Proceedings of the National Academy of Sciences of the United States of America* 100, 4328-4333.
- Geeves, M.A., Fedorov, R., and Manstein, D.J. (2005). Molecular mechanism of actomyosin-based motility. *Cell Mol Life Sci* 62, 1462-1477.
- Geeves, M.A., and Holmes, K.C. (1999). Structural mechanism of muscle contraction. *Annual review of biochemistry* 68, 687-728.
- Geeves, M.A., and Holmes, K.C. (2005). The molecular mechanism of muscle contraction. *Advances in protein chemistry* 71, 161-193.
- Gray, N.W., Fourgeaud, L., Huang, B., Chen, J., Cao, H., Oswald, B.J., Hemar, A., and McNiven, M.A. (2003). Dynamin 3 is a component of the postsynapse, where it interacts with mGluR5 and Homer. *Curr Biol* 13, 510-515.
- Gray, N.W., Kruchten, A.E., Chen, J., and McNiven, M.A. (2005). A dynamin-3 spliced variant modulates the actin/cortactin-dependent morphogenesis of dendritic spines. *Journal of cell science* 118, 1279-1290.
- Gu, X., and Verma, D.P. (1996). Phragmoplastin, a dynamin-like protein associated with cell plate formation in plants. *The EMBO journal* 15, 695-704.
- Haller, O., Frese, M., and Kochs, G. (1998). Mx proteins: mediators of innate resistance to RNA viruses. *Revue scientifique et technique (International Office of Epizootics)* 17, 220-230.
- Heaslip, A.T., Dzierszinski, F., Stein, B., and Hu, K. TgMORN1 is a key organizer for the basal complex of *Toxoplasma gondii*. *PLoS pathogens* 6, e1000754.
- Heaslip, A.T., Leung, J.M., Carey, K.L., Catti, F., Warshaw, D.M., Westwood, N.J., Ballif, B.A., and Ward, G.E. A small-molecule inhibitor of *T. gondii* motility induces the posttranslational modification of myosin light chain-1 and inhibits myosin motor activity. *PLoS pathogens* 6, e1000720.
- Henley, J.R., Krueger, E.W., Oswald, B.J., and McNiven, M.A. (1998). Dynamin-mediated internalization of caveolae. *The Journal of cell biology* 141, 85-99.
- Higuchi, H., and Takemori, S. (1989). Butanedione monoxime suppresses contraction and ATPase activity of rabbit skeletal muscle. *Journal of biochemistry* 105, 638-643.
- Hill, E., van Der Kaay, J., Downes, C.P., and Smythe, E. (2001). The role of dynamin and its binding partners in coated pit invagination and scission. *The Journal of cell biology* 152, 309-323.
- Hill, T., Odell, L.R., Edwards, J.K., Graham, M.E., McGeachie, A.B., Rusak, J., Quan, A., Abagyan, R., Scott, J.L., Robinson, P.J., and McCluskey, A. (2005). Small molecule inhibitors of dynamin I GTPase activity: development of dimeric tyrphostins. *Journal of medicinal chemistry* 48, 7781-7788.
- Hill, T.A., Gordon, C.P., McGeachie, A.B., Venn-Brown, B., Odell, L.R., Chau, N., Quan, A., Mariana, A., Sakoff, J.A., Chircop, M., *et al.* (2009). Inhibition of dynamin mediated endocytosis by the dynoles--synthesis and functional activity of a family of indoles. *Journal of medicinal chemistry* 52, 3762-3773.

- Hill, T.A., Odell, L.R., Quan, A., Abagyan, R., Ferguson, G., Robinson, P.J., and McCluskey, A. (2004). Long chain amines and long chain ammonium salts as novel inhibitors of dynamin GTPase activity. *Bioorganic & medicinal chemistry letters* *14*, 3275-3278.
- Hinshaw, J.E., and Schmid, S.L. (1995). Dynamin self-assembles into rings suggesting a mechanism for coated vesicle budding. *Nature* *374*, 190-192.
- Hirokawa, N., Niwa, S., and Tanaka, Y. (2010). Molecular motors in neurons: transport mechanisms and roles in brain function, development, and disease. *Neuron* *68*, 610-638.
- Hoepfner, D., van den Berg, M., Philippsen, P., Tabak, H.F., and Hettema, E.H. (2001). A role for Vps1p, actin, and the Myo2p motor in peroxisome abundance and inheritance in *Saccharomyces cerevisiae*. *The Journal of cell biology* *155*, 979-990.
- Imoto, M., Tachibana, I., and Urrutia, R. (1998). Identification and functional characterization of a novel human protein highly related to the yeast dynamin-like GTPase Vps1p. *Journal of cell science* *111* (Pt 10), 1341-1349.
- Ishihara, N., Nomura, M., Jofuku, A., Kato, H., Suzuki, S.O., Masuda, K., Otera, H., Nakanishi, Y., Nonaka, I., Goto, Y., *et al.* (2009). Mitochondrial fission factor Drp1 is essential for embryonic development and synapse formation in mice. *Nature cell biology* *11*, 958-966.
- Jones, B.A., and Fangman, W.L. (1992). Mitochondrial DNA maintenance in yeast requires a protein containing a region related to the GTP-binding domain of dynamin. *Genes & development* *6*, 380-389.
- Jones, S.M., Howell, K.E., Henley, J.R., Cao, H., and McNiven, M.A. (1998). Role of dynamin in the formation of transport vesicles from the trans-Golgi network. *Science (New York, N.Y)* *279*, 573-577.
- Kagawa, M., Sato, N., and Obinata, T. (2006). Effects of BTS (N-benzyl-p-toluene sulphonamide), an inhibitor for myosin-actin interaction, on myofibrillogenesis in skeletal muscle cells in culture. *Zoological science* *23*, 969-975.
- Kamitani, A., Yamada, H., Kinuta, M., Watanabe, M., Li, S.A., Matsukawa, T., McNiven, M., Kumon, H., and Takei, K. (2002). Distribution of dynamins in testis and their possible relation to spermatogenesis. *Biochemical and biophysical research communications* *294*, 261-267.
- Kang, S.G., Jin, J.B., Piao, H.L., Pih, K.T., Jang, H.J., Lim, J.H., and Hwang, I. (1998). Molecular cloning of an Arabidopsis cDNA encoding a dynamin-like protein that is localized to plastids. *Plant molecular biology* *38*, 437-447.
- Kasai, K., Shin, H.W., Shinotsuka, C., Murakami, K., and Nakayama, K. (1999). Dynamin II is involved in endocytosis but not in the formation of transport vesicles from the trans-Golgi network. *Journal of biochemistry* *125*, 780-789.
- Kim, Y.W., Park, D.S., Park, S.C., Kim, S.H., Cheong, G.W., and Hwang, I. (2001). Arabidopsis dynamin-like 2 that binds specifically to phosphatidylinositol 4-phosphate assembles into a high-molecular weight complex in vivo and in vitro. *Plant physiology* *127*, 1243-1255.
- Klockow, B., Tichelaar, W., Madden, D.R., Niemann, H.H., Akiba, T., Hirose, K., and Manstein, D.J. (2002). The dynamin A ring complex: molecular organization and nucleotide-dependent conformational changes. *The EMBO journal* *21*, 240-250.
- Kochs, G., and Haller, O. (1999a). GTP-bound human MxA protein interacts with the nucleocapsids of Thogoto virus (Orthomyxoviridae). *The Journal of biological chemistry* *274*, 4370-4376.
- Kochs, G., and Haller, O. (1999b). Interferon-induced human MxA GTPase blocks nuclear import of Thogoto virus nucleocapsids. *Proceedings of the National Academy of Sciences of the United States of America* *96*, 2082-2086.

- Koenig, J.H., and Ikeda, K. (1989). Disappearance and reformation of synaptic vesicle membrane upon transmitter release observed under reversible blockage of membrane retrieval. *J Neurosci* 9, 3844-3860.
- Koenig, J.H., and Ikeda, K. (1999). Contribution of active zone subpopulation of vesicles to evoked and spontaneous release. *Journal of neurophysiology* 81, 1495-1505.
- Koenig, J.H., and Ikeda, K. (2007). Release and recycling of the readily releasable vesicle population in a synapse possessing no reserve population. *Journal of neurophysiology* 97, 4048-4057.
- Koenig, J.H., Kosaka, T., and Ikeda, K. (1989). The relationship between the number of synaptic vesicles and the amount of transmitter released. *J Neurosci* 9, 1937-1942.
- Kosaka, T., and Ikeda, K. (1983a). Possible temperature-dependent blockage of synaptic vesicle recycling induced by a single gene mutation in *Drosophila*. *Journal of neurobiology* 14, 207-225.
- Kosaka, T., and Ikeda, K. (1983b). Reversible blockage of membrane retrieval and endocytosis in the garland cell of the temperature-sensitive mutant of *Drosophila melanogaster*, *shibirets1*. *The Journal of cell biology* 97, 499-507.
- Labrousse, A.M., Shurland, D.L., and van der Bliek, A.M. (1998). Contribution of the GTPase domain to the subcellular localization of dynamin in the nematode *Caenorhabditis elegans*. *Molecular biology of the cell* 9, 3227-3239.
- Labrousse, A.M., Zappaterra, M.D., Rube, D.A., and van der Bliek, A.M. (1999). *C. elegans* dynamin-related protein DRP-1 controls severing of the mitochondrial outer membrane. *Molecular cell* 4, 815-826.
- Lad, P.M., Nielsen, T.B., Preston, M.S., and Rodbell, M. (1980). The role of the guanine nucleotide exchange reaction in the regulation of the beta-adrenergic receptor and in the actions of catecholamines and cholera toxin on adenylate cyclase in turkey erythrocyte membranes. *The Journal of biological chemistry* 255, 988-995.
- Lee, Y.H., Gallant, C., Guo, H., Li, Y., Wang, C.A., and Morgan, K.G. (2000). Regulation of vascular smooth muscle tone by N-terminal region of caldesmon. Possible role of tethering actin to myosin. *The Journal of biological chemistry* 275, 3213-3220.
- Leprince, C., Le Scolan, E., Meunier, B., Fraissier, V., Brandon, N., De Gunzburg, J., and Camonis, J. (2003). Sorting nexin 4 and amphiphysin 2, a new partnership between endocytosis and intracellular trafficking. *Journal of cell science* 116, 1937-1948.
- Leprince, C., Romero, F., Cussac, D., Vayssiere, B., Berger, R., Tavitian, A., and Camonis, J.H. (1997). A new member of the amphiphysin family connecting endocytosis and signal transduction pathways. *The Journal of biological chemistry* 272, 15101-15105.
- Lombardi, R., and Riezman, H. (2001). Rvs161p and Rvs167p, the two yeast amphiphysin homologs, function together in vivo. *The Journal of biological chemistry* 276, 6016-6022.
- Lopez, M.A., Pardo, P.S., Cox, G.A., and Boriek, A.M. (2008). Early mechanical dysfunction of the diaphragm in the muscular dystrophy with myositis (Ttnmdm) model. *American journal of physiology* 295, C1092-1102.
- Low, H.H., and Lowe, J. (2006). A bacterial dynamin-like protein. *Nature* 444, 766-769.
- Marks, B., Stowell, M.H., Vallis, Y., Mills, I.G., Gibson, A., Hopkins, C.R., and McMahon, H.T. (2001). GTPase activity of dynamin and resulting conformation change are essential for endocytosis. *Nature* 410, 231-235.
- Masaike, Y., Takagi, T., Hirota, M., Yamada, J., Ishihara, S., Yung, T.M., Inoue, T., Sawa, C., Sagara, H., Sakamoto, S., *et al.* (2007). Identification of dynamin-2-mediated endocytosis as a new target of osteoporosis drugs, bisphosphonates. *Molecular pharmacology* 77, 262-269.
- McMacken, R., Ueda, K., and Kornberg, A. (1977). Migration of *Escherichia coli* dnaB protein on the template DNA strand as a mechanism in initiating DNA replication.

- Proceedings of the National Academy of Sciences of the United States of America *74*, 4190-4194.
- McNiven, M.A., Cao, H., Pitts, K.R., and Yoon, Y. (2000a). The dynamin family of mechanoenzymes: pinching in new places. *Trends in biochemical sciences* *25*, 115-120.
- McNiven, M.A., Kim, L., Krueger, E.W., Orth, J.D., Cao, H., and Wong, T.W. (2000b). Regulated interactions between dynamin and the actin-binding protein cortactin modulate cell shape. *The Journal of cell biology* *151*, 187-198.
- McPherson, P.S., Garcia, E.P., Slepnev, V.I., David, C., Zhang, X., Grabs, D., Sossin, W.S., Bauerfeind, R., Nemoto, Y., and De Camilli, P. (1996). A presynaptic inositol-5-phosphatase. *Nature* *379*, 353-357.
- Mears, J.A., Lackner, L.L., Fang, S., Ingerman, E., Nunnari, J., and Hinshaw, J.E. (2010). Conformational changes in Dnm1 support a contractile mechanism for mitochondrial fission. *Nature structural & molecular biology* *18*, 20-26.
- Melen, K., Ronni, T., Broni, B., Krug, R.M., von Bonsdorff, C.H., and Julkunen, I. (1992). Interferon-induced Mx proteins form oligomers and contain a putative leucine zipper. *The Journal of biological chemistry* *267*, 25898-25907.
- Miyagishima, S.Y., Nishida, K., and Kuroiwa, T. (2003). An evolutionary puzzle: chloroplast and mitochondrial division rings. *Trends in plant science* *8*, 432-438.
- Morgan, D.O. (1997). CYCLIN-DEPENDENT KINASES: Engines, Clocks, and Microprocessors. *Annu. Rev. Cell Dev. Biol.* *13*, 261-291.
- Muhlberg, A.B., Warnock, D.E., and Schmid, S.L. (1997). Domain structure and intramolecular regulation of dynamin GTPase. *The EMBO journal* *16*, 6676-6683.
- Nguyen, C., and Bibb, J.A. (2003). Cdk5 and the mystery of synaptic vesicle endocytosis. *The Journal of cell biology* *163*, 697-699.
- Nguyen, M.D., Mushynski, W.E., and Julien, J.P. (2002). Cycling at the interface between neurodevelopment and neurodegeneration. *Cell death and differentiation* *9*, 1294-1306.
- Nothwehr, S.F., Conibear, E., and Stevens, T.H. (1995). Golgi and vacuolar membrane proteins reach the vacuole in vps1 mutant yeast cells via the plasma membrane. *The Journal of cell biology* *129*, 35-46.
- Obar, R.A., Collins, C.A., Hammarback, J.A., Shpetner, H.S., and Vallee, R.B. (1990). Molecular cloning of the microtubule-associated mechanochemical enzyme dynamin reveals homology with a new family of GTP-binding proteins. *Nature* *347*, 256-261.
- Odell, L.R., Howan, D., Gordon, C.P., Robertson, M.J., Chau, N., Mariana, A., Whiting, A.E., Abagyan, R., Daniel, J.A., Gorgani, N.N., *et al.* (2010). The phthaladyns: GTP competitive inhibitors of dynamin I and II GTPase derived from virtual screening. *Journal of medicinal chemistry* *53*, 5267-5280.
- Okamoto, P.M., Tripet, B., Litowski, J., Hodges, R.S., and Vallee, R.B. (1999). Multiple distinct coiled-coils are involved in dynamin self-assembly. *The Journal of biological chemistry* *274*, 10277-10286.
- Olichon, A., Baricault, L., Gas, N., Guillou, E., Valette, A., Belenguer, P., and Lenaers, G. (2003). Loss of OPA1 perturbs the mitochondrial inner membrane structure and integrity, leading to cytochrome c release and apoptosis. *The Journal of biological chemistry* *278*, 7743-7746.
- Oliver, T.N., Berg, J.S., and Cheney, R.E. (1999). Tails of unconventional myosins. *Cell Mol Life Sci* *56*, 243-257.
- Otsuga, D., Keegan, B.R., Brisch, E., Thatcher, J.W., Hermann, G.J., Bleazard, W., and Shaw, J.M. (1998). The dynamin-related GTPase, Dnm1p, controls mitochondrial morphology in yeast. *The Journal of cell biology* *143*, 333-349.
- Otsuka, A., Abe, T., Watanabe, M., Yagisawa, H., Takei, K., and Yamada, H. (2009). Dynamin 2 is required for actin assembly in phagocytosis in Sertoli cells. *Biochemical and biophysical research communications* *378*, 478-482.

- Park, J.M., Cho, J.H., Kang, S.G., Jang, H.J., Pih, K.T., Piao, H.L., Cho, M.J., and Hwang, I. (1998). A dynamin-like protein in *Arabidopsis thaliana* is involved in biogenesis of thylakoid membranes. *The EMBO journal* *17*, 859-867.
- Park, J.M., Kang, S.G., Pih, K.T., Jang, H.J., Piao, H.L., Yoon, H.W., Cho, M.J., and Hwang, I. (1997). A dynamin-like protein, ADL1, is present in membranes as a high-molecular-mass complex in *Arabidopsis thaliana*. *Plant physiology* *115*, 763-771.
- Pavlovic, J., Schroder, A., Blank, A., Pitossi, F., and Staeheli, P. (1993). Mx proteins: GTPases involved in the interferon-induced antiviral state. *Ciba Foundation symposium* *176*, 233-243; discussion 243-237.
- Pelloquin, L., Belenguer, P., Menon, Y., and Ducommun, B. (1998). Identification of a fission yeast dynamin-related protein involved in mitochondrial DNA maintenance. *Biochemical and biophysical research communications* *251*, 720-726.
- Pelloquin, L., Belenguer, P., Menon, Y., Gas, N., and Ducommun, B. (1999a). Fission yeast Msp1 is a mitochondrial dynamin-related protein. *Journal of cell science* *112* (Pt 22), 4151-4161.
- Pelloquin, L., Ducommun, B., and Belenguer, P. (1999b). Interaction between the fission yeast nim1/cdr1 protein kinase and a dynamin-related protein. *FEBS letters* *443*, 71-74.
- Phillips, G.R., Huang, J.K., Wang, Y., Tanaka, H., Shapiro, L., Zhang, W., Shan, W.S., Arndt, K., Frank, M., Gordon, R.E., *et al.* (2001). The presynaptic particle web: ultrastructure, composition, dissolution, and reconstitution. *Neuron* *32*, 63-77.
- Pitossi, F., Blank, A., Schroder, A., Schwarz, A., Hussi, P., Schwemmler, M., Pavlovic, J., and Staeheli, P. (1993). A functional GTP-binding motif is necessary for antiviral activity of Mx proteins. *Journal of virology* *67*, 6726-6732.
- Pitts, K.R., Yoon, Y., Krueger, E.W., and McNiven, M.A. (1999). The dynamin-like protein DLP1 is essential for normal distribution and morphology of the endoplasmic reticulum and mitochondria in mammalian cells. *Molecular biology of the cell* *10*, 4403-4417.
- Pollard, T.D., Doberstein, S.K., and Zot, H.G. (1991). Myosin-I. *Annual review of physiology* *53*, 653-681.
- Poodry, C.A., and Edgar, L. (1979). Reversible alteration in the neuromuscular junctions of *Drosophila melanogaster* bearing a temperature-sensitive mutation, shibire. *The Journal of cell biology* *81*, 520-527.
- Post, P.L., Bokoch, G.M., and Mooseker, M.S. (1998). Human myosin-IXb is a mechanochemically active motor and a GAP for rho. *Journal of cell science* *111* (Pt 7), 941-950.
- Praefcke, G.J., Geyer, M., Schwemmler, M., Robert Kalbitzer, H., and Herrmann, C. (1999). Nucleotide-binding characteristics of human guanylate-binding protein 1 (hGBP1) and identification of the third GTP-binding motif. *Journal of molecular biology* *292*, 321-332.
- Prakash, B., Praefcke, G.J., Renault, L., Wittinghofer, A., and Herrmann, C. (2000a). Structure of human guanylate-binding protein 1 representing a unique class of GTP-binding proteins. *Nature* *403*, 567-571.
- Prakash, B., Renault, L., Praefcke, G.J., Herrmann, C., and Wittinghofer, A. (2000b). Triphosphate structure of guanylate-binding protein 1 and implications for nucleotide binding and GTPase mechanism. *The EMBO journal* *19*, 4555-4564.
- Preller, M., Chinthalapudi, K., Martin, R., Knolker, H.J., and Manstein, D.J. Inhibition of Myosin ATPase activity by halogenated pseudilins: a structure-activity study. *Journal of medicinal chemistry* *54*, 3675-3685.
- Ramamurthy, B., Yengo, C.M., Straight, A.F., Mitchison, T.J., and Sweeney, H.L. (2004). Kinetic mechanism of blebbistatin inhibition of nonmuscle myosin IIb. *Biochemistry* *43*, 14832-14839.

- Ramaswami, M., Krishnan, K.S., and Kelly, R.B. (1994). Intermediates in synaptic vesicle recycling revealed by optical imaging of *Drosophila* neuromuscular junctions. *Neuron* *13*, 363-375.
- Rayment, I., Holden, H.M., Whittaker, M., Yohn, C.B., Lorenz, M., Holmes, K.C., and Milligan, R.A. (1993). Structure of the actin-myosin complex and its implications for muscle contraction. *Science (New York, N.Y)* *261*, 58-65.
- Reems, J.A., Wang, W., Tsubata, K., Abdurrahman, N., Sundell, B., Tijssen, M.R., van der Schoot, E., Di Summa, F., Patel-Hett, S., Italiano, J., Jr., and Gilligan, D.M. (2008). Dynamin 3 participates in the growth and development of megakaryocytes. *Experimental hematology* *36*, 1714-1727.
- Reubold, T.F., Eschenburg, S., Becker, A., Kull, F.J., and Manstein, D.J. (2003). A structural model for actin-induced nucleotide release in myosin. *Nature structural biology* *10*, 826-830.
- Reubold, T.F., Eschenburg, S., Becker, A., Leonard, M., Schmid, S.L., Vallee, R.B., Kull, F.J., and Manstein, D.J. (2005). Crystal structure of the GTPase domain of rat dynamin 1. *Proceedings of the National Academy of Sciences of the United States of America* *102*, 13093-13098.
- Ridley, A.J. (2001). Rho family proteins: coordinating cell responses. *Trends in cell biology* *11*, 471-477.
- Robinson, P.J., Sontag, J.M., Liu, J.P., Fykse, E.M., Slaughter, C., McMahan, H., and Sudhof, T.C. (1993). Dynamin GTPase regulated by protein kinase C phosphorylation in nerve terminals. *Nature* *365*, 163-166.
- Rosenblatt, J.E., del Carmen, R., and Wyatt, R.J. (1980). A high affinity GTP binding site in rat brain. *European journal of pharmacology* *64*, 365-366.
- Rothman, J.H., Raymond, C.K., Gilbert, T., O'Hara, P.J., and Stevens, T.H. (1990). A putative GTP binding protein homologous to interferon-inducible Mx proteins performs an essential function in yeast protein sorting. *Cell* *61*, 1063-1074.
- Saiz, A., Dalmau, J., Butler, M.H., Chen, Q., Delattre, J.Y., De Camilli, P., and Graus, F. (1999). Anti-amphiphysin I antibodies in patients with paraneoplastic neurological disorders associated with small cell lung carcinoma. *Journal of neurology, neurosurgery, and psychiatry* *66*, 214-217.
- Sasaki, N., Ohkura, R., and Sutoh, K. (2002). Dictyostelium myosin II as a model to study the actin-myosin interactions during force generation. *Journal of muscle research and cell motility* *23*, 697-702.
- Sasaki, N., Ohkura, R., and Sutoh, K. (2003). Dictyostelium myosin II mutations that uncouple the converter swing and ATP hydrolysis cycle. *Biochemistry* *42*, 90-95.
- Savoia, A., De Rocco, D., Panza, E., Bozzi, V., Scandellari, R., Loffredo, G., Mumford, A., Heller, P.G., Noris, P., De Groot, M.R., *et al.* Heavy chain myosin 9-related disease (MYH9 - RD): neutrophil inclusions of myosin-9 as a pathognomonic sign of the disorder. *Thrombosis and haemostasis* *103*, 826-832.
- Savoia, A., Germeshausen, M., De Rocco, D., Henschel, B., Kratz, C.P., Kuhlen, M., Rath, B., Steuhl, K.P., Wermes, C., and Ballmaier, M. MYH9-related disease: Report on five German families and description of a novel mutation. *Annals of hematology* *89*, 1057-1059.
- Schafer, D.A. (2002). Coupling actin dynamics and membrane dynamics during endocytosis. *Current opinion in cell biology* *14*, 76-81.
- Schafer, D.A. (2004). Regulating actin dynamics at membranes: a focus on dynamin. *Traffic (Copenhagen, Denmark)* *5*, 463-469.
- Schumacher, B., and Staeheli, P. (1998). Domains mediating intramolecular folding and oligomerization of MxA GTPase. *The Journal of biological chemistry* *273*, 28365-28370.
- Sellers, J.R. (1999). Unphosphorylated crossbridges and latch: smooth muscle regulation revisited. *Journal of muscle research and cell motility* *20*, 347-349.

- Sellers, J.R. (2000). Myosins: a diverse superfamily. *Biochimica et biophysica acta* 1496, 3-22.
- Sesaki, H., and Jensen, R.E. (1999). Division versus fusion: Dnm1p and Fzo1p antagonistically regulate mitochondrial shape. *The Journal of cell biology* 147, 699-706.
- Sever, S., Damke, H., and Schmid, S.L. (2000a). Dynamin:GTP controls the formation of constricted coated pits, the rate limiting step in clathrin-mediated endocytosis. *The Journal of cell biology* 150, 1137-1148.
- Sever, S., Damke, H., and Schmid, S.L. (2000b). Garrotes, springs, ratchets, and whips: putting dynamin models to the test. *Traffic (Copenhagen, Denmark)* 1, 385-392.
- Sever, S., Muhlberg, A.B., and Schmid, S.L. (1999). Impairment of dynamin's GAP domain stimulates receptor-mediated endocytosis. *Nature* 398, 481-486.
- Shepard, K.A., and Yaffe, M.P. (1999). The yeast dynamin-like protein, Mgm1p, functions on the mitochondrial outer membrane to mediate mitochondrial inheritance. *The Journal of cell biology* 144, 711-720.
- Shupliakov, O., Low, P., Grabs, D., Gad, H., Chen, H., David, C., Takei, K., De Camilli, P., and Brodin, L. (1997). Synaptic vesicle endocytosis impaired by disruption of dynamin-SH3 domain interactions. *Science (New York, N.Y)* 276, 259-263.
- Sivadon, P., Bauer, F., Aigle, M., and Crouzet, M. (1995). Actin cytoskeleton and budding pattern are altered in the yeast *rvs161* mutant: the *Rvs161* protein shares common domains with the brain protein amphiphysin. *Mol Gen Genet* 246, 485-495.
- Slebos, R.J., and Rodenhuis, S. (1992). The ras gene family in human non-small-cell lung cancer. *Journal of the National Cancer Institute*, 23-29.
- Slepnev, V.I., Ochoa, G.C., Butler, M.H., and De Camilli, P. (2000). Tandem arrangement of the clathrin and AP-2 binding domains in amphiphysin 1 and disruption of clathrin coat function by amphiphysin fragments comprising these sites. *The Journal of biological chemistry* 275, 17583-17589.
- Slepnev, V.I., Ochoa, G.C., Butler, M.H., Grabs, D., and De Camilli, P. (1998). Role of phosphorylation in regulation of the assembly of endocytic coat complexes. *Science (New York, N.Y)* 281, 821-824.
- Smirnova, E., Griparic, L., Shurland, D.L., and van der Bliek, A.M. (2001). Dynamin-related protein Drp1 is required for mitochondrial division in mammalian cells. *Molecular biology of the cell* 12, 2245-2256.
- Smirnova, E., Shurland, D.L., Newman-Smith, E.D., Pishvae, B., and van der Bliek, A.M. (1999). A model for dynamin self-assembly based on binding between three different protein domains. *The Journal of biological chemistry* 274, 14942-14947.
- Smirnova, E., Shurland, D.L., Ryazantsev, S.N., and van der Bliek, A.M. (1998). A human dynamin-related protein controls the distribution of mitochondria. *The Journal of cell biology* 143, 351-358.
- Song, B.D., Leonard, M., and Schmid, S.L. (2004a). Dynamin GTPase domain mutants that differentially affect GTP binding, GTP hydrolysis, and clathrin-mediated endocytosis. *The Journal of biological chemistry* 279, 40431-40436.
- Song, B.D., and Schmid, S.L. (2003). A molecular motor or a regulator? Dynamin's in a class of its own. *Biochemistry* 42, 1369-1376.
- Song, B.D., Yarar, D., and Schmid, S.L. (2004b). An assembly-incompetent mutant establishes a requirement for dynamin self-assembly in clathrin-mediated endocytosis in vivo. *Molecular biology of the cell* 15, 2243-2252.
- Stowell, M.H., Marks, B., Wigge, P., and McMahon, H.T. (1999). Nucleotide-dependent conformational changes in dynamin: evidence for a mechanochemical molecular spring. *Nature cell biology* 1, 27-32.
- Sweitzer, S.M., and Hinshaw, J.E. (1998). Dynamin undergoes a GTP-dependent conformational change causing vesiculation. *Cell* 93, 1021-1029.

- Taguchi, N., Ishihara, N., Jofuku, A., Oka, T., and Mihara, K. (2007). Mitotic phosphorylation of dynamin-related GTPase Drp1 participates in mitochondrial fission. *The Journal of biological chemistry* 282, 11521-11529.
- Takei, K., McPherson, P.S., Schmid, S.L., and De Camilli, P. (1995). Tubular membrane invaginations coated by dynamin rings are induced by GTP-gamma S in nerve terminals. *Nature* 374, 186-190.
- Takei, K., Mundigl, O., Daniell, L., and De Camilli, P. (1996). The synaptic vesicle cycle: a single vesicle budding step involving clathrin and dynamin. *The Journal of cell biology* 133, 1237-1250.
- Takei, K., Slepnev, V.I., Haucke, V., and De Camilli, P. (1999). Functional partnership between amphiphysin and dynamin in clathrin-mediated endocytosis. *Nature cell biology* 1, 33-39.
- Tanabe, K., and Takei, K. (2009). Dynamic instability of microtubules requires dynamin 2 and is impaired in a Charcot-Marie-Tooth mutant. *The Journal of cell biology* 185, 939-948.
- Tanaka, A., and Youle, R.J. (2008). A chemical inhibitor of DRP1 uncouples mitochondrial fission and apoptosis. *Molecular cell* 29, 409-410.
- Tomizawa, K., Ohta, J., Matsushita, M., Moriwaki, A., Li, S.T., Takei, K., and Matsui, H. (2002). Cdk5/p35 regulates neurotransmitter release through phosphorylation and downregulation of P/Q-type voltage-dependent calcium channel activity. *J Neurosci* 22, 2590-2597.
- Tomizawa, K., Sunada, S., Lu, Y.F., Oda, Y., Kinuta, M., Ohshima, T., Saito, T., Wei, F.Y., Matsushita, M., Li, S.T., *et al.* (2003). Cophosphorylation of amphiphysin I and dynamin I by Cdk5 regulates clathrin-mediated endocytosis of synaptic vesicles. *The Journal of cell biology* 163, 813-824.
- Tsiavaliaris, G., Fujita-Becker, S., Batra, R., Levitsky, D.I., Kull, F.J., Geeves, M.A., and Manstein, D.J. (2002). Mutations in the relay loop region result in dominant-negative inhibition of myosin II function in *Dictyostelium*. *EMBO reports* 3, 1099-1105.
- Tuma, P.L., and Collins, C.A. (1994). Activation of dynamin GTPase is a result of positive cooperativity. *The Journal of biological chemistry* 269, 30842-30847.
- Urrutia, R., Henley, J.R., Cook, T., and McNiven, M.A. (1997). The dynamins: redundant or distinct functions for an expanding family of related GTPases? *Proceedings of the National Academy of Sciences of the United States of America* 94, 377-384.
- van der Blik, A.M. (1999). Functional diversity in the dynamin family. *Trends in cell biology* 9, 96-102.
- van der Blik, A.M., and Meyerowitz, E.M. (1991). Dynamin-like protein encoded by the *Drosophila shibire* gene associated with vesicular traffic. *Nature* 351, 411-414.
- Veugelers, M., Bressan, M., McDermott, D.A., Weremowicz, S., Morton, C.C., Mabry, C.C., Lefavre, J.F., Zunamon, A., Destree, A., Chaudron, J.M., and Basson, C.T. (2004). Mutation of perinatal myosin heavy chain associated with a Carney complex variant. *The New England journal of medicine* 351, 460-469.
- Vizeacoumar, F.J., Vreden, W.N., Fagarasanu, M., Eitzen, G.A., Aitchison, J.D., and Rachubinski, R.A. (2006). The dynamin-like protein Vps1p of the yeast *Saccharomyces cerevisiae* associates with peroxisomes in a Pex19p-dependent manner. *The Journal of biological chemistry* 281, 12817-12823.
- Volchuk, A., Narine, S., Foster, L.J., Grabs, D., De Camilli, P., and Klip, A. (1998). Perturbation of dynamin II with an amphiphysin SH3 domain increases GLUT4 glucose transporters at the plasma membrane in 3T3-L1 adipocytes. Dynamin II participates in GLUT4 endocytosis. *The Journal of biological chemistry* 273, 8169-8176.
- Walsh, R., Rutland, C., Thomas, R., and Loughna, S. (2010a). Cardiomyopathy: a systematic review of disease-causing mutations in myosin heavy chain 7 and their phenotypic manifestations. *Cardiology* 115, 49-60.

- Walsh, V.L., Raviv, D., Dror, A.A., Shahin, H., Walsh, T., Kanaan, M.N., Avraham, K.B., and King, M.C. (2010b). A mouse model for human hearing loss DFNB30 due to loss of function of myosin IIIA. *Mamm Genome* 22, 170-177.
- Watanabe, M., Yumoto, M., Tanaka, H., Wang, H.H., Katayama, T., Yoshiyama, S., Black, J., Thatcher, S.E., and Kohama, K. (2010). Blebbistatin, a myosin II inhibitor, suppresses contraction and disrupts contractile filaments organization of skinned taenia cecum from guinea pig. *American journal of physiology* 298, C1118-1126.
- Waterham, H.R., Koster, J., van Roermund, C.W., Mooyer, P.A., Wanders, R.J., and Leonard, J.V. (2007). A lethal defect of mitochondrial and peroxisomal fission. *The New England journal of medicine* 356, 1736-1741.
- Wechsler-Reya, R., Elliott, K., Herlyn, M., and Prendergast, G.C. (1997a). The putative tumor suppressor BIN1 is a short-lived nuclear phosphoprotein, the localization of which is altered in malignant cells. *Cancer research* 57, 3258-3263.
- Wechsler-Reya, R., Sakamuro, D., Zhang, J., Duhadaway, J., and Prendergast, G.C. (1997b). Structural analysis of the human BIN1 gene. Evidence for tissue-specific transcriptional regulation and alternate RNA splicing. *The Journal of biological chemistry* 272, 31453-31458.
- Wechsler-Reya, R.J., and Barres, B.A. (1997). Retinal development: communication helps you see the light. *Curr Biol* 7, R433-436.
- Wells, A.L., Lin, A.W., Chen, L.Q., Safer, D., Cain, S.M., Hasson, T., Carragher, B.O., Milligan, R.A., and Sweeney, H.L. (1999). Myosin VI is an actin-based motor that moves backwards. *Nature* 401, 505-508.
- Wienke, D.C., Knetsch, M.L., Neuhaus, E.M., Reedy, M.C., and Manstein, D.J. (1999). Disruption of a dynamin homologue affects endocytosis, organelle morphology, and cytokinesis in *Dictyostelium discoideum*. *Molecular biology of the cell* 10, 225-243.
- Wilsbach, K., and Payne, G.S. (1993). Vps1p, a member of the dynamin GTPase family, is necessary for Golgi membrane protein retention in *Saccharomyces cerevisiae*. *The EMBO journal* 12, 3049-3059.
- Wong, E.D., Wagner, J.A., Gorsich, S.W., McCaffery, J.M., Shaw, J.M., and Nunnari, J. (2000). The dynamin-related GTPase, Mgm1p, is an intermembrane space protein required for maintenance of fusion competent mitochondria. *The Journal of cell biology* 151, 341-352.
- Wylie, S.R., Wu, P.J., Patel, H., and Chantler, P.D. (1998). A conventional myosin motor drives neurite outgrowth. *Proceedings of the National Academy of Sciences of the United States of America* 95, 12967-12972.
- Yang, Z., Li, H., Chai, Z., Fullerton, M.J., Cao, Y., Toh, B.H., Funder, J.W., and Liu, J.P. (2001). Dynamin II regulates hormone secretion in neuroendocrine cells. *The Journal of biological chemistry* 276, 4251-4260.
- Yoo, J., Jeong, M.J., Cho, H.J., Oh, E.S., and Han, M.Y. (2005). Dynamin II interacts with syndecan-4, a regulator of focal adhesion and stress-fiber formation. *Biochemical and biophysical research communications* 328, 424-431.
- Yoon, B.I., Jung, S.Y., Hur, K., Lee, J.H., Joo, K.H., Lee, Y.S., and Kim, D.Y. (2000). Differentiation of hamster liver oval cell following *Clonorchis sinensis* infection. *The Journal of veterinary medical science / the Japanese Society of Veterinary Science* 62, 1303-1310.
- Yoon, Y., Pitts, K.R., Dahan, S., and McNiven, M.A. (1998). A novel dynamin-like protein associates with cytoplasmic vesicles and tubules of the endoplasmic reticulum in mammalian cells. *The Journal of cell biology* 140, 779-793.
- Yoon, Y., Pitts, K.R., and McNiven, M.A. (2001). Mammalian dynamin-like protein DLP1 tubulates membranes. *Molecular biology of the cell* 12, 2894-2905.
- Yumura, S., and Uyeda, T.Q. (2003). Myosins and cell dynamics in cellular slime molds. *International review of cytology* 224, 173-225.

- Zanna, C., Ghelli, A., Porcelli, A.M., Karbowski, M., Youle, R.J., Schimpf, S., Wissinger, B., Pinti, M., Cossarizza, A., Vidoni, S., *et al.* (2008). OPA1 mutations associated with dominant optic atrophy impair oxidative phosphorylation and mitochondrial fusion. *Brain* *131*, 352-367.
- Zhang, Z., Hong, Z., and Verma, D.P. (2000). Phragmoplastin polymerizes into spiral coiled structures via intermolecular interaction of two self-assembly domains. *The Journal of biological chemistry* *275*, 8779-8784.
- Zurcher, T., Pavlovic, J., and Staeheli, P. (1992a). Mechanism of human MxA protein action: variants with changed antiviral properties. *The EMBO journal* *11*, 1657-1661.
- Zurcher, T., Pavlovic, J., and Staeheli, P. (1992b). Mouse Mx2 protein inhibits vesicular stomatitis virus but not influenza virus. *Virology* *187*, 796-800.
- Zurcher, T., Pavlovic, J., and Staeheli, P. (1992c). Nuclear localization of mouse Mx1 protein is necessary for inhibition of influenza virus. *Journal of virology* *66*, 5059-5066.

Curriculum Vitae

s.jayashankar@gmail.com

First Name : Jayashankar
 Family Name : Selvadurai
 Date of Birth : 14.09.1982
 Languages Known : Tamil, English
 Father's Name : Selvadurai
 Mother's Name : Vetrikkodi

Education Profile

Degree	Board of study	Year	Percentage	Class/Grade
M.Sc Biophysics	University of Madras	2003 - 2005	72	First
B.Sc Physics	Bharathidashan University	2000 - 2003	71	First
Higher Sec.	Central board of secondary education (CBSE)	1998 - 2000	72	First

Conference and Workshops

Directed Evolution Approaches in Structural Biology

Poster presented with the title: *A Rational Approach to Study Structure and Function of Dynamins*

Wed 30th & Thu 31st January 2008 at EMBL Grenoble, France.

BIOXHIT/BCO COURSE: Remote datacollection at the ESRF and the CCP4 structure determination pipeline

Mon 21st – Fri 25th April 2008 University of Oulu, Finland

4th International symposium on Recent trends in Macromolecular Structure and Function

Wed 21st – Sat 23rd January 2010, University of Madras, India

EBI-EMBO practical course - Computational aspects of protein structure determination and analysis: from data to structure to function

Mon 6th – Fri 10th September 2010, EBI, Hinxton

Research visit, Cambridge Institute for Medical Research,

Department of Clinical Biochemistry

10th Sep -2 nd October 2010, Cambridge